DEPARTMENT OF GEOPHYSICS • STANFORD UNIVERSITY

APOLLO 14 AND 16 ACTIVE SEISMIC EXPERIMENTS
AND
APOLLO 17 LUNAR SEISMIC PROFILING

Final Report

April 1976

Prepared for

NATIONAL AERONAUTICS AND SPACE ADMINISTRATION
Johnson Spacecraft Center, Houston, Texas
Contract No. NAS 9-5632

DEPARTMENT OF GEOPHYSICS
STANFORD UNIVERSITY
STANFORD, CALIFORNIA

APOLLO 14 AND 15 ACTIVE SEISMIC EXPERIMENTS

APOLLO 17 LUNAR SEISMIC PROFILING

Contract No. NAS 9-5632

Final Report
April 1976

Prepared for

NATIONAL AERONAUTICS AND SPACE ADMINISTRATION
Johnson Spacecraft Center, Houston, Texas

TABLE OF CONTENTS

	Page
Introduction	1
A Seismic Refraction System for Lunar Use	3
A Lunar Engineering Seismic System	12
The Active Seismic Experiment	24
Seismic Data from Man-Made Impacts on the Moon	38
Active Seismic Experiment (Apollo 14 Preliminary Science Report)	46
Apollo 14 Active Seismic Experiment	58
Active Seismic Experiment (Apollo 16 Preliminary Science Report)	60
The Velocity Structure of the Lunar Crust	74
The Lunar Seismic Profiling Experiment	87
Lunar Seismic Profiling Experiment (Apollo 17 Preliminary Science Report)	93
Apollo 17 Seismic Profiling: Probing the Lunar Crust	105
Seismic Investigation of the Lunar Regolith	108
The Structure of the Lunar Crust at the Apollo 17 Site	122
Lunar Near Surface Structure	134
Energy, Frequency and Distance of Moonquakes at the Apollo 17 Site	152

Introduction

Seismic refraction experiments were successfully carried out on the Moon by Apollo astronauts during missions 14, 16, and 17 as part of an integrated set of geophysical experiments called ALSEP (Apollo lunar surface experiments package). This final report summarizes, through a collection of published papers, the seismic data pertinent to the near surface of the Moon.

The principal objective of the lunar seismic refraction experiments was to determine the near-surface elastic properties of the Moon. Several specific questions were addressed. What was the depth of the fragmental layer, the regolith, which covers much of the lunar surface? What is the structure of the regolith (is it layered? Is it laterally homogeneous?). How does the seismic velocity increase with depth in the upper 5 km of the Moon - smoothly or stepwise?

The principal conclusions from the lunar active seismic experiments can be summarized as follows. Seismic velocities of 104, 108, 92, 114 and 100 m/s were inferred for the lunar regolith at the Apollo 12, 14, 15, 16 and 17 landing sites, respectively. These data indicate that the process of fragmentation and commiution by meteoroid impacts has produced a layer of remarkably uniform seismic properties moonwide. Brecciation and high porosity are the probable causes of the very low velocities observed in the lunar regolith.

Apollo 17 seismic data revealed that the seismic velocity increases very rapidly with depth in the near-lunar surface increasing to 4.7 km/sec at a depth of 1.4 km. These data are not compatible with the idea that a cold rock powder extends to a depth of 1 km or so in the Moon. The observed magnitude of this velocity change with depth and the inplied steep velocity-depth gradient of > 2 km/sec/km are much larger than have been observed on laboratory experiments on granular materials. Such a large velocity change is more suggestive of compositional and textural

changes and in view of geologic observations is compatible with a model of fractured basaltic flows overlying the presumably anorthositic breccias that form the lunar highlands. "Thermal" moonquakes were also detected at the Apollo 17 site, becoming increasingly frequent after surise and reaching a maximum at sunset. The source mechanism of these moonquakes remains an enigma but landsliding can be the source without a complete degradation of all lunar slopes.

Robert L. Kovach
Joel S. Watkins

A SEISMIC REFRACTION SYSTEM FOR LUNAR USE

BY

B. D. McALLISTER, J. KERR, J. ZIMMER, R. L. KOVACH AND J. WATKINS

Reprinted from IEEE TRANSACTIONS
ON *GEOSCIENCE ELECTRONICS*
Volume GE-7, Number 3, July, 1969
pp. 164-171

A Seismic Refraction System for Lunar Use

BRUCE D. McALLISTER, MEMBER, IEEE, JAMES KERR, JOHN ZIMMER, ROBERT L. KOVACH, AND JOEL WATKINS

Abstract—A miniaturized seismic refraction system has been constructed for possible use on early manned lunar landings. The detection system consists of three geophones, a three-channel amplifier, a geophone calibrator, and a logarithmic compressor system. A grenade launching device and an astronaut-held thumper staff are used as the sources of seismic energy. Seismic energy from the explosive sources is detected, amplified, logarithmically compressed, converted to digital form, and formatted for real-time transmission to earth. Total weight of the seismic detection system and ancillary electronics, exclusive of the explosive sources, is 6.25 lb.

Introduction

A SEISMIC refraction system has been developed for possible use on manned lunar landings. This system, called the Active Seismic Experiment (ASE), is part of the Apollo Lunar Surface Experiments Package (ALSEP) planned to be deployed by astronauts during their exploration of the moon.

A main objective of a seismic refraction experiment on the moon is to determine its near-surface elastic properties. The primordial lunar surface may be buried to an extent not observable to the astronaut and a seismic refraction experiment may provide the only data to enable the characteristics of the near surface layers of the moon to be properly interpreted [1].

During a traverse on the lunar surface one of the astronauts will emplace three seismometers at 150 foot intervals from the ALSEP. After emplacement of the distant detector he will walk back along the line of detectors inducing seismic energy into the ground with a hand-held thumper staff. A launching device, capable of launching four explosive grenades to ranges of 500, 1000, 3000, and 5000 feet is then emplaced near the ALSEP. The grenades are launched by command from earth after departure of the astronauts. The three miniature seismometers and associated electronics comprise the lunar seismic detection system.

Ranging of the grenades is accomplished by measuring the parameters of an assumed ideal ballistic trajectory. The launching device contains electronics to measure the time of flight, angle of launch and initial velocity of the grenades. The range is calculated to within ± 5 percent and time of detonation is known to within ± 0.1 ms.

Seismic energy from the explosive sources is detected, amplified, logarithmically compressed, converted to digital form, and formatted for real-time transmission to earth. This paper describes the seismic refraction system which has been developed for use on the moon.

Manuscript received October 24, 1968; revised December 16 1968. This work was supported by NASA under Contract NAS 9-5632. Fabrication of flight hardware was supported by the Bendix Aerospace Systems Division under Contract NAS 9-5829. Evaluation of this system for post-Apollo use is supported under NASA Grant NGL 05-020-232.

B. D. McAllister and R. L. Kovach are with the Department of Geophysics, Stanford University, Stanford, Calif. 94305.

J. Kerr is with Geotech, a Teledyne Company, Garland, Tex.

J. Zimmer is with Bendix Aerospace Systems Division, Ann Arbor, Mich.

J. Watkins is with the Department of Geology, University of North Carolina, Chapel Hill, N. C.

System Description

Geophones

The miniature seismometers, or geophones, developed for lunar use are of the moving coil-magnet type. The coil is the inertial mass suspended by springs in the magnetic field. Above the resonant frequency of such a device the output is proportional to ground velocity; below the resonant or natural frequency the output drops off at 12 dB per octave.

Existing commercial geophone designs were not suitable for lunar use. First, spring parameters needed to be changed to be compatible with lunar gravity. Second, it was apparent that significant increases in sensitivity could be achieved while still reducing weight and size by use of better magnet materials and more efficient coil windings. Other considerations such as various methods by which the astronaut could implant the device and the need to protect the springs from the vibration and shock levels encountered in testing and transit also suggested a new design. A significant increase in available signal power with some savings in size and weight were realized while satisfying the other design objectives including matching the coil resistance to the optimum amplifier source impedance.

The design goal for the overall system response was that it be flat to ground velocity down to 3 Hz. For geophones of small size and weight the minimum resonant frequency for reliable operation can be expected to be somewhat higher than 3 Hz, particularly with the springs used for operation at lunar gravity. Preemphasis in the succeeding electronics was used to give the desired response at frequencies below geophone resonance.

For a state-of-the-art junction transistor in an appropriate configuration, the power spectral density of the equivalent input noise is very nearly constant down to about 20 Hz. Below this frequency it increases with a slope of $1/f$. Thus preemphasis at frequencies lower than resonance amplifies the $1/f$ noise decreasing the signal-to-noise ratio for signals at higher frequencies. This effect is a strong incentive to make the geophone's

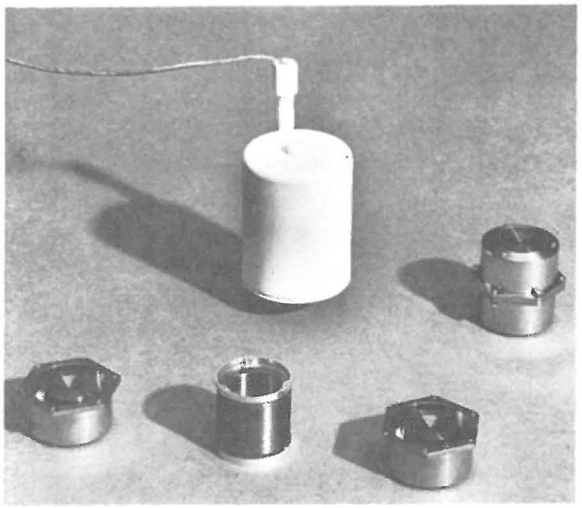

Fig. 1. Three geophones showing the unit in its outer case, the assembled magnet cup, and the magnet cup disassembled with the coil and springs. Diameter of geophone is 1.54 inches.

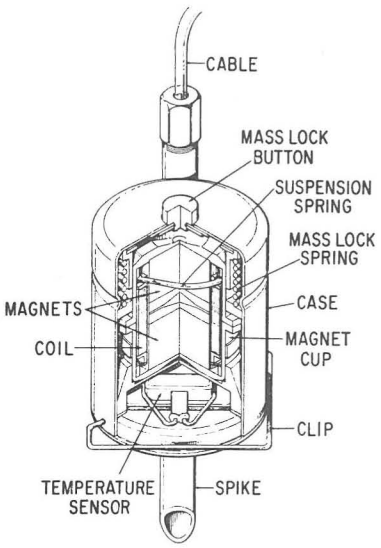

Fig. 2. Cutaway view of a geophone in its outer case. This is the geophone which includes the temperature sensor.

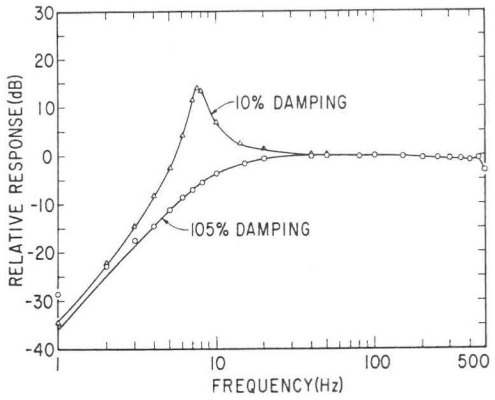

Fig. 3. Relative response curves for the lunar geophone with a constant velocity input and damping 10 percent and 105 percent of critical.

natural frequency the lowest possible consistent with small size and weight and adequate mechanical ruggedness. These constraints led to a choice of 7.5 Hz for the lunar geophone's natural frequency.

The optimum source impedance for low noise operation of a junction transistor amplifier is about 2000 to 5000 ohms. It can be increased or decreased by effectively connecting several transistors in parallel or series at the input. An amplifier with a differential input was used and the source resistance was determined to be at a broad optimum at about 6000 ohms.

Fig. 1 shows three geophones in various stages of assembly. In the foreground the internal assembly of a geophone is disassembled into its three major components; the two halves of the magnet cup and the coil with springs attached. Each half of the magnet cup is identical and includes magnetic pole pieces and pole caps as shown. Fabricated of ALNICO-9, they are charged so that the fields in each half oppose each other, making a closed flux path for each half of the cup. The average flux in the gap for each half ranges from 19 000 to 20 000 maxwells. The unit on the right shows the magnet cup assembled; the one in the background shows the completed geophone in its external case with mass lock button on the top.

The coil is wet wound using Shell EPON 828 on a mandrel between end pieces also cast from EPON 828, with nickel–silver threaded inserts encapsulated in them. 13 600 turns of no. 43 type ML copper magnet wire are used. The screws that secure the springs to the coil, and the springs themselves, serve as conductors from the coil.

Fig. 2 is a cutaway view of the assembled geophone. The position of the coil in the magnetic flux path is shown. The internal assembly is supported within the outer case by parts machined from EPON-828 for thermal and mechanical stability. When the mass lock button at the top of the case is held in the depressed position, three nickel–silver fingers extending inside the inner case assembly (the magnet cup) hold the coil firmly against the lower stops. This mass lock insures that the unit can survive the shock and vibration encountered in environmental testing and transit to the moon. The spring loaded mass lock buttons are released automatically when the geophones are removed from a carrying fixture and deployed by the astronauts.

The sensitivity and frequency response characteristics of the resulting geophone are excellent. Fig. 3 shows typical damped and undamped geophone response to a constant velocity input. An open circuit generator constant of about 235 V/(m/s) was achieved using a coil resistance of 6200 ohms. Open circuit damping is about 5 percent of critical. For comparison, a standard 4.5 Hz HS-1 Hall–Sears geophone has a generator constant of about 24 V/(m/s) with a coil resistance of 215 ohms and open circuit damping of about 23 percent of critical. Adjusting for the differing coil resistances and ignoring differences in open circuit damping, the available signal power from the lunar geophone is about

three times greater than that from the commercial geophone. The magnetic cup assembly of the commercial unit measures 1.88 inches high by 1.62 inches in diameter. Weight is about 9.5 oz. Equivalent specifications for the lunar geophone are 1.095 inches diameter, 1.25 inches high, and 4.16 oz. Complete with outer case the unit weighs 6.25 oz.

Testing of the lunar model geophones on earth presents a problem as the inertial mass rests on the lower stops in the earth's gravitational field. A device was developed which introduced a dc current into the geophone's coil just large enough to offset about 5/6 of the weight of the inertial mass at earth gravity. This value of current could be calculated accurately for each geophone from its measured generator constant and was nominally 0.74 mA. High voltage batteries and a large dropping resistance were used to obtain a quiet current source. Large capacitors inserted in the amplifier input blocked any dc current from the amplifier.

A second concern was verifying the linearity of the geophone at the very low signal amplitudes expected. The system sensitivity is such as to give clearly discernible signals to ground motion of 1 mμ zero-to-peak at 10 Hz. Testing to these levels, below normal background seismic noise levels on earth, required use of a quiet site and an isolation drive system to excite the geophones.

Low-level tests were accomplished in a 50-foot deep cased hole at the Geotech, Garland, Tex., facility. The operating mechanism from a Johnson–Matheson vertical seismometer was used as the isolation drive unit. This unit has a natural frequency of 0.8 Hz. A signal generator was the driving source and signal levels required for a given displacement were calculated using the large seismometer's calibrated generator constant. The three geophones were mounted directly on the 18-kg mass of the JM seismometer and lunar gravity was simulated using the quiet current source described previously. By testing very late at night good data was obtained down to displacements of 1 mμ peak-to-peak at 10 Hz. There were no measurable deviations from linearity at these low amplitudes.

During the rather lengthy storage time of the system on the moon (up to one year), the possibility exists that some geophone parameters might drift. A calibrator system is included in the succeeding electronics for testing for this drift. During manufacture, all the pertinent geophone parameters, natural frequency, open circuit damping, and generator constant are calibrated for each unit. The calibrator has demonstrated the capability of measuring these parameters to within 10 percent of the values determined by low-level and other tests in the laboratory.

The geophone cable assembly is constructed of four twisted pair, shielded, polyimide insulated cables. Three pairs connect each geophone to its respective amplifier input and the fourth connects a temperature sensor in the near geophone to the proper data circuitry. The

Fig. 4. A suited astronaut implanting the geophone on a simulated lunar surface.

three geophones are spaced at 150 feet intervals on the cable automatically providing the proper separation during deployment by the astronaut. Black and white markers on the cable are used to indicate the thumper firing points. Fig. 4 shows how the geophones suspended by the cable are implanted by the astronaut. The astronaut raises the geophone to a vertical position with his toe and then forces the spike into the lunar surface.

Amplifier, Calibrator, and Log Compressor

A three-channel amplifier conditions the geophone signals prior to their conversion into a digital format. Since a seismic thumper device will be used for short range shots (of the order of feet), seismic signals containing energy at frequencies of 100 Hz and higher can be generated. A system time resolution of ± 1 ms was selected. This dictates a minimum sampling frequency of 500 Hz which, in turn, specifies the filter response at high frequencies necessary to minimize data contamination from sideband folding. The low signal-to-noise ratio expected from the distant grenade explosions and the lack of a priori knowledge as to the character of the expected waveforms make it desirable to widen the frequency response as much as possible within this constraint. Fig. 5 shows the overall frequency response for the lunar active seismic detection system.

Each amplifier consists of a differential input dc preamplifier, essentially a five stage differential amplifier, together with associated calibrator circuitry at the input

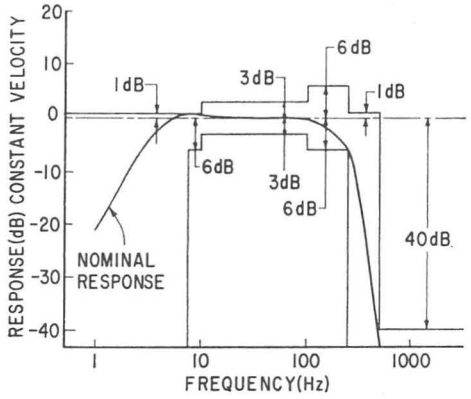

Fig. 5. The overall frequency response of the system. Both nominal response and specified limits are shown.

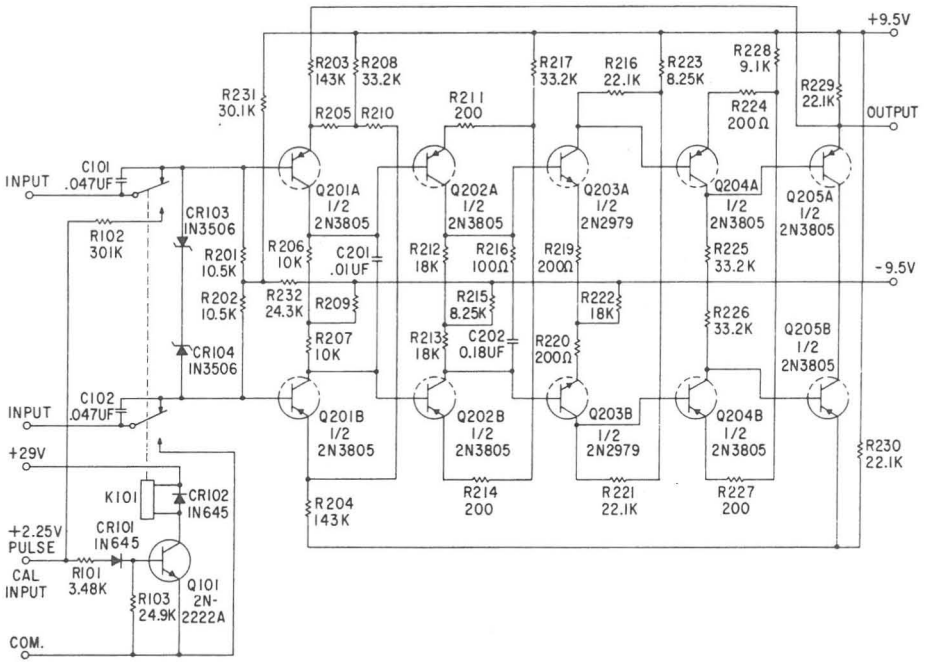

Fig. 6. The geophone preamplifier and calibrator circuits for a typical channel.

of the preamplifier and an active filter section. The purpose of the calibrator circuitry is to provide a means of checking for any changes in the parameters of the geophones during lunar operation.

Fig. 6 is a schematic drawing of the geophone preamplifier and calibrator circuits. The values for the resistances R201 and R202 are selected to yield 115 percent of critical damping of the geophone. A 2.25-volt dc calibration pulse applies a current pulse to the geophones through resistance R102. Because of the changed circuit configuration, specifically insertion of series capacitors C101 and C102, the impedance seen by the geophone is increased to essentially the 301-kΩ value of R102 and the geophone is now underdamped. The resultant ringing frequency and rate of decay are the means used to measure the natural frequency and generator constant of the geophones on the moon.

Fig. 7 is a schematic of the filter section of the active seismic detection system. This section consists of 5 active stages utilizing field-effect transistors in a source follower configuration together with an operational amplifier output stage. The first stage supplies the low-frequency preemphasis required to compensate for the low-frequency roll off of the geophone's response. The last four stages form a low pass filter with a roll off of 48 dB per octave above 250 Hz. The capacitively coupled operational amplifier supplies more than enough gain to offset insertion loss due to the previous stages and also adds an additional roll off of about 6 dB per octave above 300 Hz.

The wide dynamic range of signals expected, the overall timing resolution desired, and telemetry bit rate constraints made some form of data compression before telemetering to earth desirable. For example, the dynamic range of the linear system is nominally 80 dB. The maximum bit rate available to the ASE was 10.6 Kbit-S. With a minimum sampling frequency of 500 Hz, uniform sampling in time, and three channels of seismic

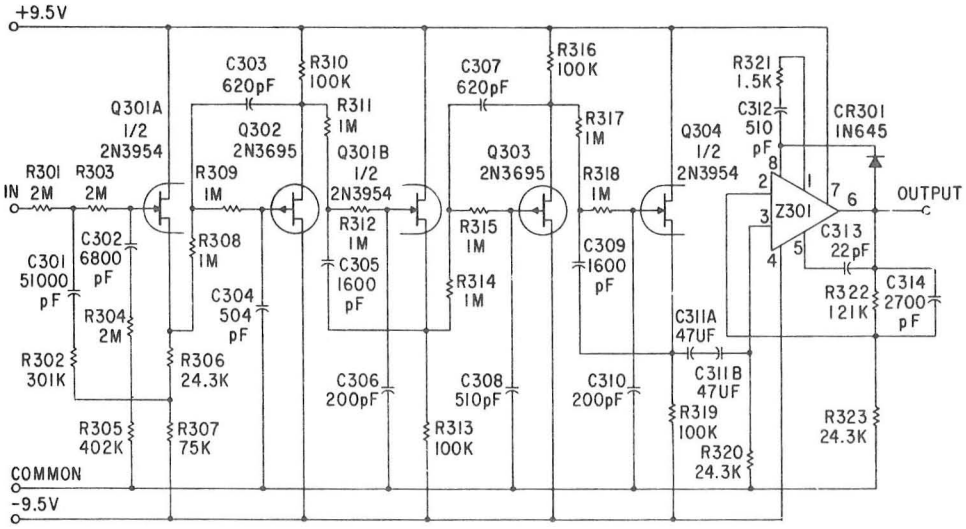

Fig. 7. The active filter circuit for a single channel.

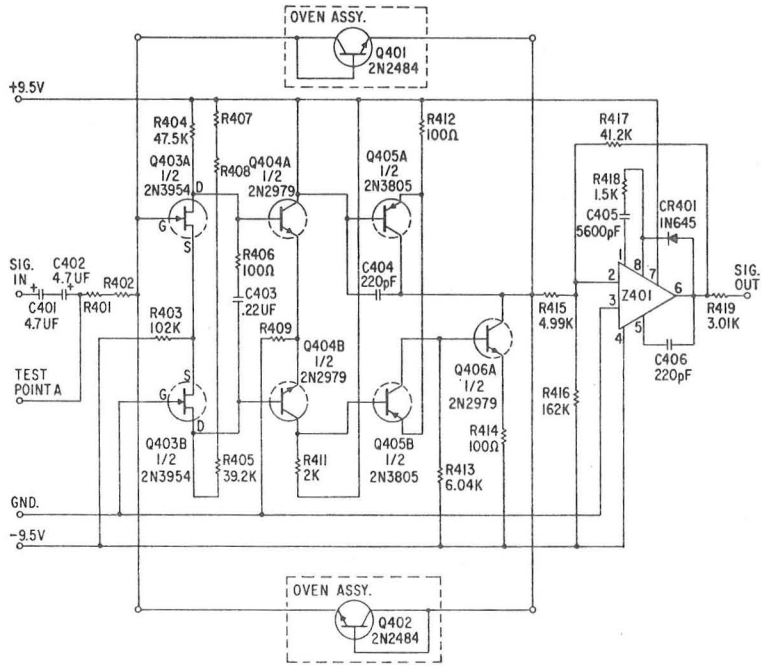

Fig. 8. The logarithmic compressor circuit for a single channel.

data required, a maximum of only 5 bits per geophone data subword are available. In a linear digitization system this would have led to unacceptably poor resolution at the very low signal levels expected from the distant grenade shots. Since signal levels were expected to be distributed throughout the system's dynamic range, the most desirable compression scheme was one that gave signal resolution as some constant fraction of signal amplitude. This is the principle characteristic of logarithmic compression and thus this form of data compression was chosen.

The logarithmic compressor circuit is shown in Fig. 8. The logarithmic relationship of voltage and current in the base emitter diodes of Q401 and Q402 are used to generate this function. One diode is used for each signal polarity. Since this logarithmic relationship is a sensitive function of temperature these diodes are maintained at a constant temperature of 105°C by an oven over the electronic environmental temperature range of −20 to +85°C.

We can express the logarithmic transfer function for the compressor and amplifier system as

$$V_{out} = K_1 \ln V_{in} + K_2; \qquad V_{in} > 0. \tag{1}$$

The constant K_1 determines the slope of the log transfer function whereas K_2 is specified by the dc offset of the compressor output and the system noise level. Nominal values of these constants for input signals of each polarity are

$$V_{out} = 0.2687 \ln |V_{in}^{+}| + 4.1473; \qquad V_{in} > 0$$

$$V_{out} = -0.2687 \ln |V_{in}^{-}| + 0.2927; \qquad V_{in} < 0.$$

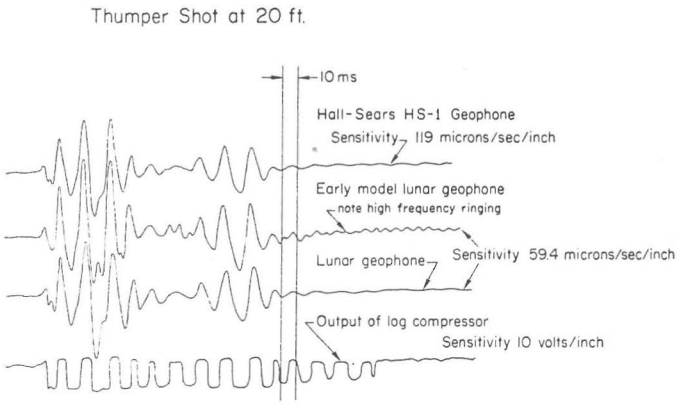

Fig. 9. Tracings of seismograms from a thumper shot at 20 feet for the lunar geophone compared with a commercial geophone. Note differences in sensitivity. Bottom trace accurately depicts the actual output from the logarithmic compressor.

For actual flight hardware the values of these constants are calibrated for each channel. Log compression accuracy is specified at ± 10 percent referred to the linear input of the system. However, the accuracies typically achieved have been ± 3 to 5 percent.

The linear portion of the system has a minimum dynamic range of 80 dB. The constants in the log transfer function are chosen such that an input dynamic range of 80 dB is compressed to a maximum voltage of 5.0 volts peak-to-peak centered at the output about a zero reference voltage of 2.42 volts. These constants also adjust the system noise level so that the first quantization level in the succeeding analog-to-digital converter is down in the noise, nominally at the rms noise level. Fig. 9 gives a typical seismogram as recorded at the output of the linear portion of the system and the output of the log compressor.

The principal effect of log compression of data on resolution can be most easily evidenced by substituting in the log transfer function, $V_{\text{in}} = V_{\text{in}} \pm \Delta V_{\text{in}}$ and $V_{\text{out}} = V_{\text{out}} \pm \Delta V_{\text{out}}$. ΔV_{in} and ΔV_{out} are the equivalent incremental changes in voltage at the compressor input and output, respectively. An expression for ΔV_{out} as a function of V_{in} and ΔV_{in} can easily be derived:

$$\pm \Delta V_{\text{out}} = K_1 \ln\left(1 \pm \frac{\Delta V_{\text{in}}}{V_{\text{in}}}\right). \tag{2}$$

One can see that log compression of data in a digital system yields signal resolution to some constant fraction of signal amplitude over the system's dynamic range, as opposed to some fraction of the full scale value in a linear system. For this system, where 5 bits including the sign bit are available, the fractional amplitude resolution is ± 2.67 dB, or $+36$ percent and -27 percent of signal amplitude.

Calibration of each log compressor is accomplished as a part of flight acceptance tests and separate functions are derived for positive and negative signals. The techniques used are straightforward. Testing of the calibrator's operation is somewhat less straightforward since the data are only seen after log compression. A key requirement is that use of the calibrator permit measuring the geophone's natural frequency, generator constant, and damping factor to an accuracy of 10 percent, relative to the calibrated values.

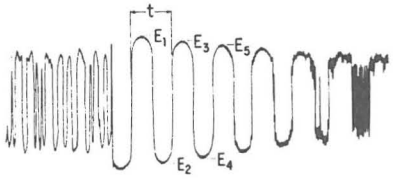

Fig. 10. Tracing of actual ultraviolet recording showing response of the system to the calibrate pulse as seen at the output of the logarithmic compressor.

Fig. 10 is a recording of the analog waveform at the output of the log compressor resulting from operation of the calibrator. Several characteristics of this process are pertinent. First, the nature of the log transfer function is such that the system noise appears greatly amplified making determination of an ac zero reference line from the recording difficult. Second, use of the calibrator itself introduces a small dc step in voltage due to bias changes and upon which the ac ring down of the geophone is superimposed. Last, the nature of the log transfer function is such that the exponential decay of the ring down becomes linear at the log compressor output; because of the dc shift the successive positive and successive negative peaks have different slopes. The technique described below circumvents these problems. We can write

$$G = 280 f_0 b_t \text{ V/(m/s)} \tag{3}$$

$$f_0 = \frac{m}{t_m}\sqrt{(1 - b_t^2)} \text{ Hz} \tag{4}$$

$$\frac{V_n}{V_{n+m}} = \exp\left(2\pi m \frac{b_t}{\sqrt{1 - b_t^2}}\right) \tag{5}$$

where

b_t = resonant system damping factor, expressed as a fraction of the critical damping value,
f_0 = geophone undamped natural frequency in Hz,
G = geophone generator constant relating output voltage to ground velocity in V/(m/s),
m = a positive even integer,
n = a positive integer,
t_m = the period of $m/2$ cycles of the system response to the calibrate pulse,
V_n = zero-to-peak value of the nth half cycle of the uncompressed system response to the calibrate pulse, and
V_{n+m} = zero-to-peak value of the $n+m$th half cycle of the uncompressed system response to the calibrate pulse.

Equation (5) relates successive peaks in a damped linear resonant system to the damping factor. Recalling from (1) that

$$E_n = K_1 \ln (V_n) + K_2$$

where

E_n = zero to peak value of the nth half cycle of the compressed system response to the calibrate pulse

we can define

$$\Delta E_m = E_n - E_{n+m}$$

where

ΔE_m = the difference in zero-to-peak values of m successive half cycles of the compressed system response to the calibrate pulse.

We can then solve for an expression relating the damping constant b_t to the amplitude decrement of succeeding peaks in the system response at the log compressor's output

$$b_t = \frac{\Delta E_m}{\sqrt{\Delta E_m{}^2 + (2\pi m K_1)^2}} \cdot \tag{7}$$

Furthermore, the difference in the slopes of the negative and positive peaks can be compensated for by averaging the two slopes:

$$\Delta E_m = (\Delta E_{m_-} + \Delta E_{m_+})/2. \tag{8}$$

Equations (8), (7), (4), and (3) are used to calculate the geophone parameters b_t, f_0, and G from the analog data recorded at the log compressor output. A 10 percent accuracy relative to the more precise laboratory calibrations is easily attainable.

Digital Portions of the System

A 16-channel commutator, an 8-bit analog-to-digital converter, and logic circuitry associated with data formatting and command functions comprise the bulk of the remaining ASE electronics. Fig. 11 is a block diagram of this portion of the system.

The 16-channel commutator switches analog voltages from the three seismic data channels and 13 channels of engineering and housekeeping data to the eight bit converter. For the seismic data only the five most significant bits are used. Engineering data formatted include the mortar box attitude (2 axes), temperatures in the mortar box and electronics package, and calibration voltage levels for the geophones and the converter. Since operation of the ASE uses all the telemetry capacity, five channels are provided for housekeeping data from the rest of ALSEP.

The general outline of the data format used is shown in Fig. 12. A data frame consists of thirty-two 20-bit words, each of which is normally broken down into four 5-bit subwords. Subwords 2–4 in each word are usually the 3 seismic data subwords, while the first subword is used for engineering data. Engineering data is quantified in 8 bits, and each parameter is transmitted

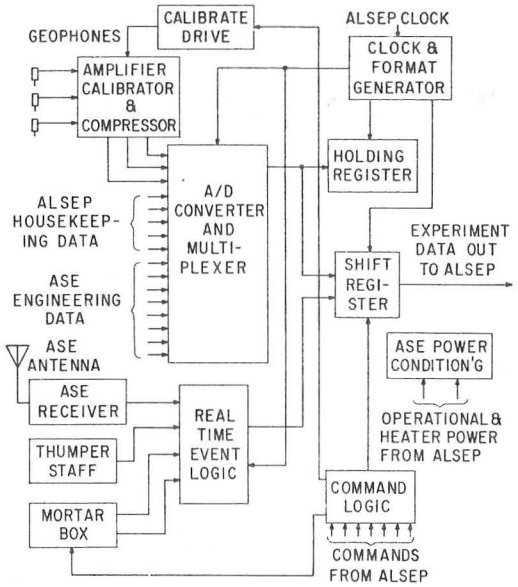

Fig. 11. Block diagram of the active seismic experiment.

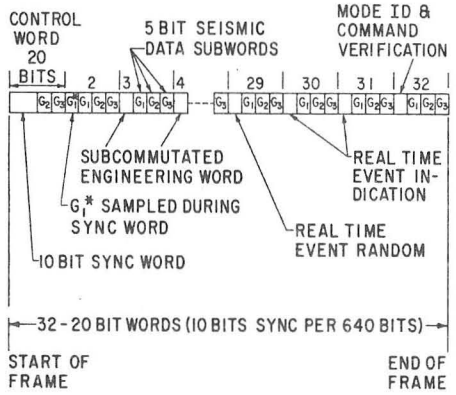

Fig. 12. The active seismic experiment data format.

in two parts. An exception to the above is the 10 bits of synchronization required in each data frame, transmitted in bits 1–10 of the first, or control, word of each frame. The 5 bits of geophone data so displaced are delayed and transmitted in the first subword of the following word.

It is crucial that the time of occurrence of certain events be transmitted with greater resolution than that normally afforded by the system. These events are those associated with launch and impact of the grenades and the firing of the thumper staff. A *real-time event* (RTE) feature of the telemetry format provides the capability of time resolution to ± 0.1 ms. This feature uses the first subword in words 29–31 in each data frame. If a RTE has occurred in the previous data frame a distinctive code 00100 appears in this subword. The subwords in words 30 and 31 give the time within the previous frame that the RTE occurred to the nearest 0.1 ms.

A command system provides for nine commands associated with the ASE. Two commands turn the ASE

TABLE I

TYPICAL ASE PERFORMANCE FIGURES

Sensitivity: 21.0 dB rms signal-to-rms noise ratio for a displacement of 1 mμ 0 to peak at 10 Hz. (Amplifier input noise voltage for a 6-kΩ source is 0.72 μV rms).

Dynamic Range: 74 dB for the linear system. All channels are within 6 dB.

Logarithmic Compression Accuracy: Worst case referred to the compressor input is ±4 percent.

Quantizer Resolution: Engineering data—±0.20 percent of full scale. Seismic data—+36 and −27 percent of signal amplitude.

Quantizer Accuracy: Peak rms error through the A/D converter and the multiplexer is better than: engineering data—±0.33 percent of full scale; seismic data—+6.0 and −5.6 percent of signal amplitude.

Calibrator Accuracy: ±10 percent of laboratory calibration values.

Crosstalk: Less than 70 dB at 100 Hz.

Common Mode Rejection:—50 dB

TABLE II

ASE PHYSICAL DIMENSIONS AND POWER REQUIREMENTS

Item	Dimensions	Weight
Geophone	Length 1.94 inches Diameter 1.54 inches Overall length including spike 4.81	6.25 oz max. each without temp. sensor 6.40 oz max. with temp. sensor
Cables	Length 16.5 ft, 166.5 ft., and 316.5 ft	2.0 lb
Amplifier, calibrator, filter, and compressor package	Length 5.25 inches Width 3.06 inches Height 1.00 inch	12.0 oz
Electronics package (includes amplifier, etc., above)	Length 6.77 inches Width 6.18 inches Height 2.75 inches	3.07 lb
Mortar box (includes grenades)	Length 15.6 inches Width 6.2 inches Height 9.5 inches	14.96 lb
Thumper	Length (folded) 14.5 inches Length (deployed) 44.5 inches	4.01 lb
	TOTAL	25.22 lb

Power Requirements

Operational	8.0 watts
Thermal control (standby)	1.75 watts

on and off and place the ALSEP data processor in the high bit rate (10.6 kbit-s) mode. Five commands are associated with firing grenades; four commands are used to fire each grenade individually, and one is an alternative automatic sequential command. One command arms the grenade rocket motors and firing circuits in each grenade. It must be activated prior to a "FIRE" command. Finally, one command initiates the 1-second geophone calibrate pulse.

When the ASE experiment is turned on the full output format with RTE capability is operational even if the "ARM" and "FIRE" commands are not activated. It is in this mode that the thumper staff is operated. This also provides a passive listening capability by which the experiment can periodically monitor the lunar seismic background noise.

When the ASE experiment is turned off, certain engineering parameters are made available through the ALSEP telemetry format for monitoring the experiment's condition and its environment. These data are the temperature of the near geophone, the mortar box, and the electronics package. Monitoring these data are helpful for selecting the appropriate time during lunar twilight to activate the grenade launching phase of the experiment. A time will be chosen such that the declining surface temperatures have cooled the geophones and cables thus minimizing noise from these sources. The mortar box and electronics, with their longer thermal time constants, will also be well within their optimum operating temperature range.

A summary of the performance specifications, physical dimensions, and power requirements of the lunar seismic refraction system are given in Tables I and II.

REFERENCES

[1] R. L. Kovach and F. Press, "Lunar seismology," *Proc. Conf. on Lunar Exploration*, Bull. 152, Virginia Polytechnic Institute, vol. 56, 1962

[2] R. L. Kovach, "Lunar seismic exploration," in *The Physics of the Moon*, vol. 3, American Astronautical Society Science and Technology Series, pp. 189–198, 1967.

Reprinted from Bulletin of the Association of Engineering Geologists,
Fall 1969, Volume VI, Number 2

JOEL S. WATKINS
J. H. WHITCOMB
E. L. WEEKS
T. J. GRAVES
R. L. KOVACH
R. H. GODSON

A Lunar Engineering Seismic System

ABSTRACT

An engineering seismic system is planned for one of the Apollo manned landings on the surface of the moon. The system is expected to provide data regarding elastic and inelastic parameters to depths of 75 feet.

Supporting research conducted on earth indicates that the seismic data can be interpreted in terms of porosity and extent of fracturing and layering in the lunar soil and substrate. Results of the supporting research have been applied to terrestrial groundwater investigations and cavity detection.

An engineering seismic experiment is now planned for the fourth manned lunar landing in the National Aeronautics and Space Administration's Apollo series of lunar missions. The experiment is designed to (1) determine the depth of the fragmental layer which appears to cover much of the lunar surface, (2) investigate the structure of the fragmental layer (is it layered? is it laterally homogeneous?), (3) determine the porosity of the fragmental and subjacent layer and (4) estimate the extent of fracturing in the subjacent rock. Similar experiments conducted during following missions may be useful for locating and delineating near-surface cavities but this capability will not be intentionally used during the initial experiment. Data from the initial experiment will contribute to studies of bearing strength, traffic ability and excavatability required for follow-on missions.

This paper describes the system designed to accomplish these objectives and reviews results of research conducted in support of the

experiment. Differences between this instrumentation and instrumentation designed to accomplish the same objectives on earth are reviewed. Some of the new instrumentation, the authors believe, merits consideration for use on earth. A substantial body of research has been accomplished in support of the experiment. Results of some of this research have already been applied to terrestrial problems. Other results suggest methods which may be eventually refined to the point that they are sufficiently precise and indicative to be used as terrestrial tools.

THE SYSTEM

The Apollo Lunar Surface Experiments Packages (ALSEP) include three seismic systems. One system is analogous to a conventional station seismograph in that it continuously records low frequency seismic signals generated by moonquakes and by medium to large meteorite impacts. A second unit is analogous to a seismic refraction system with a spread length of approximately one mile. This system records seismic waves generated by explosives. Data from this system provide information about the structure of the lunar near-surface to maximum depths of 1,000–2,000 feet. The system is capable of processing reflections, although our knowledge of lunar structure suggests that reflections are unlikely. The third system is the engineering seismic system capable of investigating the structure of the lunar near-surface in some detail to a depth of about 75 feet.

These systems, along with other ALSEP scientific experiments, share common power and data transmission modules. In addition, the long-range refraction system and the engineering seismic systems use common geophones, amplifiers and data compression devices but have different command networks and seismic sources. The two systems are designed to operate as an integral unit and are collectively designated as the ALSEP Active Seismic Experiment (ASE). Kovach (1967) describes overall objectives and operation of the ASE and McAllister et al. (1969) describes the instrumentation of the ASE.

Once on the moon the astronauts will deploy the engineering seismic system as shown in Figure 1. The "Thumper" serves as a holder for the geophones, geophone cable, and Thumper cable during flight when it is folded into a compact unit approximately $13 \times 8 \times 7$ inches. Upon landing, the Thumper is unfolded and functions as a reel from

which geophones and cables are deployed. After deployment of cables and geophones, the astronaut returns along the geophone line and sequentially fires 21 Apollo Standard Initiators (ASI's) located in the base of the Thumper to provide the seismic energy. The ASI's are similar to squibs and small pressure cartridges. ASI's are found throughout the spacecraft where they are used to separate modular components, help sever umbilical cords, etc. Each ASI contains about 100 milligrams of explosive and generates seismic energy slightly less than the seismic energy output of a blasting cap. ASI's fire directly into a coupling plate which distributes the seismic energy over a

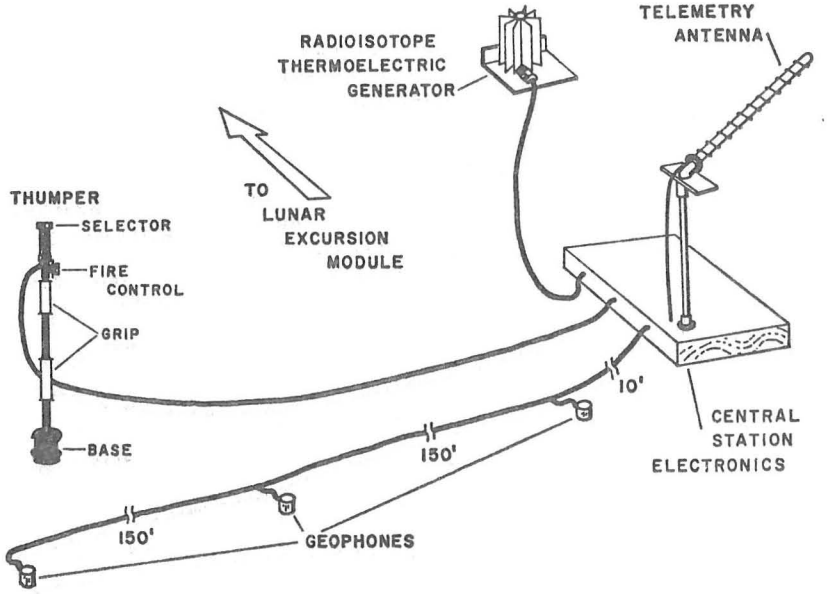

FIGURE 1. Sketch of the active seismic experiment deployed in the engineering seismic mode

wider area than that of the ASI alone. The Thumper, cables, and geophones weigh 7.1 lb.; the electronics weigh 3.1 lb.

The astronaut selects an ASI by turning the selector on top of the Thumper. He then charges the capacitor for about 5 seconds by turning the fire control knob a quarter turn. Pushing in on the fire control knob discharges the capacitor into the selected ASI.

The radioisotope thermoelectric generator (RTG) provides the current to charge the capacitor as well as power to operate telemetry and command systems. The current is conducted to the Thumper through the cable connecting the Thumper to the Central Station Electronics

(CSE). This cable also transmits a signal to the CSE at the instant the ASI fires. This signal is generated by a pressure transducer located in the Thumper base and actuated by the pressure of the exploding gases filling the volume between the ASI mounting and the coupling plate.

The seismic energy generated by the ASI travels through the ground and is picked up by three geophones deployed along a 300-foot line. The geophones are similar to terrestrial geophones except for a weaker spring used to compensate for lower lunar gravity.

The seismic signals are transmitted to the CSE for processing and transmission to the telemetry antenna. In the CSE the signals are amplified, logarithmically compressed, digitized, and multiplexed for the telemetering to earth.

The engineering seismic system data stream requires a telemetry bit rate mode of 10,600 bps activated only during the Thumper operation. The 10.6 kbps data are transmitted to earth in real time. A portion of the data is demultiplexed immediately upon receipt on earth in order to verify proper functioning of the system. Complete demultiplexing and exponentiation occurs a few days after the lunar operation, when the data tapes are received at the University of North Carolina.

Logarithmic Data Compression

Engineering objectives of the experiment are the determination of thickness, structure, porosity, and extent of fracturing of the fragmental layer. Standard seismic refraction analysis will tell us what the thickness of the fragmental layer is, something about the structure of the fragmental layer and provide us with an estimate of the porosity of the fragmental layer. Attenuation of seismic energy tells us about the extent of fracturing (essentially, the more fracturing in a rock, the more seismic energy the rock will "soak up"). Surface wave dispersion analysis will confirm the structure deduced from refraction analysis. Surface wave analysis has the further advantage that surface wave characteristics are sensitive to elastic properties of the rock or soil to which refraction data are insensitive. Specifically, ice-filled pores, low velocity layers and cavities are often identifiable from surface wave analysis but are seldom identifiable from refraction analysis.

Analysis of refraction data, attenuation of seismic energy, and surface wave dispersion requires a considerable quantity of data—such

a quantity, in fact, that multiple recordings at different amplification levels are required using most terrestrial seismic instruments. In addition, several trial explosions are usually required on earth to determine initial amplitude settings. Trials and multiple recordings are not feasible on the surface of the moon; therefore, lunar instrumentation must accurately record arrival times and waveforms of waves with a wide range of amplitudes. The problem is further complicated by lunar data transmission limitations. If lunar telemetry could transmit 100,000 bps, there would be no serious problem, but lunar telemetry has a maximum transmission rate of 10,600 bps.

To overcome this problem, we transmit the logarithm of the amplitude rather than transmitting the actual amplitude. The data are then exponentiated by computer and original amplitudes are plotted on a Calcomp plotter. One difficulty remains. The effective amplitude resolution of the plotting techniques we use is about one part in 10^2. Since the lunar data have a maximum amplitude resolution of almost one part in 10^4, multiple computer plots will probably be required to analyze the data! The reader is referred to McAllister et al. (1969) for details of logarithmic compression and data transmission.

ENERGY COUPLING

The second major change in design relative to terrestrial instrumentation was in the energy coupling mechanism. A series of experiments conducted at atmospheric pressure showed that seismic energy, generated by detonation of small explosives mounted in 1.25-in. diameter cylinders closed at one end and in contact with the ground at the open end, was optimal in tubes attached to inverted cones which distributed the gas pressure over the ground surface (Watkins and Whitcomb, 1968). When the experiments were repeated at low ambient pressures, the seismic pressure pulse at the mouth of the tube decreased with decreasing ambient pressure (Fig. 2). Further experimentation at low pressures (Fig. 3) showed that the efficiency of energy transfer varied as the distance from the pyrotechnic to the body in which the seismic energy was to be induced. Maximum efficiency occurred when the pyrotechnic was fired directly into the body with no intervening space (Watkins and Whitcomb, 1968).

When the design of the Thumper was modified so that the ASI's

fired directly into a base plate or coupling plate, it was found that small fragments of burning pyrotechnic and the metal end plate enclosure of the ASI were ejected laterally from the Thumper base, some with energies sufficient to damage the astronaut suit material. The final design incorporates a skirt fitted over the upturned edge of the coupling plate to prevent ejection of these fragments.

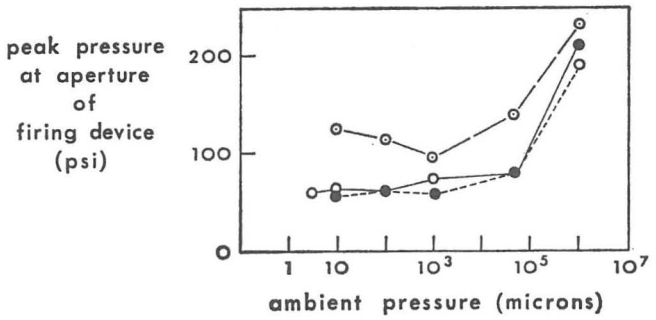

FIGURE 2. Peak pressure observed at firing device aperture as a function of ambient pressure

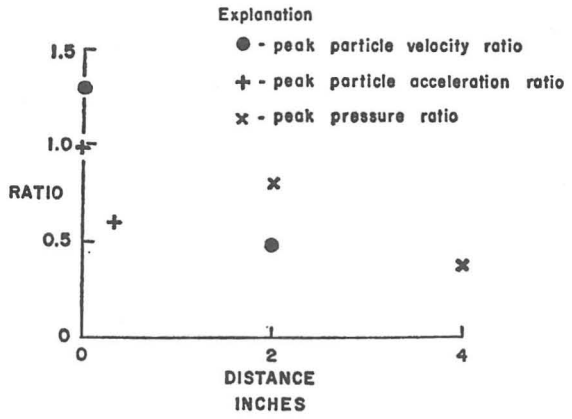

FIGURE 3. Ratio of peak pressures observed at firing device aperture in vacuum and at one atmosphere as a function of ASI–aperture distance

SUPPORTING RESEARCH

Supporting research has been most successful in (1) relating in situ compressional wave velocities and porosities, (2) relating head-wave attenuation and degree of fracturing, (3) cavity detection, and

(4) shear wave detection. Results of these investigations are briefly reviewed in the remainder of this report.

Compressional wave velocities in dry porous rocks. In situ compressional wave velocities and porosities from nonsaturated rocks of 15 areas in Arizona, California, and New Mexico will be reported by Watkins and Walters (in preparation). Sites were selected to provide maximum variation in porosity. Lithologies include granite, sandstone, quartzite, limestone, andesite, basalt, rhyolite, and diatomite. Porosities range from 2 to 84 percent.

Data collected by Watkins and Walters are shown in Figure 4. An empirical least squares fit yields

$$\phi = 0.52 \ln \alpha - 1.81 \quad (1)$$

where ϕ is total porosity (expressed in decimal fractions, e.g., 0.1, 0.2, etc.) and α is the compressional wave velocity (km-sec^{-1}). The root-mean-square error of the data relative to (1) is 20 percent. Data in Figure 4 in and of themselves do not preclude discontinuities or characteristics other than a smooth curve in the region $1.0 \leq \alpha \leq 2.0$ km-sec^{-1}. Abundant data from measurements made on saturated rocks clearly suggest a smooth curve in this region. Therefore, a smooth curve is drawn through the data points. Additional data should be collected in the region $1.0 \leq \alpha \leq 2.0$ km-sec^{-1}, however. These data permit estimation of porosities in porous lunar rock and soil from compressional wave velocity data.

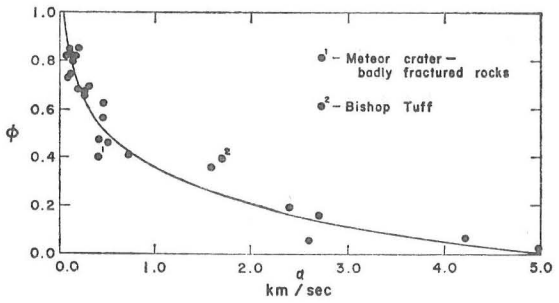

FIGURE 4. In situ measurements of compressional seismic wave velocities α as a function of fractional porosity ϕ

The immediate application of these results has been in groundwater exploration (Eaton and Watkins, in press; Watkins and Spieker, in press) where determination of rock or soil porosity is a

primary objective. Data in Figure 4 together with data from a number of other sources were used by the senior author (J.S.W.) to obtain an empirical equation relating compressional wave velocity α to grain density p, porosity ϕ, and pressure P (Watkins, in preparation). The equation is as follows:

$$\alpha = (2.3p + 0.023p[\ln P] - 0.72 - 0.1[\ln P])P^{0.06p^{-1}\phi^{-5.2}} \quad (2)$$

Details of the derivation are lengthy and will not be reviewed herein.

Headwave attenuation. Attenuation of compressional headwaves has been discussed by DeBremaecker et al. (1966) and Godson et al. (1965). Results of these investigations have not produced a quantitative relation between attenuation and fracturing as was the case for compressional wave velocities and porosities. However, it is possible to qualitatively relate the product of two seismic parameters, Q and α, to the degree of fracturing in the rock units investigated.

The parameters, Q and α, were used by DeBremaecker et al. (1966) in their formulation of a headwave attenuation function, as:

$$A = Nd^{-2} \exp(-\pi dQ^{-1} f\alpha^{-1}), \quad (3)$$

where A is the amplitude, d the distance, Q the attenuation constant, f the frequency, α the compressional wave velocity, and N a constant, is consistent with field observations.

Godson et al. (1965) examined the variations of Q and $Q\alpha$ as a function of α measured in situ in 10 rocks. They found that data from individual rock units tended to cluster in relatively well-defined groups. The $Q\alpha$ vs. α groupings were closely related to the extent of fracturing present in the rock units. In Figure 5, Kana-a lava flow second layer, which was shown by drilling to be relatively unfractured, had a higher $Q\alpha$ product than rocks of comparable compressional wave velocities occurring in the Southern Coulee second layer and S.P. andesite lava flow, both of which are extensively fractured. Figure 5 shows that badly fractured rocks, including cinders and blocky lava, have $Q\alpha$ products less than 3.5×10^{-3}, moderately fractured rocks have $Q\alpha$ products between 3.5×10^{-3} and 9.0×10^{-3} and unfractured rocks have $Q\alpha$ products greater than 9.0×10^{-3} m-sec^{-1}.

The $Q\alpha$-fracturing relationship may not be practical on earth where drilling and excavation are relatively uncomplicated procedures but on the surface of the moon, where even 3 m are difficult to drill, the seismic data provide the best estimate of the degree of fracturing in the rock substrate beneath the lunar soil.

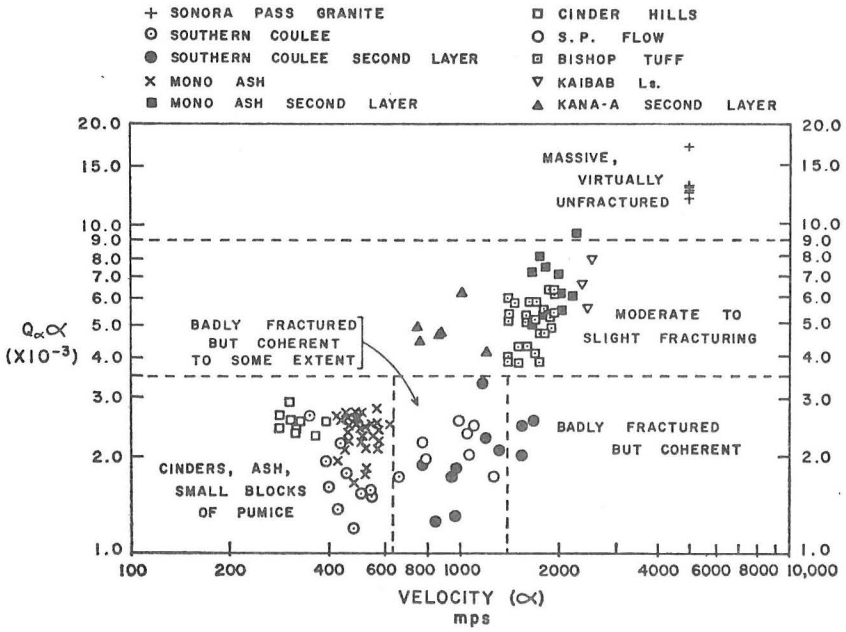

FIGURE 5. Relationship between compressional wave velocities α, attenuation parameter $Q_\alpha\alpha$ and extent of fracturing in selected rock types. $Q_\alpha\alpha$ units are mps.

Cavity investigations. Watkins et al. (1967) investigated the seismic response of two lava tunnels and one cavity formed by an underground nuclear explosion. They found that it was possible to generate resonant vibrations in the cavities. Fundamental modes of the vibrations had frequencies near those predicted by theory.

The probability of the single seismic spread proposed for the Apollo program partially overlapping a near-surface lunar cavity is very small, but seismic cavity location may be attempted in later missions. Cavities, and in particular lava tunnels, can provide shelter for astronauts and their equipment during meteor showers but constitute a hazard to astronauts traversing the lunar surface.

Godson and Watkins (1968) attempted to locate a cavity in the Anchor Reservoir, Wyoming. Resonance was observed in an area where a previous gravity survey had identified a gravity minimum. An open crack located to one side of the area of the gravity low tended to support the inference of a subsurface cavity, but the cavity has not been located by drilling.

Shear wave detection. The detection of shear headwaves has been

the object of numerous investigations during the past two decades. The need for such a technique is obvious since, given the density, shear wave velocity, and compressional wave velocity of a rock or other elastic medium, we can immediately calculate the elastic moduli of the medium. Compressional wave velocities are relatively easy to measure, and it has been previously shown that porosities (and therefore bulk densities) can be deduced from compressional wave velocities.

Measurement of shear wave velocities is difficult because shear wave velocities are always lower than compressional wave velocities and therefore arrive at the same time as the wave train following the compressional headwave and subsequent compressional waves.

It was hoped that a satisfactory shear wave detection technique could be developed and incorporated into the engineering seismic experiment, but it was not until after the general nature of the engineering seismic instrumentation was defined that Whitcomb (1966 and in press) reported results of his investigations of the shear wave detection problem. He found that, for short distances from an ordinary explosive source, shear waves could be detected by angular accelerometers because of the rotational component in shear waves which is absent in compressional waves.

The shear wave detection technique developed by Whitcomb may be incorporated into later Apollo missions. Application of the technique on earth is limited by the high cost and imperfect response of currently available angular accelerometers.

SUMMARY

The engineering seismic system is planned as part of the Apollo program on the fourth manned landing on the moon. It will provide information on the thickness and porosity of the lunar soil and on the porosity and extent of fracturing of the underlying rock substrate.

Instrumentation is similar to that used on earth but with important modifications which yield a large dynamic range and improve transmission of seismic energy from the lunar energy source to the lunar soil.

Supporting research included investigation of the porosity–compressional wave velocity relationship, cavity detection, and shear wave detection. Results of these investigations will be used to inter-

pret data returned from the moon and to design future lunar instrumentation. The results of some of these investigations have been applied to some terrestrial engineering problems and have suggested novel solutions to other terrestrial engineering problems.

ACKNOWLEDGMENTS

The authors wish to acknowledge the contributions of colleagues at the U.S. Geological Survey Center for Astrogeology, Flagstaff, Arizona, especially L. H. Strom and D. L. Kieffer who assisted in the design of the instrumentation and carried out much of the supporting research. The Bendix Aerospace Division, Ann Arbor, Michigan, fabricated the flight model. The experiment and the supporting research were supported by NASA contracts T-57397-G and T-25091-G to the U.S. Geological Survey and NAS-9-6532 to Stanford University.

REFERENCES

DEBREMAECKER, J. C., GODSON, R. H., and WATKINS, J. S., "Attenuation Measurements in the Field," *Geophysics*, Vol. 31, 1966, pp. 526–569.

EATON, G. P., and WATKINS, J. S., "The Use of Seismic Refraction and Gravity Methods in Hydrological Investigations," *Can. Cent. Comm. Mining and Groundwater Geophysics*, in press.

GARDNER, G. H. F., WYLLIE, M. R. J., and DROSCHAK, D. M., "Effects of Pressure and Fluid Saturation and the Attenuation of Elastic Waves in Sands," *Journal of Petroleum Technology*, Vol. 16, 1964, pp. 189–198.

GODSON, R. H., WATKINS, J. S., and LONEY, R. A., "Velocities and Attenuation of Headwave Amplitudes Observed in Lunar Analog Rocks," *in* Investigation of in situ physical properties of surface and subsurface site materials, Engineering Geophysical Techniques Project Annual Report, Part F, 1965, 25 pp.

———, and WATKINS, J. S., "Seismic Resonance Investigation of a Near-Surface Cavity in Anchor Reservoir, Wyoming," *BAEG*, Vol. 5, 1968, pp. 27–36.

KOVACH, R. L., "Lunar Seismic Exploration," in Singer, S. F., ed., *Physics of the Moon*, American Astronautical Society of Science and Technology Service, Vol. 13, 1967, pp. 189–198.

MCALLISTER, B. D., KERR, JAMES, ZIMMER, JOHN, KOVACH, R. L., and WATKINS, J. S., "A Seismic Refraction System for Lunar Use," *Transactions of IEEE*, Vol. GE-7, 1969, pp. 164–171.

WATKINS, J. S., and SPIEKER, A. M., *Seismic Refraction Survey of Pleistocene Drainage Channels in the Lower Great Miami River Valley, Ohio*, U.S. Geological Survey Prof. Paper 605-B, in press.

WATKINS, J. S., 1969, "Lunar Velocity Profiles to 70 km," in preparation.

———, GODSON, R. H., and WATSON, K., *Seismic Detection of Near-Surface Cavities*, U.S. Geological Survey Prof. Paper 599–A, pp. A1–A12, 1967.

———, and WALTERS, L. A., "In Situ Compressional Wave Velocities in Porous Unsaturated Rock," in preparation.

———, and WHITCOMB, J. H., *Thumper Final Report, ALSEP Active Seismic Experiment*, U.S. Geological Survey Interagency Report, Astrogeology 4, 1968, 72 pp.

WHITCOMB, J. H., "Shear-wave Detection in Near-surface Seismic Refraction Studies," *Geophysics*, Vol. 31, 1966, pp. 981–983.

———, *Detection of SH-type Seismic Shear Waves Using Angular Accelerometers*, U.S. Geological Survey Prof. Paper 599–D, in press.

The Active Seismic Experiment

J. R. McDOWELL

Determining the existence or nonexistence of a lunar crust, the origins and internal structures of the lunar maria and the lunar highlands, and the origin of the lunar soil is fundamental to an understanding of the origin and evolution of the moon, the earth, and the terrestrial planets. As a step in this direction, a seismic refraction system has been developed for use on manned lunar landings to provide information concerning the lunar-subsurface geologic structure to depths of 75 to 500 feet. The system, known as the Active Seismic Experiment (ASE), is a part of the Apollo Lunar Surface Experiments Package (ALSEP); it has been deployed on Apollo 14 and is scheduled for deployment again on Apollo 16. The experiment involves the generation and monitoring of artificial seismic waves ranging in frequency from 3 to 250 hertz in the lunar surface and near-subsurface. The seismic waves are artificially produced by two different explosive devices and are detected by miniature seismometers or geophones. The data that result are telemetered to earth for study and interpretation.

INTRODUCTION

The scientific objective of the Active Seismic Experiment (ASE) is to determine the physical properties of lunar near-surface materials. Seismic energy is artificially produced by two different explosive devices, transmitted through the lunar surface materials, and detected by miniature seismometers (geophones); the resulting wave trains (in the 3- to 250-hertz range) are telemetered to earth for interpretation. The ASE is also used, for short periods of time, to monitor natural lunar seismic waves in the same frequency range. Penetration of seismic energy to varying depths (down to approximately 500 feet) is achieved, and wave velocities through several layers of near-surface materials are investigated, by varying the explosion-to-detector distance and the size of the explosive charge. The velocities of the compressional seismic waves, their frequency spectra, and their attenuations are all functions of the physical constants of the lunar near-surface rocks. Interpretation of these data permits rock type and character, as well as degree of induration and lunar-material bearing strength, to be inferred.

EXPERIMENT DESCRIPTION

During a lunar mission on which the Active Seismic Experiment is carried, the astronauts deploy a line of geophones at intervals of 10, 160, and 310 feet from the ALSEP Central Station. These three geophones are used to detect seismic waves induced in the lunar subsurface both while the astronauts are on the moon and after their departure.

In the first instance, the astronaut walks back along the deployed geophone line, using a "thumping" device to induce seismic energy into the lunar soil. The thumper contains 21 Apollo standard initiators (ASI's), which are fired by the astronaut at 15-foot intervals marked along the 300 feet of geophone cable. Since the thumper is used to stow and deploy the geophones and cabling, the assembly is referred to as the thumper/geophone assembly.

In the second instance, the seismic energy is produced by a launching device, capable of launching four rocket-propelled, explosive grenades to lunar ranges of 500, 1000, 3000, and 5000 feet. The grenades contain 0.1, 0.3, 0.6, and 1.0 pound of high explosive, respectively. The device, known as the mortar package assembly, is emplaced by the astronaut so that its firing line is aligned to be 180 degrees from the deployed geophone line. The grenades are launched by earth command after the departure of the astronauts, for a period of up to one year following lunar deployment.

If the distance between the geophones and the energy source is known, the velocity of the seismic waves can be determined by analysis of the time interval between the energy (explosion) instant and the detection of the seismic-wave arrivals. In the thumper mode, the range determination is based on a

---

The basic scientific requirements for the Active Seismic Experiment were developed under the direction of Principal Investigator R. L. Kovach (Department of Geophysics, Stanford University) and Co-Principal Investigator J. Watkins (Department of Geology, University of North Carolina).

THIS PAGE INTENTIONALLY

LEFT BLANK.

knowledge of the marked interval on the geophone cable at which the astronaut fires the ASI. The instant of ASI initiation is detected by a pressure switch and telemetered as a real-time event (RTE). In the grenade mode, the range determination is based on the parameters of a ballistic trajectory assumed to be ideal. The launch angle of the grenade is determined from measurements made of the pitch and roll angles of the mortar package prior to each launch. Initial velocity data are provided by range-line breakwire circuits, which are broken at the beginning and at the end of a 25-foot interval of line deployed at launch, the breaks being telemetered as real-time events. Time of flight is furnished by a transmitter in each grenade which is activated at launch and destroyed upon explosive impact; loss of the transmitter signal occurs at the instant of explosion and is also telemetered as a real-time event. Using these parameters (launch angle, velocity, and time of flight), grenade range can be determined to within ±5 percent. The time of thumper ASI initiation and the time of grenade detonation are known to within ±0.1 millisecond.

The seismic detectors are three identical geophones—electromagnetic transducers that translate high-frequency seismic energy into electric signals. The outputs of the three geophones are applied to separate logarithmic compression amplifiers to obtain maximum dynamic range and maximum sensitivity.

The Active Seismic Experiment uses seven commands transmitted from the Manned Space Flight Network to arm and fire the grenades and to effect geophone calibration. Other commands are used to effect power distribution to the ASE from the ALSEP data subsystem and to place the data subsystem in the active seismic mode. The three channels of seismic data generated by the ASE, along with 13 channels of engineering data, are converted to digital form within the experiment for transmission to earth. A 20-bit digital word format and a 10,600-bit-per-second data rate are used in the ASE to ensure accurate encoding and transmission of critical real-time-event data and to provide a relatively high frequency seismic-data-handling capability. The higher bit rate and the longer word length are incompatible with the normal ALSEP format and preclude the usual data collection from other experiments during the time the ASE is activated. Five significant measurements from the ALSEP electric power subsystem are included in the ASE telemetry format as engineering data. The experiment formats the seismic and engineering data and applies them to the data-subsystem modulator for modulation and downlink transmission.

EXPERIMENT DESIGN

The Active Seismic Experiment, the components of which are shown in Figure 1, is made up of three major subsystems: the thumper/geophone assembly, the mortar package assembly, and the Central Station electronics. The experiment weighs 34.66 pounds. Size and weight data for each of the subsystems are presented in Table I; system power requirements are listed in Table II.

Thumper/Geophone Assembly

The thumper/geophone assembly is constructed almost entirely of magnesium alloy and is so designed that it folds into three sections for stowage. It is electrically connected to the ALSEP Central Station by 318 feet of flat, four-conductor, H-film cable, which is stowed on a split spool on the upper end of the thumper handle and unwound by the astronaut during deployment. Also stowed on the thumper until deployment are the three geophones, the geophone cabling, and an aluminum-alloy geophone flag. The geophone cabling is wound on a reel at the lower end of the thumper. The geophones are mounted in individual stowage sockets in the reel assembly and held in by removable clips. The geophone flag is similarly stowed in a socket in the reel assembly and is deployed at the second geophone emplacement to aid the astronaut in the visual alignment of the geophones. The thumper is held horizontally during

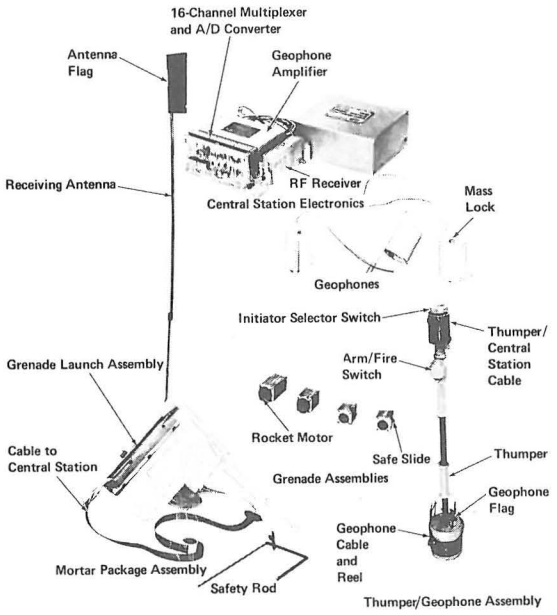

Figure 1 The Active Seismic Experiment

Table I Active Seismic Experiment Subsystem Parameters

Subsystem or Component	Parameter	Value
Thumper/Geophone Assembly	Length (folded)	14.5 inches
	Weight	7.59 pounds
• Thumper	Length (deployed)	44.5 inches
	Weight (including cables and initiators)	4.64 pounds
• Geophones	Height (including spike)	4.80 inches
	Diameter	1.66 inches
	Weight (three geophones with cables)	2.95 pounds
Mortar Package	Envelope Height	11.5 inches
	Envelope Width	6.0 inches
	Envelope Length	15.25 inches
	Weight	17.00 pounds
• Mortar Box Assembly	Height	11.5 inches
	Width	6.0 inches
	Length	15.25 inches
	Weight (including antenna and cables)	6.39 pounds
• Grenade Launch Assembly	Width	9.0 inches
	Length	13.7 inches
	Depth	6.23 inches
	Weight (including grenades)	10.88 pounds
• Grenades	Cross Section	2.7 inches
	Length	4-6 inches
	Weight[a]	8.08 pounds
Central-Electronics Assembly	Height	2.75 inches
	Width	6.18 inches
	Length	6.77 inches
	Weight	3.22 pounds
Mortar-Package Pallet Assembly	Width	24.0 inches
	Length	26.0 inches
	Weight	6.85 pounds

[a] Grenades 1, 2, 3, and 4 weigh 2.67, 2.19, 1.70, and 1.52 pounds, respectively.

Table II System Power Requirements

Type	Amount
Voltage	
ASE-Activated	+29, +15, −12, and +5 volts d.c.
ASE-Deactivated	+29 volts d.c.
Power	
Operational	8.0 watts (maximum)
	6.0 watts (nominal)
Thermal Control (standby)	3.00 watts

deployment, as shown in Figure 2, and rotating handles on the staff assembly allow both the power- and the geophone-cable reels to rotate freely for cable deployment.

The thumper contains 21 Apollo standard initiators (ASI's), rated at 1 ampere "no-fire" and 3 amperes "all-fire." The ASI, as a component, generates a pressure of approximately 650 pounds per square inch in a 10-cubic-centimeter volume. The initiators are threaded into a magnesium mounting plate, which forms a portion of the thumper base. The ASI's are individually fired directly into a forged-aluminum impact plate, which is spring-loaded

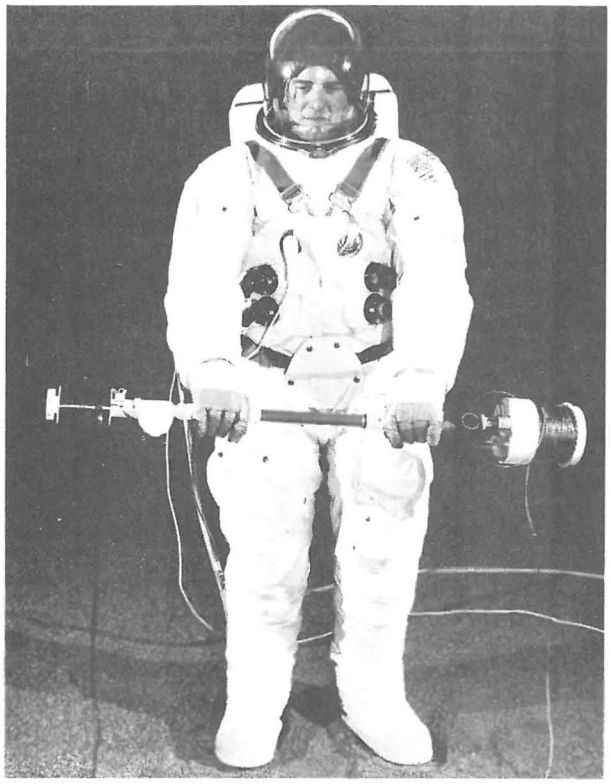

Figure 2 Deployment of Thumper/Geophone Assembly

against the mounting plate. As illustrated in Figure 3, the gas pressure resulting from an initiator discharge drives the impact plate sharply downward, imparting a thump to the adjacent lunar surface. The initiator-discharge gases are immediately vented around the edges of the impact plate and are deflected downward by a ring which is part of the mounting plate. A pressure switch, installed in the mounting plate, closes from the pressure generated from an initiator firing. The switch closure causes an RTE signal to be generated in the ASE central electronics, indicating the instant of explosion. The end of each ASI mounted in the mounting plate is covered with a coating of silicone rubber to protect the initiator from the pressure and debris from adjacent initiator

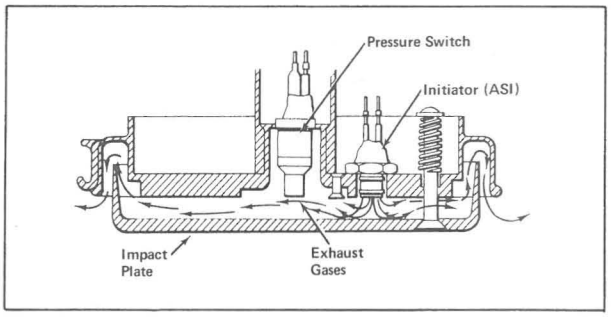

Figure 3 Operation of Thumper Base Section

firings, which might otherwise cause sympathetic deflagration. Extensive test firings have demonstrated the adequacy of this protection.

The thumper is so designed that all the initiators are internally shorted by the ASI rotary selector switch when the selector switch is in the zero position. In any other position (numbered 1 through 21), one ASI is connected to the firing circuitry and the other twenty remain shorted out. Simple rotation of the switch to a position other than zero will not in itself fire an ASI, even with power applied; a definite two-step firing operation with a time delay is required. After ASI selection by rotation of the selector switch to a numbered position, the thumper is armed by rotating the ARM/FIRE knob approximately 90 degrees and holding it at that position for a minimum of 4 seconds. This switch is then pushed in, applying a capacitor charge across the ASI and causing it to fire. The ARM/FIRE control is so designed that the firing switch cannot be actuated until the arming switch has been activated. If for any reason it should be necessary to stop the firing sequence after the thumper is armed, release of the ARM/FIRE control permits it to return to its normal unactivated position, and the arming capacitors are automatically discharged in a matter of milliseconds. In the normal position, the control provides a low impedance across the firing capacitors, both to prevent them from picking up a static charge and to discharge them if they are charged but have not fired through an ASI.

The thumper is shown in the firing position in Figure 4.

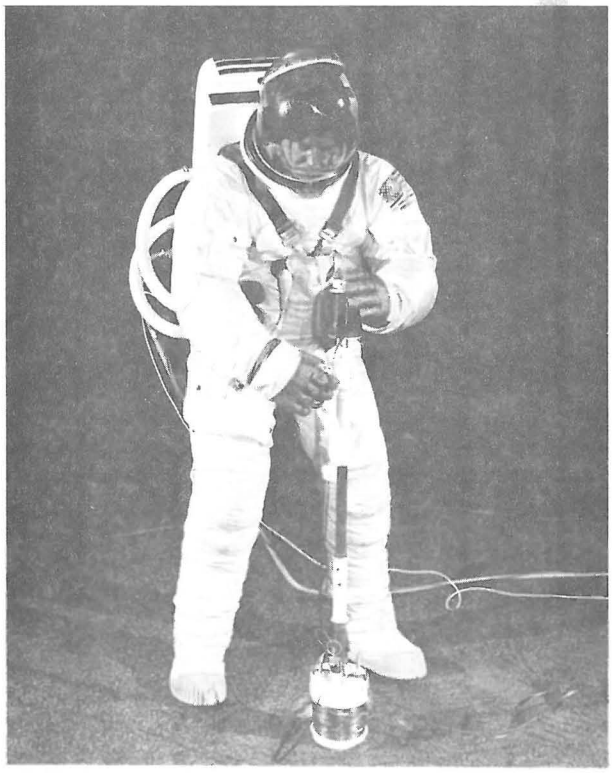

Figure 4 Thumper in Firing Position

Mortar Package Assembly (MPA)

The mortar package, shown in a deployed configuration in Figure 5, consists of a mortar box assembly and a grenade launch assembly (GLA). The mortar box is an L-shaped fiberglass box, with a magnesium frame and folding legs. The grenade launch assembly is made up of four fiberglass launch tubes, each containing a rocket-launched explosive grenade. The GLA is mounted in the mortar box. The mortar box contains the electronic circuitry for arming and firing the grenade rocket motors, along with a receiving antenna, two SAFE/ARM switches, and a thermal bag. The antenna, used in conjunction with the grenade transmitters, is mounted to the side of the mortar box and folded along the edge of the package during transport. A flag is mounted on the antenna top section to aid the astronaut during deployment. The two SAFE/ARM switches disable both the arming and the firing circuits and short out the rocket-motor firing capacitors and initiators for astronaut safety during lunar deployment. The forward end of the mortar box is beveled at 45 degrees,

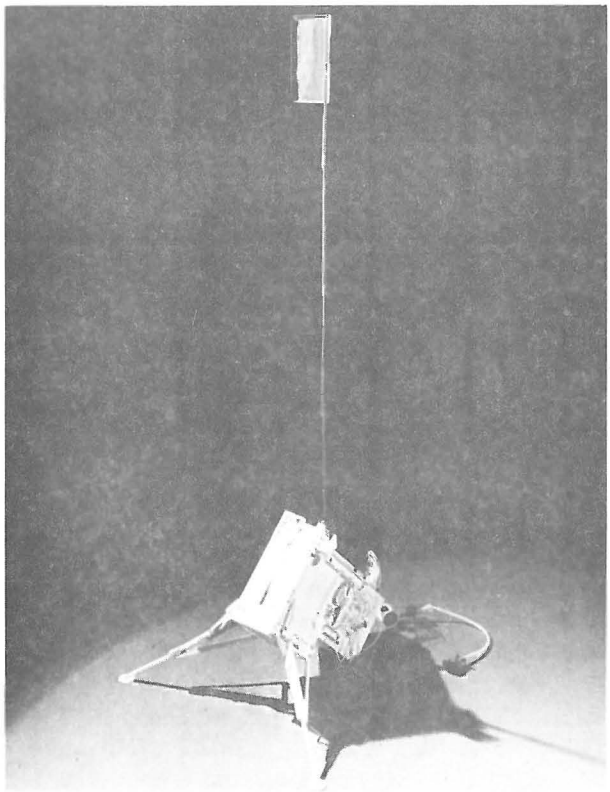

Figure 5 Deployed Mortar Package Assembly

and in the deployed position the MPA rests upon the 45-degree bevel. The remainder of the package is supported by two legs, which are stored along the side of the box during transport and folded down and locked into place during deployment. The mortar box is attached to an aluminum-skin pallet assembly in the final deployed configuration. The pallet has four 7-inch stakes mounted to its underside and, when placed on the lunar surface, provides a stable base for a 45-degree grenade launch.

The mortar package assembly is designed to survive on the lunar surface for a period of one year. A temperature ranging between -60°C during lunar night and +85°C during lunar day is maintained by a thermal control design incorporating thermal isolation and insulation as well as electronic heaters inside the mortar box. Isolation is provided by a multilayer aluminized-Mylar thermal bag, which is installed down inside the mortar box. The electronic heaters are mounted on the walls of this bag. Insulation is provided by a multilayer aluminized-Mylar fiberglass cover along the top of the mortar box. This cover remains in place throughout lunar storage until the first grenade is launched through it; it also serves as a radio-frequency-interference shield, completely enclosing the grenade launch assembly. The mortar-box firing circuits are designed with low-pass input filters, and all firing capacitors and initiators have resistors across them to reduce the effects of electrostatic charge. The fragile bottom of the thermal bag disintegrates when the grenades are launched. Two fiberglass blowout panels, each extending over two launch tubes, enclose the bottom of the mortar box and blow away upon grenade ignition.

GLA Configuration

The grenade launch assembly, pictured in Figure 6, is a fiberglass launch-tube assembly (LTA) consisting of four rocket-launched grenades, a grenade safety-pin assembly, three microswitches, three temperature sensors, and two vertical sensors. Each of the four launch tubes has a cross section of 3 inches. Two tubes are 9 inches long and the other two are 6.5 inches long. Around the outside of each tube is wound a range line, a thin stranded stainless steel cable, to which the grenade is attached. Two fine copper wires are looped around each range line, so spaced that the first breaks when the grenade is separated from the launch tube by about 16 inches and the second breaks when this distance is increased by exactly 25 feet. Loop-breaking starts and stops a range gate pulse, establishing a time interval for determination of grenade velocity.

Grenade construction is detailed in Figure 7. The four grenades are similar, differing only in the size of

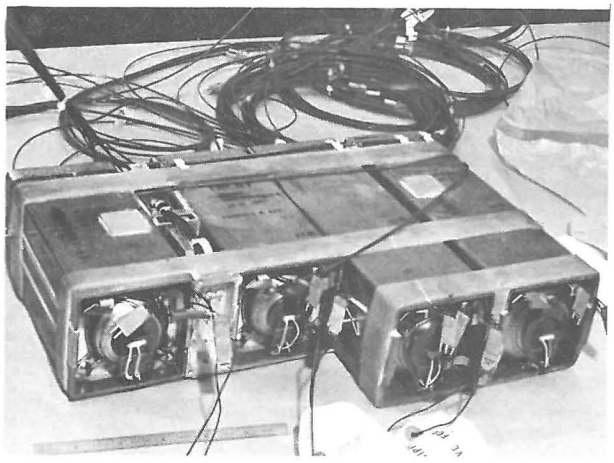

Figure 6 Grenade Launch Assembly

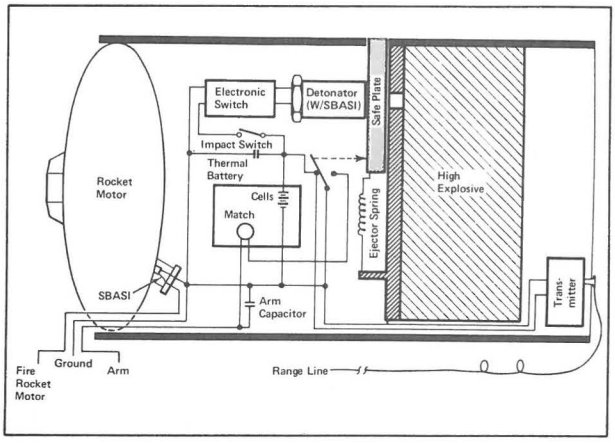

Figure 7 Grenade Construction

the motor and the amount of propellant and high explosive. Each has a thin fiberglass casing and a 2.7-inch-square cross section; they range in length from 4 to 6 inches. Inside the casing are the rocket motor, a safe-slide plate, a high-explosive charge, a detonating cartridge, an omnidirectional impact switch, a thermal battery, and a 30-megahertz transmitter. The range line is attached to the output terminal of the transmitter and serves as a half-wave end-feed antenna as it trails the grenade in flight.

The launch tubes for grenades 2, 3, and 4 each contain a microswitch that closes when the grenade is launched. Each switch connects the firing command from a sequential grenade-firing circuit to the next grenade to be launched.

Two temperature sensors are located between tubes 1 and 2 of the LTA; a third is located between tubes 3 and 4. One of the sensors provides an analog signal indicating GLA temperature to the data handling function of the Active Seismic Experiment. The other two sensors are part of the mortar-box heater control circuitry.

Two bubble-type electrolytic vertical sensors are mounted between tubes 3 and 4. These single-axis sensors indicate angular tilt (±12 degrees) in pitch and roll from the local vertical to provide grenade-launch-angle deviation from the 45-degree deployment angle. The vertical sensor is qualified for a 100-*g* shock resulting from grenade launch.

Grenade Launch

The mortar package is activated by ARM GRENADES and FIRE GRENADES commands from earth. The ARM GRENADES command is applied to and gated through the experiment central-electronics command gating to the grenade-arming circuit, which charges the regular and sequential firing capacitors in the mortar box and in each of the four grenades by applying a 24-volt arming signal. After arming, a FIRE GRENADE command for each of the grenades is applied to the command gating and gated to the appropriate firing circuit in the mortar box; this causes the firing capacitor to discharge and to ignite the grenade propellant through a single-bridgewire Apollo standard initiator (SBASI). As the grenade leaves the launch tube, the safe slide is spring-ejected; this permits a microswitch in the grenade to close, discharging the grenade-arming capacitor across a thermoelectric match and, in turn, activating the thermal battery. The thermal battery, when activated, provides internal grenade power for driving the transmitter and charging the detonator storage capacitors.

The first of the two range-line breakwires is broken upon grenade launch, initiating the range gate pulse to the real-time-event logic in the central electronics. Rocket propellant in the grenade is exhausted before the grenade exits the tube. The second range-line breakwire is broken when the grenade is 25 feet into trajectory; this terminates the range gate pulse to the real-time-event logic and provides time/distance data for subsequent determination of grenade velocity. The grenade transmitter, activated at launch and utilizing the grenade range-line as an antenna, transmits until it is destroyed upon grenade impact. The omnidirectional impact switch in the grenade allows the detonator capacitor to discharge, firing a detonator to set off the grenade high explosive upon impact. The 30-megahertz signal from the transmitter is received by the antenna mounted on the mortar box and is conducted by coaxial cable to the receiver in the Central Station electronics. The received signal is applied, through a level detector, to the real-time-event logic for application to the data handling function. The grenade transmitter signal provides an indication of time of flight and instant of detonation, and thus a second calculation of range, enhancing the confidence factor for the range calculation that is based on launch-angle and grenade-velocity data generated from the vertical sensors and the range-line breakwires.

Grenade 2 (3000 feet) is fired first, followed sequentially by grenade 4 (500 feet), grenade 3 (1000 feet), and grenade 1 (5000 feet). This firing order results in optimum mortar-package firing stability. A redundant arming and firing circuit is provided for sequential firing in the event of failure of one or all of the regular firing circuits. This so-called sequential circuit is armed by the normal ARM GRENADES command. A series of interlocking microswitches connect the sequential firing circuit to the next grenade-firing circuits as the grenades are launched.

Grenade Design Features

The safe slide in each grenade constitutes a mechanical block between the detonator and the explosive block. It is held in place while the grenade is in the launch tube and is spring-ejected at launch. While it is in place, inadvertent detonator ignition will not set off the high-explosive charge. The safe slide also keeps a microswitch so positioned as to isolate the thermal battery output from the high-explosive firing circuitry, and provides a low impedance to the firing capacitors to prevent their being charged by a static charge.

The thermal battery in each grenade contains a thermoelectric match, which has a no-fire rating of 0.75 ampere for 10 milliseconds and an all-fire rating of 2.0 amperes for 10 milliseconds. The hermetically sealed battery output is rated at a nominal 15 volts (a 13-volt minimum for 1-second activation to a maximum of 19 volts) and is capable of providing 100 milliamperes for 1 minute (minimum).

The grenade transmitter has a ruggedized, subminiature, encapsulated cordwood construction. It operates at a continuous-wave frequency of 30 megahertz ±100 kilohertz, with a power output of 200 milliwatts for a minimum of 1 minute. Both the transmitter and the thermal battery are designed to survive a grenade-launch shock of 2465 *g*'s and are qualified at 3200 *g*'s.

The grenade high-explosive charge is plastic-bonded hexanitrostilbene (HNS).* The selection of HNS for use in the Active Seismic Experiment was made on the basis of vacuum stability, thermal stability, friction sensitivity, impact (shock) sensitivity, shelf life, and radiation sensitivity. The material does not decompose in a vacuum, prolonged exposure resulting in a weight loss of less than 0.06 percent, and this due primarily to evaporation of residual solvents. From a

*Developed by the Naval Ordnance Laboratory, White Oak, Maryland.

thermal standpoint, HNS is an excellent explosive material. It does not begin to melt until exposed to temperatures well above 500°F for prolonged periods, making it extremely safe to handle in any normal temperature environment. It is in no way sensitive to friction, and as a raw material it is very insensitive to impact shock. It has been dropped from great heights onto solid concrete without detonating; its impact sensitivity as measured in Military Standard Laboratory tests is well above the minimum military standard of 60 centimeters. With respect to shelf life, military tests predict a decomposition of only 1 percent over a 500-year period at 212°F. Radiation sensitivity tests indicate that HNS is in no way sensitive to radiation. From these criteria, it was concluded that HNS could be handled, tested, flown on a spacecraft, and deployed by astronauts with relative safety. For the Active Seismic Experiment, raw HNS is blended with Teflon to yield a 90-percent-HNS/10-percent-Teflon composition. The blend is pressed into a plastic block under pressures of approximately 30,000 pounds per square inch, and the block is then machined into the flight configuration seen in the X ray of a completed grenade launch assembly shown in Figure 8.

Grenade design also features a fast-ignition motor, with an extremely short thrust duration (6 to 10.5 milliseconds) and a stable launch platform. Stability is attained by utilizing recoilless launch techniques, with open-end launch tubes operating on the rocket-motor action/reaction principle for grenade launch. During the development phase of the Active Seismic Experiment, a trade-off study was conducted and tests were performed to compare the feasibility of open-tube rocket-launched grenades with that of a closed-tube mortar approach. Mortar launch offered the advantage of good reproducibility, provided that a lightweight, stable platform could be achieved; moreover, all the propellant would burn while the grenade was still in the closed tube. However, the high reaction load imparted to the launch platform presented a problem in that it necessitated a mechanically strong and predictably heavy design. The logical alternative to the mortar approach was to attach a motor to the grenade to form a miniature rocket and use an open launch tube. The motor developed has so short a burn time that it is burned out completely by the time the grenade travels the length of the 6.5-inch or 9-inch tube. Since there is little reaction load on the launcher, the design is suitably lightweight. There are two basic motor sizes, with different propellant loadings to achieve the different burn times. Nozzle sizes of 0.5 and 0.8 inch are used for the two motors to yield the required thrust levels, the nozzle being an orifice rather than a conventional nozzle. A further requirement imposed on the motor is that it be hermetically sealed but ignite reliably even if the seal should be lost during the year of lunar storage. The motors are therefore individually sealed with a 0.003-inch stainless steel diaphragm stitch-welded across the nozzle; the diaphragm blows out upon ignition. The initiators are also welded in.

The solid propellant used* was selected for its burn rate, temperature stability, friction sensitivity, impact sensitivity, and vacuum stability. An extruded cylinder of the magnesium/Teflon-composition propellant 0.205 inch in diameter is sliced into wafers 0.013 to 0.018 inch thick, as dictated by thrust/time curve requirements. The wafers are retained behind a conical screen welded inside the motor assembly, in numbers varying from 570 to 2365. Two views of the rocket motor assembly and a cutaway showing the conical screen are seen in Figure 9. The motors are elliptical in shape, being formed by 2:1 elliptical

*A classified (NOTS PL6670) military propellant.

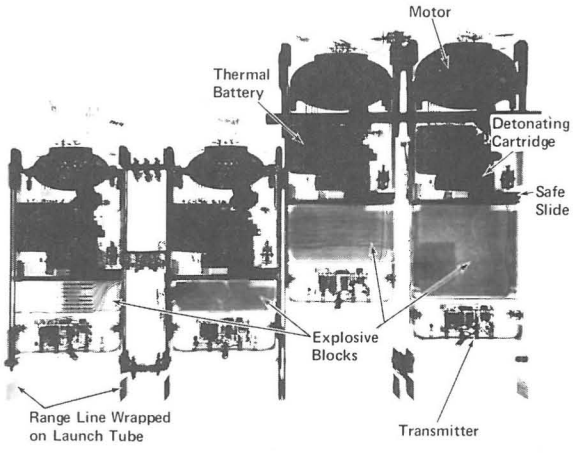

Figure 8 X Ray of Flight-Configuration Grenade Launch Assembly

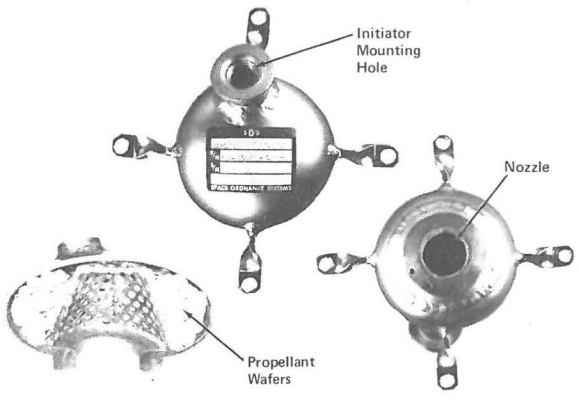

Figure 9 Grenade Rocket Motor

Parameter	Grenade			
	1	2	3	4
Range (ft)	5000	3000	1000	500
Weight (gm)	1261	1024	775	695
High-Explosive Charge Weight (lb)	1.0	0.60	0.30	0.10
Rocket-Motor Mean Peak Thrust (lb)	5000	2500	1700	1250
Mean Velocity (ft/sec)	163	126	73	52
Lunar Flight Time (sec)	44	32	19	13
Rocket-Motor Propellant Weight (gm)	42	27	15	10
Number of Propellant Pellets	2365	1520	620	570
Launch Angle	45°	45°	45°	45°
Rocket-Motor Thrust Duration (msec)	6.0	7.5	10.5	8.5

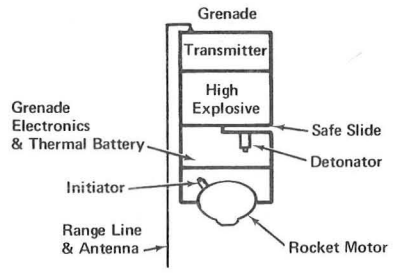

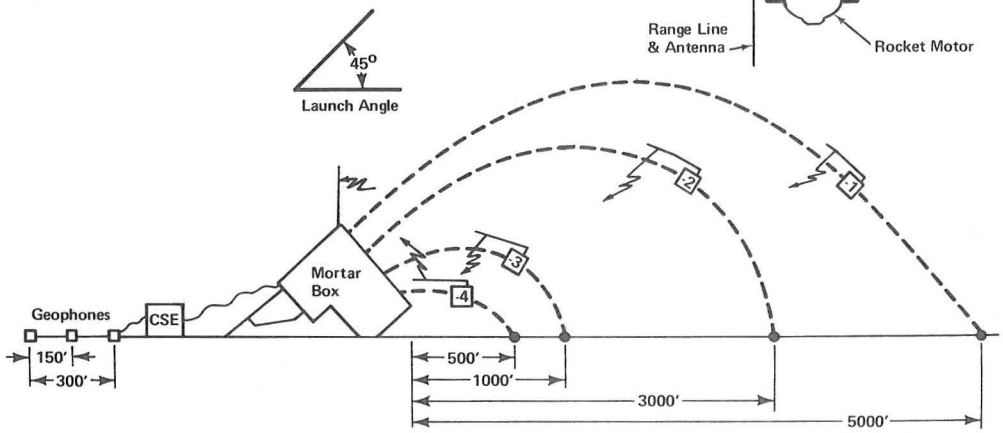

Figure 10 Grenade Design and Performance Parameters

domes of 4130 chrome/molybdenum steel, heat-treated to a minimum yield strength, welded together, of 180,000 to 200,000 pounds per square inch.

Grenade design and performance parameters are summarized in Figure 10.

Central Station Electronics (CSE)

The ASE central-electronics subsystem, shown in Figure 11, is hard-mounted to the ALSEP Central Station thermal plate and electrically and thermally controlled by that station. The subsystem contains power protection circuitry, temperature sensors, calibration, timing, and control-logic circuitry, and data handling and processing capability. Included as subassemblies are the 16-channel multiplexer and analog-to-digital converter, the ASE receiver, and the geophone amplifier.

The power protection circuitry contains current-sensitive relays that prevent overvoltage from damaging the ASE subsystems. It also prevents an ASE subsystem from overloading the ALSEP power distribution unit in the event of a malfunction. The circuitry is assembled on a printed-circuit board (power protection module). The circuits are designed to trip at an overload equal to 200 percent of the normal operating load. Operating and standby (survival) power is supplied to the Active Seismic Experiment from the ALSEP power distribution unit at +5, +15, -12, and +29 volts d.c.

Two temperature sensors, mounted on the discrete-component board, provide central-electronics temperature data in the ON and SURVIVAL modes. The discrete-component board also includes arming and firing circuitry and calibration voltage circuitry. The calibration circuits perform two functions: They

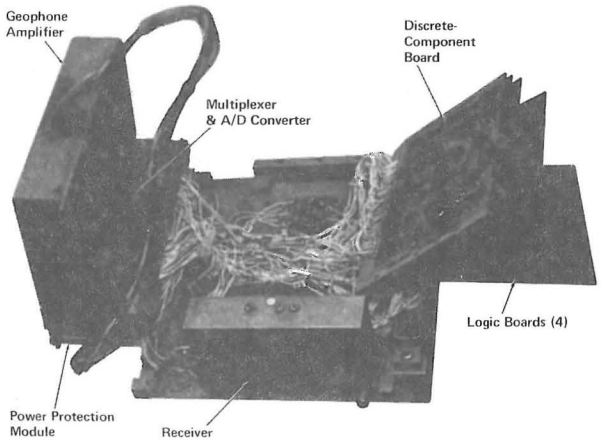

Figure 11 Active Seismic Experiment Central Electronics

provide a two-point calibration to the multiplexer and analog-to-digital converter, and, actuated by earth command, they provide a calibration signal to the geophones for lunar test and calibration comparison.

The timing and control circuitry is basically digital logic, which operates the Active Seismic Experiment using a 10.6-kilohertz clock signal in conjunction with seven commands from earth. The data rate of the ASE logic is 10.6K bits per second. The basic timing is obtained from the 10.6-kilohertz square wave received from the ALSEP data processor. The shift-register multiplexing logic selects the data to be loaded into the shift register through the analog-to-digital-converter frame, holding, and control gates. A START pulse is applied to the multiplexer and analog-to-digital converter from the decoder of the timing and control function. When a real-time event (RTE) occurs (as in the case of thumper firing, range-line-velocity START and STOP breakwires, or loss of transmitter signal upon grenade explosion), the RTE logic, in conjunction with the sequence counters and holding register, provides a MARK EVENT signal to indicate the event occurrence in the prior telemetry frame. The word and bit in which the event occurred are also identified.

Data handling and processing are accomplished by the application of 16 analog-voltage channels to the ASE multiplexer and analog-to-digital converter. Three analog channels are used for geophone outputs, two for mortar-box launch angle outputs, three for calibration, three for ASE temperature and power measurements, and the other five for ALSEP electric-power-subsystem temperature and power measurements. The analog signals are multiplexed, converted to digital signals, and formated for shifting to the ALSEP central data subsystem and downlink transmission.

Subword, word, and frame signals are derived from the sequence counters through the decoder of the timing and control function. The ASE data format is made up of 32 20-bit words per frame, each word consisting of four 5-bit subwords. Geophones 2 and 3 are sampled and read out in every word of the frame; geophone 1 is sampled and read out in all but the first word. In the first word, geophone 1 is sampled and stored, then read out in the first subword of the second word. The first two subwords of word 1 comprise a 10-bit frame-synchronizing signal. The first three bits of subword 1 of word 32 provide a mode-identification signal. The binary signals from the multiplexer converter are applied to the shift-register multiplexer gates, which are controlled by the shift-register multiplexing logic. A storage buffer is provided between the converter multiplexer and the shift-register multiplexer gates. The ASE data are shifted out in the 32-word telemetry-frame format to the biphase modulator of the ALSEP data subsystem for modulation and downlink transmission.

The ASE receiver is a subminiature, low-power r.f. receiver, capable of receiving a continuous-wave signal transmitted from the in-flight grenade transmitter. The receiver is located in the central-electronics package and is connected by coaxial cable to its antenna, which is mounted on the mortar box. The functions of the receiver are to acquire, track, and amplify the continuous-wave transmitter signal and to provide an output to the central electronics to indicate signal acquisition or loss. The receiver has a center frequency of 30 megahertz, with a minimum acquisition and tracking bandwidth of ±100 kilohertz.

The geophone amplifier assembly is a subassembly of the central-electronics subsystem. The amplifier, together with the geophones and cabling carried on the thumper, form what is known as the active seismic detection system (ASDS). Since the ASDS was designed, developed, and tested as a subsystem, it is described separately in the section that follows.

Active Seismic Detection System (ASDS)

The active seismic detection system is designed to monitor seismic waves in the frequency range between 3 and 250 hertz. Three electromagnetic geophones, three logarithmic-compression amplifiers, and the interconnecting cabling constitute its major elements. The geophones can be excited mechanically by natural or artificial seismic waves or electrically by a GEOPHONE CALIBRATE command. Sensing induced or natural seismic activity which creates motion in the lunar surface, each geophone generates an electric (a.c.) signal that is proportional to the amplitude and frequency of the ground motion. This signal is supplied to the geophone amplifier assembly in the central electronics, where it is first amplified by a linear amplifier. It is then filtered to eliminate frequencies of more than twice the sampling rate and to flatten the frequency response in the passband of 3 to 250 hertz by enhancing signals with frequencies below the geophone natural frequency. After filtering, the signal is logarithmically compressed by one of two identical logarithmic compressor circuits in each geophone-channel log compressor; two such compressor circuits are required – the one to process positive and the other negative signals – because the geophone signals are bipolar and logarithmic compression is a function of the instantaneous amplitude. The log-compressed signal is connected to a multiplexer gate, which is controlled by the ASE format-generator logic to properly time-sample the data.

Because ASDS response may change in the course of 1-year lunar operation and storage, a pulse-type calibration is included with the amplifiers to provide a relative-calibration function. This function is activated by applying a GEOPHONE CALIBRATE command to the ASE command gating. The command is gated to the calibration circuitry when a pulse 1 second in width is generated and applied to the ASDS calibrate driver, electrically exciting the geophones. Geophone excitation permits measurement of geophone resonant frequency, generator constant, and damping coefficient relative to the preflight calibration. A temperature sensor mounted in geophone 1 (that closest to the Central Station) provides temperature data whenever the ASE is not activated.

Geophone Design

The geophones developed for lunar use are of the moving-coil/magnet type. The coil is the inertial mass, suspended by springs in the magnetic field. Above the resonant frequency of such a device, its output is proportional to ground velocity; below its resonant or natural frequency, the output drops off at the rate of 12 decibels per octave.

Previously existing commercial geophone designs were evaluated but found to be unsuitable for lunar use. Spring parameters had to be changed to be compatible with lunar gravity. Moreover, it was apparent that significant increases in sensitivity could be achieved with simultaneous reductions in weight and size if better magnet materials and more efficient coil windings were used. Design changes were also suggested by such considerations as the methods available to the astronaut for implanting the device and the need to protect the springs from the vibration and shock levels encountered during testing and transit. The final design saw a significant increase in available signal power with some savings in size and weight, as well as the satisfaction of such other design objectives as the matching of the coil resistance to the optimum amplifier source impedance.

The design goal for overall ASDS response was that it be flat to ground velocity down to 3 hertz. The minimum resonant frequency for reliable operation of geophones of small size and weight can be expected to be somewhat higher than 3 hertz, particularly with the springs used for operation at lunar gravity. Preemphasis in the succeeding electronics was used to provide the desired response at frequencies below geophone resonance frequencies.

For state-of-the-art junction transistors in appropriate configurations, the power spectral density of the equivalent input noise is very nearly constant down to about 20 hertz. Below this frequency it increases with a slope of $1/f$. Preemphasis at frequencies lower than the resonance frequency thus amplifies the $1/f$ noise, decreasing the signal-to-noise ratio for signals at higher frequencies. This effect constitutes a strong incentive to select as the natural frequency of the geophone the lowest possible frequency consistent with small size and weight and adequate mechanical ruggedness. These constraints led to the choice of 7.5 hertz as the natural frequency for the lunar geophone.

Figure 12 is a cutaway view of the assembled geophone, showing the position of the coil in the magnetic flux path. The internal assembly is supported within the outer case by parts machined from Epon® 828 for thermal and mechanical stability. When the mass-lock button at the top of the case is held in the depressed position, three nickel/silver fingers extending inside the inner case assembly (the magnet cup) hold the coil firmly against the lower stops. This mass lock ensures that the unit can survive the shock and vibration encountered in environmental testing and transit to the moon. The spring-loaded mass-lock buttons are released automatically when the geophones are removed from the thumper and deployed by the astronauts.

®Epon is the registered trademark of Shell Chemical Corporation for a family of resins.

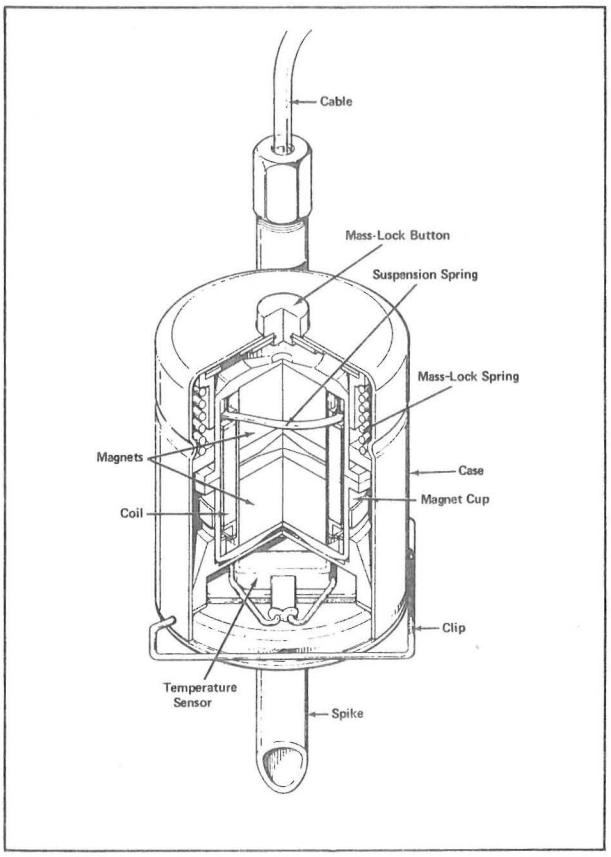

Figure 12 Cutaway View of Assembled Geophone

The coil is wet-wound, using Epon 828 on a mandrel between end pieces also cast from Epon 828, with nickel/silver-threaded inserts, encapsulated in them; 13,600 turns of No. 43-type ML copper magnet wire are used. The screws that secure the springs to the coil, and the springs themselves, serve as conductors from the coil. The two halves of the magnet cup are identical and include magnet pole pieces and pole caps, as shown in the figure. Fabricated of Alnico 9, they are so charged that the fields in the two halves oppose one another, creating a closed flux path for each half of the cup. The average flux in the gap for each half ranges from 19,000 to 20,000 maxwells. The sensitivity and frequency-response characteristics of the resulting geophone are excellent. An open-circuit generator constant of about 235 volts per meter per second is achieved, using a coil resistance of 6200 ohms; open-circuit damping is about 5 percent of critical. By way of comparison, a standard 4.5-hertz geophone* has a generator constant of about 24 volts per meter per second, with a coil resistance of 215 ohms and open-circuit damping of about 23 percent of critical. Adjusting for differing coil resistances and ignoring differences in open-circuit damping, the available signal power from the lunar geophone is about three times that from a commercial geophone. The magnetic cup assembly of the commercial unit is 1.88 inches high and 1.62 inches in diameter and weighs about 9.5 ounces. The lunar geophone is 1.25 inches high and 1.095 inches in diameter and weighs 4.16 ounces. Complete with outer case, the unit weighs 6.25 ounces.

Geophone Testing

Testing of the lunar geophone on earth presents a problem because the inertial mass rests on the lower stops in the earth's gravitational field. To overcome this problem, a device was developed which introduces into the coil of the geophone just enough direct current to offset about five-sixths of the weight of the inertial mass at earth gravity. The necessary current was accurately calculated for each geophone on the basis of its measured generator constant and was nominally 0.74 milliampere. High-voltage batteries and a large dropping resistance were used to obtain a quiet current source. Large capacitors were inserted in the amplifier input to block any d.c. flow from the amplifier.

Verification of geophone linearity at the very low signal amplitudes expected presents another problem. The system sensitivity is such as to provide clearly discernible signals in response to ground motions of 1 millimicron zero-to-peak at 10 hertz. Testing at these levels, which are lower than normal background seismic-noise levels on earth, requires the use of a quiet site and an isolation drive system to excite the geophones.

Low-level tests** were performed in a 50-foot-deep cased hole. The operating mechanism from a vertical seismometer† with a natural frequency of 0.8 hertz was used as the isolation drive unit. A signal generator was the driving source, and signal levels required for a given displacement were calculated, using the calibrated generator constant of the large seismometer. The three geophones were mounted directly to the 18-kilogram mass of the seismometer, and lunar gravity was simulated using the quiet current source previously described. Testing very late at night, good data were obtained down to displacements of 1 millimicron peak-to-peak at 10 hertz. There were no measurable deviations from linearity at these low amplitudes.

Cable Assembly

The geophone cable assembly consists of four twisted-pair, shielded polyimide-insulated cables. Three of the pairs connect the three geophones to their respective amplifier inputs; the fourth connects a temperature sensor in the near geophone to the proper data circuitry. The three geophones are spaced at 150-foot intervals on the cable, automatically providing the proper separation upon deployment by the astronaut. White markers on the cable indicate the thumper firing points.

Amplifier Design

A three-channel amplifier conditions the geophone signals prior to their conversion into digital format. Since the seismic thumper device is used for short-range shots (of the order of feet), seismic signals containing energy at frequencies of 100 hertz and higher can be generated. A system time resolution of ±1 millisecond was selected. This dictated a minimum sampling frequency of 500 hertz, which, in turn, specifies the filter response at high frequencies necessary to minimize data contamination from sideband folding. The low signal-to-noise ratio expected from the distant grenade explosions and uncertainty as to the character of the waveforms to be generated made it desirable to widen the frequency response as much as possible within the aforementioned constraint. The

*Hall-Sears model HS-1.

**For greater detail, see "The Active Seismic Detection System Final Report," Geotech Technical Report No. 69-44, Garland, Texas, 7 August 1969.

†The Johnson-Matheson vertical seismometer.

overall frequency response for the active seismic detection system is shown in Figure 13.

The wide dynamic range of the expected signals, the overall timing resolution desired, and telemetry bit-rate constraints suggested the desirability of some form of data compression prior to transmission to earth. The dynamic range of the linear system is nominally 80 decibels. The maximum bit rate available to the Active Seismic Experiment is 10.6K bits per second. With a minimum sampling frequency of 500 hertz, uniform sampling in time, and three channels of seismic data required, a maximum of only 5 bits per geophone-data subword would be available. In a linear digitization system, this would lead to unacceptably poor resolution at the very low signal levels expected from the distant grenade shots. Since signal levels are likely to be distributed throughout the dynamic range of the system, the compression scheme of choice was one that would give signal resolution as some constant fraction of signal amplitude. Logarithmic compression was selected because this is its principal characteristic.

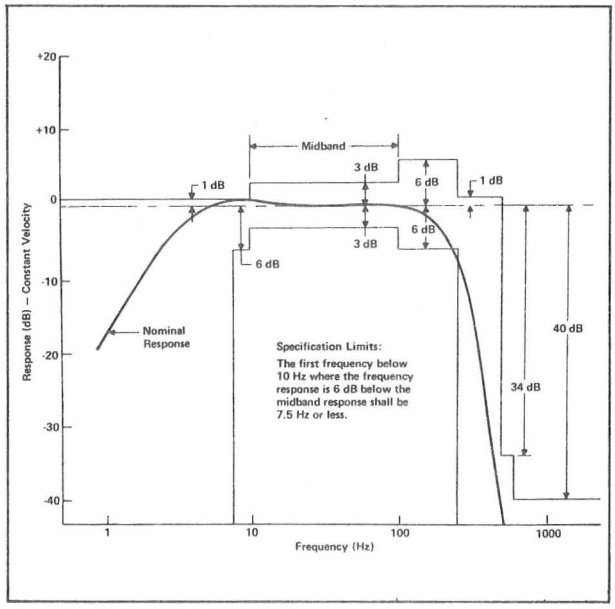

Figure 13 Active Seismic Detection System Nominal Frequency Response

THIS PAGE INTENTIONALLY LEFT BLANK.

Reprinted from
6 November 1970, Volume 170, pp. 620-626

SCIENCE

Seismic Data from Man-Made Impacts on the Moon

G. Latham, M. Ewing, J. Dorman, F. Press, N. Toksoz, G. Sutton, Rolf Meissner, F. Duennebier, Y. Nakamura, R. Kovach and M. Yates

Seismic Data from Man-Made Impacts on the Moon

Abstract. *Unusually long reverberations were recorded from two lunar impacts by a seismic station installed on the lunar surface by the Apollo 12 astronauts. Seismic data from these impacts suggest that the lunar mare in the region of the Apollo 12 landing site consists of material with very low seismic velocities near the surface, with velocity increasing with depth to 5 to 6 kilometers per second (for compressional waves) at a depth of 20 kilometers. Absorption of seismic waves in this structure is extremely low relative to typical continental crustal materials on earth. It is unlikely that a major boundary similar to the crust-mantle interface on earth exists in the outer 20 kilometers of the moon. A combination of dispersion and scattering of surface waves probably explains the lunar seismic reverberation. Scattering of these waves implies the presence of heterogeneity within the outer zone of the mare on a scale of from several hundred meters (or less) to several kilometers. Seismic signals from 160 events of natural origin have been recorded during the first 7 months of operation of the Apollo 12 seismic station. At least 26 of the natural events are small moonquakes. Many of the natural events are thought to be meteoroid impacts.*

Impacts on the lunar surface of the Apollo 12 Lunar Module (LM) ascent stage and the third stage of the Apollo 13 Saturn booster (S-IVB) generated seismic signals that were recorded by the seismometers installed on the moon by the Apollo 12 astronauts on 19 November 1969. The seismometers are part of the emplaced science station called ALSEP (Apollo Lunar Surface Experiments Package). [For details of the lunar seismic experiment, see (*1*).] Approximately 160 events of natural origin have been recorded by the seismometers during the first 7 months of operation. However, few criteria have emerged for estimating the time or location of these natural events from the study of their seismograms. Hence, the man-made impacts, whose time and location are well known from the National Aeronautics and Space Administration's tracking information, have emerged as extremely important tools for the seismic exploration of the moon. It is expected that NASA will include impacts of both the LM and the spent S-IVB stage of the Apollo booster on all future Apollo missions.

At least 26 of the natural lunar seismic events are believed to be shallow moonquakes. All of these events occur within 3 days of the time when the moon comes closest to the earth (perigee) during its monthly orbital cycle. At least one quake has been detected at each perigee crossing. Tidal strains, produced within the moon by the gravitational interaction between the earth and the moon, reach maximum values at perigee. Thus, tidal strains, which are much larger in the moon than in the earth, appear to be an important factor in the release of seismic energy in the outer shell of the moon.

All the moonquakes are small. The magnitude of the largest events is between 1 and 2 on the Richter scale. The magnitude of the lunar signals is obtained through Richter's empirical relationship between energy and magnitude. An earthquake of this magnitude would normally be barely perceptible even by persons in the immediate vicinity of the epicenter. The rate of lunar seismic energy release implied by these data is very low compared with the rate of seismic energy release in the earth. If the moon were as active as the earth and if the seismic sources were uniformly distributed throughout the outer shell of the moon, between 10 and 100 quakes with energy release equal to or greater than that of the S-IVB impact would have been recorded during the 7 months of operation considered in this report. No quakes of this magnitude have been recorded thus far. However, neither the recording period nor the area covered by lunar seismic stations is sufficient to permit generalizations on this point. Zones of high seismicity may be localized in regions far from the Apollo 12 station. Despite these qualifications, it is almost certain that the concept of plate tectonics as it applies to the earth, with large-scale deformation of the crust of the earth to form folded mountains and great trenches, does not apply to the moon at this point in its evolution. Nor do we see visual evidence of such tectonic activity in the past from study of the surface features of the moon. The outer shell of the moon appears to be very old and quite stable except for the disruptive influences of tidal stresses. Some of the natural events are believed to be produced by meteoroid impacts, which can usually be distinguished from the moonquake signals by their higher frequency content and their relatively peaked spectra. When Hawkins' (*2*) flux estimate is used, the rate of occurrence of the impact events is in approximate agreement with the number of meteoroids in the kilogram mass range that are expected to collide with the lunar surface within a radius of a few hundred kilometers from the seismic station. The study of these signals will eventually provide a quantitative estimate of the numbers and masses of meteoroids in space in the kilogram mass range and more detailed information on the internal structure of the moon.

Table 1. Expended LM ascent stage and S-IVB impact parameters. The Apollo 12 seismic station is located at 3°03′S, 23°25′W.

Parameter	LM	S-IVB
Time of impact (G.M.T.)	$22^h17^m16.4^s$	$01^h09^m39.0^s \pm 0.2^s$
Mass (kg)	2,383	13,925
Impact velocity (km/sec)	1.68	2.58
Kinetic energy of impact (ergs)	$3.36(10)^{16}$	$4.63(10)^{17}$
Equivalent energy of impact (lb of TNT)	$1.77(10)^3$	$2.44(10)^4$
Angle of impact from horizontal	3.7°	76.4°
Distance between point of impact and seismic station (km)	73	135
Azimuth from seismic station	112°	274°
Latitude	3°57′S	2°45′S
Longitude	21°12′W	27°52′W

The locations of the Apollo 12 seismic station and the impact points are shown in Fig. 1. Pertinent impact and seismometer parameters are listed in Table 1. The LM struck the lunar surface 73 km from ALSEP at a velocity of 1.68 km/sec and at an angle to the lunar surface of only 3.7°; it was moving toward ALSEP at the time of impact. The S-IVB struck the surface at nearly normal incidence, 135 km from ALSEP, with a velocity of 2.58 km/sec, headed toward the northeast.

The region of the impacts is located in the southeastern edge of Oceanus Procellarum. The relatively smooth area, particularly between the LM impact point and ALSEP, is believed to be covered by igneous rock, which flooded the region early in the moon's history. Several separate episodes of flooding may have occurred. The rough terrain between the S-IVB impact point and ALSEP presumably consists of older lunar material, which extends up through the lava fill. The nature of the older material is unknown. It may be primitive lunar material that accreted during the final stage of lunar evolution; it may be material thrown out from large craters; or it may be igneous rock formed during an early stage of melting. On the basis of the apparent flooding of older craters, we estimate the overlying mare material to be approximately 1 to 2 km thick between the LM impact point and the seismic station and to be variable in thickness from 0 to 2 km between the S-IVB impact point and the station; however, these estimates are subject to considerable uncertainty (*3*).

The impact signals are shown on a compressed time scale in Fig. 2, along with the signals from the two largest events of natural origin recorded thus far. The signal from a missile impact recorded at White Sands, New Mexico, by Latham *et al.* (*4*) is also shown for comparison. All the lunar signals are clearly similar in character but, as a class, are quite different from the White Sands missile impact signals. The following remarks can be made concerning the general characteristics of the lunar signals.

1) The lunar signals have extremely long duration. The LM impact signal was detectable for about 1 hour, and the S-IVB impact signal was detectable for more than 4 hours. A missile impact signal on earth would last only a few minutes at an equivalent distance. The lunar signals build up gradually to a maximum and then decay very gradually. The LM impact signal reaches its maximum intensity approximately 7 minutes after its beginning, and the S-IVB impact signal reaches its maximum value after approximately 12 minutes. The smoothed envelopes of the signals reach maximum peak-to-peak ground displacement amplitudes of 9.5 and 75 nm for the LM and S-IVB, respectively.

Table 2. Travel times and velocities for seismic waves recorded from LM and S-IVB impacts.

Impacts	Wave type	Travel time (sec)	Velocity (km/sec)
LM	*P*	$23.5^{+2.1}_{-3.7}$	3.1 (2.9–3.7)
	S	40.4	1.8
S-IVB	*P*	29.1	4.64
	PP	34.8	3.88
	S	54.0	2.50

2) The earth missile impact signal contains distinct phases corresponding to the arrival of various types of seismic waves. Such phases are less distinct in the lunar signals.

3) Spectra of the impact signals (shown in Fig. 3) are relatively broad for samples taken near the beginnings of the wave trains. For the S-IVB signals, the spectra of samples taken at later times in the wave trains show a gradual decrease of energy in the high-frequency end of the spectrum, owing, presumably, to the greater absorption of high-frequency seismic energy. The gradual loss of high-frequency energy tends to narrow the spectra, thus emphasizing a single dominant spectral

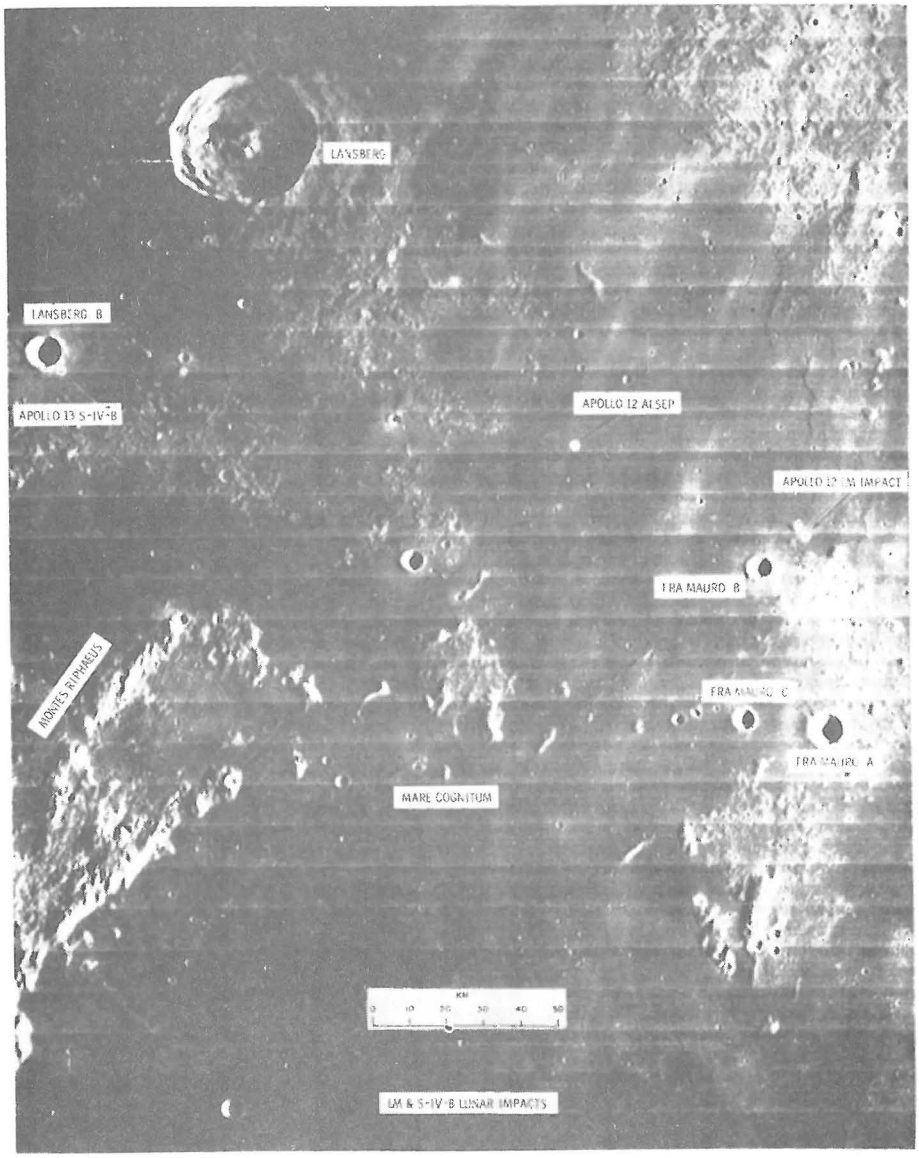

Fig. 1. Locations of the LM and S-IVB impacts and the Apollo 12 seismic station. The region shown is in the southeastern edge of Oceanus Procellarum. The coordinates of these sites are listed in Table 1.

Table 3. Summary of seismic energies and conversion efficiencies for impact signals.

Impacts	Calculated seismic energy coupled into the lunar structure (ergs)		Conversion efficiency (ratio of seismic energy to impact kinetic energy)	
	Scattering hypothesis	Dispersion hypothesis	Scattering hypothesis	Dispersion hypothesis
LM	$1.5 \cdot 10^{10}$	$2.8 \cdot 10^{10}$	$4.5 \cdot 10^{-7}$	$8.3 \cdot 10^{-7}$
S-IVB	$8.5 \cdot 10^{11}$	$4.7 \cdot 10^{12}$	$1.8 \cdot 10^{-6}$	$1.0 \cdot 10^{-5}$

peak for the later portions of the signals. The spectra of LM impact signals remain relatively broad. Although the peak frequency is relatively stable with time for each signal, it does vary from signal to signal. The spectral maxima are at 1.1 and 0.40 hz for the LM and S-IVB signals, respectively. Low-frequency energy (below 0.25 hz) is notably absent in the signals.

4) The impact signals are complex with little or no phase correlation between any two components of motion, except for the very early parts of the wave trains at times of body wave arrivals.

The beginnings of the impact signals are shown on an expanded time scale in Fig. 4. Signals corresponding to the arrival of compressional waves (P) and shear waves (S), waves that travel through the body of the moon, can be identified on the seismic records. The identification of these arrivals is based primarily on their associated particle motions and on their relative times of arrival. The first arrival from the LM impact is very small in amplitude, and it is difficult to specify the exact arrival time. This arrival may correspond to a wave that has reflected once from the lunar surface (PP), as will be discussed below. The prominent signal that nearly obscures the P wave onset from the LM impact was produced by a sudden tilt of the instrument. Such tilts are produced at random by thermal expansion and contraction of the Mylar insulating blanket that surrounds the instrument. The remaining phases are more easily distinguished. The travel times and wave speeds are listed in Table 2.

Our objective in the interpretation of the lunar impact seismograms is to derive a model for the outer shell of the moon that is consistent with the observed travel times of seismic body waves and that will explain the unusual characteristics of the remainder of the wave train. With data from only two artificial impacts recorded at a single station, detailed answers are difficult to achieve.

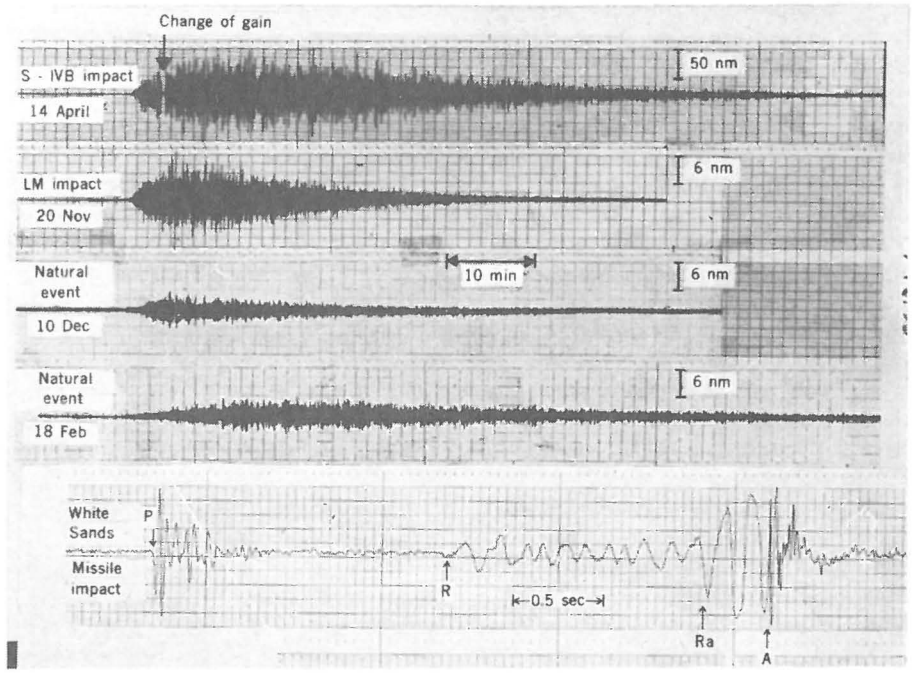

Fig. 2. Signals from the LM and S-IVB impacts and from two of the largest natural events recorded to date. All signals were recorded on the long-period vertical component seismometer. A record of the seismic signal from a missile impact recorded at the White Sands Missile Range is also shown for comparison. For the White Sands record: $P = P$ wave; $R =$ Rayleigh wave; $Ra =$ air-coupled Rayleigh wave; $A =$ atmospheric acoustic arrival; distance, 1.5 km; kinetic energy, $1.5 \cdot 10^{15}$ ergs. Note that the time scale of the White Sands impact signal is greatly expanded relative to that of the lunar signals.

An independent source of information is provided by measurement of seismic velocities on returned lunar samples. The laboratory measurements are obtained by placing a rock sample under pressure and measuring the speeds of waves passing through it by ultrasonic techniques. Since increasing pressure is equivalent to increasing depth within the moon, estimates of seismic velocities as a function of depth within the moon are thus obtained. Experimental results of this type have been reported for the Apollo 11 samples by Kanamori *et al.* (*5*) and Schreiber *et al.* (*6*).

The sample analyzed by Kanamori *et al.* (sample 10057) is a basalt, which contains numerous voids and microfractures. It appears to be moderately shocked, presumably by the meteoroid impact that blasted it out of the lunar material and deposited the rock on the lunar surface. The sample has a bulk density of 2.88 g/cm^3 and an intrinsic density of 3.38 g/cm^3. The data given by Schreiber *et al.* were obtained from a fine-grained vesicular rock (sample 10017) which has a bulk density of 3.1 g/cm^3. Both sets of experimental data show very low surface velocities and a rapid increase in velocity with depth in the upper 20 km of the moon to between 4.8 and 5.6 km/sec for compressional waves. The low surface velocities result from the presence of open pores and microfractures in the samples. The rapid increase in velocity with depth is produced by the closing of cracks and voids under pressure. Complete consolidation of rock material may not occur under the low lunar gravity until depths of at least 20 km have been reached.

Low seismic velocities for the upper few meters of lunar material have been confirmed by measurement of seismic signals generated by the LM and from Surveyor results. From LM signals, a compressional velocity of 108 m/sec for the top several meters of material has been reported (*7*). From Surveyor data, a compressional velocity of 45 m/sec and a shear velocity of 23 m/sec for the top few centimeters of material have been derived (*8*).

The time-distance curves for seismic compressional and shear waves con-

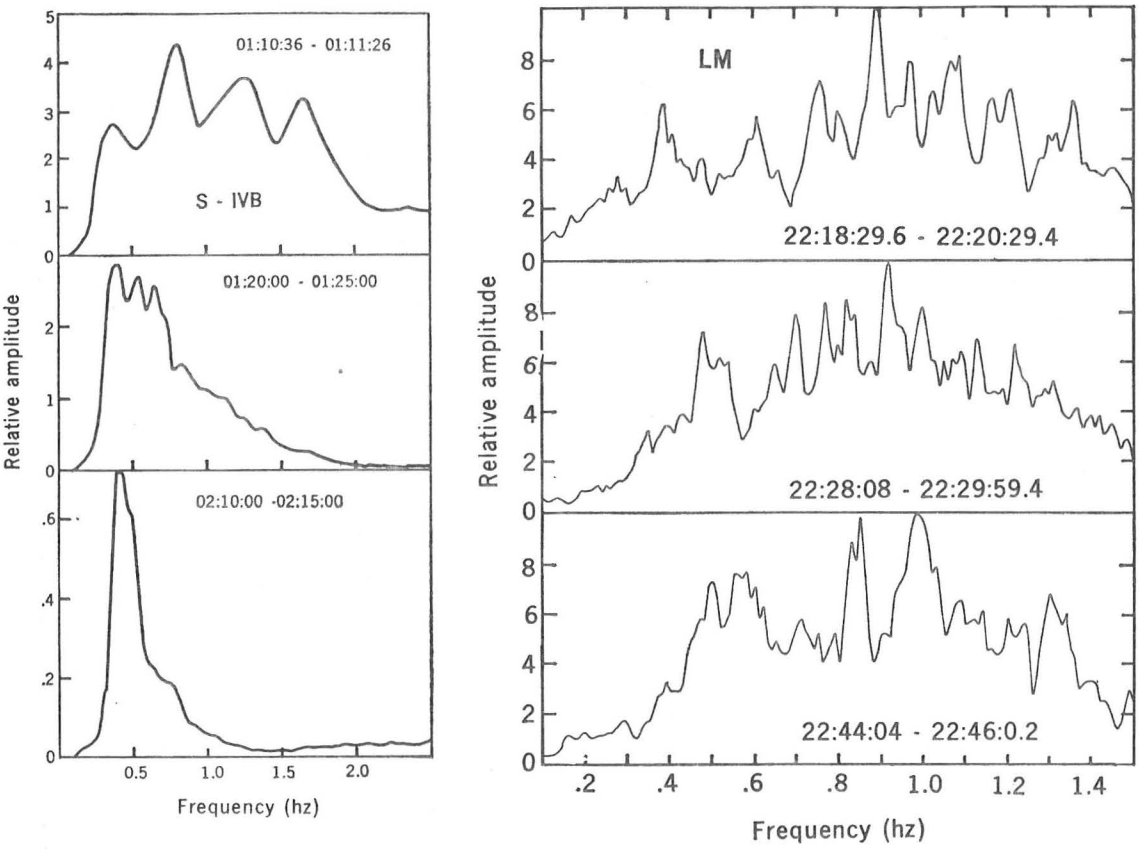

Fig. 3. Frequency spectra of impact signals. The S-IVB signal spectra are corrected for instrument response; the LM spectra are not corrected. Times (G.M.T.) for the beginning and ending of each sample are given on the spectral plots.

structed from the laboratory data are plotted in Fig. 5. The observed travel times of waves from the impacts are also indicated. Seismic waves traveling downward in a medium in which the velocity increases with depth will be refracted according to Snell's law, along curved ray paths that are concave upward, and they will eventually return to the surface at a time that increases with distance as indicated by the time-distance curve. Rays may reflect from the surface one or more times before reaching the detector. The *PP* phase, for example, corresponds to a compressional wave that reflects once from the surface at a point midway between the source and the receiver (for a source at the surface). Thus the travel time for the *PP* phase is equal to twice that of the direct *P* wave, which would be recorded at half the distance. The travel time of the *PP* phase from the S-IVB can, therefore, be plotted on the *P* wave curve at a distance of 67.5 km. In this connection, we note that the ground motion amplitude for the *PP* phase is approximately twice the amplitude of the *P* wave for the S-IVB impact. Thus, it is possible that the first arrival detected from the LM impact is *PP* and that the earlier *P* wave was too small to be detected. In Fig. 5 we have also plotted the LM first arrival on the alternate assumption that it is the *PP* phase.

The velocity-depth curves derived from laboratory measurements are applicable only if the outer 20 to 40 km of Oceanus Procellarum, which corresponds to the greatest depth of penetration of seismic waves from the impacts, consists of rock material similar to the crystalline rocks used in the measurements. The approximate agreement between the travel-time curves observed from the impacts and those computed from the laboratory measurements indicates that this similarity may exist. If so, no major boundary similar to the crust-mantle interface on earth, where an abrupt increase in velocity to about 8.1 km/sec occurs, is present in the outer 20 km of the mare.

The assumption of a model consisting of homogeneous rock under self-compaction leads to a travel-time curve with no sharp changes of slope. This simple model is consistent with the few travel-time data obtained so far, but future impact observations may necessitate its modification. It is clear that the material found at the surface of the mare is too dense to constitute the entire moon unless internal temperatures are high enough so that thermal expansion offsets the effects of compression (*9*). Alternately, the density of the material sampled in the mare may be anomalously high (*10*).

Quality factor Q *of lunar material.* Attenuation of energy in a vibrating system is frequently specified by the quantity Q (quality factor) for the system; or $1/Q$ is the dissipation function, where $2\pi/Q$ is the fractional loss of energy per cycle of vibration of the system. Thus, a high Q implies low attenuation. The Q of a system can be determined by measuring the rate of decay of system energy with time. The value of Q for the lunar material in the region of the Apollo 12 site, as measured by the rate of decay of the LM and S-IVB signal amplitudes, is approximately 3000. This value is in contrast with values of Q between 10 and 300 for most materials of the earth's continental crust.

The relatively high Q inferred for the lunar material may be a consequence of the nearly complete absence of fluids within the outer shell of the moon. Some experimental evidence that supports this possibility has been presented by Pandit and Tozer (*11*). These authors state that evacuation of porous terrestrial rocks to pressures of 10^{-2} torr typically increases the Q of the sample by a factor of 5 over the value measured at 1 atmosphere. Low

temperatures in the mare material might also increase the Q. However, no substantive information on subsurface lunar temperatures are available at present.

Lunar seismic reverberation. To explain the unexpectedly long duration of the impact signals, we must either assume that the effective source mechanism was prolonged in some manner or that the long duration is a propagation effect. However, the fact that signals from events of internal origin (moonquakes) and events of external origin (impacts) both show the reverberation is strong evidence for a propagation effect.

The possible propagation mechanisms fall into two general categories: true dispersion effects, where coherent waves propagate at differing group velocities dependent upon wavelength; or scattering effects, where the effective path lengths are increased owing to numerous reflections from acoustic discontinuities. An explanation must take into account that a surface impact source is expected to generate most of its seismic energy in the form of surface waves. Normally, surface waves appear on earthquake or shallow explosion records as trains of sinusoidal waves dispersed by variation of velocity with wavelength due to a vertical gradient of elastic properties in the wave guide. There are usually clear and consistent phase relations between the horizontal and vertical components of motion. Consistent phase relations are lacking in the extended wave trains of the lunar impact signals, as was previously described.

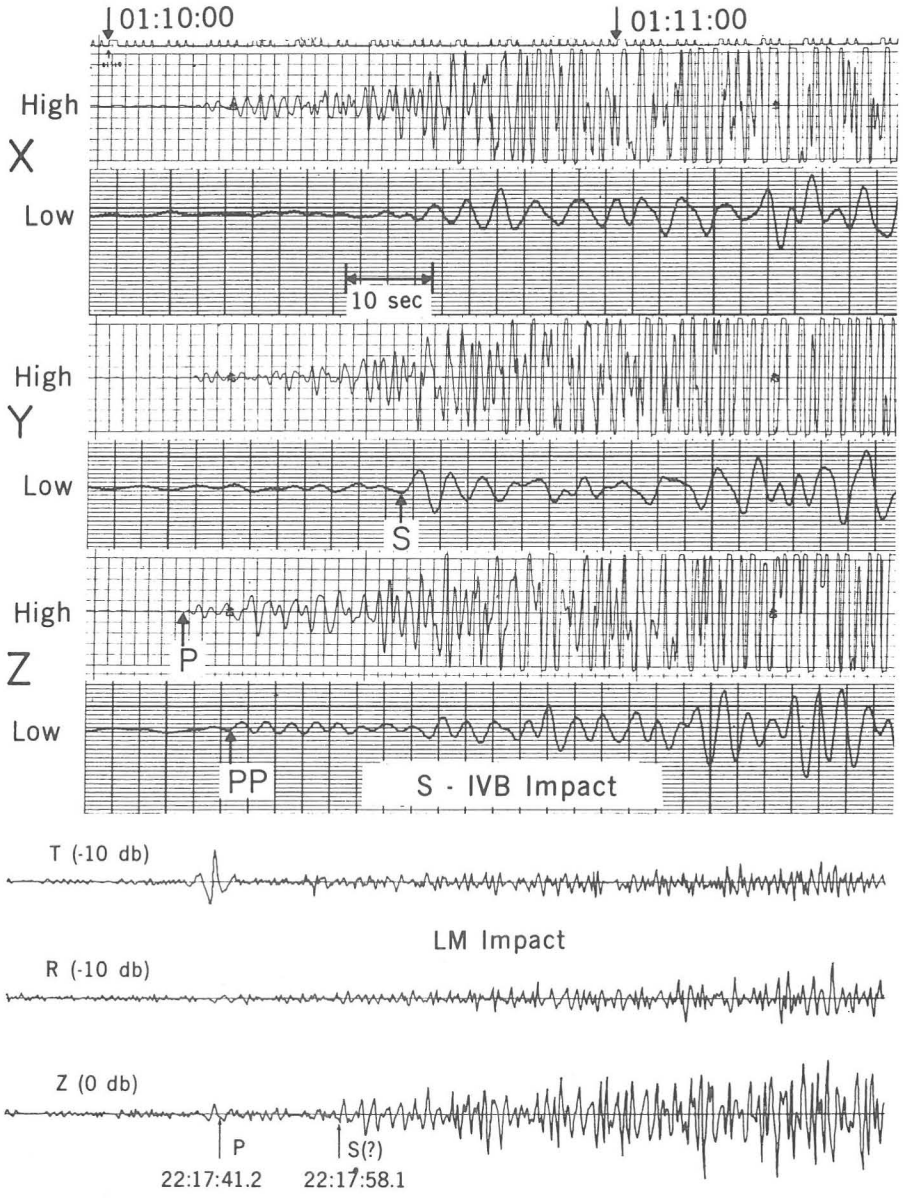

Fig. 4. Initial portions of impact signals on an expanded time scale. (Top) S-IVB signal with high-pass filtering (*High*) to emphasize the P wave, and low-pass filtering (*Low*) to emphasize the PP and S waves (filter corners are at 5 seconds). (Bottom) LM impact signal showing P (or PP) and S phases. For the S-IVB signal, X and Y are horizontal component seismometers, and Z is the vertical component. The X and Y components are approximately transverse and radial, respectively, for the S-IVB impact. For the LM signal, R and T are the radial and transverse (horizontal) components and Z is the vertical component. The S-IVB PP phase is also plotted on the P travel-time curve at half the distance and half the travel time. The LM P phase is also plotted in this manner under the assumption that it may actually be a PP arrival (see text). Time on the records is the time at which the data are recorded at the receiving station on earth.

Scattering hypothesis. The scattering hypothesis explains the character of the impact signals by postulating that the moon not only has a high Q but is also very heterogeneous, at least in the near-surface region of the mare. If the lunar medium contains inhomogeneities comparable in scale to the wavelength of the propagating seismic waves, significant scattering will occur. Scattering would tend to increase the duration of the observed seismic waves, would suppress the appearance of distinct phases within the wave train, and would reduce coherence between the horizontal and vertical components of surface motion.

That the outer shell of the moon might be highly heterogeneous is not surprising in view of the extreme age of the surface. Meteoroid bombardment would certainly have shattered the original lunar material to depths approaching 50 km, and the terrestrial geologic processes that remove these scars would be absent. Also, the surface lava is reported to have a very low viscosity and a high thermal coefficient of expansion (*12*). A lava with these properties might form extensive networks of lava tubes within the flow and would fracture extensively after solidifying. Alternately, the heterogeneity might simply be characteristic of the structure produced by the influx of blocks of material during the final stages of accumulation of the moon.

If scattering is sufficiently intense, the propagation of seismic waves might properly be described by diffusion theory, in which seismic energy "flow" is proportional to the gradient of energy density. With proper selection of parameters, the envelopes of the impact reverberations can be fit quite accurately by diffusion theory except for the first few minutes, when scattering would not be expected to be the predominant mechanism (*13*). If scattering is an im-

portant factor in lunar seismic wave transmission, heterogeneity must exist within the lunar material on a scale of from several hundred meters, or less, to several kilometers. An alternate approach to the scattering problem has been given by Steg and Klemens (*14*).

Dispersion hypothesis. At least two seismic wave guides are likely to occur in the outer shell of the moon. One is the unconsolidated surface debris layer (the lunar regolith) which, together with a shattered crystalline layer, forms a low-velocity zone overlying the more competent, higher-velocity basement rocks. A deeper wave guide is formed by the velocity gradient in the basement rock, which is inferred from the pressure coefficient of velocity measured in the laboratory on lunar crystalline rocks.

Both of these wave guides would "trap" surface waves (Love waves and Rayleigh waves), but important distinctions between their effects are to be expected. The very high modes of the basement wave guide can be thought of as multiply reflected body waves analogous to the Sofar channel in the oceans or as a "whispering gallery" phenomenon. Neither low nor high modes of surface waves in the basement channel can account for the prolonged reverberation without invoking scattering, because the difference between the maximum and minimum group velocities is small for the frequencies of interest. The situation is different for the surface low-velocity zone, where the dispersion curves (Fig. 6) for Rayleigh waves of the fundamental mode show a maximum group velocity of 1660 m/sec and a minimum group velocity of 30 m/sec for the period range of from 1.2 to 1.5 seconds. For this model, surface waves with predominant periods of from 1.2 to 1.5 seconds and a duration of 74 minutes for the S-IVB source distance of 135 km would be expected. The predominant period varies directly with the thickness of the low-velocity surface layer, and inversely with the shear velocity. The observed signal for the S-IVB impact shows a lower frequency than does the LM impact, which implies a thicker surface layer (or lower shear velocity) for the S-IVB wave path, or excitation of a higher mode by the LM impact. The signal duration predicted by this model is satisfactory for the LM but requires some multipathing for the S-IVB impact. Multipath propagation or a mixture of modes is also required to explain the lack of correlation between the three components of ground motion.

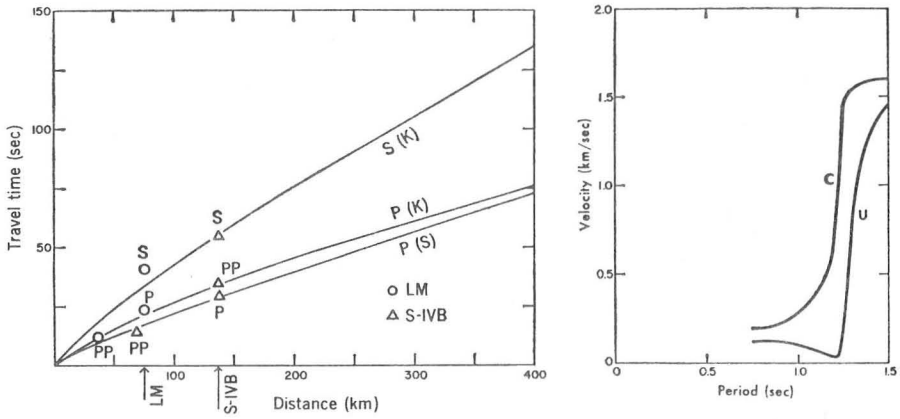

Fig. 5 (left). Travel times of seismic waves from the lunar impact signals. Solid curves are derived from laboratory measurements of seismic velocities on returned lunar samples. $P(S)$ = compressional wave velocities measured for a lunar rock sample by Schreiber *et al.* (*6*); $P(K)$, $S(K)$ = compressional and shear wave velocities measured for a lunar rock sample by Kanamori *et al.* (*5*). Fig. 6 (right). Phase (C) and group velocity (U) curves for Rayleigh waves of the fundamental mode. The model consists of a 30-m low-velocity layer with shear velocity of 0.1 km/sec, which overlies basement material with shear velocity of 1.8 km/sec.

The closest terrestrial analog to the lunar impact signals discovered thus far are surface waves (first-shear-mode Rayleigh waves) recorded on the ocean bottom from shallow focus earthquakes originating in the Mid-Atlantic Ridge (*15*). These signals show a gradual buildup and decay, very long duration with nearly constant period, and inferred Q values from 1500 to 2000 for the oceanic wave guide. The signals are observed only when significant amounts of unconsolidated sediments are present along the path between the source and the receiver. If we ignore the water layer, the oceanic structure may be quite similar to the lunar structure, with the sediment layer being equivalent to the low-velocity outer zone of the moon.

The presence of a thick permafrost zone overlain by 100 to 200 m of low-velocity material, as suggested by Shubert *et al.* (*16*), might also provide a model consistent with this interpretation.

The terrestrial oceanic signals clearly demonstrate that the major features of the lunar seismic reverberation can be explained by dispersion in a high Q wave guide that contains material of low shear velocity. If the lunar signals are higher-mode Rayleigh waves, this would also explain the absence of low-frequency energy in these signals, since higher modes cannot propagate at frequencies below a fixed cutoff frequency. The observed differences in the reverberation frequencies of the natural events would be explained by the dispersion hypothesis as resulting from lateral variations in the shear velocity or thickness of the surficial layer.

Efficiencies of impacts as seismic sources. The calculation of seismic energy coupled into the lunar structure by the impacts is dependent on whether we assume scattering or dispersion to be the predominant mechanism that explains the seismic reverberations. Calculated seismic energies based on both hypotheses are given in Table 3. For these calculations, we have assumed a density of lunar material of 3.3 g/cm^3; Q of 3000; constant signal frequencies of 1 and 0.5 hz for the LM and S-IVB, respectively; and cylindrical spreading of energy with thicknesses of layers through which the waves are transmitted of 2 and 4 km for the LM and S-IVB signals, respectively.

The efficiency of the S-IVB impact is 4 to 12 times greater than that of LM impact (see Table 3). This difference was anticipated, since the LM struck the surface at a very shallow angle and would thus have transferred a small fraction of its momentum to the surface at the primary impact point, whereas the S-IVB struck the surface at a much steeper angle and would have transferred essentially all of its momentum at the primary impact point.

Conversion efficiencies of between $1 \cdot 10^{-5}$ and $5 \cdot 10^{-5}$ were obtained for missile impacts at White Sands, New Mexico (*3*). McGarr *et al.* (*17*) obtained efficiencies of between $8 \cdot 10^{-7}$ and $6 \cdot 10^{-5}$ for various target materials for hypervelocity impacts. Thus, the efficiency of the S-IVB impact for production of seismic energy is in approximate agreement with efficiencies

obtained for impact experiments on earth.

Conclusions. We summarize below in four major conclusions:

1) Body wave velocities measured from the LM and S-IVB impacts are in reasonably close agreement with the velocities predicted from laboratory measurements on lunar rock samples. This result implies that the rock material collected at the surface of the mare near the Apollo 12 landing site is similar to the material that forms the mare to depths of at least 20 km.

Present data for the mare region near the Apollo 12 landing site suggest that the outer shell of the moon consists of low-velocity material near the surface, with velocity increasing rapidly with depth in the upper 20 km. It is unlikely that a major discontinuity similar to the Mohorovicic discontinuity, which defines the lower limit of the crust of the earth, exists in the outer 20 km of the moon.

The fact that NASA was able to achieve such high targeting accuracy for the S-IVB and that the resulting seismic signals were so large suggests that planned future impacts can be extended to ranges up to at least 500 km and that the data returned will provide information on lunar structure to depths of several hundred kilometers.

2) The lunar seismic reverberation can be explained equally well as resulting from dispersion of surface waves or from scattering or, perhaps more likely, from a combination of these mechanisms. Scattering of surface waves implies the presence of heterogeneity in the outer shell of the moon on a scale from several hundred meters, or less, to several kilometers. Surface irregularities may contribute significantly to the scattering. The dispersion hypothesis requires the presence of a low-velocity outer zone. The presence of this zone to depths of several meters has been confirmed by measurements of seismic waves from sources associated with the LM and from Surveyor measurements. Very low absorption of seismic wave energy in the lunar material is inferred, independent of the assumed mode of propagation. This may be a consequence of the absence of fluids in the near-surface materials or low temperature or a combination of these factors.

3) Estimates of the fraction of impact kinetic energy that is converted to seismic wave energy are reasonably close to results obtained from impact experiments on earth.

4) Seismic signals of natural origin are produced by moonquakes and by meteoroid impacts. The low level of detectable lunar seismic activity relative to the earth suggests that the outer shell of the moon is tectonically stable as compared with the lithosphere of the earth. Tidal stresses appear to be an important factor in the occurrence of moonquakes. Meteoroid flux in the kilogram mass range, as it has been inferred from seismic data, is in approximate agreement with the Hawkins flux estimate (*2*).

G. Latham, M. Ewing, J. Dorman
Lamont-Doherty Geological Observatory of Columbia University, Palisades, New York 10964

F. Press, N. Toksoz
Department of Geology and Geophysics, Massachusetts Institute of Technology, Cambridge 02139

G. Sutton, Rolf Meissner
F. Duennebier
Institute of Geophysics, University of Hawaii, Honolulu 96822

Y. Nakamura
General Dynamics Corporation, Fort Worth, Texas 76101

R. Kovach
Department of Geophysics, Stanford University, Stanford, California 94305

M. Yates
Bellcomm Corporation, Washington, D.C. 20024

References and Notes

1. G. Latham, M. Ewing, F. Press, G. Sutton, *Science* **165**, 241 (1969).
2. G. Hawkins, "The Meteor Population," Research Report 3, NASA Document CR-51365 (1963).
3. R. Eggleton, personal communication.
4. G. Latham, W. McDonald, H. Moore, *Science* **168**, 242 (1970).
5. H. Kanamori, A. Nur, D. Chung, D. Wones, G. Simmons, *ibid.* **167**, 726 (1970).
6. E. Schreiber, O. Anderson, N. Soga, N. Warren, C. Scholz, *ibid.*, p. 732.
7. G. Latham, M. Ewing, F. Press, G. Sutton, J. Dorman, Y. Nakamura, N. Toksoz, R. Wiggins, R. Kovach, "Apollo 12 Preliminary Mission Science Report" (NASA SP-235, 1970), section 3, p. 39.
8. G. Sutton and F. Duennebier, *J. Geophys. Res.*, in press.
9. Y. Nakamura and G. Latham, *ibid.* **74**, 3771 (1969).
10. J. Wood, J. Dickey, U. Marvin, B. Powell. "Proceedings of the Apollo 11 Lunar Science Conference," *Geochim. Cosmochim. Acta Suppl. 1* **1**, 965 (1970).
11. B. Pandit and D. Tozer, *Nature* **226**, 335 (1970).
12. T. Murase and A. R. McBirney, *Science* **167**, 1491 (1970).
13. G. Latham, M. Ewing, F. Press, G. Sutton, J. Dorman, Y. Nakamura, N. Toksoz, R. Wiggins, J. Derr, F. Duennebier, "Proceedings of the Apollo 11 Lunar Science Conference," *Geochim. Cosmochim. Acta Suppl. 1* **3**, 2309 (1970).
14. R. Steg and P. Klemens, *Phys. Rev. Lett.* **24**, 381 (1970).
15. R. Anderson and G. Latham, *J. Geophys. Res.* **74**, 2747 (1969).
16. G. Shubert, R. Lingenfelter, S. Peale, *Rev. Geophys. Space Phys.* **8**, 199 (1970).
17. A. McGarr, G. Latham, D. Gault, *J. Geophys. Res.* **74**, 5981 (1969).
18. We thank L. Sykes and C. Scholz for reviewing the manuscript and offering helpful suggestions. Supported by the National Aeronautics and Space Administration under contracts NAS9-5957 and NAS9-5632. Computer facilities were provided by the NASA Goddard Space Flight Center, Institute for Space Studies, New York. Lamont-Doherty Geological Observatory Contribution 1586. Hawaii Institute of Geophysics Contribution 345.

9 July 1970; revised 25 August 1970

7. Active Seismic Experiment

Robert L. Kovach,[a]† *Joel S. Watkins,*[b] *and Tom Landers* [a]

The purpose of the active seismic experiment (ASE) is to generate and monitor seismic waves in the lunar near surface and to use these data to study the internal structure of the Moon to a depth of approximately 460 m (1500 ft). Two seismic energy sources are used: an astronaut-activated thumper device containing 21 small explosive initiators and a mortar package containing four high-explosive grenades. The grenades are rocket launched by command from Earth and are designed to impact at ranges of about 150, 300, 900, and 1500 m (about 500, 1000, 3000, and 5000 ft). A secondary objective of the experiment is to monitor high-frequency seismic activity during periodic listening modes.

Analysis to date of the seismic signals generated by the astronaut-activated thumper has revealed important information concerning the near-surface structure of the Moon. Two compressional wave (P-wave) seismic velocities were measured at the Fra Mauro site. The near-surface material possesses a seismic-wave velocity of 104 m/sec (340 ft/sec). Underlying this surficial layer at a depth of 8.5 m (28 ft), the lunar material has a velocity of 299 m/sec (980 ft/sec). The measured thickness of the upper unconsolidated debris

[a] Stanford University.
[b] University of North Carolina.
† Principal investigator.

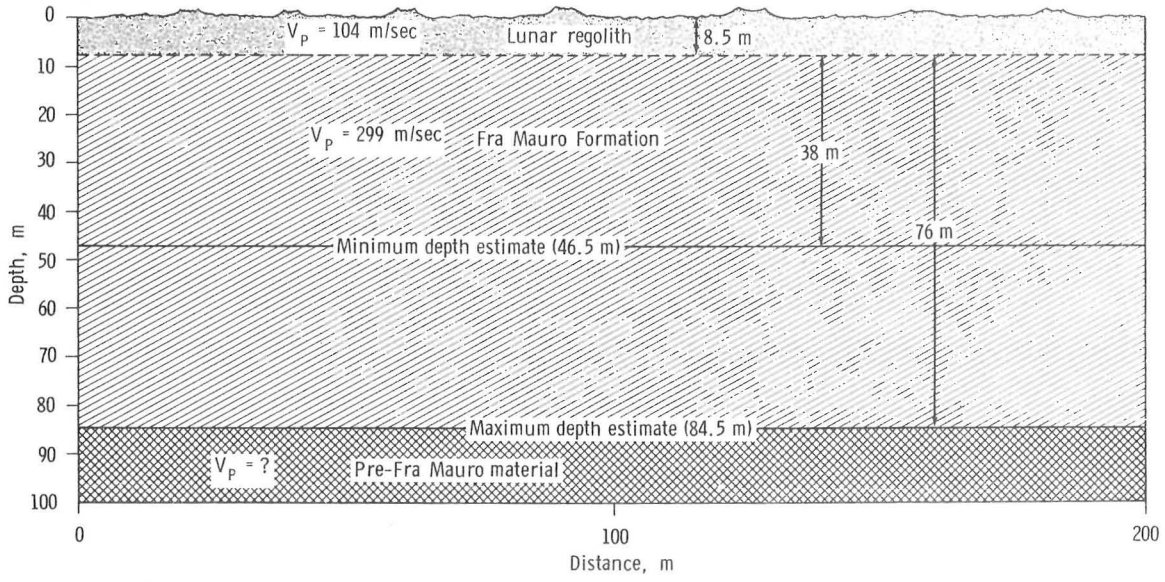

FIGURE 7–1.—Seismic cross section at Fra Mauro landing site. (V_P = seismic-wave velocity.)

layer is in good agreement with geological estimates of the thickness of the regolith at this site.

By combining the seismic-refraction results from the ASE with the lunar module (LM) ascent seismic data recorded by the Apollo 14 passive seismic experiment (PSE), estimates of the thickness of the underlying material can be made (fig. 7–1). These estimates range from 38 to 76 m (124 to 250 ft) and may be indicative of the thickness of the Fra Mauro Formation at this particular site. More definitive conclusions must await the seismic results from the four grenade firings.

Interesting signals, similar to some events recorded by the PSE, have also been recorded during the intermittent passive listening periods of the ASE. Analysis of these signals together with similar data from the PSE may shed light on the origin of these signals.

Instrument Description and Performance

The ASE consists of a thumper and geophones, a mortar package assembly, electronics within the Apollo lunar-surface experiments package (ALSEP) central station, and interconnecting cabling. The components of the ASE are shown schematically in figure 7–2.

The astronaut-activated thumper is a short staff (fig. 7–3) used to detonate small explosive charges—single bridgewire Apollo standard initiators. Twenty-one initiators are mounted perpendicular to the base plate at the lower end of the staff. A pressure switch in the base plate detects the instant of initiation. An arm-fire switch and an initiator-selector switch are located at the upper end of the staff. A cable connects the thumper to the central station to transmit real-time event data. The thumper also stores the three geophones and connecting cables until deployment on the lunar surface. In figure 7–4, the lunar module pilot (LMP) is shown beginning to unwind the

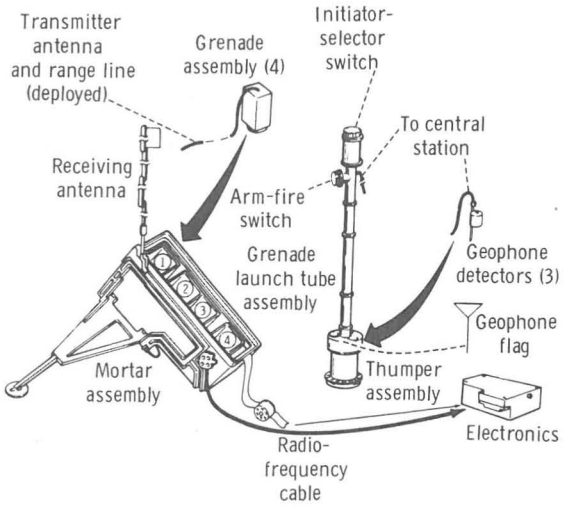

FIGURE 7–2.—Schematic diagram of the ASE.

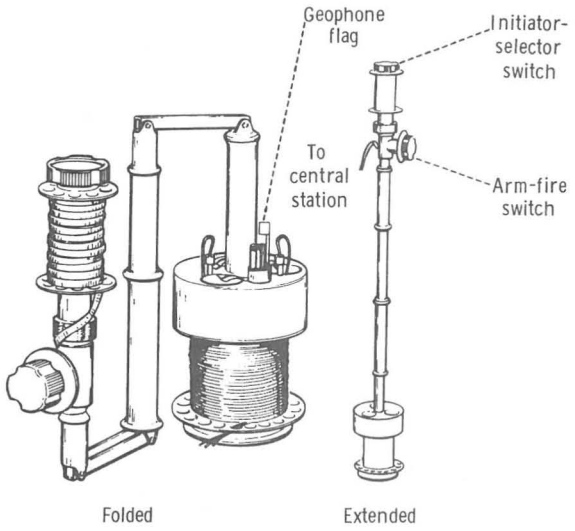

FIGURE 7–3.—Schematic diagram of the thumper in the folded and extended positions.

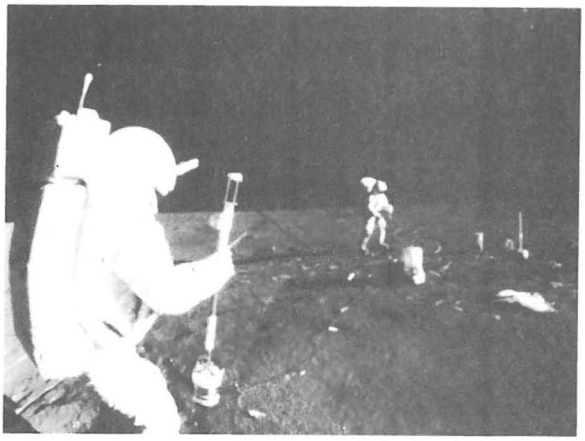

FIGURE 7–4.—Enlargement of 16-mm sequence camera photograph showing the LMP with hand-held thumper (S–71–19509).

geophone line from the thumper on the Moon just before activation of the ASE at 17:59 G.m.t. on February 6, 1971.

The three identical geophones are miniature seismometers of the moving coil-magnet type. The coil is the inertial mass suspended by springs in the magnetic field. Above the natural resonant frequency of the geophones (7.5 Hz), the output is proportional to ground velocity. The geophones are deployed at 3-, 49-, and 94-m (10-, 160-, and 310-ft) intervals in a linear array from the central station and connected to it by cables.

A three-channel amplifier and log compressor condition the geophone signals before conversion into a digital format for telemetering to Earth. The low signal-to-noise ratios expected and the lack of knowledge as to the character of the expected waveforms made it desirable to widen the frequency response as much as possible within the constraints of the digital sampling frequency of 500 Hz. Because signal levels were expected to be distributed throughout the system dynamic range, a logarithmic compression scheme was selected to give signal resolution as some constant fraction of signal amplitude. The system deployed on the Moon has the properties listed in table 7–I, and

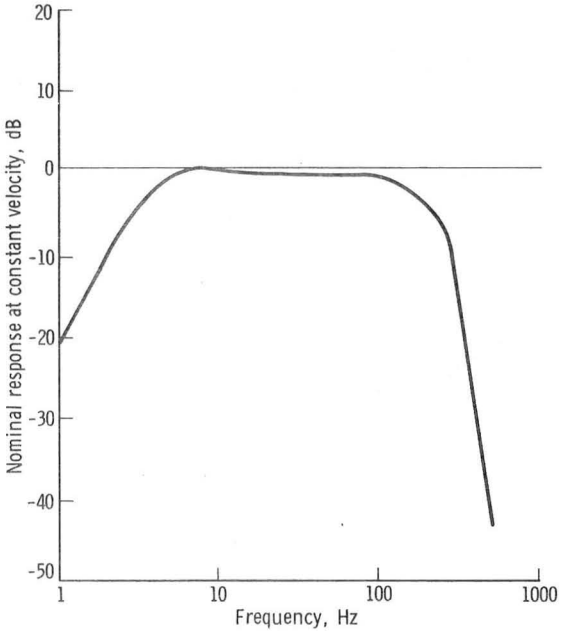

FIGURE 7–5.—Frequency response of the ASE.

TABLE 7–I. *Apollo 14 ASE Characteristics*

Component characteristics	*Channel no.*		
	1	*2*	*3*
Geophones:			
Generator constant, V/m/sec	250.4	243.3	241.9
Frequency, Hz	7.32	7.22	7.58
Resistance, ohm	6065	6157	6182
Amplifiers:			
Noise level, μV rms at input	0.300	0.325	0.272
Dynamic range, rms signal to rms noise in dB	86.8	86.5	87.5
Gain (at 10 Hz and V_{input} = 0.005 V rms)	666.7	666.7	675.7
Log compressor (compression accuracy for temperature range 15° to 50° C):			
Positive signal error, percent	3.79	4.71	2.00
Negative signal error, percent	2.07	1.32	3.33
System:			
Signal-to-noise ratio (rms signal to rms noise in dB for a 1-nm peak-to-peak signal at 10 Hz)	33.6	33.1	32.9
Calibrator accuracy:			
Generator constant, percent error	4.21	9.70	6.40
Natural frequency, percent error	3.28	4.99	8.58

TABLE 7–II. *Apollo 14 ASE Grenade Parameters*

Parameter	Grenade no.			
	1	2	3	4
Range, m	1 500	900	300	150
Mass, g	1 236	1 020	810	719
High-explosive-charge mass, g	454	272	136	45.4
Rocket-motor mean peak thrust, N	20 460	11 450	7005	5337
Mean velocity, m/sec	49	40	23	16
Lunar flight time, sec	44	32	19	13
Rocket-motor-propellant mass, g	47	31	16.8	11.5
Quantity of propellant pellets, number	2 435	1 596	648	550
Launch angle, deg	45	45	45	45
Rocket-motor thrust duration, msec	7.0	8.2	12.5	12.5

the nominal frequency response shown in figure 7–5.

The mortar assembly comprises a mortar box, a grenade-launch-tube assembly, and interconnecting cables. To provide an optimum launch angle for the grenades, the mortar package is deployed at an angle approximately 45° to the lunar surface. A two-axis inclinometer provides pitch- and roll-angle (deviation from the vertical) information on the mortar package. The mortar box is a rectangular fiber-glass-and-magnesium construction in which is mounted the grenade-launch-tube assembly containing four grenades.

Each grenade is attached to a range line, which is a thin-stranded cable wound around the outside of the launch tube. Two fine copper wires are looped around each range line. The first loop is spaced so that it will break when the grenade is approximately 0.4 m (16 in.) from the launch tube. A second loop is spaced to break when the range line has deployed an additional 8 m (25 ft) from the first breakwire. Breaking the loops starts and stops a range-gate pulse to establish a time interval for the determination of the initial grenade velocity.

The four grenades are similar but differ in the amount of propellant and high explosive (table 7–II). Each grenade possesses a square cross section with a thin fiber-glass casing. The casing contains the rocket motor, safe slide plate, high-explosive charge, ignition and detonation devices, thermal battery, and a 30-MHz transmitter. The range line is attached to the transmitter to serve as a half-wave end-feed antenna.

In operation, an arm command from ground control applies a pulse to charge condensers in the mortar box and grenade; a fire command discharges the condenser through an initiator, which ignites the rocket motor. When the grenade leaves the tube, a spring-ejected safe slide is removed, activating a microswitch in the grenade.

A thermal battery and the electronics in the grenade make up the firing circuit. The microswitch discharges a condenser across a thermal match to activate the thermal battery, which in turn powers the transmitter and produces a capacitor charge for the detonator. At impact, an omnidirectional impact switch closes, discharging the capacitor into the detonator to ignite the explosive. The explosion terminates radiofrequency transmission as an indication of detonation time. The critical parameters measured are the detonation time, time of flight, initial velocity, and launch angle. Because of the ballistic trajectory followed by the grenades in the lunar vacuum, the necessary data are available to determine grenade range. The planned mortar mode of operation for the ASE is shown in figure 7–6.

Because some of the geophone parameters might drift on the lunar surface, a calibrator circuit is provided in the system to measure these parameters to within 10 percent of the preflight values. The damping resistance across the geophone is altered to underdamp the geophone, and

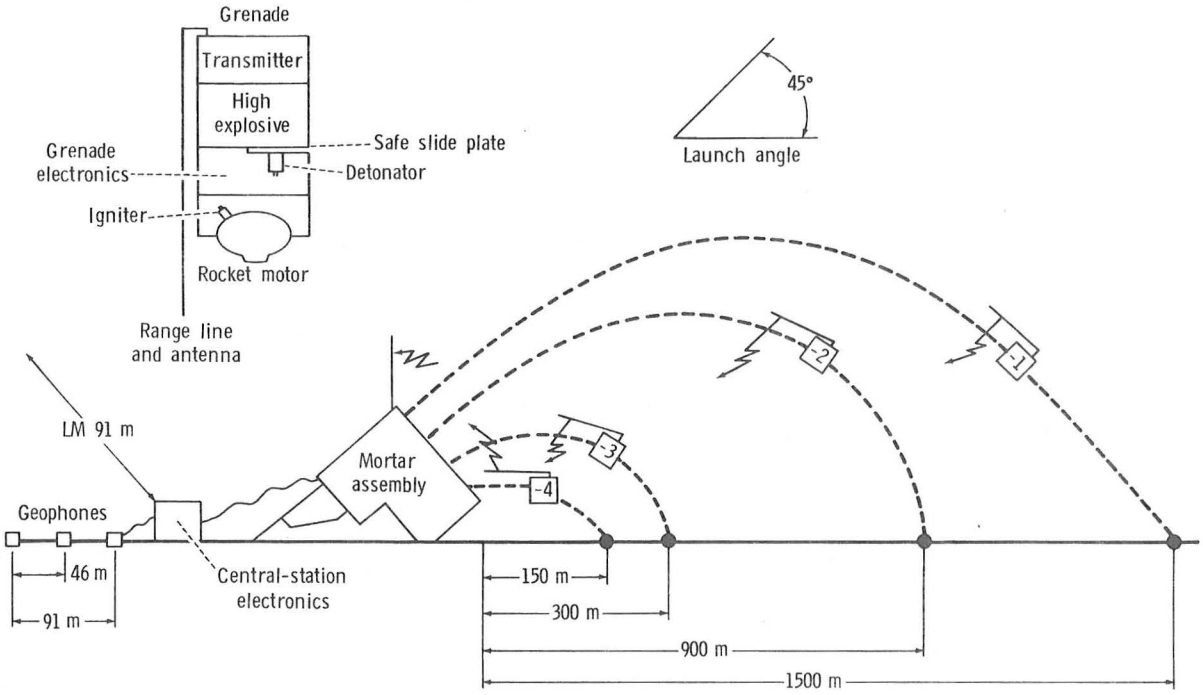

FIGURE 7–6.—Schematic diagram showing the mortar mode of operation for the ASE.

current is introduced into the geophone coil to react with the magnetic field of the geophone, producing a force on the geophone coil. This force moves the coil and, with an underdamped geophone, the signal from the geophone is a logarithmically decaying sinusoidal signal. A typical calibration pulse recorded on the three geophones on February 12 is shown in figure 7–7. Analysis of similar calibration pulses transmitted between thumper operations on the Moon demonstrated close agreement of the natural frequency and generator constant of the geophones with measured preflight values.

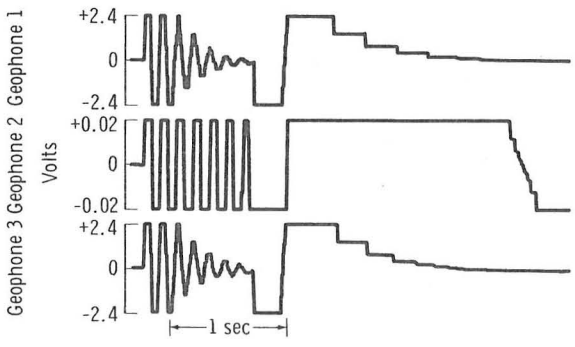

FIGURE 7–7.—Calibration pulse recorded on February 12 during passive listening mode.

The ASE system is controlled from Earth by a number of commands that control such functions as switching to the high-bit data rate and firing the grenades from the mortar box assembly. Further technical details of the ASE, particularly of the electronics, can be found in reference 7–1.

Thermal Control

The ASE electronics are part of the ALSEP central station and do not require separate thermal control. The ASE mortar package assembly was designed to be maintained between —60° and 85° C. Thermal control of the mortar package assembly is accomplished with multilayer aluminized Mylar insulation used in conjunction with small heaters. Heater operation begins automatically at a temperature of about —17° C when the ASE is in the standby mode of operation. Four temperatures are monitored in this mode: central-electronics temperature, grenade-launch-tube-assembly temperature, mortar-package tempera-

ture, and temperature of the geophone closest to the ALSEP.

Deployment

At the Apollo 14 site, the three geophones are alined in a southerly direction from the ALSEP central station (fig. 3–1 in sec. 3). No difficulty was experienced in deploying and arming the mortar package. The mortar package is positioned to fire the four grenades in a northerly direction in alinement with the geophone line. The mortar package assembly is shown in figure 7–8 as deployed on the lunar surface. A view looking downrange from the mortar package is shown in figure 7–9. The geophone line appears in the right foreground.

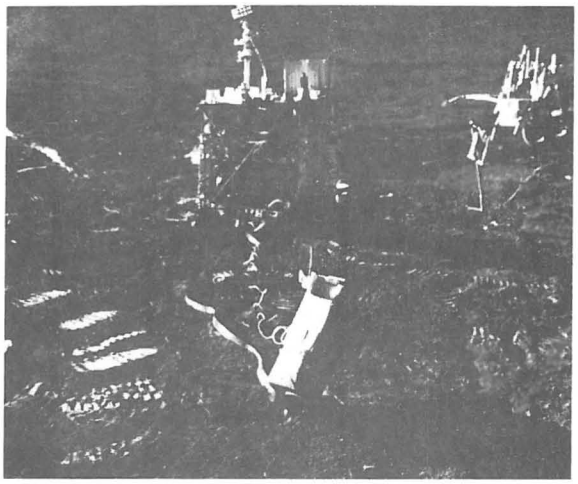

FIGURE 7–8.—Mortar assembly deployed on the lunar surface (AS14–67–9361).

For convenience, the geophone closest to the ALSEP is designated "geophone 1" and the most distant is designated "geophone 3." No difficulty was experienced in implanting the geophones and maintaining them vertically in the lunar soil. Before beginning thumper operations at geophone 3, it was noted that the alinement flag at geophone 2 had fallen over. Because of time constraints, thumper operations were begun at geophone 3 before returning to check the flag and geophone at the middle position.

Thumper operations were begun at 18:09 G.m.t. and continued until 18:37 G.m.t. Thumper firings were begun with shot 1 at geophone 3 and continued at 4.6-m (15-ft) intervals along the geophone line to shot 21 at geophone 1. In figure 7–10, the LMP is shown firing the thumper along the geophone line on the lunar surface. The thumper failed to fire after several attempts at

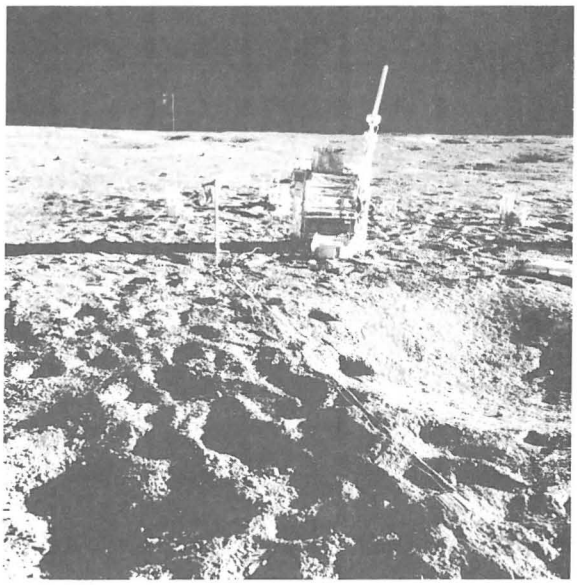

FIGURE 7–9.—Photograph looking downrange from mortar assembly on lunar surface. Geophone line is deployed in right foreground (AS14–67–9377).

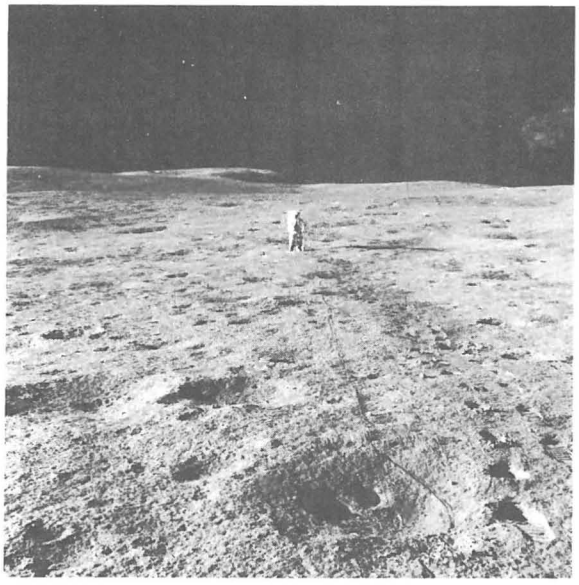

FIGURE 7–10.—The LMP firing thumper along geophone line on the lunar surface (AS14–67–9374).

several initiator positions, and several firing positions were skipped to gain extravehicular activity (EVA) time. Successful thumper shots were recorded at positions 1 (located at geophone 3); 2, 3, 4, 7, 11 (located at geophone 2); 12, 13, 17, 18, 19, 20, and 21 (located at geophone 1).

Upon reaching position 11, at the middle geophone, the LMP observed that this geophone had pulled out of the ground, apparently because of the effects of set or elastic memory in the cable. After repositioning the geophone, he resumed thumping operations. Even though geophone 2 was resting on its side during the first five thumper firings, usable seismic data were recorded. The net result of tipping a vertical-component geophone off vertical is to translate the mass and effectively increase the natural frequency. Analysis of the calibration pulse sent before beginning thumping operations showed that the effective natural frequency of geophone 2 had increased from 7.5 to 13.4 Hz. The total time spent on thumping operations was 28 min, within allowable EVA constraints, and valuable lunar seismic data were obtained.

Several thumper shots were attempted while the commander was moving on the lunar surface near the ALSEP central station. Unfortunately, his movements generated seismic energy that was recorded by the highly sensitive geophones. As a result, his movements had to be restricted during the remaining thumper operations. However, it still may be possible to conduct thumper operations on the Moon and allow the second astronaut to move about, provided he is sufficiently far removed from the central station and geophone line.

Description of Recorded Seismic Signals

Thumper Mode

During thumper operations on the lunar surface, the LMP was instructed to stand still for 20 sec before and 5 sec after each firing. Therefore, 5 sec of seismic data were recorded for each thumper firing. The seismic data recorded for thumper shots 18 and 20 are shown in figure 7–11. Characteristically, the seismic signals produced by thumper firings within 9 m (30 ft) of a geophone have extremely impulsive beginnings and saturate the dynamic range of the amplifier for about 0.5 sec. The predominant frequency of these signals range from 27 to 29 Hz.

As the distance between the thumper firings and the geophones is increased, the seismic signals possess more emergent beginnings. In figure 7–12, a record section is alined in time to the same instant of firing for thumper shots 18 to 21 as recorded at geophone 2. The wave trains build up to a maximum amplitude within the first 0.25 to 0.5 sec from onset of signal and then gradually decrease in amplitude. This effect can best be seen in figure 7–11 by comparing the seismic signals recorded at 14, 32, and 41 m (45, 105, and 135 ft). Little difficulty exists in picking the onset of the seismic signals out to a distance of 46 m (150 ft); but, at greater distances, uncertainty arises in determining the beginning of the seismic wave arrival because the signals are much weaker. The peak amplitude of the recorded signals typically decreases by a factor of approximately 60 in 61 m. More refined data-analysis techniques applied to the recorded seismic signals from the thumper mode of operation are underway.

Passive Listening Mode

The ASE is also capable of operating in a passive listening mode and is commanded into this high-bit-rate mode for a 30-min period each week. Several interesting signals have been recorded in this mode of operation. Two of these events, recorded on February 19, are shown in figure 7–13. The signals have the largest amplitude on a single geophone, although the signal is definitely discernible above the ambient noise level, but greatly reduced in amplitude on the other geophone channels.

The signal recorded on geophone 1 beginning at about 15:29:41 G.m.t. has a predominant frequency of approximately 36 Hz, whereas the signal recorded by geophone 2 at approximately 15:38:46 G.m.t. has a frequency of approximately 47 Hz. Both of these signals have impulsive beginnings and relatively short durations of 6 to 10 sec. Maximum amplitudes occur at the beginning of the wave train.

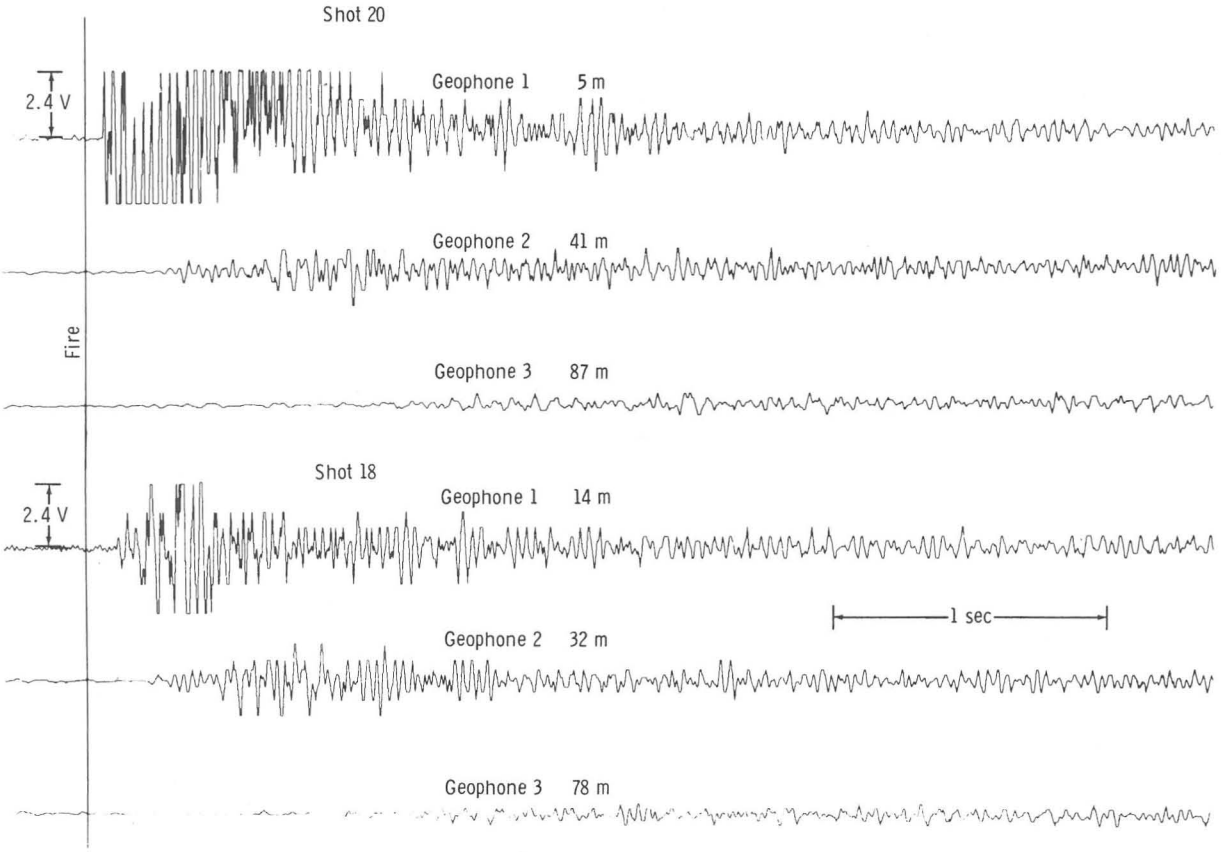

FIGURE 7–11.—Seismic signals produced by thumper firings 18 and 20 on the lunar surface.

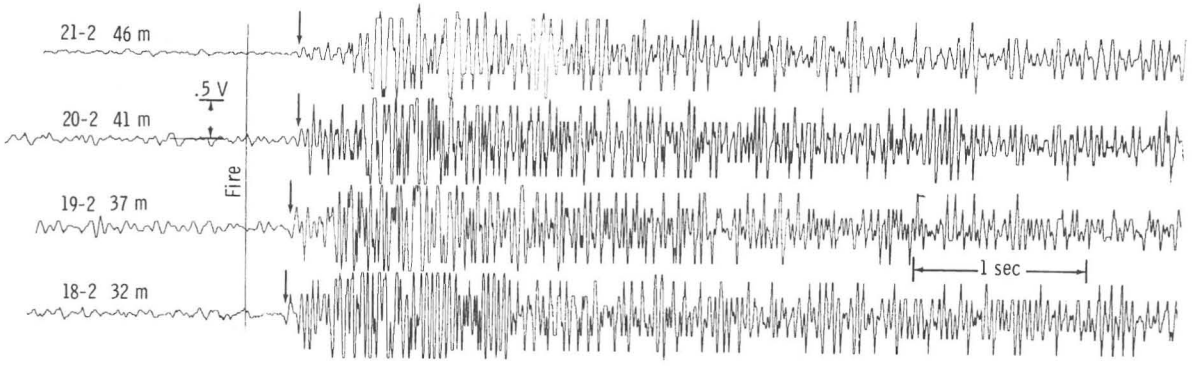

FIGURE 7–12.—Seismic signals produced by thumper firings 18 to 21 as recorded at geophone 2. The traces are alined to the same relative instant of the firing of the thumper. The small arrows point to the onset of the seismic signal.

One can note a gross similarity to the seismic signals produced by thumper firings close to a geophone, although the amplitude of these signals is approximately 100 to 200 times smaller than the thumper-generated signals. These events are also strikingly similar to the type X events (impulsive beginnings and relatively short durations—normally less than 10 sec) recorded during the

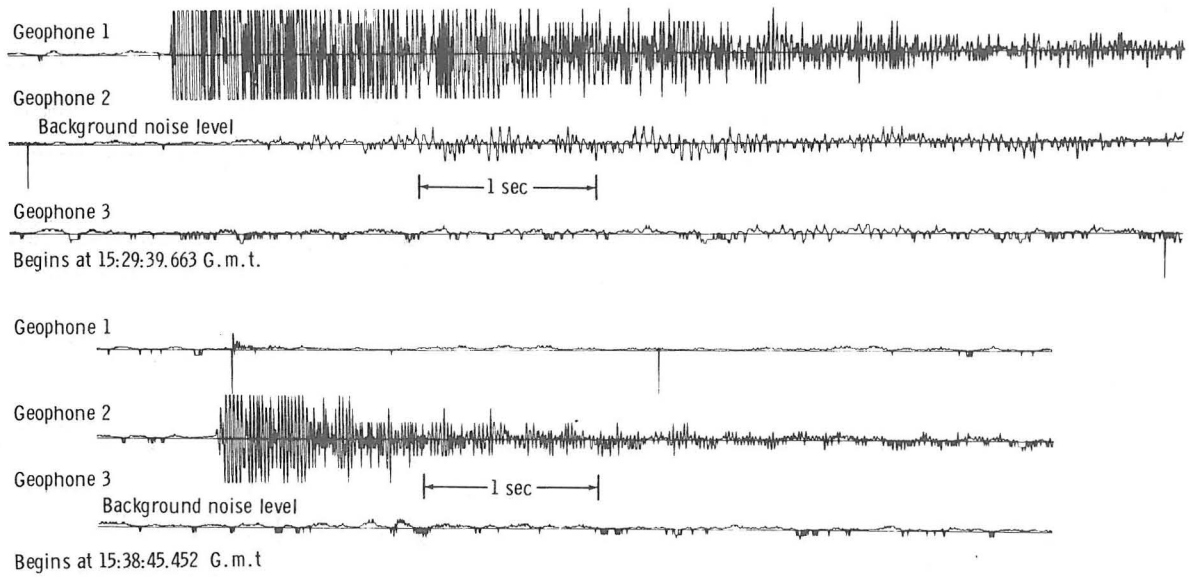

FIGURE 7–13.—Signals recorded during the passive listening mode on February 19; all plots clipped at 0.01 V.

Apollo 11 mission (ref. 7–2) that were speculated to be produced by direct micrometeoroid impacts on the PSE. Continuing work is being directed toward detailed analysis of these events.

Discussion

A preliminary interpretation of the traveltime/distance data (fig. 7–14) obtained from the thumper firings is rewardingly consistent in that

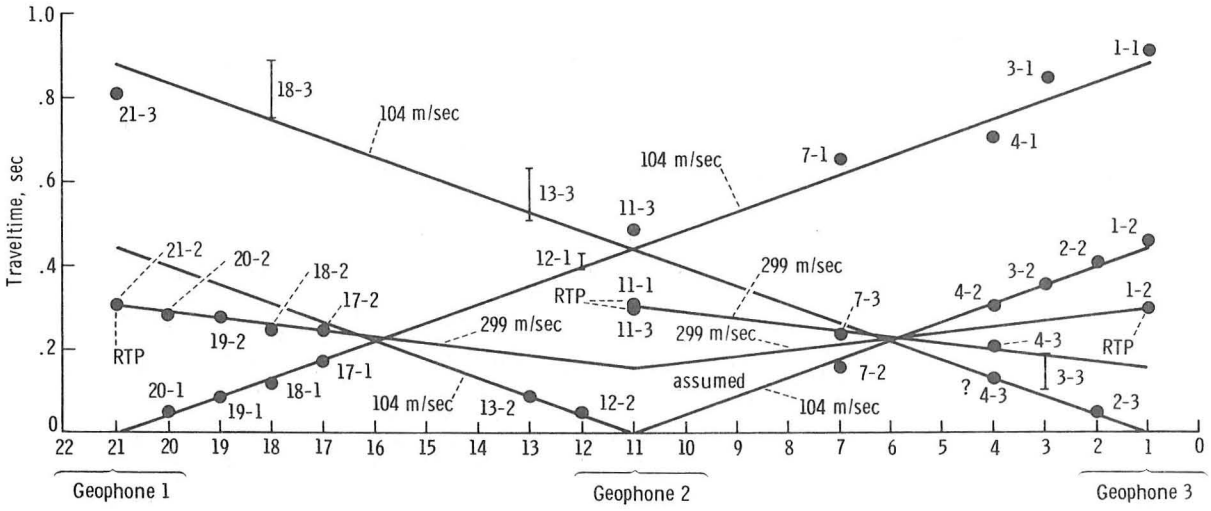

FIGURE 7–14.—Seismic arrivals from the thumper firings plotted on a traveltime/distance graph. The data points are shown as black circles; the first number refers to the thumper firing, the second number to the geophone on which the data were recorded. Reverse tie points are indicated as RTP; distance between thumper shot locations is 4.6 m.

very good agreement exists in reverse tie points (RTP); that is, the principle of seismic reciprocity states that traveltimes must be identical when the positions of a geophone and a shot (thumper firing) are interchanged. For example, the traveltime for thumper shot 21 to geophone 2 and thumper shot 11 to geophone 1 should be identical. The near identity of reverse tie points 21–2 and 11–1 and of 11–3 and 1–2 lends strength to the data interpretation. Agreement between reverse tie points 1–1 and 21–3 is somewhat poorer, but it should be remembered that the more distant thumper firings produced much weaker seismic signals for which it is difficult to determine unambiguously an initial onset. An example of traveltimes that cannot be precisely determined is 18–3, and the range of possible traveltimes is shown by the line.

Two P-wave velocities are evident in the traveltime data. A direct arrival is observed with a P-wave velocity of 104 m/sec together with a faster arrival possessing a velocity of 299 m/sec. No apparent variation exists in P-wave velocities across the section sampled as is evidenced by the conformance of seismic velocities measured along the geophone line.

The depth to the 299-m/sec refracting horizon is 8.5 m. It is proposed that this thin upper layer possessing a seismic velocity of 104 m/sec represents the fragmental veneer of unconsolidated particulate debris—the lunar regolith that covers the surface at the Fra Mauro site. If the discontinuity between the 104-m/sec and the 299-m/sec material is accepted as the base of the regolith, the thickness of the regolith is very similar to that estimated solely on geological evidence. By photographic studies of the depth at which blocky floors appear in fresh craters, it has been inferred that the fragmental, surficial layer that overlies the more consolidated or semiconsolidated substrate at the Fra Mauro site ranges in thickness from 5 to 12 m (ref. 7–3).

From measurement of the elapsed time between engine ignition and signal arrival at the Apollo 12 PSE for the reaction control system test firings and for the LM ascent, the compressional velocity of the lunar-surface material at the Apollo 12 site was determined to be approximately 108 m/sec

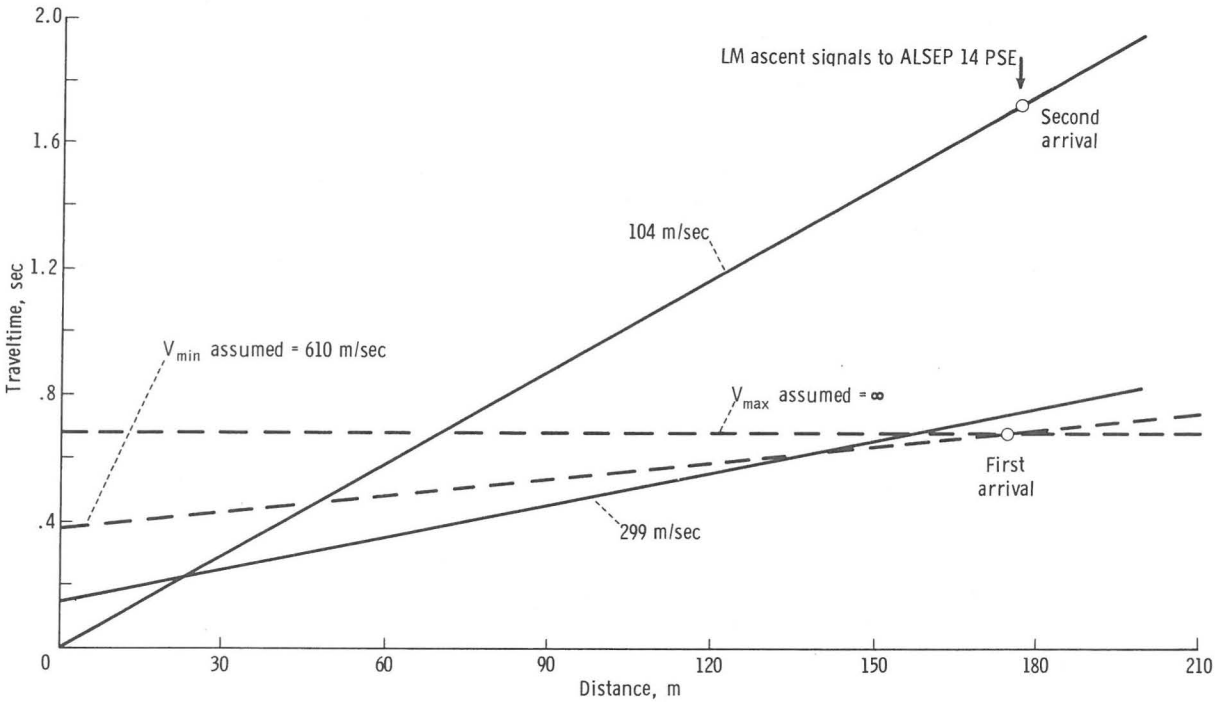

FIGURE 7–15.—First and second arrivals from the LM ascent as recorded by the PSE compared to the extrapolated traveltime/distance data derived from the thumper firings.

[55]

(ref. 7–4). This value is in exceedingly close agreement with that measured for the surface material at the Apollo 14 Fra Mauro site and is also consistent with estimates derived on the basis of mechanical properties measured by Surveyor (ref. 7–5). Therefore, it can be argued that the fragmental and comminuted layer that covers much of the lunar surface, although locally variable in thickness, possesses remarkably similar seismic or acoustic properties.

One other piece of evidence lends support to this hypothesis. Seismic signals were also generated by the LM ascent and recorded by the Apollo 14 PSE at a distance of 178 m (584 ft). These data are shown in figure 7–15 compared with the extrapolated traveltime/distance curves derived from the thumper firings of the ASE. The observed traveltime for the second arrival is nearly identical to that predicted for a direct seismic wave propagating with a velocity of 104 m/sec. A first arrival is observed with a traveltime somewhat faster than that predicted by a refraction from the top of the 299-m/sec horizon, suggesting that a material with a faster intrinsic compressional-wave velocity lies beneath the 299-m/sec material.

If the assumption is made that this underlying material possesses an infinite compressional-wave velocity V and that the traveltime curve behaves in the manner shown in figure 7–15, a maximum estimate to the thickness of the 299-m/sec material can be derived. Similarly, if only a modest increase in seismic velocity, such as to 610 m/sec (2000 ft/sec), in the underlying material is proposed, then a minimum estimate is obtained. These assumptions lead to a minimum thickness estimate of 38 m and a maximum thickness estimate of 76 m.

At this writing, it is somewhat premature to speculate what the 299-m/sec material represents other than to comment that this velocity is similar to that measured in situ in blocky basalt flows near Flagstaff, Ariz., or in blocky pumice deposits such as found at the Southern Coulee of the Mono Craters, California (ref. 7–6). However, no inference to a specific rock type should be made because a wide range of velocities is often determined for similar rocks, and similar velocities are often measured for widely different rock types. Nevertheless, it is interesting to point out that the thickness estimate of 38 m to 76 m for this material is not in disagreement with the postulated thickness of 100 m or so for the Fra Mauro Formation (ref. 7–3).

The relatively low compressional wave velocities that were measured by the ASE argue against the presence of substantial amounts of permafrost in the lunar near surface at this particular site. Measured velocities in permafrost vary greatly—depending on such factors as lithology, porosity, and degree of interstitial freezing—but typically range from 2438 to 4572 m/sec (8000 to 15 000 ft/sec) (ref. 7–7).

It has also been proposed (ref. 7–8) that the unconsolidated surface debris layer (the lunar regolith) together with a shattered crystalline layer forms a surface low-velocity zone to "trap" seismic surface waves effectively; this proposal helps to explain the prolonged reverberations recorded by the Apollo 12 PSE after the impact of the Apollo 12 LM and the Apollo 13 SIVB. However, the assumed working model consisted of a 30-m-thick, surface, low-velocity layer overlying crystalline material that has an intrinsic seismic velocity some 20 times greater than that of the surface-debris layer. To date, the results of the ASE argue against this hypothesis on a moonwide basis. Further details concerning the deeper structure of the lunar near surface of the Fra Mauro site must await the results from the ASE grenade firings.

References

7–1. McAllister, Bruce D.; Kerr, James; Zimmer, John; Kovach, Robert L.; and Watkins, Joel: A Seismic Refraction System for Lunar Use. IEEE Trans. Geosci. Electron., vol. GE–7, no. 3, July 1969, pp. 164–171.

7–2. Latham, G. V.; Ewing, M.; Press, F.; et al.: Passive Seismic Experiment. Sec. 6 of Apollo 11 Preliminary Science Report. NASA SP–214, 1969.

7–3. Offield, T. W.: Geologic Map of the Fra Mauro Site—Apollo 13, Scale 1:5000. USGS map, 1970.

7–4. Latham, G. V.; Ewing, M.; Press, F.; et al.: Passive Seismic Experiment. Sec. 3 of Apollo 12

Preliminary Science Report. NASA SP–235, 1970.

7–5. SUTTON, GEORGE H.; AND DUENNEBIER, FREDERICK: Elastic Properties of the Lunar Surface From Surveyor Spacecraft Data. J. Geophys. Res., vol. 75, no. 35, Dec. 1970, pp. 7439–7444.

7–6. WATKINS, J. S.: Annual Report, Investigation of In Situ Physical Properties of Surface and Subsurface Site Materials by Engineering Geophysical Techniques. NASA Contract T–25091 (G), July 1966.

7–7. BARNES, D. F.: Geophysical Methods for Delineating Permafrost. Proc. Int. Conf. Permafrost, NAS–NRC pub. 1287, 1965, pp. 349–355.

7–8. LATHAM, G. V.; EWING, M.; DORMAN, J.; PRESS, F.; ET AL.: Seismic Data From Man-Made Impacts on the Moon. Science, vol. 170, no. 3958, Nov. 1970, pp. 620–626.

Apollo 14 Active Seismic Experiment

Abstract. *Explosion seismic refraction data indicate that the lunar near-surface rocks at the Apollo 14 site consist of a regolith 8.5 meters thick and characterized by a compressional wave velocity of 104 meters per second. The regolith is underlain by a layer with a compressional wave velocity of 299 meters per second. The thickness of this layer, which we interpret to be the Fra Mauro Formation, is between 16 and 76 meters. The layer immediately beneath this has a velocity greater than 370 meters per second. We found no evidence of permafrost.*

A seismic refraction experiment was carried out during the Apollo 14 mission with the purpose of determining the near-surface properties of the moon to a depth of approximately 460 m (1500 feet). This experiment, called the Active Seismic Experiment (ASE), differs from the Passive Seismic Experiment in that it utilizes explosive sources and an array of geophones. The experiment also operates in a passive mode during intermittent listening periods.

Two seismic energy sources are used, a thumper device activated by the astronauts and a mortar package containing four high-explosive grenades. The grenades are launched by rocket by command from the earth and are designed to impact at ranges up to 1524 m (5000 feet).

Apollo 14 astronauts detonated 13 of 21 explosive initiators and deployed the mortar package during the mission. Because of possible hazards to other experiments in the vicinity, the four grenades will be launched later, when the collection of essential data in other experiments is complete. The instrumentation for the experiment has been described elsewhere (*1*).

Typical seismic data recorded from thumper shots are shown in Fig. 1. The ASE operates in a passive listening mode for a 30-minute period each week. (Since the ASE data stream preempts all other experimental data, the experiment cannot be left on continuously.) Data for two events, recorded in the passive mode on 19 February 1971, are shown in Fig. 2. The signal amplitude is largest at a single geophone. The signal is discernible above the ambient noise level but greatly reduced in amplitude on the other geophone channels.

The signals recorded in the passive mode are similar to those produced by thumper firings close to a geophone but 100 to 200 times smaller in amplitude. They are also strikingly similar to the signals for type-X events (impulsive beginnings and relatively short durations, normally less than 10 seconds) recorded during the Apollo 11 mission (*2*). The latter may have been produced by direct micrometeoroid impacts on the Passive Seismic Experiment (PSE).

Figure 3 is a section of a composite record of all the thumper data recorded by geophone 2. This figure shows the change in wave form and shift in arrival time of wavelets as a function of the distance from source to receiver.

Two P-wave (compressional wave) velocities are represented in the travel-time data, 104 m/sec for a direct arrival and 299 m/sec for a faster arrival. The layers of material characterized by these velocities are designated A (104 m/sec) and B (299 m/sec). No variation appears in P-wave velocities across the section sampled.

Seismic signals were also generated by the ascent of the lunar module and recorded by the Apollo 14 PSE at a distance of 178 m (584 feet). The travel time for the second arrival is nearly identical to that predicted for a direct seismic wave propagating with a velocity of 104 m/sec. A first arrival has a travel time somewhat faster than that predicted from a refraction from the top of the horizon (layer B), which suggests that a material with a faster intrinsic compressional wave velocity lies beneath layer B.

If the assumption is made that this underlying material possesses an infinite compressional wave velocity, a maximum estimate of the thickness of layer B can be derived. Similarly, if it is assumed that the critical distance for the arrival of the head wave traveling through the underlying material is 100 m (that is, at the end of the geophone line), a minimum velocity of 370 m/sec is obtained in this layer, which is designated layer C. Calculations indicate that the range of possible thicknesses for layer B is between 16 and 76 m.

The velocity 104 m/sec is characteristic of a porous and highly brecciated rock material such as the lunar regolith. This layer (A) is 8.5 m thick. The nature of layer B is less clear. The geophone line lies in part on Eratosthenian Crater cluster material, which Offield (*3*) interpreted as having been derived from clusters of primary craters or secondary craters of an unknown source. Craters from which such cluster material is derived are not large (300 to 400 m in diameter), and the minimum thickness of 16 m that we calculate for layer B is more than one would expect from craters of this size.

A more likely explanation for the origin of this layer is that it is either the smooth terrain material of Offield (*3*) or the Fra Mauro Formation. According to Offield, the smooth terrain material is "similar to nearby plains material of presumed volcanic origin . . . of uncertain thickness," and the Fra Mauro Formation consists of "material

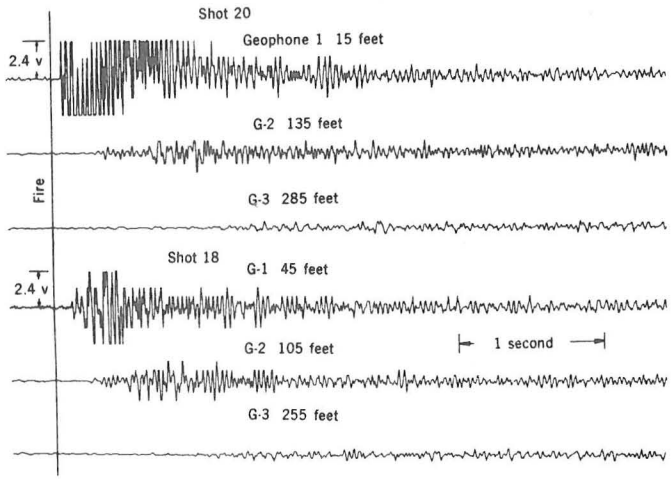

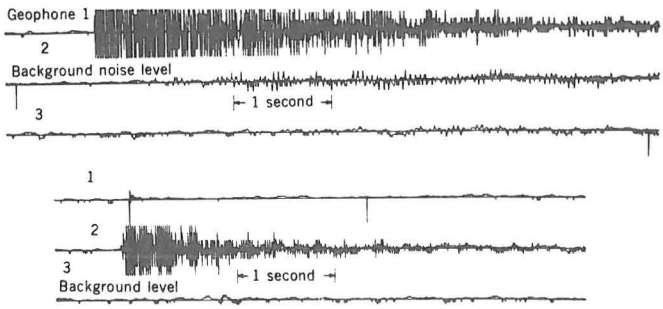

Fig. 1 (left). Seismic signals produced by thumper firings 18 and 20 on the lunar surface (1 foot = 0.3 m). Fig. 2 (right). Signals recorded during the passive listening mode on 19 February 1971.

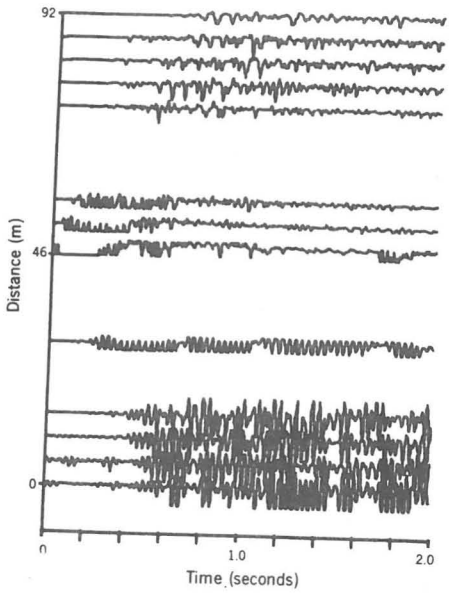

Fig. 3. Seismic signals produced by thumper firings, as recorded at geophone 2. The traces are aligned at the instant of firing of the thumper.

of ejecta blanket surrounding the Imbrium basin."

We have examined two aspects of the Apollo 14 seismic data in an attempt to deduce evidence supporting one or the other of the above models, that is, smooth terrain material or Fra Mauro Formation. First, we calculated the thicknesses of overlapping ejecta blankets from craters near the Apollo 14 site. We considered only those craters younger than the Fra Mauro Formation and extended our calculations to a maximum distance of 1000 km. Details of the results of these calculations are forthcoming [see Hu and Watkins(*4*)]. The calculation scheme was empirical but appears to have given good results.

For the Apollo 14 site, the calculated regolith thickness is 3.9 to 7.2 m. The calculated range of thickness of the Fra Mauro Formation is 5.5 to 15.6 m (*4*). The observed thickness of layer A and the minimum thickness of layer B calculated from seismic data are thus approximately the same as the maximum thicknesses calculated for the regolith and the Fra Mauro Formation, respectively (*4*).

Watkins *et al.* (*5*) measured in situ velocities in a number of different rock types with possible lunar analogs. Their results are compared with lunar data in Fig. 4. Lunar data and data from the Meteor Crater, Arizona, ejecta blanket are shown in solid circles. The porosity of the Apollo 14 regolith was assumed to be the same as that of the Apollo 11 regolith (*6*). The relatively lower velocities of the lunar rocks in comparison with terrestrial rocks of comparable porosities is probably due to the greater degree of brecciation of the lunar and Meteor Crater rocks.

Because of brecciation in lunar rock, it is more meaningful to estimate the porosity of layer B and compare it with the porosities of terrestrial rocks than to compare the velocities directly. A solid line in Fig. 4 indicates our estimated range of porosity of layer B, 35 to 55 percent. Watkins *et al.* (*5*) include three terrestrial rock units whose velocities or structure, or both, might be appropriate: (i) ejecta blanket, Meteor Crater, porosity 40 percent; (ii) rhyolite ash and lapilli, Mono Craters, California, porosity 46 percent; and (iii) S. P. andesitic lava flow, Arizona, porosity 56 percent.

We conclude that layer A is the lunar regolith. The layer is 8.5 m thick beneath the geophone line at the Apollo 14 site, and it appears to be comprised mainly of overlapping ejecta blankets from post-Fra Mauro craters.

This layer is underlain by a layer whose thickness is calculated to be from 16 to 76 m and whose characteristic wave velocity is 299 m/sec. The abrupt change in seismic velocity and, by inference, in other physical properties of layer B indicate a major change in the nature of the evolution of lunar near-surface rocks. The estimated porosity of layer B, between 35 and 55 percent (layer A has an inferred porosity of 48 percent), indicates that it is not solid rock, but is very porous and possibly highly fractured.

The calculated thickness of the Fra Mauro Formation at the Apollo 14 site is slightly less than the minimum thickness inferred for layer B, but, if variations in the thickness of the Fra Mauro Formation and inaccuracies in the calculations are taken into account, the discrepancy does not seem unreasonable.

Photogeologic mapping of the area around the Apollo 14 site suggests that layer B might consist of Fra Mauro material or possibly of volcanics. Both explanations are consistent with the observed velocities. However, if layer B is volcanic, it is difficult to understand why so few igneous rocks were returned by Apollo 14 astronauts (*7*), since a number of young craters in the vicinity have penetrated into and through the layer.

The velocity and inferred porosity of layer B are comparable with those observed in the upper part of Meteor Crater ejecta (40 percent porosity) and, thus, quite reasonable for ejecta from Mare Imbrium. The change in inferred

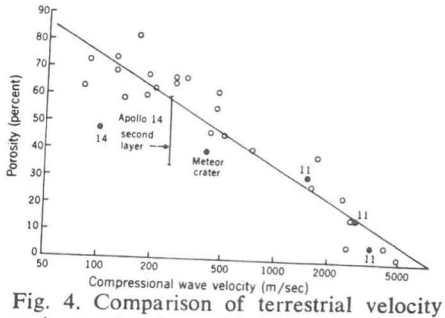

Fig. 4. Comparison of terrestrial velocity and porosity data with lunar data. (Open circles) Terrestrial data. (Solid circles) lunar data of Meteor Crater, Arizona, data. The numbers refer to the Apollo missions that provided the data.

porosity between layer A and layer B is small but significant. For a porous, highly fractured rock such as one would expect in the Mare Imbrium ejecta, continued bombardment and diminution of particle size would increase the porosity only slightly. We, therefore, conclude that layer B is the Fra Mauro Formation.

Evidence regarding the underlying layer (C) is inconclusive at the present time. The relatively low compressional wave velocities that were measured by the ASE argue against the presence of substantial amounts of permafrost in the lunar near-surface at this particular site. Velocities in permafrost vary greatly—depending on such factors as lithology, porosity, and degree of interstitial freezing—but typically range from 2438 to 4572 m/sec (*8*).

JOEL S. WATKINS
Department of Geology, University of North Carolina, Chapel Hill 27514
ROBERT L. KOVACH
Department of Geophysics, Stanford University, Stanford, California 94305

References and Notes

1. R. L. Kovach, J. Watkins, T. Landers, *Apollo 14 Preliminary Science Report* (NASA SP-272, National Aeronautics and Space Administration, Washington, D.C., 1971), p. 163.
2. G. V. Latham, M. Ewing, F. Press, G. Sutton, J. Dorman, N. Toksoz, R. Wiggins, Y. Nakamura, J. Derr, F. Duennebier, *Apollo 11 Preliminary Science Report* (NASA SP-214, National Aeronautics and Space Administration, Washington, D.C., 1969), p. 143.
3. T. W. Offield, *U.S. Geologic Survey Map ORB-III-S-23* (*25*) (U.S. Geological Survey, Washington, D.C., 1970).
4. T. Hu and J. S. Watkins, *Trans. Amer. Geophys. Union* **52**, 273 (1971).
5. J. S. Watkins, L. A. Walters, R. H. Godson, *Geophysics*, in press.
6. N. Costes, W. Carrier, J. Mitchell, R. Scott, *Science* **167**, 739 (1970).
7. P. R. Brett and members of the Apollo 14 Preliminary Examination Team, *Trans. Amer. Geophys. Union* **52**, 265 (1971).
8. D. F. Barnes, in *Proceedings of an International Conference on Permafrost* (NAS-NRC 1287, National Academy of Sciences–National Research Council, Washington, D.C., 1966), p. 349.
9. Supported by NASA contract NAS 9-5632.

24 September 1971; revised 9 December 1971

10. Active Seismic Experiment

Robert L. Kovach,[a†] Joel S. Watkins,[b] and Pradeep Talwani[a]

The purpose of the active seismic experiment (ASE) is to generate and monitor seismic waves to study the lunar near-surface structure. Specifically, how thick is the lunar regolith at the Apollo 16 site? What are the acoustic or seismic properties of the lunar near-surface material? Are there any distinct seismic horizons and do they correlate with our estimates of geological horizons? Is there a characteristic difference in the shallow seismic velocities between the maria and the highlands? Several seismic energy sources are used: an astronaut-activated thumper device, a mortar package that contains rocket-launched grenades, and the impulse produced by the lunar module (LM) ascent.

To date, analysis of some seismic signals recorded by the ASE has provided data concerning the near-surface structure at the Descartes landing site. Two compressional (P-wave) seismic velocities have so far been recognized in the seismic data. The lunar surface material (fig. 10-1) has a seismic wave velocity of 114 m/sec. Underlying this surficial material at a depth of 12.2 m, the lunar rocks have a velocity of 250 m/sec. The 114-m/sec material velocity is assigned to the lunar regolith and agrees closely with the surface velocity measured at the Apollo 12, 14, and 15 landing sites; this agreement indicates that no major regional difference exists in the near-surface acoustical properties of the Moon.

The material underlying the regolith does not indicate that competent lava flows exist in the Cayley Formation at the Apollo 16 site. Instead, this velocity of 250 m/sec is suggestive of brecciated material or impact-derived debris of as yet undetermined thickness. Further analyses of the ASE grenade seismic signals should give more information on the deeper structure at the Apollo 16 landing site.

[a]Stanford University.

[b]University of North Carolina.

[†]Principal Investigator.

INSTRUMENT DESCRIPTION AND PERFORMANCE

The ASE consists of a thumper and geophones, a mortar package assembly (MPA), electronics within the Apollo lunar surface experiments package (ALSEP) central station, and interconnecting cabling. The components of the ASE are shown in figure 10-2.

The astronaut-activated thumper is a short staff used to detonate small explosive charges – single bridgewire Apollo standard initiators. Twenty-one initiators are mounted perpendicular to the base plate at the lower end of the staff. A pressure switch in the base plate detects the instant of initiation. An arm-fire switch and an initiator-selector switch are located at the upper end of the staff. A cable connects the thumper to the central station to transmit real-time event data. The thumper also stores the three geophones and connecting cables until deployment on the lunar surface.

The three identical geophones are miniature seismometers of the moving coil-magnet type. The coil is the inertial mass suspended by springs in the magnetic field. Above the natural resonant frequency of the geophones (7.5 Hz), the output is proportional to ground velocity. The geophones are deployed at 3-, 48-, and 93-m (10-, 160-, and 310-ft) intervals in a linear array from the central station and are connected to it by cables.

A three-channel amplifier and a logarithmic compressor condition the geophone signals before conversion into a digital format for telemetry to Earth. The low signal-to-noise ratios expected and the lack of knowledge as to the character of the expected waveforms made it desirable to widen the frequency response as much as possible within the constraints of the digital sampling frequency of 500 Hz. Because signal levels were expected to be distributed throughout the system dynamic range, a logarithmic compression scheme was selected to give signal resolution as some constant fraction of signal amplitude. The Apollo 16 system has the properties listed in table 10-I.

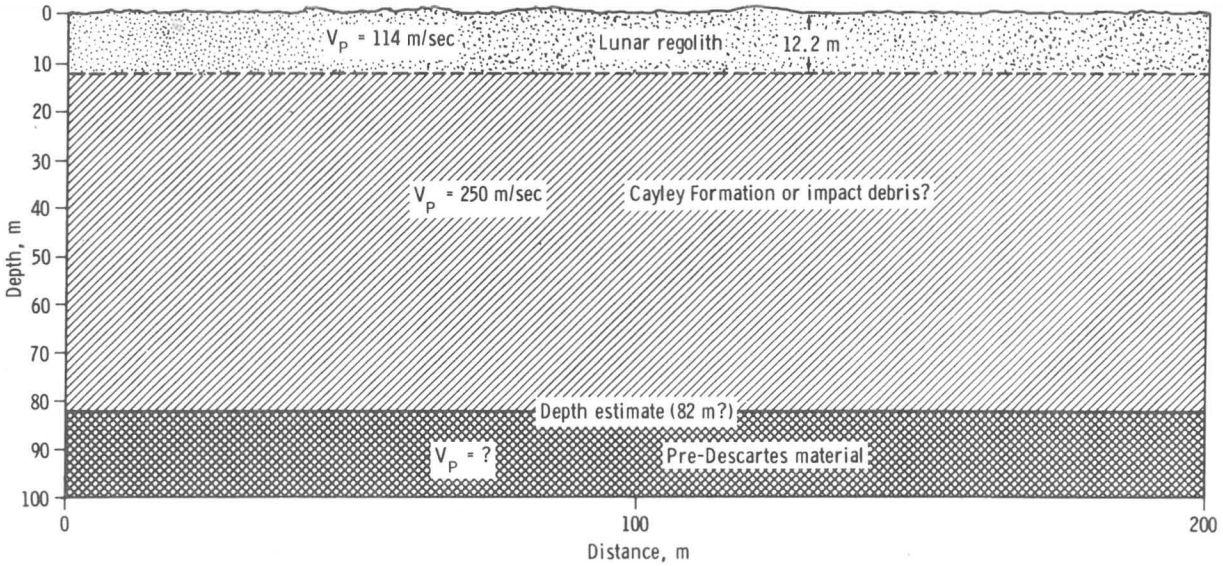

FIGURE 10-1.–Seismic cross section at the Descartes landing site (V_p = seismic wave velocity).

The MPA comprises a mortar box, a grenade-launch-tube assembly, and interconnecting cables. To provide an optimum launch angle for the grenades, the MPA is deployed at an angle approximately 45° to the lunar surface. A two-axis inclinometer provides pitch- and roll-angle (deviation from the 45° nominal and vertical) information on the MPA. The mortar box is rectangular and is made of fiber glass and magnesium; the grenade-launch-tube assembly containing four grenades is mounted in the mortar box.

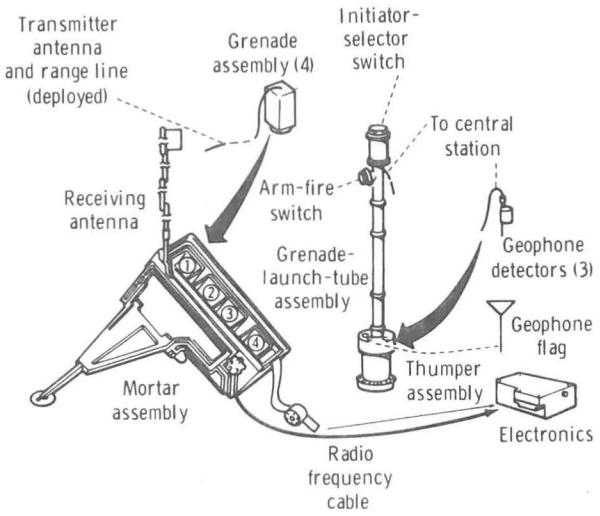

FIGURE 10-2.–Drawing of the ASE.

The forward end of the mortar box is beveled at 45° so that, in the deployed position, the MPA rests upon the 45° bevel. The remainder of the package is supported by two legs that are unfolded and locked into place during deployment. The mortar box is anchored to a pallet assembly in the final deployment. Four 17.8-cm (7-in.) stakes are mounted on the underside of the pallet to provide a stable platform for the grenade launchings.

Each grenade is attached to a range line, which is a thin-stranded cable wound around the outside of the launch tube. Two fine copper wires are looped around each range line. The first loop is spaced so that it will break when the grenade is approximately 0.4 m (16 in.) from the launch tube. A second loop is spaced to break when the range line has deployed an additional 8 m (25 ft) from the first breakwire. Breaking the loops starts and stops a range-gate pulse to establish a time interval for the determination of the initial grenade velocity.

The four grenades are similar but differ in the amount of propellant and high explosive (table 10-II). Each grenade has a square cross section with a thin fiber-glass casing. The casing contains the rocket motor, safe slide plate, high-explosive charge, ignition and detonation devices, thermal battery, and a 30-MHz transmitter. The range line is attached to the transmitter to serve as a half-wave end-feed antenna.

In operation, an arm command from ground

TABLE 10-I.– Apollo 16 ASE Characteristics

Component characteristics	*Channel no.*		
Geophones:	1	2	3
Generator constant, V/m/sec	255	255	257
Frequency, Hz	7.42	7.44	7.39
Resistance, ohm	6090	6212	6204
Amplifiers:			
Noise level, mV rms at input	.266	.100	.133
Dynamic range, rms signal to rms noise in dB at 10 Hz	84.4	92.4	90
Gain (at 10 Hz) and V_{input} = 2.75 mV peak to peak	698	684	709
Log compressor (compression accuracy for temperature range 288° to 323° K):			
Positive signal error, percent	4.04	3.63	4.83
Negative signal error, percent	2.46	1.87	1.88
System:			
Signal-to-noise ratio (rms signal to rms noise in dB for a 10-nm peak-to-peak signal at 10 Hz)	38.9	37.9	45.0
Minimum discernible signal (based on 0.5-mV zero-to-peak input equal to 1 digital unit at low level)			
Zero to peak at 1 Hz, nm	4	4	4
Zero to peak at 4 Hz, nm	.3	.3	.3
Zero to peak at 10 Hz, nm	.1	.1	.1
Zero to peak at 20 Hz, nm	.05	.05	.05

TABLE 10-II.– Apollo 16 Nominal ASE Grenade Parameters

Parameter	*Grenade no.*			
	1	*2*	*3*	*4*
Range, m	1 500	900	300	150
Mass, g	1 261	1 024	775	695
High-explosive-charge mass, g	454	272	136	45
Rocket-motor mean peak thrust, N	22 224	11 112	7556	5556
Mean velocity, m/sec	50	38	22	16
Lunar flight time, sec	44	32	19	13
Rocket-motor-propellant mass, g	42	27	15	10
Propellant pellets, no.	2 365	1 520	620	570
Launch angle, deg	45	45	45	45
Rocket-motor thrust duration, msec	6.0	7.5	10.5	8.5

control applies a pulse to charge condensers in the mortar box and the grenade; a fire command discharges the condenser through an initiator, which ignites the rocket motor. When the grenade leaves the tube, a spring-ejected safe slide is removed, activating a microswitch in the grenade.

A thermal battery and the electronics in the grenade make up the firing circuit. The microswitch discharges a condenser across a thermal match to activate the thermal battery, which in turn powers the transmitter and produces a capacitor charge for the detonator. At impact, an omnidirectional impact switch closes, discharging the capacitor into the detonator to ignite the explosive. The explosion terminates radio frequency transmission as an indication of detonation time. The critical parameters

measured are the detonation time, time of flight, initial velocity, and launch angle. Because of the ballistic trajectory followed by the grenades in the lunar vacuum, the necessary data are available to determine grenade range. The mortar mode of operation for the ASE is shown in figure 10-3.

Because some of the geophone parameters might change on the lunar surface, a calibrator circuit is provided to measure these parameters to within 10 percent of the preflight values. The damping resistance across the geophone is altered to underdamp the geophone, and current is introduced into the geophone coil to react with the magnetic field of the geophone, producing a force on the geophone coil. This force moves the coil and, with an underdamped geophone, the signal from the geophone is a logarithmically decaying sinusoidal signal. Analysis of similar calibration pulses transmitted after thumper operations on the Moon demonstrated close agreement of the natural frequency and generator constant of the geophones with measured preflight values.

The ASE system is controlled from Earth by a number of commands that control such functions as switching to high bit rate and firing the grenades from the mortar box assembly. Further technical details of the ASE can be found in references 10-1 and 10-2.

DEPLOYMENT

At the Apollo 16 site, the three geophones are alined on a highly cratered uneven area at a bearing of 287° (clockwise from north) from the ALSEP central station (fig. 6-13, sec. 6). Figure 10-4 shows the commander (CDR) standing at the middle geophone flag during thumper operations.

Minor difficulty was experienced in the deployment of the MPA pallet, and one of the four stakes was not implanted. The MPA was leveled and armed to fire the four grenades on command to distances of 150, 300, 900, and 1500 m in a direction bearing 287° clockwise from north. Figure 10-5 shows the deployed MPA on the lunar surface. A closeup view of the MPA on the special pallet is shown in figure 10-6. Near the end of the third period of extravehicular activity (EVA), the MPA roll sensor was observed to be reading off scale. However, a television panorama taken near the end of the EVA

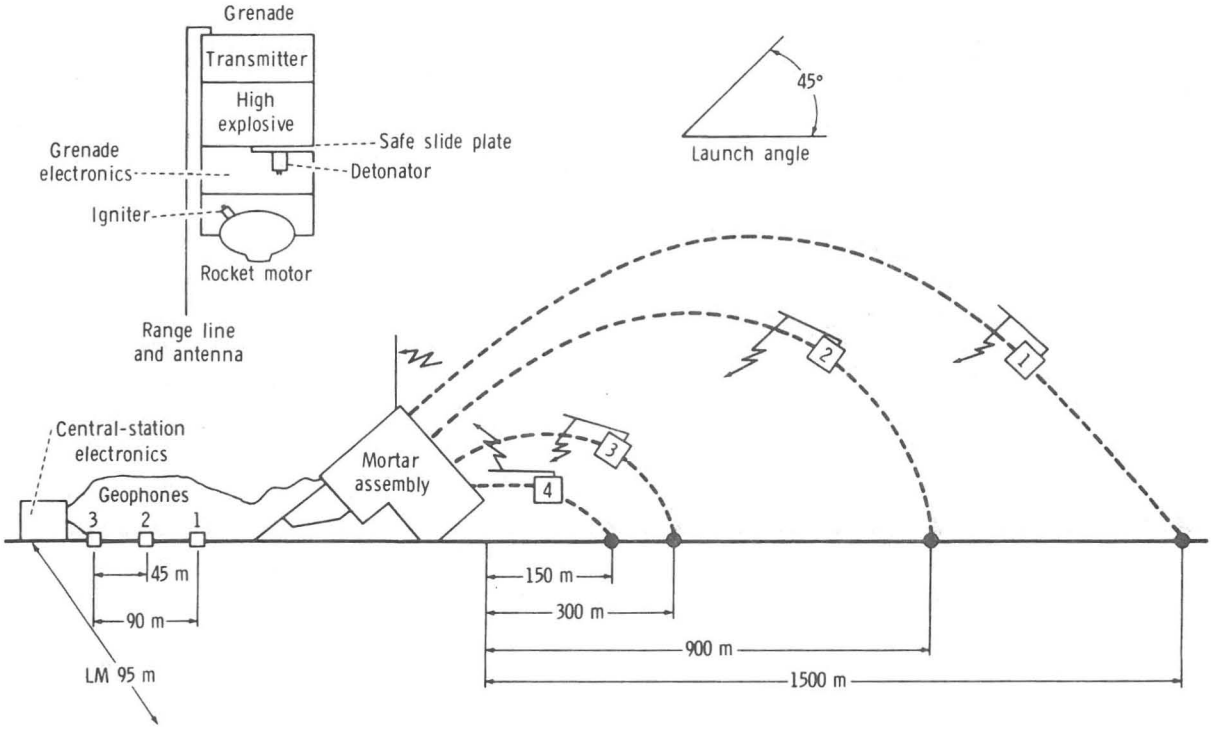

FIGURE 10-3.–Schematic drawing showing the mortar mode of operation for the ASE.

verified that the MPA was properly positioned and alined, suggesting that the roll sensor was inoperative.

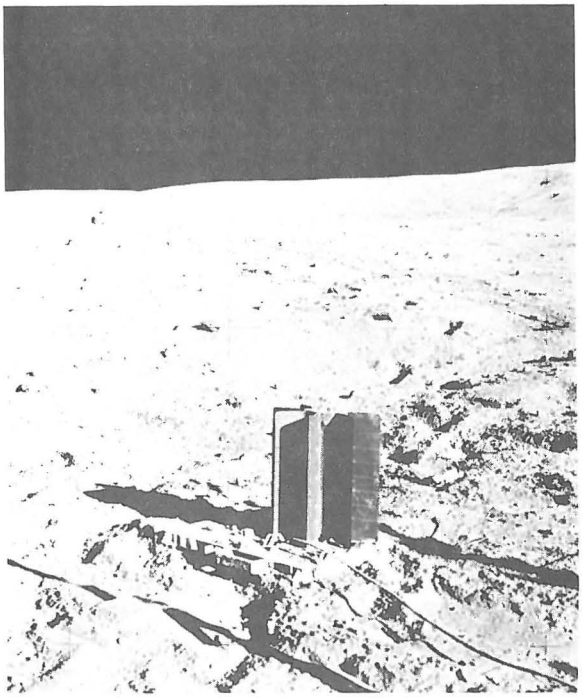

FIGURE 10-4.–The CDR firing the thumper along the geophone line on the lunar surface (AS16-113-18352).

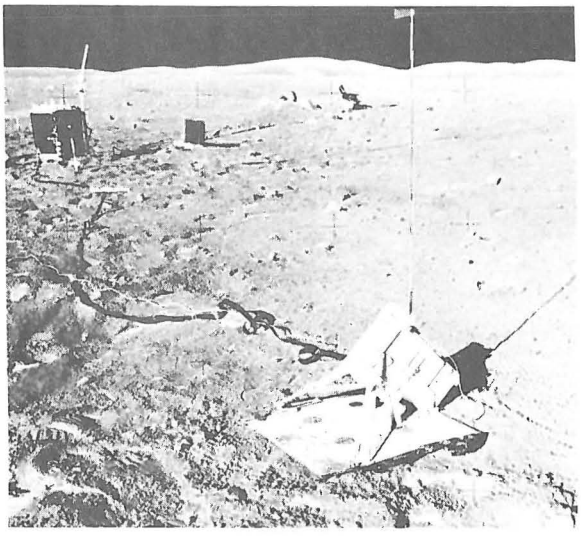

FIGURE 10-5.–Photograph of the deployed mortar assembly on the lunar surface. The MPA is aimed to fire to the right, parallel to the geophone line (AS16-113-18379).

The ALSEP central station was commanded to the high-bit-rate mode at 19:54:30 G.m.t. on April 21, 1972, to record the ASE/thumper mode of operation. Thumping operations began at 20:01:52 G.m.t. at geophone 3 (farthest from the ALSEP central station) and proceeded at 4.75-m (15-ft) intervals (except between positions 11 and 12 and positions 18 and 19, which are at 9.5-m (30-ft) intervals) toward geophone 1 (nearest to the central station). The final thumper shot was fired at 20:16:08 G.m.t., which resulted in a 14-min time line.

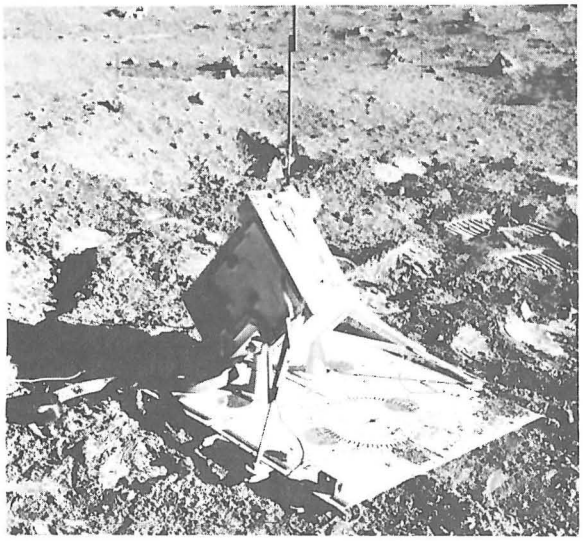

FIGURE 10-6.–Closeup view of the deployed MPA on the lunar surface (AS16-113-18380).

The central station was commanded to normal bit rate at 20:16:32 G.m.t. The thumper was fired at 19 cable positions. Two attempts were needed to fire the thumper at position 2, but this was not due to equipment malfunction. Analysis of the real-time data records shows that the thumper was not armed for the necessary 5 sec prior to firing. Seismic signals were recorded at all three geophones for all 19 thumper firings.

The ALSEP central station was also commanded to high bit rate at 01:06:00 G.m.t. on April 24 to record the impulse produced by the LM ascent. A large seismic signal was recorded by the geophone array. The ALSEP central station is periodically scheduled for the high-bit-rate mode for passive listening to detect seismic signals and to verify experiment operational capability.

On May 23, the ALSEP was commanded to high bit rate between 05:20:00 and 06:44:00 G.m.t. for the ASE/mortar mode of operation. Three of the four high-explosive grenades in the MPA were successfully launched to distances of approximately 900, 150, and 300 m. The decision was made not to launch grenade number 1 (1500 m) because the grenade launch assembly pitch angle sensor went off scale high. This off scale indication made the pitch position of the launch assembly uncertain.

Analyses of the engineering data recorded during the grenade firings indicated that the range line apparently malfunctioned so that initial grenade velocity data were lost. Nevertheless, range data were obtained from knowledge of the initial angle of launch and the time of flight by using the equations

$$T = \frac{2V_I \sin\theta}{g} \qquad R = V_I \cos\theta\, T \qquad (10\text{-}1)$$

where T = time of flight
V_I = computed initial velocity
θ = launch angle
g = lunar gravity
R = range

The validity of this approach was confirmed because of seismic data overlap from the LM ascent.

DESCRIPTION OF RECORDED SEISMIC SIGNALS

Thumper Mode

During thumper operations on the lunar surface, the CDR was instructed to stand still for 10 sec before and 10 sec after each firing. Therefore, 10 sec

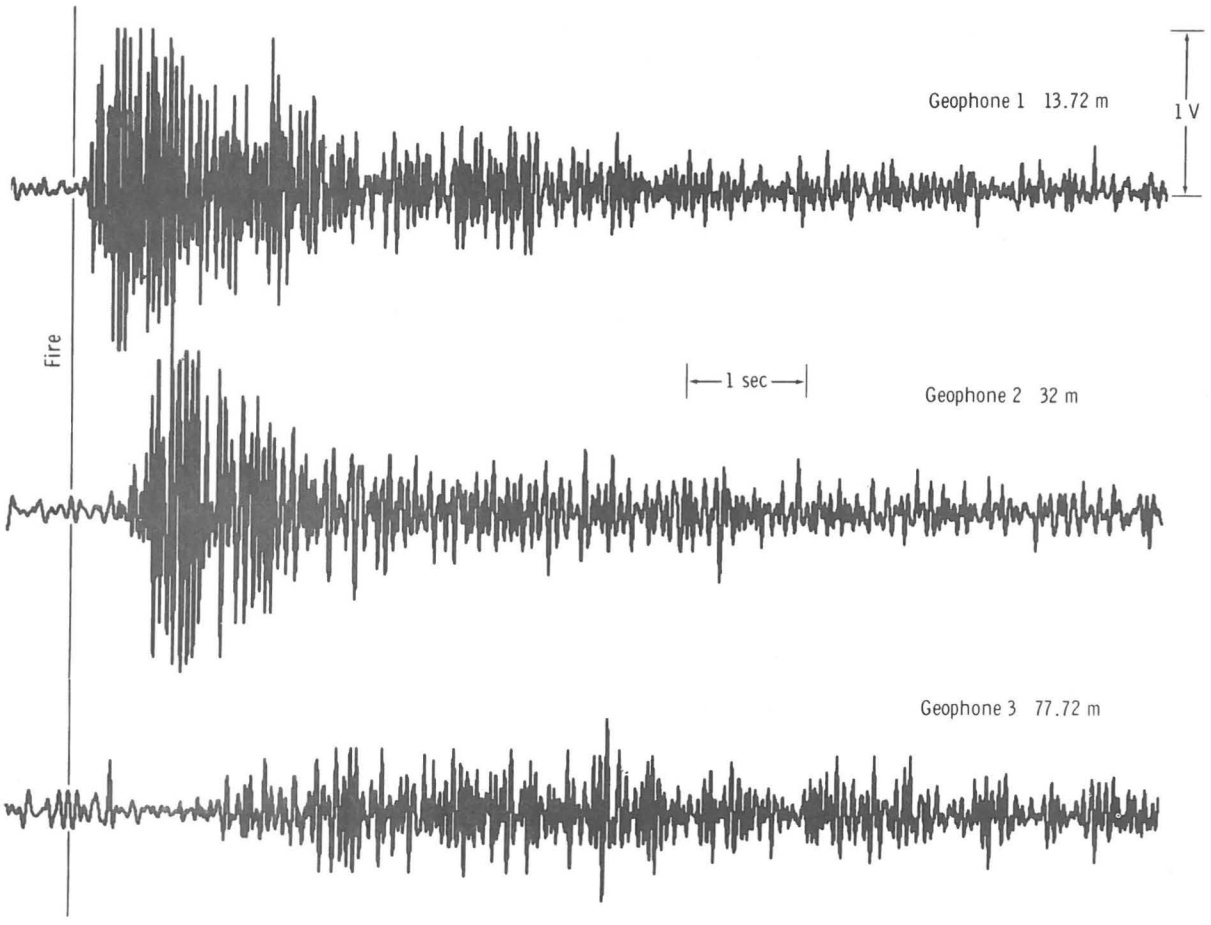

FIGURE 10-7.–Seismic signals produced by thumper firing 17 on the lunar surface.

of seismic data were recorded for each thumper firing. The seismic data recorded for thumper shot 17 are shown in figure 10-7. Examination of these signals reveals that thumper firings within approximately 15 m of a geophone have impulsive beginnings and that the seismic signals have more emergent beginnings with increasing distance. Power spectra for a typical thumper shot are shown in figure 10-8. The spectra are uncorrected for instrument response inasmuch as the ASE has a flat response to input ground velocity over the frequency band from 3 to 100 Hz. The predominant frequency of the thumper signals is 22 Hz.

Figure 10-9 is a record section alined in time to the same instant of firing for thumper shots 2 to 10 as recorded at geophone 2. Little difficulty exists in selecting the onset of the seismic signals to a distance of 41 m; however, at greater distances, uncertainty arises in determining the beginning of the seismic wave arrival because of the more emergent onset. Figure 10-10 is an expanded time scale record section for thumper shots 2 to 9 as recorded at geophone 3. The arrows point to unambiguous onsets of clear first and second arrivals.

Lunar Module Ascent

A signal of particular interest was generated by the thrust of the LM ascent engine. The resulting seismic signal was recorded by the ASE geophone array at distances of 95, 121, and 157 m (fig. 10-11). The arrows point to the measured first and second seismic wave arrivals at the individual geophones. Power spectra of the seismic signals produced by the LM ascent (fig. 10-12) show that most of the signal is concentrated in the frequency band from 5 to 8 Hz. Interpretation of the traveltime curve and related data are given in the subsection entitled "Discussion."

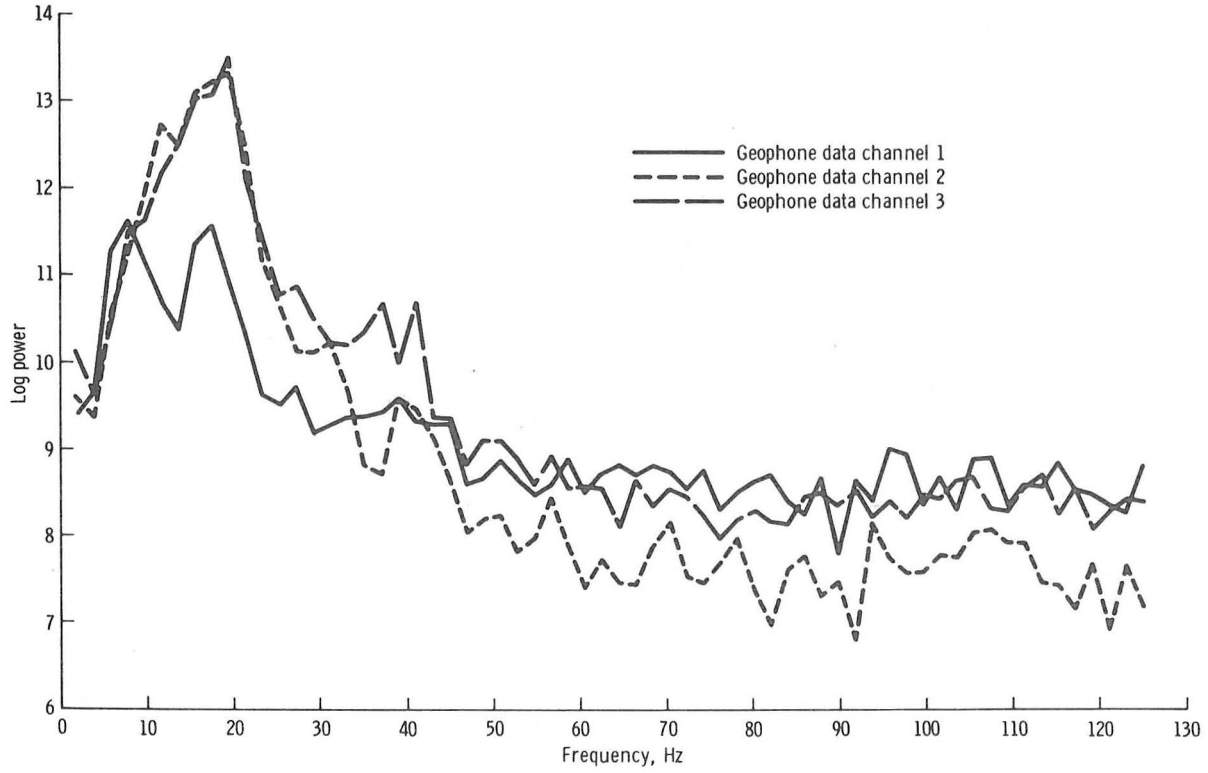

FIGURE 10-8.–Power spectra of seismic signals produced by thumper firing 8.

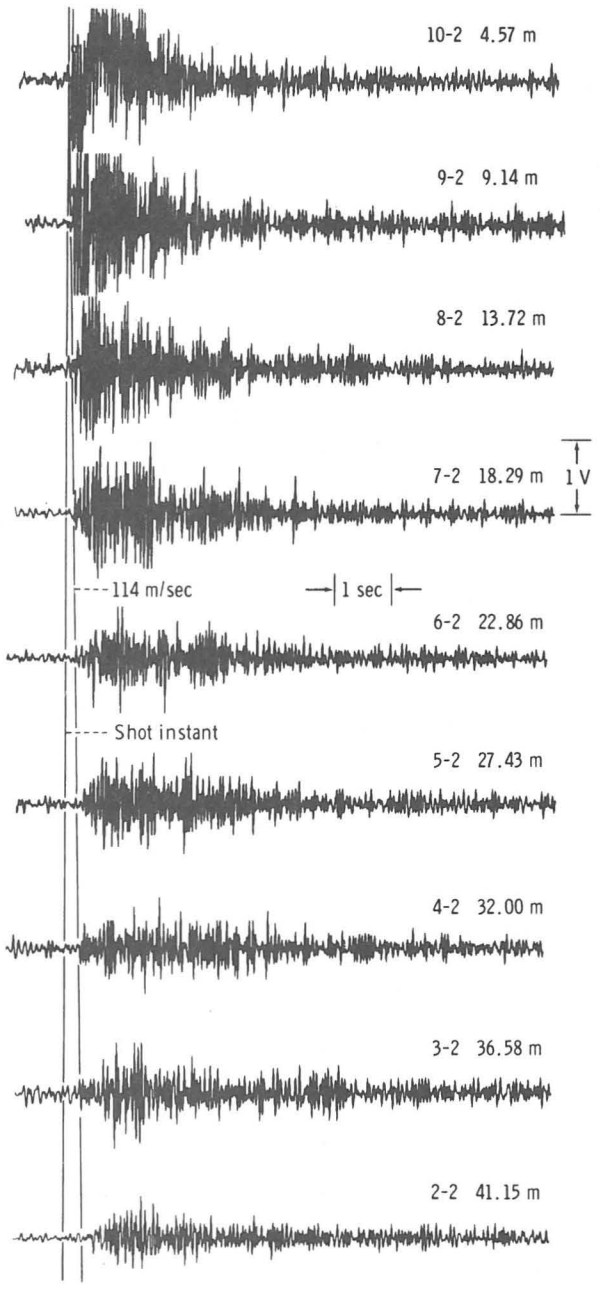

FIGURE 10-9.–Seismic signals produced by thumper firings 2 to 10 as recorded at geophone 2. The traces are alined to the same relative instant of the firing of the thumper. The line marked 114 m/sec is alined to the measured onset of the seismic signal. (The first number in the data identifier is the thumper firing, and the second number is the geophone on which the data were recorded.)

Mortar Firings

The ASE mortar package assembly was located 14 m from geophone 1, pointed to fire parallel to the geophone line and down range toward geophone 3. Firing of grenade 2 was an initial surprise in that the rocket-motor ignition produced a sufficient impulse against the mortar pallet to generate a seismic signal detected by the ASE geophones (fig. 10-13). The seismic signals produced by subsequent grenade launch "thumps" were almost identical in character and form, differing only in overall amplitude. Examination of the power spectra for a grenade launch signal (fig. 10-14) clearly shows the higher frequency content of the signal for the geophone that was closest to the MPA. The signal recorded at geophone 1 (14 m) has a spectral peak at 20 Hz, whereas the signal recorded at geophone 3 (5 m) peaks at approximately 14 Hz.

The seismic signals produced by the detonation of grenade 4 are shown in figure 10-15. This grenade was launched at an angle of 33.67° and had a flight time of 10.785 sec, which resulted in a distance of 48 m from this impact to geophone 3. The seismic records are noisy prior to the onset of the impact signal because the signals produced by the grenade launch itself have not completely decayed to low-level prefiring conditions. Nevertheless, the desired signal can be recognized on the basis of a change in frequency, inasmuch as the power spectra for the impact signals reveal a predominant signal frequency of 10 Hz (fig. 10-16), compared to 15 to 20 Hz for the grenade launch signal. It is expected that narrow band pass and velocity filtering will enhance the desired signals. Furthermore, because the individual grenade launch signals were closely reproducible from launch to launch, a simple noise subtraction procedure can be used. Work is still proceeding on analyses of the grenade 2 (900 m) and 3 (300 m) detonation signals.

DISCUSSION

The traveltime/distance data obtained from the thumper firings are shown in figure 10-17. An example of traveltimes that cannot be precisely determined is shot 10-3, and the range of possible traveltimes is shown by the height of the line. Thumper firings beyond a distance of approximately

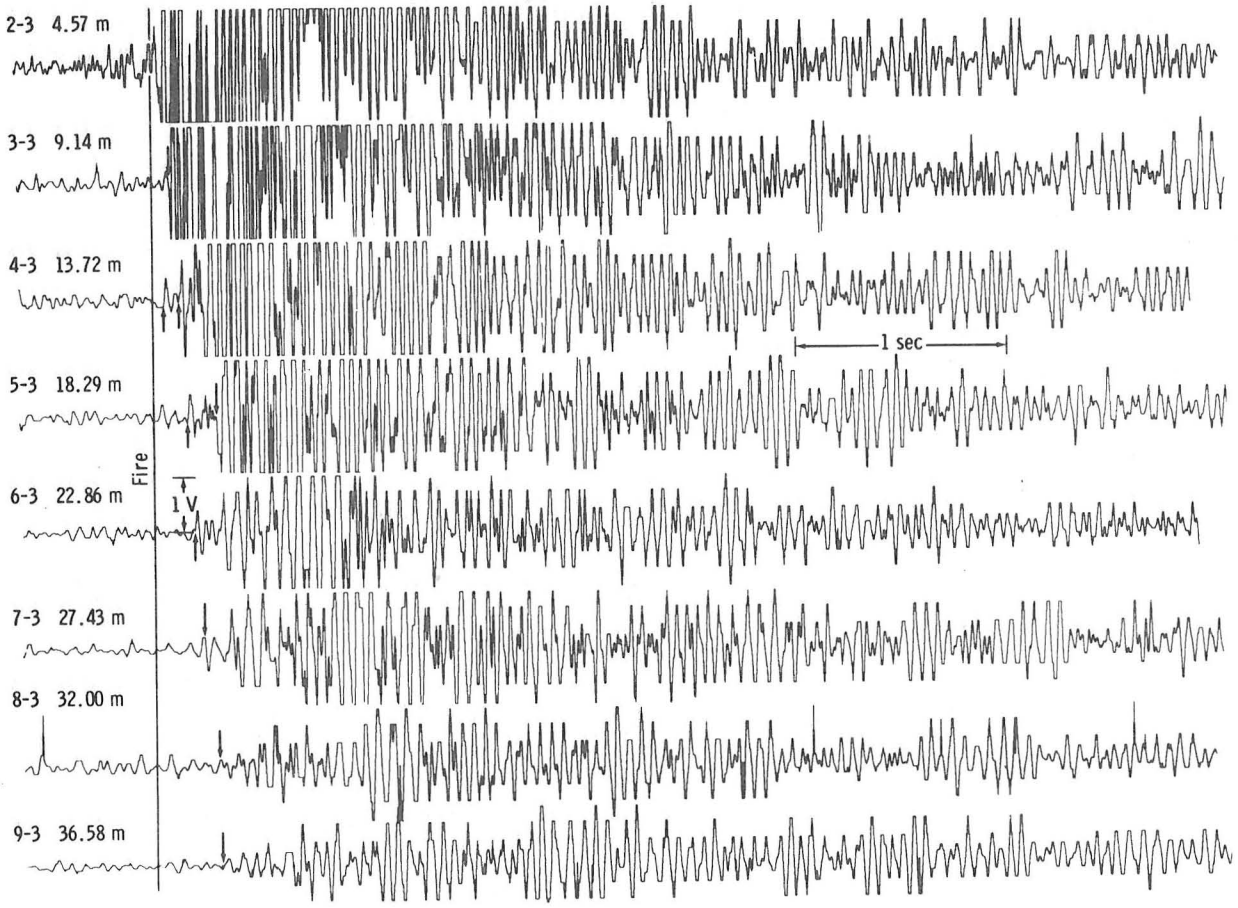

FIGURE 10-10.–Expanded time playouts of seismic signals produced by thumper firings 2 to 9 as recorded at geophone 3. The traces are alined to the same firing instant, and the arrows point to the onset of the seismic signal. (The first number in the data identifier is the thumper firing, and the second number is the geophone on which the data were recorded.)

40 m produced weak seismic arrivals for which it is difficult to determine unambiguously an initial onset.

Only one P-wave velocity is evident in the thumper traveltime data. A direct arrival is observed with a P-wave velocity of 114 m/sec. No detected variation exists in the P-wave velocity across the section sampled, as is evidenced by the uniformity of the velocity across the geophone line. This velocity can be compared to the regolith velocities of 104, 108, and 92 m/sec measured at the Apollo 12, 14, and 15 sites, respectively (refs. 10-3 and 10-4). Even though there is some minor variability from site to site, the fragmental and comminuted layer that covers much of the lunar surface has surprisingly similar seismic or acoustic properties.

Traveltime data from the seismic signals produced by the LM ascent, the grenade 4 detonation, and a grenade launcher thump are shown in figure 10-18. The effective instant of fire for the grenade launches was fixed by "anchoring" the 0.12-sec traveltime (fig. 10-13) for the impulse to the nearest geophone (geophone 1 at 14 m) to agree with thumper firing data at the same distance. This anchoring was necessary because of the finite buildup time for which the impulse of the grenade launch was transmitted to the lunar surface. The data are compared

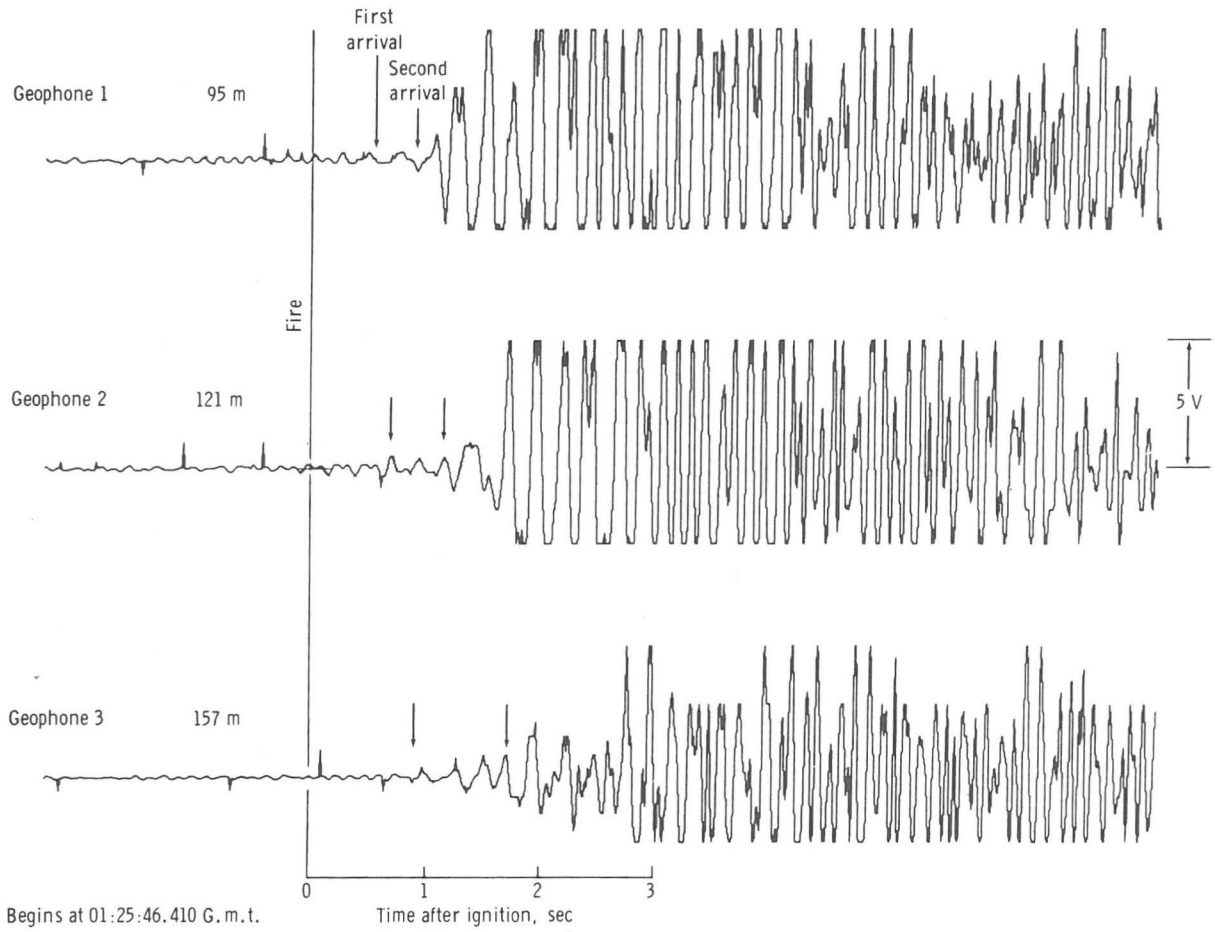

FIGURE 10-11.–Signals recorded by the ASE geophones from the lift-off of the LM ascent stage.

with the extrapolated traveltime/distance curve derived from the thumper firings of the ASE.

A faster arrival having a velocity of 250 m/sec is observed. The depth to the 250-m/sec refracting horizon is 12.2 m. It is proposed that the surface layer, which has a seismic velocity of 114 m/sec, represents the regolith at the Apollo 16 site. Estimates of the regolith thickness at the Apollo 16 site based solely on geological considerations are somewhat ambiguous. Regolith thicknesses are commonly estimated from the total crater population with a higher density of craters implying a greater regolith thickness. If all craters observed on the Cayley Formation are assumed to be impact craters, the indicated mean regolith thickness is 22 m (ref. 10-5). On the other hand, analyses of only concentric craters suggest a regolith thickness of approximately 7 m. Results of the Apollo 16 ASE would thus lend support to the lower estimate.

The underlying material having a seismic velocity of 250 m/sec is certainly not indicative of competent lava flows that typically on Earth have seismic velocities greater than approximately 800 m/sec (ref. 10-6). Field geological investigations have also revealed that the Cayley Formation does not consist of lava flows as had been postulated (ref. 10-7) but rather consists of perhaps interstratified breccias, and no bedrock appears to have been sampled by the Apollo 16 crew (sec. 6). The measured value of 250 m/sec can also be compared to the value of 299 m/sec measured for the underlying Fra Mauro breccias at the Apollo 14 site. Thus, it seems probable

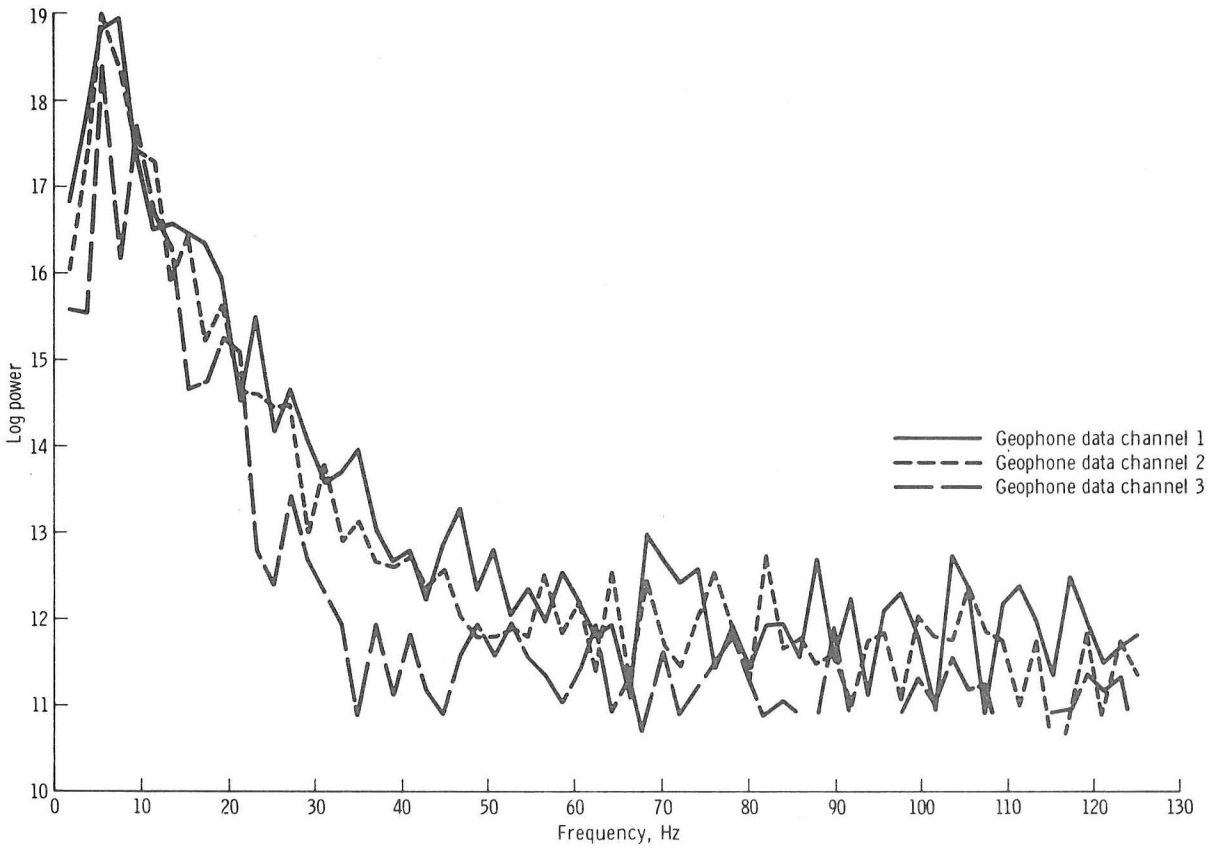

FIGURE 10-12.–Power spectra of seismic signals produced by LM ascent.

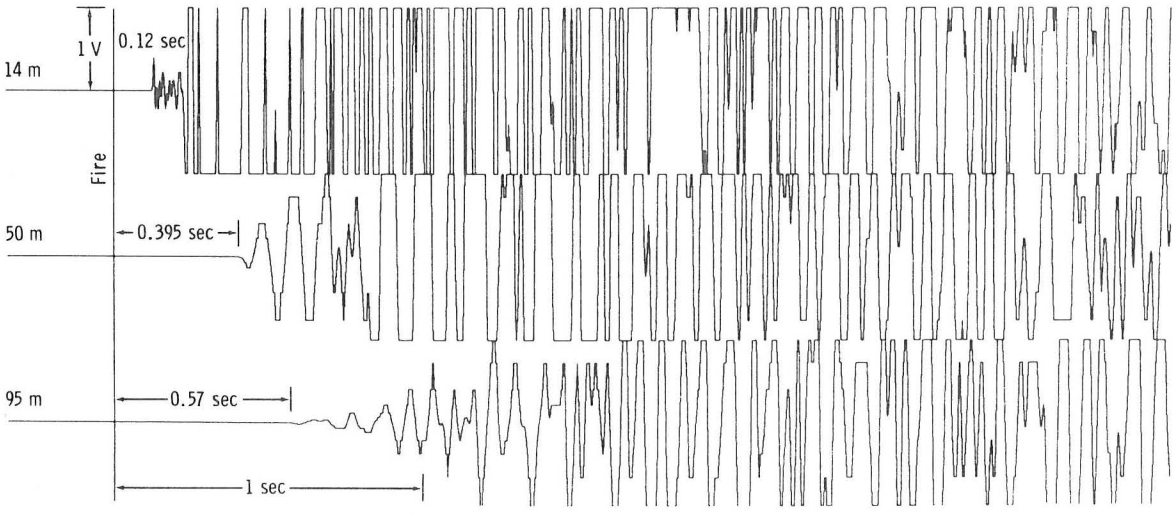

FIGURE 10-13.–Signals recorded by the ASE geophones from the launch of grenade 2.

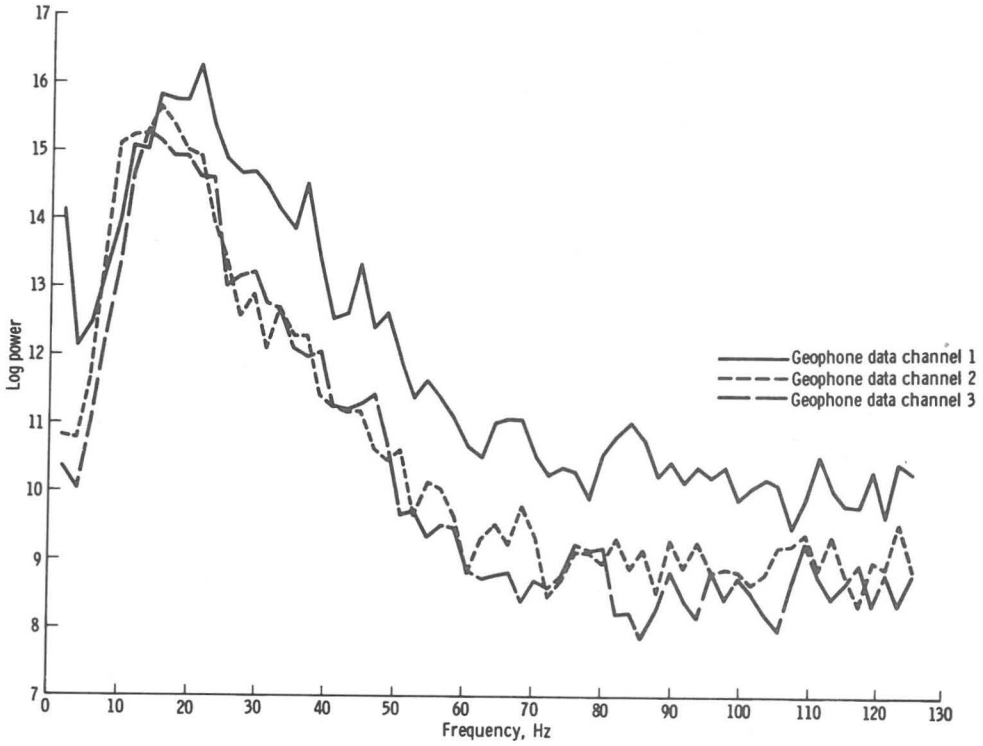

FIGURE 10-14.–Power spectra of seismic signals produced by the launch of grenade 4.

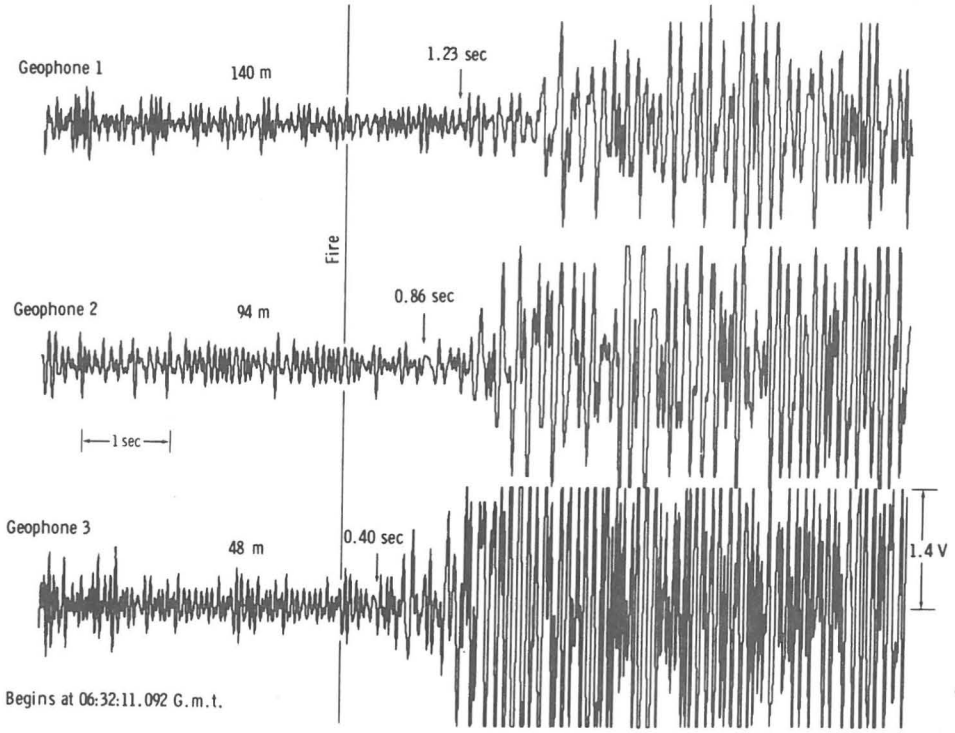

FIGURE 10-15.–Seismic signals produced by the detonation of grenade 4. The detonation time is marked by the vertical line marked fire. The small arrows point to the onset of the seismic signal.

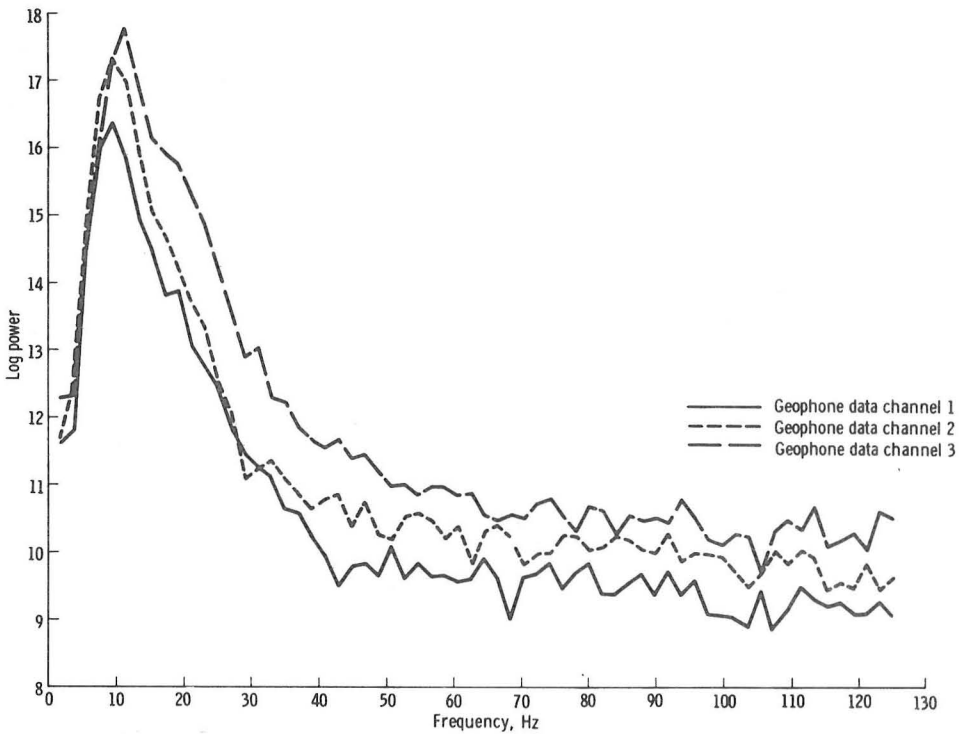

FIGURE 10-16.–Power spectra of the seismic signals produced by the detonation of grenade 4.

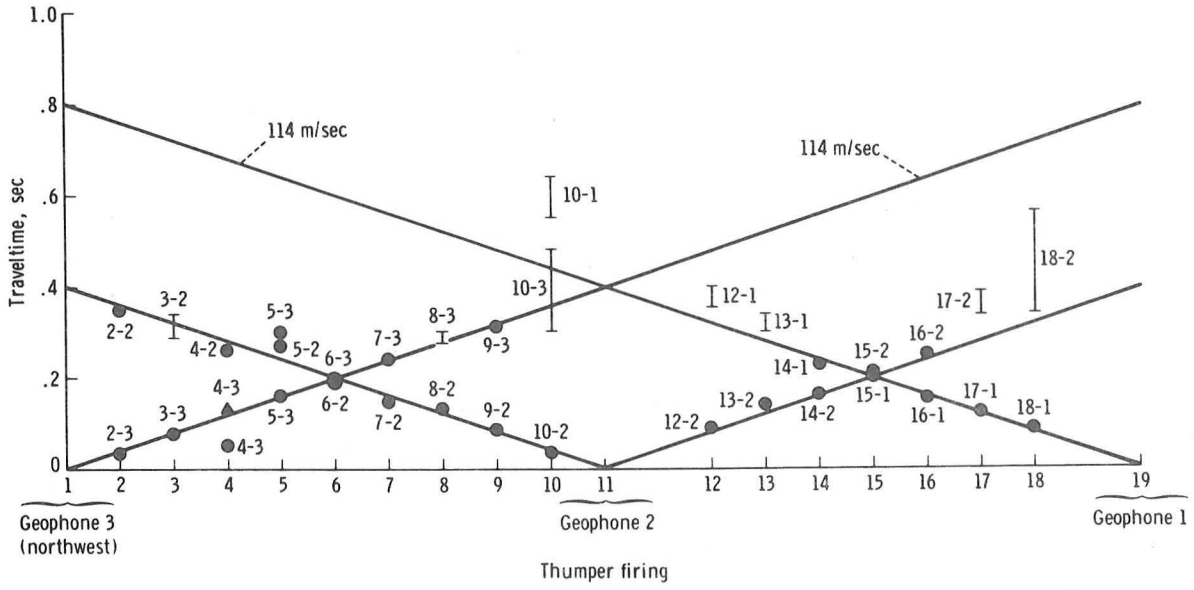

FIGURE 10-17.–Seismic arrivals from the thumper firings plotted on a traveltime/distance graph. The data points are shown as black circles. The distance between thumper shot locations is 4.75 m (except between positions 11 and 12 and positions 18 and 19, which are at 9.5-m intervals). Shot 4-3 has an anomalous early arrival. (The first number in the data identifier is the thumper firing, and the second number is the geophone on which the data were recorded.)

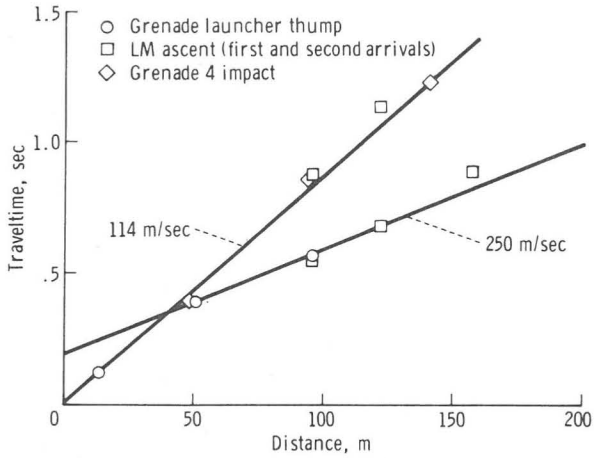

FIGURE 10-18.–Seismic arrivals from the LM ascent, grenade launch, and detonation of grenade 4 compared to extrapolated traveltime/distance data derived from the thumper firings.

that, at the Apollo 16 site, the regolith is underlain by low-velocity brecciated material or impact-derived debris.

If it is assumed that the rocks underlying the probable brecciated material at the Apollo 16 site have a seismic velocity of 1 km/sec, the thickness of the 250 m/sec material is 70 m. This thickness is likely an underestimate based on impact crater models proposed for the lunar highlands (ref. 10-8). It is anticipated that analyses of the complicated seismic signals from the grenade 2 and 3 firings will provide some definitive answers on the intriguing problem of the shallow velocity structure in the lunar highlands and of the severe velocity gradient in the lunar near-surface material (ref. 10-9).

REFERENCES

10-1. McCallister, Bruce D.; Kerr, James; Zimmer, John; Kovach, Robert L.; and Watkins, Joel: A Seismic Refraction System for Lunar Use. IEEE Trans. Geosci. Electron., vol. GE-7, no. 3, July 1969, pp. 164-171.

10-2. McDowell, Jack R.: The Active Seismic Experiment. Bendix Tech. J., vol. 4, no. 2, Summer-Autumn 1971, pp. 40-51.

10-3. Latham, Gary V.; Ewing, Maurice; Press, Frank; Sutton, George; et al.: Passive Seismic Experiment. Sec. 8 of Apollo 15 Preliminary Science Report. NASA SP-289, 1972.

10-4. Kovach, Robert L.; Watkins, Joel S.; and Landers, Tom: Active Seismic Experiment. Sec. 7 of Apollo 14 Preliminary Science Report. NASA SP-272, 1971.

10-5. Oberbeck, V. R.: Implications of Regolith Thickness in Apollo 16 Landing Site. NASA TM X-62089, 1971.

10-6. Watkins, J. S.: Annual Report, Investigation of In Situ Physical Properties of Surface and Subsurface Site Materials by Engineering Geophysical Techniques. NASA Contract T-25091 (G), July 1966.

10-7. Hodges, Carol Ann: Geologic Map of Part of the Descartes Region of the Moon. Apollo 16 Pre-Mission Map, U.S. Geol. Survey Map, 1972.

10-8. Short, Nicholas M.; and Forman, Michael L.: Thickness of Impact Crater Ejecta on the Lunar Surface. Modern Geol., vol. 3, no. 2, 1972, pp. 69-91.

10-9. Kovach, R. L.; and Watkins, J. S.: The Near-Surface Velocity Structure of the Moon. Lunar Science-III, Revised Abstracts of Papers Presented at the Third Lunar Science Conference, Houston, Tex., Jan. 10-13, 1972, Carolyn Watkins, ed., Lunar Science Institute Contribution No. 88, Feb. 18, 1972, pp. 461-462.

THE VELOCITY STRUCTURE OF THE LUNAR CRUST*

ROBERT L. KOVACH
Dept. of Geophysics, Stanford University, Stanford, Calif., U.S.A.

and

JOEL S. WATKINS
Dept. of Geology, University of North Carolina, Chapel Hill, N.C., U.S.A.

(Received 3 October, 1972)

Abstract. Seismic refraction data, obtained at the Apollo 14 and 16 sites, when combined with other lunar seismic data, allow a compressional wave velocity profile of the lunar near-surface and crust to be derived. The regolith, although variable in thickness over the lunar surface, possesses surprisingly similar seismic properties. Underlying the regolith at both the Apollo 14 Fra Mauro site and the Apollo 16 Descartes site is low-velocity brecciated material or impact derived debris. Key features of the lunar seismic velocity profile are: (i) velocity increases from 100–300 m s^{-1} in the upper 100 m to ~ 4 km s^{-1} at 5 km depth, (ii) a more gradual increase from ~ 4 km s^{-1} to ~ 6 km s^{-1} at 25 km depth, (iii) a discontinuity at a depth of 25 km and (iv) a constant value of ~ 7 km s^{-1} at depths from 25 km to about 60 km. The exact details of the velocity variation in the upper 5 to 10 km of the Moon cannot yet be resolved but self-compression of rock powders cannot duplicate the observed magnitude of the velocity change and the steep velocity-depth gradient. Other textural or compositional changes must be important in the upper 5 km of the Moon. The only serious candidates for the lower lunar crust are anorthositic or gabbroic rocks.

1. Introduction

A seismic refraction experiment was used to study the characteristics of the lunar near-surface at the Apollo 14 and 16 landing sites. The results of these experiments, together with the recording of Lunar Module (LM) ascent stage and upper stage of the Saturn rocket (S-IVB) impacts allow an interpretation of the seismic velocity structure in the lunar interior to be made. In this paper we want to examine some of the following questions: What are the acoustic or seismic properties of the lunar near-surface material? How thick is the lunar regolith at the Apollo 14 and 16 sites? Are there distinct seismic horizons and do they correlate with any geological horizons? Is permafrost present near the lunar surface? Are there characteristic differences in the shallow seismic velocities between the maria and the highlands? How do the shallow seismic results interface with the larger-scale seismic results? What are the implications, compositional or otherwise, of the seismic results for the outer lunar interior?

In the study of the Earth's crust seismic refraction profiling has often been used. The technique involves the recording of explosive charges at various distances from an array of seismometers (geophones). On the Moon a 91 m linear array of three geophones was deployed by the Apollo astronauts and several seismic energy sources were used: an astronaut-activated thumper device with small explosive initiators, a

* Paper dedicated to Professor Harold C. Urey on the occasion of his 80th birthday on 29 April, 1973.

The Moon 7 (1973) 63–75.

mortar package containing rocket launched grenades and the impulse produced by the thrust of LM-ascent stage as it departed from the lunar surface. Technical details of the experiment can be found in Kovach *et al.* (1971) and Kovach *et al.* (1972).

2. Apollo 14 Results

Apollo 14 landed at latitude 3°40′24″S, longitude 17°27′55″W in the Fra Mauro region. Here the lunar surface is covered by a stratigraphic unit, called the Fra Mauro formation, which is presumed to be the ejecta deposit produced by the large impact which formed the Imbrium basin. At the landing site the Apollo 14 crew deployed the string of three geophones in a southerly direction across the lunar surface and used the thumper device to generate seismic signals. The thumper was fired at 4.57 m intervals along the geophone line.

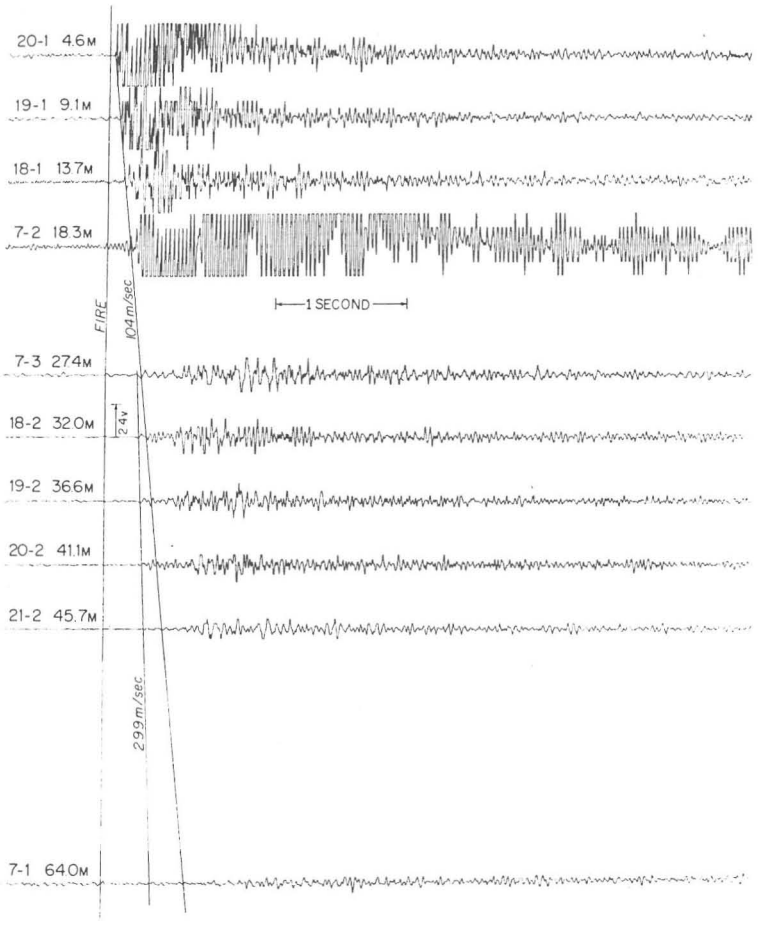

Fig. 1. Composite seismic record section aligned in time to same instant of thumper firings at the Apollo 14 site. First number refers to shot number. Second number to geophone on which recorded.

A composite seismic record section aligned in time to the same instant of thumper firings at the Apollo 14 site is shown in Figure 1. The first number refers to the thumper explosive initiator used and the second number to the geophone on which the data were recorded. The northernmost geophone which was closest to the central telemetry station was designated geophone 1.

Two compressional wave (P-wave) velocities are recognized on the composite record section. A first arrival with a P-wave velocity of 104 m s^{-1} is observed out to a distance of 22.7 m where a faster arrival with a velocity of 299 m s^{-1} is identified. No variation in P-wave velocities was observed across the horizontal section sampled, as was evidenced by the conformance of the seismic velocities measured along the geophone line. The lunar near-surface at the Apollo 14 site is thus characterized by a surface layer of 104 m s^{-1} velocity overlying material possessing a seismic velocity of 299 m s^{-1}.

Seismic signals were also generated from the rocket thrust produced by the ascent of the landing module from the Moon and recorded by the Apollo 14 passive seismometer at a distance of 178 m (584 ft). These travel-time data are shown in Figure 2 compared to the extrapolated travel-time distance curves determined from the astronaut thumper firings. The observed travel-times are in close agreement with the extrapolated travel-times. However, a first arrival was observed with a travel-time somewhat faster than that predicted by a refraction from the top of the 299 m s^{-1} horizon indicating that a material with a faster intrinsic compressional-wave velocity lies beneath the 299 m s^{-1} material.

If the assumption is made that the material underlying the 299 m s^{-1} material possesses an infinite compressional wave velocity, a maximum estimate of the 299 m s^{-1} material can be derived. Furthermore, as shown in Figure 2, if the critical distance for

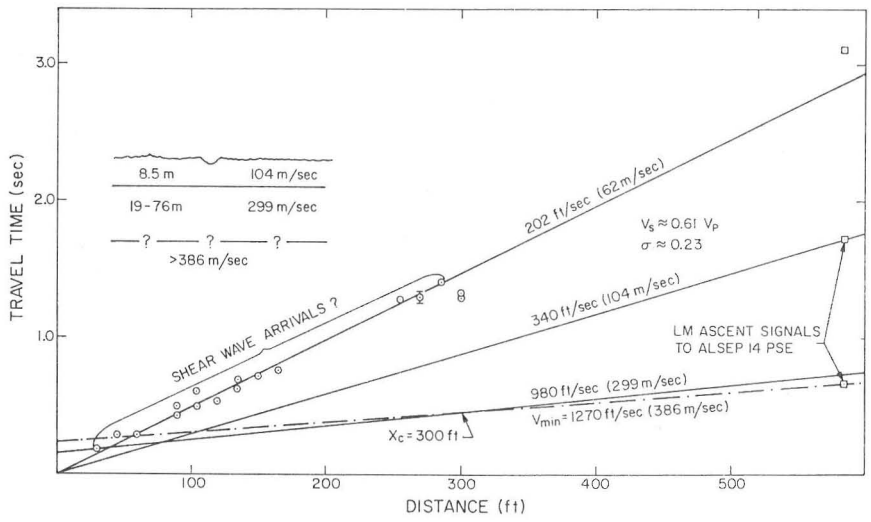

Fig. 2. Travel-times measured at the Apollo 14 site.

the arrival of the head wave traveling through the underlying material is taken as 100 m (the length of the geophone line) a minimum velocity of 386 m s^{-1} is inferred for the underlying material. The range of possible thickness, therefore, for the 299 m s^{-1} material is 17 to 88 m.

The depth to the 299 m s^{-1} refracting horizon is 8.5 m. The low seismic velocity of 104 m s^{-1} is suggestive of a porous and highly brecciated rock material and thus believed to be representative of the fragmental veneer of unconsolidated particulate debris – the lunar regolith that covers the surface of the Fra Mauro site. This measured thickness of 8.5 m for the regolith agrees well with that estimated solely on geological evidence. By photographic studies of the depth at which blocky floors appear in fresh craters, it can be inferred that the fragmental, surficial layer that overlies the more consolidated or semiconsolidated substrate at the Fra Mauro site ranges in thickness from 5 to 12 m (Offield, 1970).

A velocity of 299 m s^{-1} is comparable to that observed in the upper part of Meteor Crater ejecta material (Watkins and Kovach, 1971) and it is thus quite reasonable to assume that this velocity is representative of ejecta from Mare Imbrium. A thickness estimate of 19 to 76 m is comparable to geological estimates of 100 m or so for the Fra Mauro formation (Offield, 1970). The returned lunar samples have also definitely revealed that the Fra Mauro formation is primarily comprised of breccias (Wilshire and Jackson, 1972).

The relatively low compressional wave velocities that were measured in the lunar near-surface argue against the presence of substantial amounts of any shallow permafrost at this particular site. Measured velocities in permafrost vary greatly – depending on such factors as lithology, porosity, and degree of interstitial freezing – but typically range from 2438 to 4572 m s^{-1} (8000 to 15000 ft s^{-1}) (Barnes, 1966).

3. Apollo 16 Results

The landing site for Apollo 16 was at latitude 8°59′29″S, longitude 15°30′52″E. This location, known as the Descartes site, was chosen to sample and study the constructional units, called the Cayley formation and the associated Descartes material which are a part of the lunar highlands. It had been presumed by some that these formations were primarily volcanic in origin and that lava flows might be found at this location (Milton and Hodges, 1972).

At this site the three geophones were deployed on the Cayley formation on a highly cratered uneven area at a bearing of 287° (clockwise from north) from the central telemetry station. Geophone 3 was deployed 90 m northwest of geophone 1 (Figure 3).

Figure 4 is a record section aligned in time to the same instant of firing for thumper shots 2 to 10 as recorded at geophone 2. There is no difficulty in recognizing the onset of the seismic signals out to a distance of 40 m; but at greater distances the onset of the seismic wave arrivals are more uncertain because of the emergent beginnings. Figure 5 is an expanded time scale record section for thumper shots 2 to 9 as recorded at geophone 3.

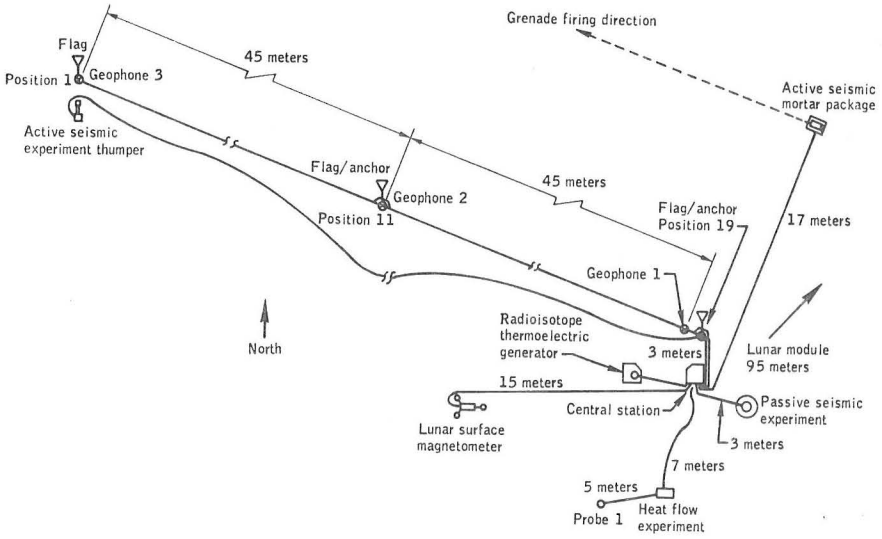

Fig. 3. Schematic diagram showing deployment of geophysical experiments at the Apollo 16 site.

The travel-time-distance data from the Apollo 16 thumper firings are shown in Figure 6. Only one compressional wave velocity is evident in these data – a direct arrival possessing a velocity of 114 m s^{-1}. Again no variation in the measured surface velocity was noted across the geophone line.

Seismic signals of particular interest at the Apollo 16 site were generated by the ascent of the lunar landing module and the detonations of rocket propelled grenades. The seismic signals from the ascent of the landing module are shown in Figure 7.

The mortar package assembly was located 14 m from geophone 1 pointed to fire parallel to the geophone line and downrange toward geophone 3 (Figure 4).

The seismic signals produced by the detonation of the nearest grenade (0.1 lb of high explosive) are shown in Figure 8. The records are noisy prior to the onset of the detonation signal because the grenade launch itself produced a disturbance which had not completely decayed to low level prefiring conditions. However, the desired signals can be recognized on the basis of a change in frequency inasmuch as the detonation signals possess a predominant signal frequency of 10 Hz compared to 15–20 Hz for the grenade launch itself. Figure 9 shows the seismic signals produced by the detonation of 0.3 lb of explosive at a distance of about 400 m. 0.6 lb of high explosives were also detonated at a distance of 1000 m from the geophone line. However, because of the reverberation produced from the grenade launch only weak surface waves could be recognized.

The travel-time data for the seismic signals recorded at the Apollo 16 site are shown in Figure 10. Seismic arrivals with velocities of 114 m s^{-1} and 250 m s^{-1} are observed. The depth to the top of the 250 m s^{-1} refracting horizon is 12.2 m. Again it is inferred that the material with a seismic velocity of 114 m s^{-1} is representative of the regolith

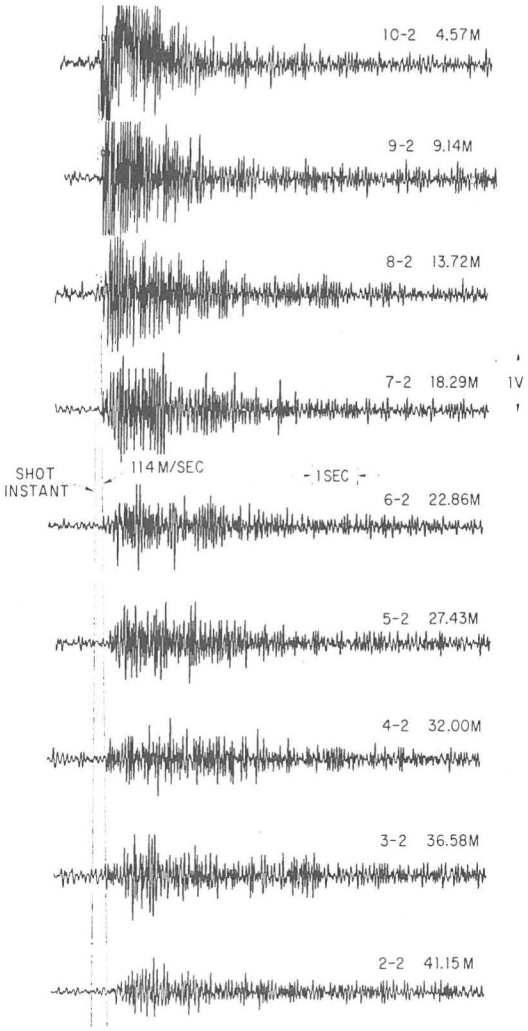

Fig. 4. Seismic record section recorded at Apollo 16 site. Line marked 114 m s^{-1} shows first arrival of P-wave.

at the Apollo 16 site. Estimates of the regolith thickness at the Apollo 16 site based solely on geological considerations can be ambiguous. Regolith thicknesses are commonly estimated from the total crater population with a higher density of craters implying a greater regolith thickness. If one assumes that all craters observed on the Cayley formation at the Apollo 16 site are impact craters, the indicated mean regolith thickness is 22 m (Oberbeck, 1971). On the other hand, restricting the analysis to only concentric craters suggested a regolith thickness of about 7 m. The refraction from the 250 m s^{-1} horizon could not be recognized out to a distance of 445 m, but if it is indeed present the maximum thickness for the 250 m s^{-1} material is 220 m.

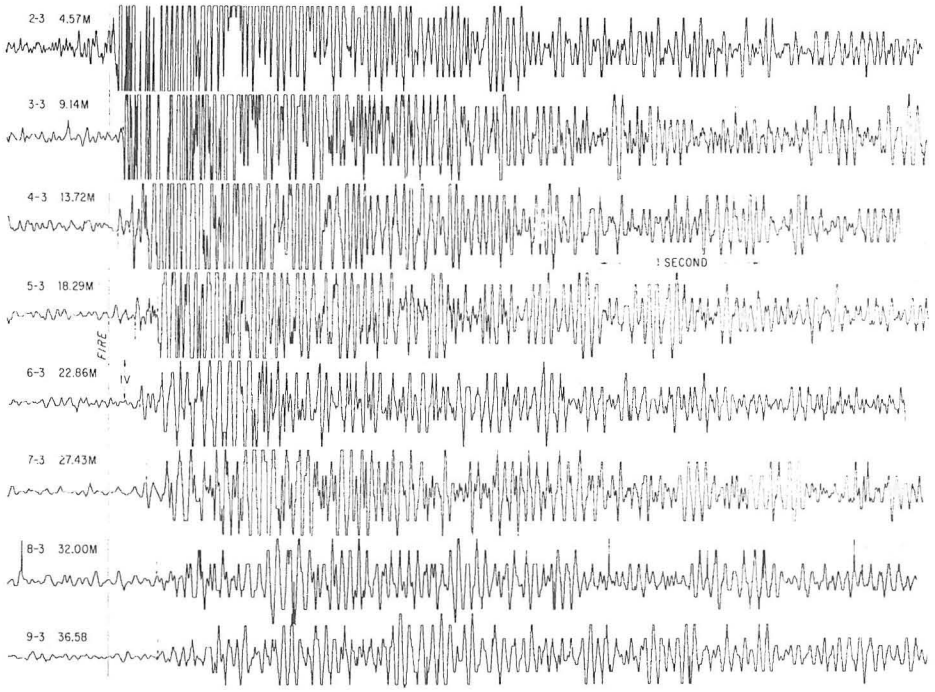

Fig. 5. Expanded time playout of thumper firings 2–9 recorded at geophone 3 at the Apollo 16 Descartes site. Arrows indicate the first arrival. Note the more emergent beginning with an increase in distance.

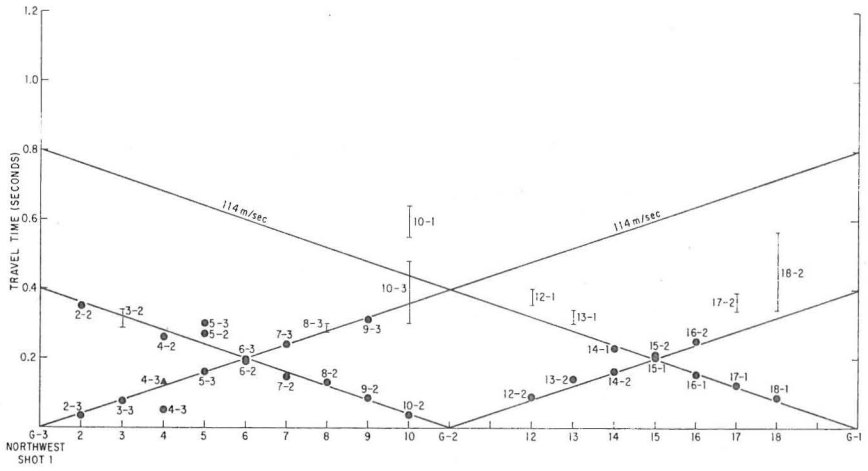

Fig. 6. Travel-time data for thumper firings at the Apollo 16 site. The data points are shown as black circles; the first number refers to the thumper firing, the second number to the geophone on which the data were recorded. Distance between firing locations (except skipped positions 11 and 19) is 4.57 m (15 ft). Note uniformity of measured velocity across section sampled.

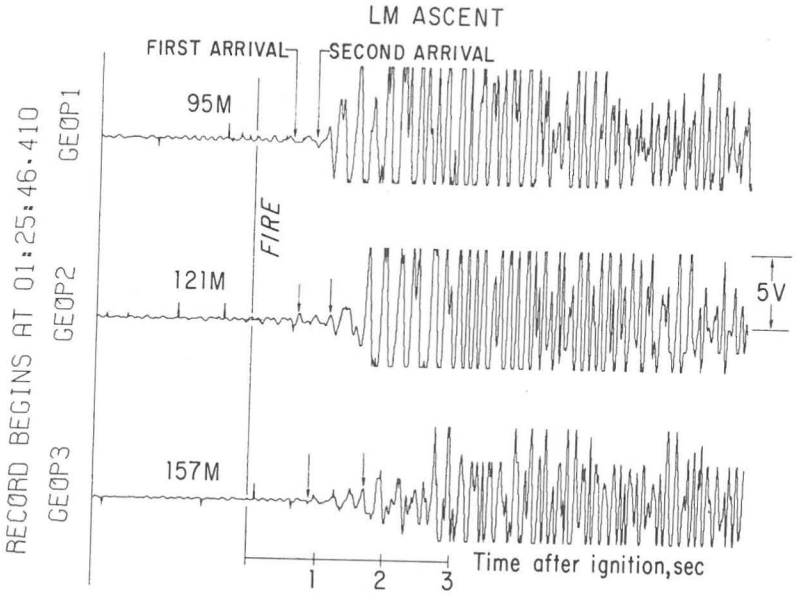

Fig. 7. Seismograms recorded on Apollo 16 geophone array from ascent of Lunar Module (LM) from lunar surface. Arrows indicate first and second arrivals.

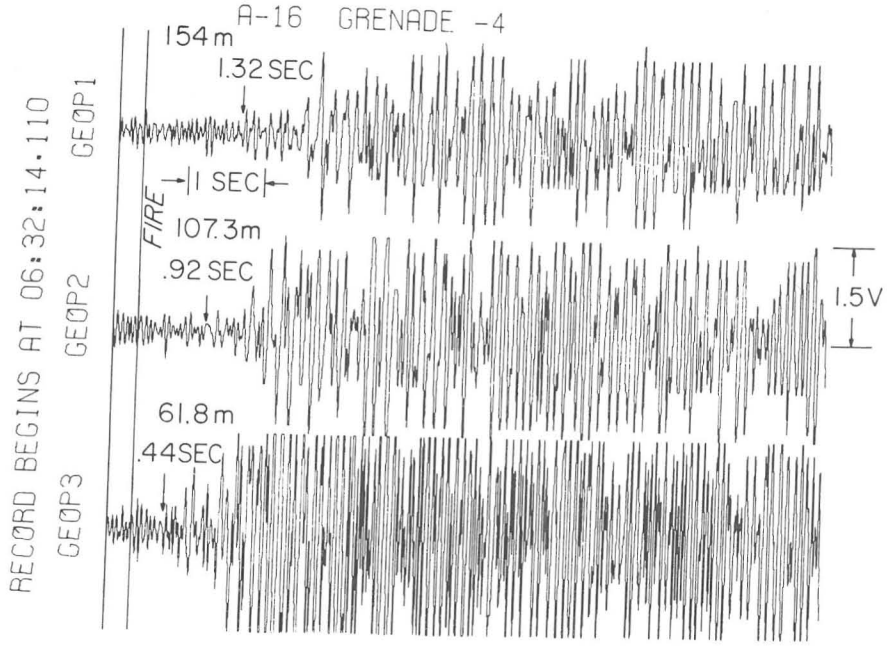

Fig. 8. Seismograms produced by detonation of 0.1 lb of high explosive at the Apollo 16 site.

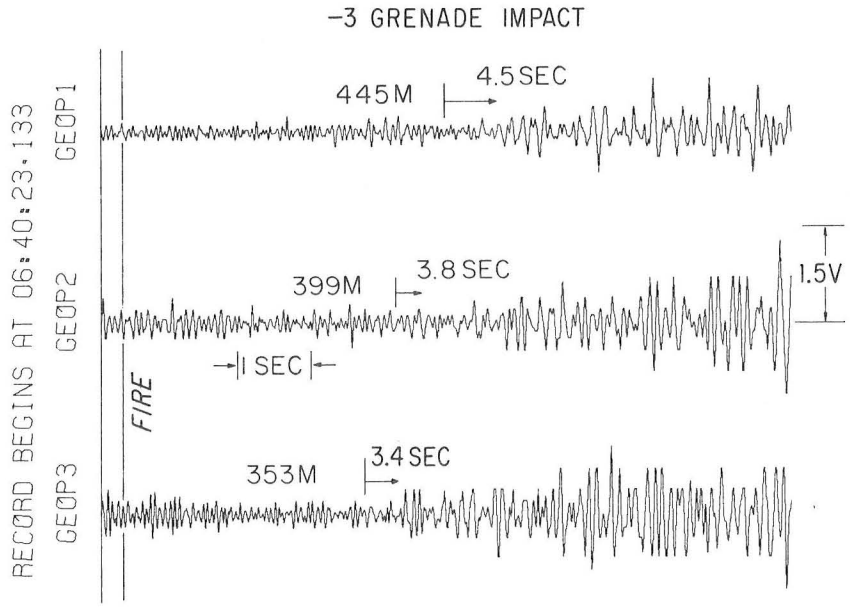

Fig. 9. Seismogram produced by detonation of 0.3 lb of high explosive at the Apollo 16 site recorded on geophone array at distances shown.

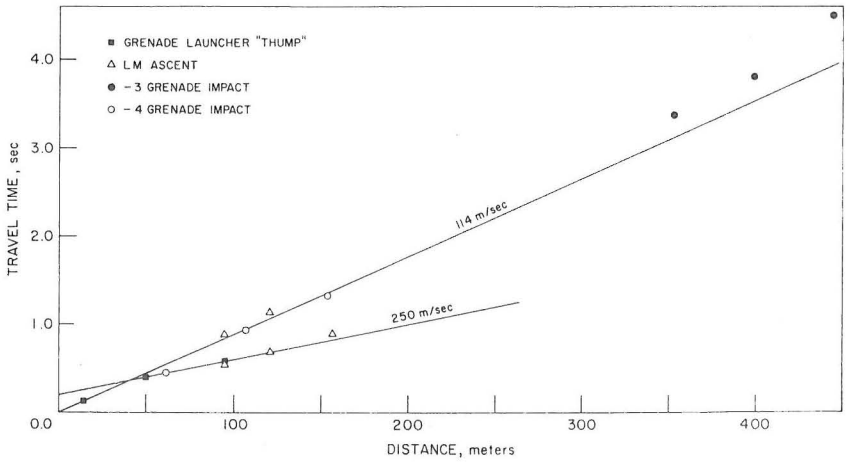

Fig. 10. Travel-times measured at the Apollo 16 site.

The underlying material with a seismic velocity of 250 m s^{-1} is certainly not indicative of competent lava flows which typically, on Earth, have seismic velocities greater than about 800 m s^{-1} (Watkins *et al.*, 1972). The returned lunar samples have also revealed that the Cayley formation does not consist of lava flows as had been postulated (Milton and Hodges, 1972), but rather consists of perhaps interstratified

breccias. No bedrock appears to have been sampled by the Apollo 16 crew. The measured value of 250 m s^{-1} is close to the value of 299 m s^{-1} measured for the underlying Fra Mauro breccias at the Apollo 14 site. Thus it seems clear that at both the Apollo 14 and 16 sites the lunar surface is underlain by low-velocity brecciated material or impact derived debris.

4. Discussion and Conclusions

The seismic velocity of the 114 m s^{-1} measured at the Descartes site can be compared to the velocities for the regolith of 104, 108 and 92 m s^{-1} measured at the Apollo 12, 14 and 15 sites respectively (Latham *et al.*, 1972; Kovach *et al.*, 1971). Even though there is some variability in the velocity from site to site the process of fragmentation and communition by meteoroid impacts has produced a layer of surprisingly similar seismic properties, arguing against any major regional difference in the near-surface acoustical properties of the Moon.

The velocity model for the upper 25 km of the Moon, compatible with the impact data recorded by the network of Apollo seismometers (Toksőz *et al.*, 1972) and the lunar seismic refraction experiments is shown in Figure 11. Several salient features can be pointed out.

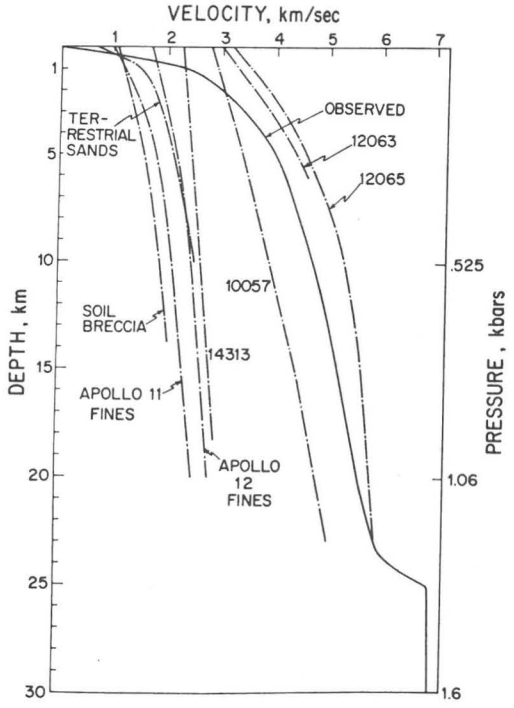

Fig. 11. Observed velocity profile for upper 30 km of Moon compared to velocities of lunar and terrestrial rocks and powders measured in laboratory as a function of pressure. Lunar rocks are identified by sample number.

(i) The seismic velocity increases very rapidly from values of 100–300 m s^{-1} in the upper 100 m or so of the Moon to a value of ~4 km s^{-1} at a depth of 5 km.

(ii) The velocity increases more gradually from ~4 km s^{-1} at 5 km depth to ~6 km s^{-1} at a depth of 25 km.

(iii) A discontinuity in seismic velocity is present at a depth of 25 km.

(iv) A nearly constant value of ~7 km s^{-1} from a depth of 25 km to about 60 km.

The exact details of the velocity variation in the upper 5–10 km of the Moon cannot yet be resolved (i.e. whether it is smooth as depicted or a stepwise increase) but one simple observation can be made. Self-compression of any rock powder such as the Apollo 11 or 12 soils or terrestrial sands cannot duplicate the observed magnitude of the lunar velocity change and the steep velocity-depth gradient (~2 km s^{-1} km^{-1}).

Experiments on returned lunar soils (Anderson *et al.*, 1970; Kanamori *et al.*, 1970, 1971; Mizutani *et al.*, 1972; Warren *et al.*, 1971) and truly hydrostatic measurements on terrestrial sands and basaltic ash (Talwani *et al.*, 1972) suggest velocity-depth gradients of 0.4 to 0.8 km s^{-1} km^{-1} but such gradients only persist to a pressure of ~50 bars (depth ≈1 km in Moon). At higher pressures the velocity gradient decreases to values 10 to 20 times less than the gradient at low pressure.

Recent experimental results on unconsolidated sands and rock powders show that no unique relation exists between seismic velocity and porosity in granular material. Secondly, velocities in unconsolidated materials do not exhibit excess pressure memory (Talwani *et al.*, 1972). Rather there is an irreversible change in porosity accompanying a completely reversible variation in velocity as the material is repeatedly cycled to pressures of 2.4 kbar (~50 km lunar depth).

In view of the lack of verifying experimental data it would seem unlikely to expect that a deep rock powder layer (of several km) with a velocity gradient of 1.35 km s^{-1} km^{-1}, as proposed by Gold and Soter (1970) and further discussed by Gold (1971a, b), can be invoked to explain the shallow lunar velocity variation. It has also been argued that plastic deformation, sintering and excess pressure memory (presumably from large meteorite impacts) make the lunar *in situ* velocities much higher than is observed in the laboratory (Jones, 1972). The important observation is that the increase of seismic velocity in the shallow lunar interior is much too large to be due simply to self-compaction of rock powders. *The implication is that other effects such as composition or textural changes must be important in the upper 5 km of the Moon.* It, of course, might be possible to invoke *ad hoc* hypotheses to explain this velocity variation but the seismic experiment planned for Apollo 17 should shed light on this important paradox. The primary purpose of the Apollo 17 seismic profiling experiment is to gather needed travel-time data in the distance range of 0.1 km to 10 km. Explosive charges will be detonated out to distances of 2.5 km and the LM ascent stage is targeted to impact within 10 km.

From about 4 km to 25 km depth the physical properties of the lunar rocks are probably dominated by cracks, pores and intergranular effects. Rocks have intercrystalline cracks and pores and have very low seismic velocities at atmospheric pressure.

Seismic velocities increase rapidly over the pressure range from zero to 1.5 kbar (~25 km depth in Moon) where velocity values change only minor amounts with a further increase in hydrostatic pressure (Nur and Simmons, 1971).

Because of this large pressure effect on seismic velocities over this depth range in the Moon, probably not much can unambiguously be said about composition. However, the observed velocity variation does lie between the measured velocity values for returned lunar basaltic rocks 10057, 12065 and 12063 suggesting compatibility with a basaltic composition.

At a depth of 25 km the seismic velocity increases only very slightly to a value of 7.0 km s^{-1} at a depth of 65 km. Because at these pressures (>1.5 kbar) much of the crack and porosity effects in rocks have been minimized it is possible to use laboratory measurements on rocks to make some compositional inferences. Temperature effects can also be excluded because at the anticipated lunar temperatures their effect is, at worst, to produce a decrease in seismic velocity by 0.1–0.2 km s^{-1}.

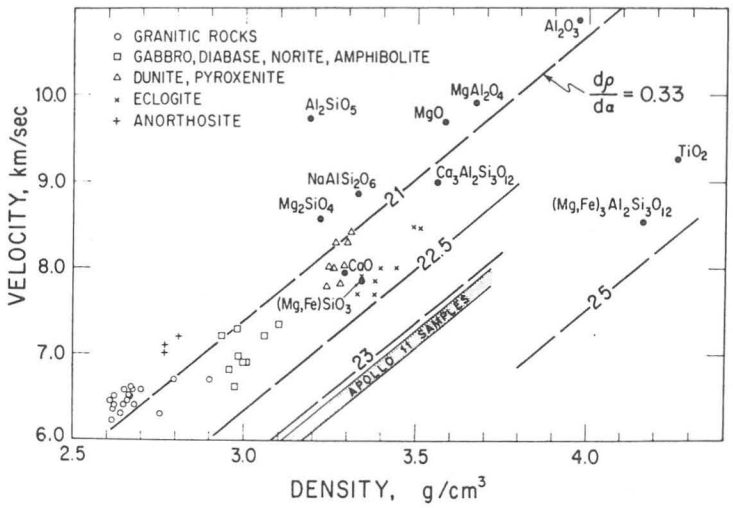

Fig. 12. Velocity and density of rocks and minerals as a function of mean atomic weight.

Figure 12 is a plot of the seismic velocity in rocks and minerals as a function of mean atomic weight. For a given mean atomic weight seismic velocity increases as the density increases. The effect of an increase in iron content is to increase the density and mean atomic weight but decrease the seismic velocity. It can be seen that for the various rocks shown only anorthosite or gabbro (including diabase, norite or amphibolite) have a seismic velocity of ~7 km s^{-1} and can be considered as serious candidates for the lower lunar crust. Eclogites, dunites and pyroxenites all have seismic velocities higher than that observed and should not be considered further. It is also obvious that seismic data alone cannot distinguish between gabbro and anorthosite and petrologic and geochemical arguments must be introduced.

Acknowledgements

This research was supported by the National Aeronautics and Space Administration under contract NAS 9-5632 and grant NGL 05-020-232.

References

Anderson, O. L., Scholz, C., Soga, N., Warren, N., and Schreiber, E.: 1970, *Proc. of the Apollo 11 Lunar Sci. Conf.* **3**, Pergamon Press, New York, p. 1959.

Barnes, D. F.: 1965, Proc. of the Intern. Conf. on Permafrost, NAS-NRC publ. 1287, p. 349.

Gold, T.: 1971a, *Proc. of the Second Lunar Sci. Conf.* **3**, MIT Press, Cambridge, Mass., p. 2675.

Gold, T.: 1971b, *Proc. Am. Phil. Soc.* **115**, 74.

Gold, T. and Soter, S.: 1970, *Science* **169**, 1071.

Jones, B. W.: 1972, 'Seismological Evidence for Deep Rock Powder on the Moon', Cornell University Center for Radiophysics and Space Research, unpublished report.

Kanamori, H., Nur, A., Chung, D. H., Wones, D., and Simmons, G.: 1970, *Science* **167**, 726.

Kanamori, H., Mizutani, H., and Yamano, Y.: 1971, *Proc. of the Second Lunar Sci. Conf.* **3**, The MIT Press, Cambridge, Mass., p. 2323.

Kovach R. L., Watkins, J. S., and Landers, T.: 1971, *Apollo 14 Preliminary Science Report*, NASA SP-272, p. 163.

Kovach, R. L., Watkins, J. S., and Talwani, P.: 1972, *Apollo 16 Preliminary Science Report*, NASA SP, in press.

Latham, G., Ewing, M., Press, F., Sutton G., Dorman, J., Nakamura, Y., Toksőz, N., Lammlein, D., and Duennebier, F.: 1972, *Apollo 15 Preliminary Science Report*, NASA SP-289, p. 81.

Milton D. J. and Hodges, C. A.: 1972, 'Geologic Maps of the Descartes Region of the Moon', *USGS Misc. Geol. Investigations Map I-748.*

Mizutani, H., Fujii, N., Hamano, Y., Osako, M., and Kanamori, H.: 1972, 'Lunar Science III', *Lunar Science Institute Cont. No. 88*, p. 547.

Nur, A. and Simmons, G.: 1969, *Earth Planetary Sci. Letters* **7**, 183.

Oberbeck, V. R.: 1971, NASA Technical Memorandum X-62, 089.

Offield, T. W.: 1970, 'Geologic Map of the Fra Mauro Site-Apollo 13', Scale 1:5000, USGS unnumbered map.

Talwani, P., Nur, A. and Kovach, R. L.: 1972, *Geophysics* **37**, in press.

Toksőz, M. N., Press, F., Anderson, K., Dainty, A., Latham, G., Ewing, M., Dorman, J., Lammlein, D., Nakamura, Y., Sutton, G., and Duennebier, F.: 1972, *The Moon* **4**, 490.

Warren, N., Schreiber, E., Scholz, C., Norrison, J. A., Norton, P. R., Kumazala, M., and Anderson, O. L.: 1971, *Proc. of the Second Lunar Sci. Conf.* **3**, The MIT Press, Cambridge, Mass., p. 2345.

Watkins, J. S. and Kovach, R. L.: 1971, *Science* **175**, 1244.

Watkins, J. S., Walters, L. A., and Godson, R.: 1972, *Geophysics* **37**, 29.

Wilshire, H. G. and Jackson, E. D.: 1972, *Geological Survey Professional Paper 785.*

The Lunar Seismic Profiling Experiment

J. E. DYE

The Lunar Seismic Profiling Experiment (LSPE), now under development and scheduled for deployment on the moon as a part of the Apollo 17 mission, is an advanced version of the Active Seismic Experiment, described elsewhere in this issue.* The LSPE consists of eight packages, each containing an explosive charge, and a central-electronics package, which is housed within the ALSEP Central Station. The explosive charges weigh from 1/8 pound to 6 pounds and are approximately equivalent to TNT in energy per pound. They will be deployed from the Lunar Roving Vehicle (LRV) by the astronauts at distances of 500 meters to 3.5 kilometers from an array of four geophones emplaced on the lunar surface. The charges will be detonated after the astronauts leave the lunar surface by an r.f. command from the ALSEP Central Station.

The detonations will generate waves of seismic energy, the velocities of which will be determined to depths of 3 to 4 kilometers on the basis of geophone detection measurements. The data obtained, in combination with known velocity/density relationships, are expected to reveal much concerning the internal structure and composition of the lunar surface. According to present plans, the Apollo 17 landing site should be near a major planetary ridge – one comparable in extent to the midoceanic ridges on earth – which may be the surface manifestation of a fundamental internal process of lunar evolution, such as differentiation and/or convection.

The Lunar Seismic Profiling Experiment and the Active Seismic Experiment have the following important similarities and differences:

- The LSPE has a maximum explosive-charge weight of 6 pounds, whereas that in the ASE is 1 pound. As a consequence, the LSPE charges can be deployed at a greater maximum distance from the geophone array – 3.5 kilometers for the LSPE as compared with 1.7 kilometers for the ASE – to yield seismic velocity measurements at greater lunar-surface depths.
- The ASE explosive charges are rocket-propelled. Those of the LSPE are carried to the desired deployment site aboard the LRV and emplaced on the lunar surface by the astronauts.
- The ASE charges detonate on impact with the lunar surface after rocket propulsion initiated by ground command. The individual LSPE charges are armed by two mechanical timers that are started by the crew at the time of deployment. Time runout and arming occur well after the crew has left the lunar surface. Detonation is accomplished via a ground-controlled r.f. link between the ALSEP Central Station and a receiver in each explosives package.
- The ASE geophone array is linear, 300 feet in length, and consists of three geophones spaced at 150-foot intervals. The LSPE geophone array is triangular in shape, with one geophone positioned at each of the apices of an equilateral triangle 300 feet on a side; a fourth geophone is positioned at the triangle center. The LSPE array provides a capability for determining the arrival angle of the induced seismic energy.
- The LSPE geophones are identical to the ASE geophones but are stowed in a different manner for transport to the lunar surface and deployment by the astronauts.
- The LSPE central electronics are similar in function and construction to the ASE central electronics. They differ in that, whereas the ASE contains a receiver, the LSPE contains a transmitter that transmits a pulse-coded r.f. signal to a receiver in the explosives package to actuate detonation at a precise time.

EXPERIMENT DESCRIPTION

The LSPE explosives package is seen in Figure 1, and a cutaway view is shown in Figure 2. The Lunar Seismic Profiling Experiment contains eight such packages, all identical except for the size of the high-explosives charge and the preset runout time of the mechanical timers. The high-explosives charge is contained within a nickel-plated fiberglass housing, which forms the bottom portion of the explosives package. The top portion – the electronics and SAFE/ARM

Robert L. Kovach, Department of Geophysics, Stanford University, is Principal Investigator for the Lunar Seismic Profiling Experiment as well as for the Active Seismic Experiment.

*J. R. McDowell, "The Active Seismic Experiment."

THIS PAGE INTENTIONALLY LEFT BLANK.

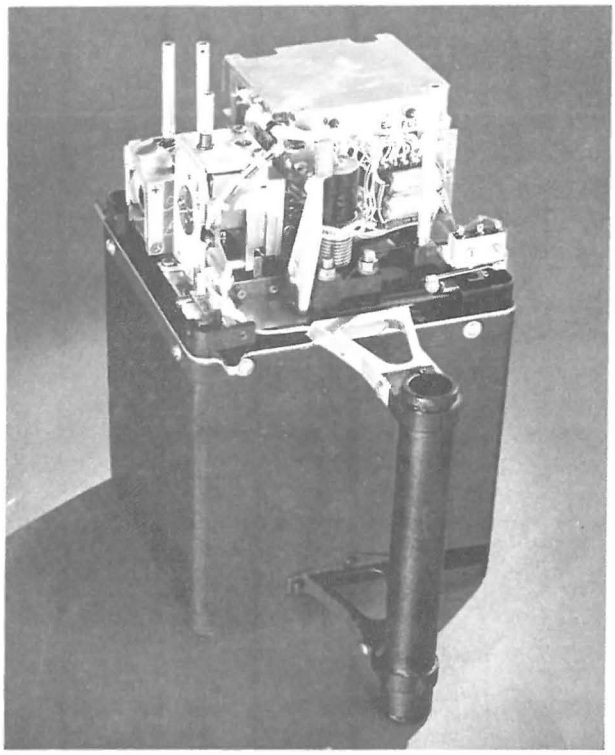

Figure 1 Lunar-Seismic-Profiling Explosives Package (Cover Removed)

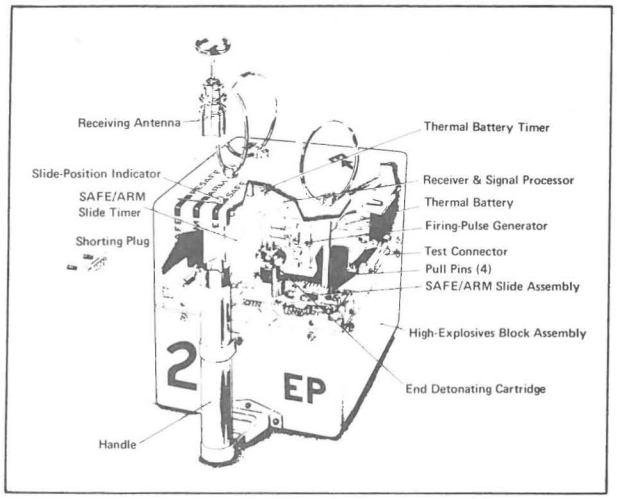

Figure 2 Lunar-Seismic-Profiling Explosives Package (Cutaway View)

assembly – consists of a magnesium baseplate upon which are mounted the following components:

- the *end detonating cartridge (EDC)*, the first component of the explosives train;
- the *SAFE/ARM slide*, the second component of the explosives train, which contains an explosive lead;
- a mechanical *SAFE/ARM slide timer*, which moves the lead into line with the EDC to complete, or arm, the explosives train;
- *receiving antenna, receiver, signal processor, and firing-pulse generator*, which function to receive the pulse-coded FIRE signal transmitted from the ALSEP Central Station, to process this coded signal, and to provide a firing pulse that fuses a bridgewire in the EDC to actuate the explosives train;
- a *thermal battery*, which supplies power to the above circuitry;
- a *thermal battery timer*, which activates the battery via impact of a firing pin onto a percussion primer in the battery.

A temperature ranging between 40°F and 170°F will be maintained for these components over the period from lunar morning to lunar noon during which the package is to be exposed to the lunar environment. Solar input at high sun angles will be minimized by multilayer insulation inside a fiberglass top cover and by a coating of white thermal paint on the exterior of the upper portion of the cover. The remaining exterior surfaces of the explosives package are painted black to permit rapid initial warm-up of the packages, which will be deployed at low sun angles when temperatures are near the minimum operating limit.

The astronauts start the two mechanical timers at the time of deployment by removing two separate pull pins. Another pull pin provides a safety back-up to the SAFE/ARM slide timer by constraining the SAFE/ARM slide in its SAFE position. A fourth pull pin, contained within the thermal battery timer, serves as a safety back-up against the possibility of premature functioning of the battery timer by constraining the firing pin from activating the battery. Each of these pins is held by a retaining-spring force that must be overcome by the astronaut during pin removal. Removal of the SAFE/ARM slide pull pin requires both rotation and pull, the two actions in sequence being constrained by a retaining-spring force. Locking features are incorporated in all pins to prevent their removal in the event of component malfunction. Should either of the timers have started to run, its pin would be locked in place and impossible to remove. Should the slide not be constrained in the SAFE position by the SAFE/ARM slide timer, the SAFE/ARM slide pull pin would lock and could not be removed. Should the firing pin be prematurely released by the timing mechanism, the pull pin constraining the firing pin within the thermal battery timer would lock in a similar manner.

EXPERIMENT OPERATION

A block diagram describing the operational sequence within an LSPE explosives package is presented in Figure 3.

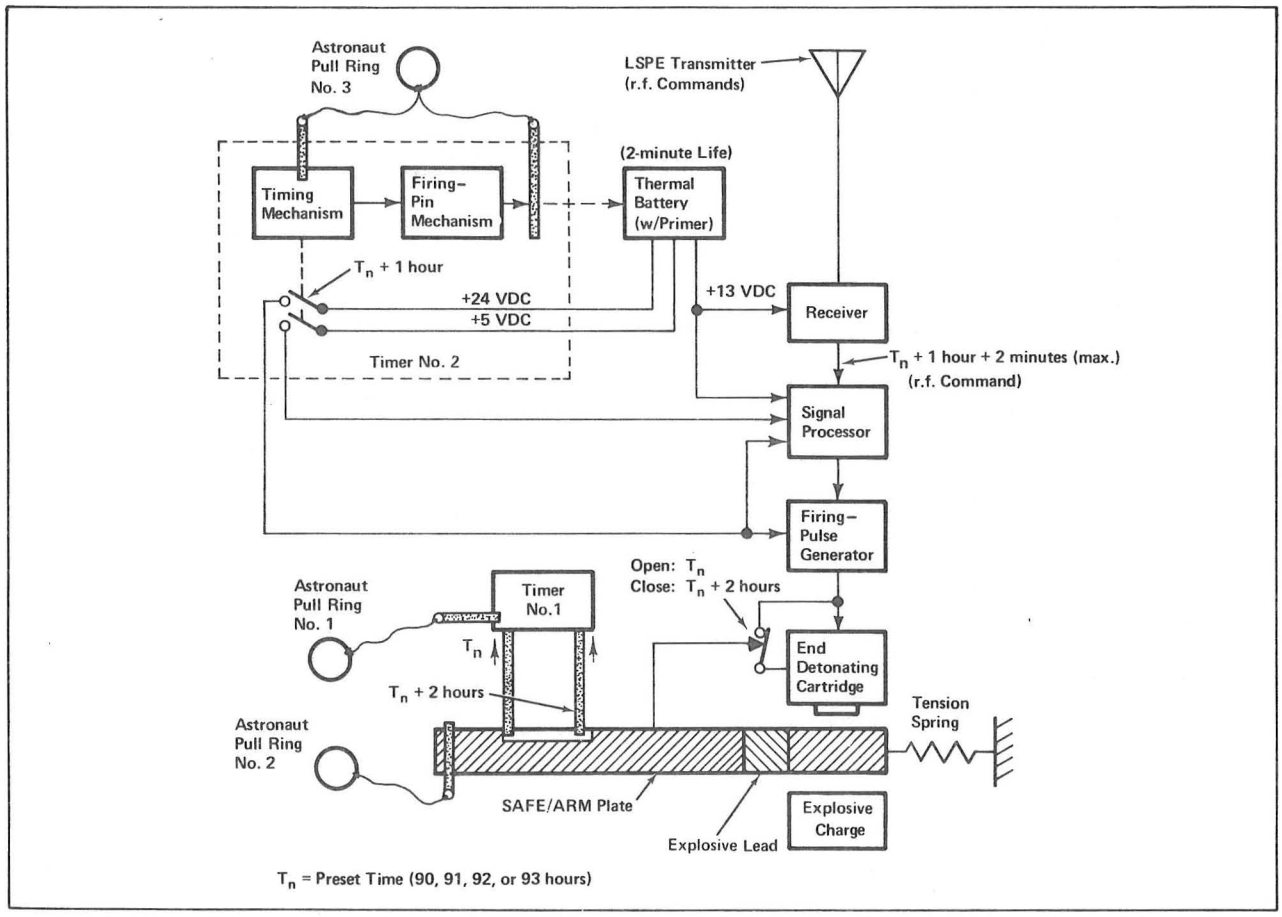

Figure 3 Explosives Package Block Diagram

When the astronaut removes the four pull pins at the time of deployment, the mechanical timers start, which, after a 90-hour timeout, remove the safety constraints holding the SAFE/ARM slide and the battery firing pin in the locked position; the prescribed order of pull-pin removal maximizes the safety that is inherent in the pull-pin locking features. The SAFE/ARM slide timer is preset to function for 90 hours, a period that assures – even in a contingency situation – that the crew will have left the lunar surface prior to the arming of any explosives package. Once this period has elapsed, a pin constraining the spring-loaded SAFE/ARM slide is retracted by the timer, permitting the slide to move to its ARM position. Motion of the slide opens a microswitch that to this point has shorted the electrical leads of the EDC. The thermal battery timer is preset to function, independently, at 91 hours, 1 hour after the SAFE/ARM slide timer has placed the slide in its ARM position. A spring-loaded firing pin within the timer is released, striking a percussion primer within the battery and activating the battery. Concurrently, two microswitches within the timer are closed, connecting the thermal battery output to the electric circuits.

The LSPE transmitter, which is located within the ALSEP Central Station, transmits a repetitive pulsed carrier signal, the time characteristics of which are detailed in Figure 4. A series of three pulses properly spaced in time is required to elicit a FIRE signal out of the signal processor within the explosives package and detonate the explosives train. Should the first set of pulses fail to accomplish this, the battery life of 2 minutes permits three additional attempts to be made. Since the seismic data subsequently collected must be accurately referenced to the instant of detonation, it is necessary to establish which specific set of pulses is effective. This is done by comparing known times of pulse-set transmission with the time of arrival at the geophones of the initial seismic data. Pulse sets are spaced at 29.55-second intervals to make such identification possible without ambiguity.

In the event of a dud, the SAFE/ARM slide timer mechanism retracts a second pin and the slide moves to a RESAFE position; this occurs at 92 hours, 2 hours after initial release of the SAFE/ARM slide. A linkage extending through the top cover of the explosives package and connected to the SAFE/ARM slide

THIS PAGE INTENTIONALLY

LEFT BLANK.

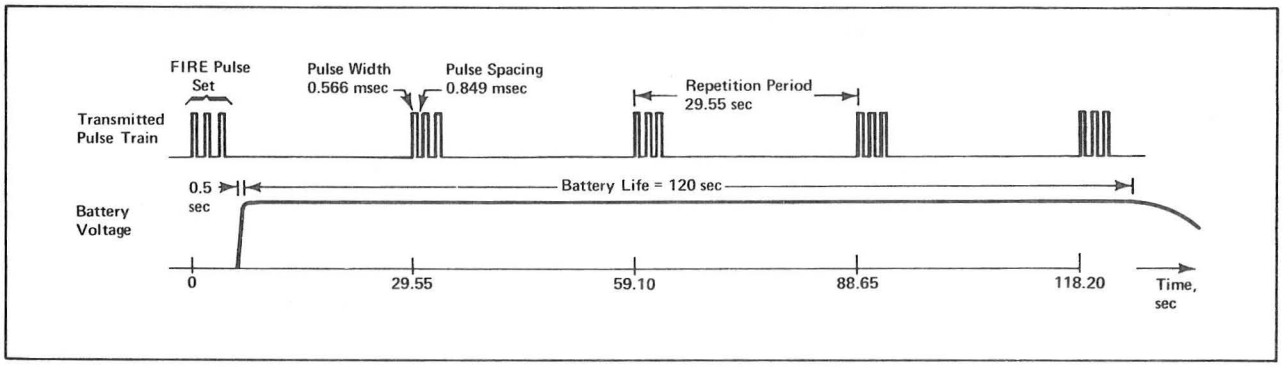

Figure 4 Time Characteristics of LSPE Transmitter Signal

indicates to the astronauts that the slide is in its initial SAFE position.

It should be noted that the explosives package is so designed as to eliminate any possibility of premature detonation endangering the lives of ground handling personnel or of the astronauts during deployment. The locking features of the pull pins and their order of removal preclude any mechanical timer-action output should either or both timers operate prematurely. Subsequent to pull-pin removal, premature detonation could occur only if both timers were to time out prematurely, each within a window of 2 hours, and if a pulse-coded spurious r.f. signal within the narrow 10-kilohertz bandwidth of the receiver were to be received during the 3-minute window of maximum battery life.

The LSPE geophones, which are identical to those used for the Active Seismic Experiment, are stowed in a geophone module as shown in Figure 5. The universal handling tool is used by the astronauts to carry this module to a deployment site about 30 feet away from the ALSEP Central Station. The tool is also used to remove the module cover; to pick up, carry, and emplace the individual geophones; and to spool out the geophone cable, which is wound on a ball-bearing-supported reel.

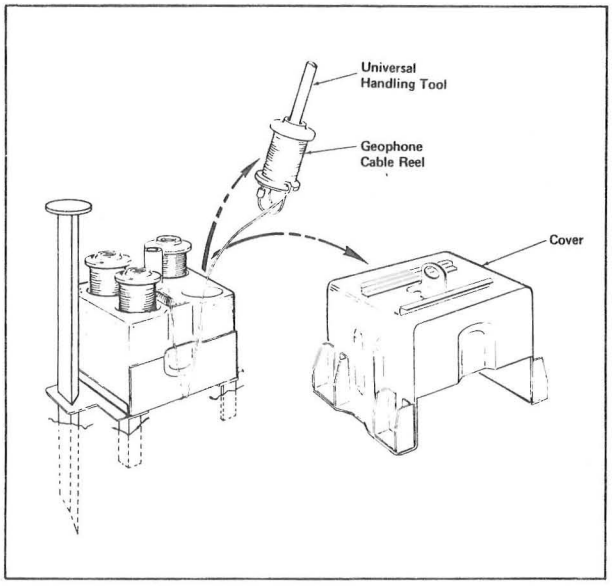

Figure 5 Geophone Module Deployment

10. Lunar Seismic Profiling Experiment

Robert L. Kovach,[a†] *Joel S. Watkins,*[b] *and Pradeep Talwani*[a]

The successful installation of a geophysical station at the Taurus-Littrow landing site of the Apollo 17 mission marked the culmination of an exciting period of manned lunar exploration and vastly improved current knowledge of the lunar interior. Before the Apollo 17 mission, there was a gap in our knowledge concerning the upper 10 km of the lunar crust because of the large hiatus in pertinent traveltime data between the coverage provided by the previous active seismic experiments on Apollo 14 and 16 and that of the earlier lunar module (LM) and SIVB impacts. In particular, it was not possible to resolve whether the seismic velocity increased smoothly or stepwise in the upper 5 km of the Moon.

The purpose of the Apollo 17 lunar seismic profiling experiment (LSPE) was to record the vibrations of the lunar surface as induced by explosive charges, by the thrust of the LM ascent engine, and by the crash of the LM ascent stage. Analyses of these seismic data were planned to determine the internal characteristics of the lunar crust to a depth of several kilometers. The traveltimes of seismic waves are inverted to determine the seismic velocity structure with depth and to provide the direct means of probing the lunar interior. A secondary objective of the LSPE was to monitor lunar seismic activity during periodic listening intervals.

Strong seismic signals were recorded from the detonation of eight explosive charges that were armed and placed on the lunar surface by the crewmen at various points along the traverses. Recording of these seismic signals generated traveltime data to a distance of 2.7 km.

One of the more significant events of the Apollo 17 mission was the recording of the seismic signals from the LM ascent stage, which struck the lunar surface 8.7 km southwest of the landing site. The characteristic reverberation from this impact spread outward and was first detected at the Apollo 17 station approximately 6 sec after impact. The seismic signals received from this impact provided a valuable traveltime datum for determining the variation of seismic velocity with depth in approximately the upper 5 km of the Moon.

The most significant discovery resulting from the analysis of the data recorded by the LSPE is that the seismic velocity increases in a marked stepwise manner beneath the Apollo 17 landing site (fig. 10-1). A surface layer with a seismic velocity of 250 m/sec and a thickness of 248 m overlies a layer with a seismic velocity of 1200 m/sec and a thickness of 927 m, with a sharp increase to approximately 4000 m/sec at the base of the lower layer. The seismic velocities for the upper layers are compatible with those for basaltic lava flows, indicating a total thickness of approximately 1200 m for the infilling mare basalts at Taurus-Littrow. Major episodes of deposition or evolution are implied by the observed abrupt changes in seismic velocity.

INSTRUMENT DESCRIPTION AND PERFORMANCE

The LSPE consists of a geophone array, eight explosive packages, and electronics within the Apollo lunar surface experiments package (ALSEP) central station. Four identical geophones are used in a triangular array; the geophones are miniature seismometers of the moving coil-magnet type. The coil is the inertial mass suspended by springs in the magnetic field. Above the natural resonant frequency of the geophones (7.5 Hz), the output is proportional to ground velocity. The LSPE geophone array was deployed without difficulty in the nominal configuration at the Apollo 17 site approximately 148 m

[a]Stanford University.
[b]The University of Texas at Galveston.
[†]Principal Investigator.

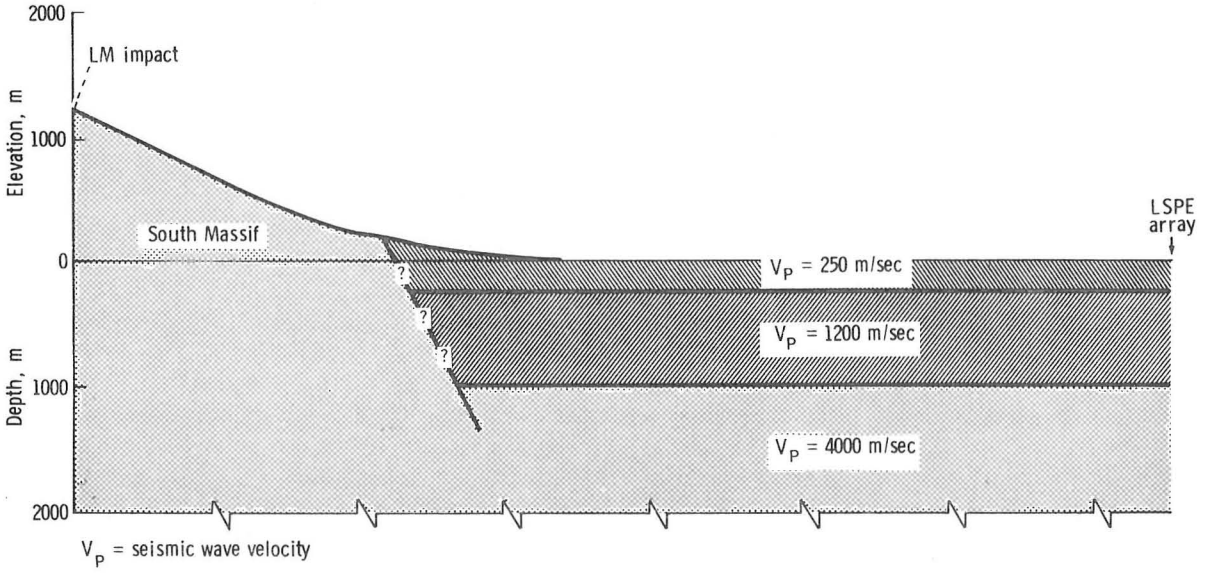

FIGURE 10-1.–Seismic cross section at the Taurus-Littrow landing site (no vertical exaggeration).

west-northwest of the LM (fig. 10-2). Figure 10-3 is a photographic panorama from geophone 2 to the LM as viewed from geophone 3.

A four-channel amplifier and a logarithmic compressor condition the geophone signals before conversion into a digital format for telemetering to Earth. Because the LSPE signal levels are distributed throughout the dynamic range of the system, logarithmic compression is used. This compression gives signal resolution as some constant fraction of signal amplitude. The logarithmic compressor used in the LSPE has the transfer function

$$V_{out} = \pm M \ln \left| V_{in} \right| + b' \qquad (10\text{-}1)$$

where V is voltage, the constant M determines the slope of the transfer function, and b' is specified by the dc offset of the compressor output and the system noise level. The values of M and b' are determined by calibration of the system to provide at least 6-percent accuracy of the data referenced to the level of the input signal. The properties of the LSPE system are listed in tables 10-I and 10-II, and the nominal frequency response is shown in figure 10-4. The output of the logarithmic compressor is referenced to 2.5 V dc.

The analog output of the logarithmic compressor is converted to a 7-bit binary element in the LSPE control electronics by an analog-to-digital converter

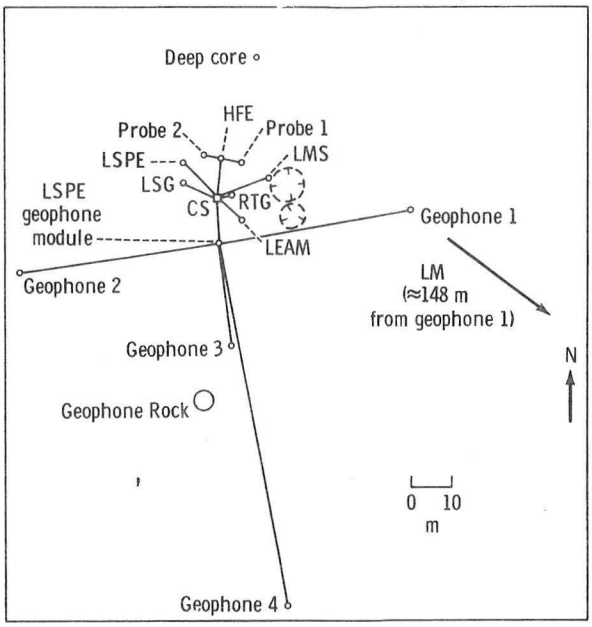

Key: CS = central station
HFE = heat flow experiment
LEAM = lunar ejecta and meteorites experiment
LMS = lunar mass spectrometer
LSG = lunar surface gravimeter
RTG = radioisotope thermoelectric generator

FIGURE 10-2.–The LSPE nominal deployment.

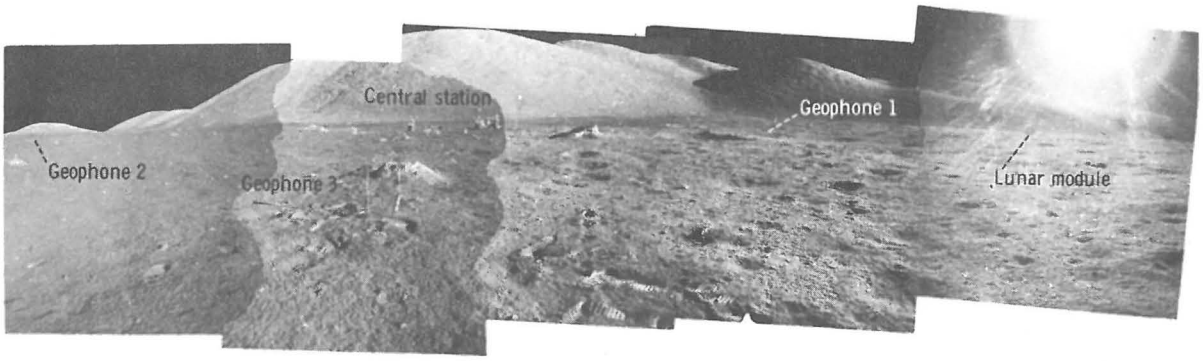

FIGURE 10-3.–Panorama from geophone 2 to the LM as viewed from behind geophone 3 (AS17-147-22546, 22548, 22550, 22552, 22554).

TABLE 10-I.–*Apollo 17 LSPE Characteristics*

Component characteristics	*Channel no.*			
	1	*2*	*3*	*4*
Amplifiers:				
Noise level, mV rms at input	0.75	0.75	0.83	0.83
Dynamic range, rms signal to rms noise in dB at 10 Hz	73.4	76.2	75.6	75.8
Geophones:				
Resistance, ohm	5970	5953	6080	6153
Generator constant, V/m/sec at 40 Hz	235.6	239.2	237.1	235.3
Natural frequency, Hz	7.38	7.31	7.40	7.35
System:				
Signal-to-noise ratio (rms signal to rms noise in dB for a 6-nm rms signal at 10 Hz)	24.4	26.9	26.8	26.8
Amplitude sensitivity (measured at input to log compressor), V/μm of peak-to-peak ground displacement at 10 Hz	7.33	7.02	7.12	7.13

TABLE 10-II.–*LSPE System Sensitivity*

Frequency, Hz	*Sensitivity, V/μm*			
	Channel 1	*Channel 2*	*Channel 3*	*Channel 4*
1	0.1	0.1	0.1	0.1
2	.7	.8	.8	.8
3	1.7	1.7	1.7	1.7
4	2.4	2.5	2.5	2.5
6	4.3	4.2	4.3	4.3
8	6.0	5.8	5.9	5.8
10	7.3	7.0	7.1	7.1
15	10.9	10.5	10.6	10.6
20	13.2	12.8	12.8	13.0

and transmitted to Earth through the ALSEP communications network. The 7-bit binary encoding provides for an amplitude resolution of 1.277 dB (≈16 percent). Each geophone channel is sampled 118 times/sec to provide a minimum of 5 samples/sec at a frequency of 20 Hz.

Digital Portions of the LSPE

The data format used is shown in figure 10-5. A data frame consists of three subframes, each consisting of twenty 30-bit words. The first word of each subframe consists of one 10-bit synchronous word

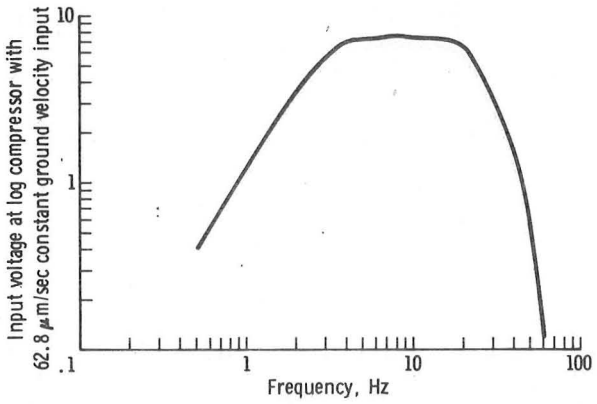

FIGURE 10-4.–Nominal frequency response of the LSPE.

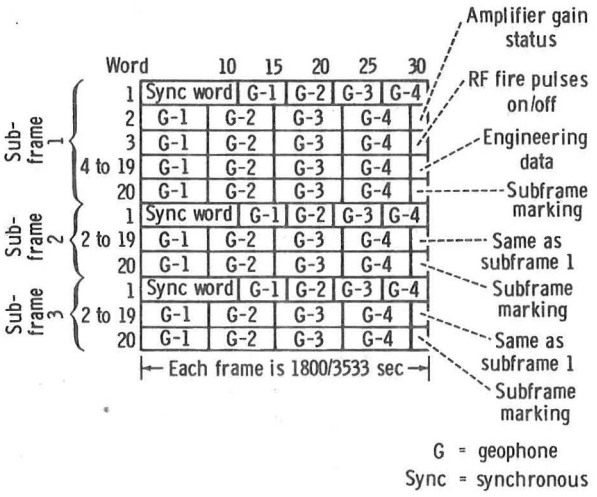

FIGURE 10-5.–The LSPE data format. Each data frame consists of three subframes of twenty 30-bit words each. Geophone data words are normally 7 bits long except for those in word 1, which are 5-bit samples.

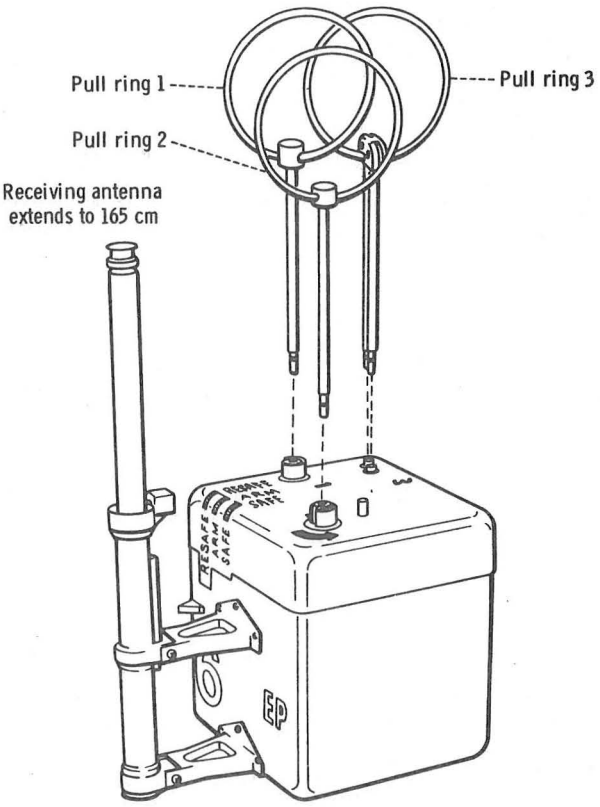

Notes: (1) Pull ring 1 - pulls one pin to start SAFE/ARM slide timer

(2) Pull ring 2 - swing up ring; rotate 90° counterclockwise; pull pin to release SAFE/ARM plate

(3) Pull ring 3 - pulls two pins to free firing pin and start thermal battery timer

FIGURE 10-6.–Arming sequence for an LSPE explosive package.

and one 5-bit seismic data sample from each of the four seismic data channels. Words 2 to 20 of each subframe are 7-bit samples from each of the four seismic data channels. Engineering data are interleaved and subcommutated, using the remaining 2 bits to form 30-bit words.

In words 2 to 19, geophone samples are sampled on the bit preceding the word on which they are read out; the most significant bit is read out first. In the first word of each subframe, the timing of the data sampling is the same as that in words 2 to 19 except that the samples are stored and read out in the last 20 bits with one 5-bit word/channel.

The time of the RF fire pulses must be accurately known. When the LSPE is commanded to the fire pulses "on" mode, a fire pulse set is transmitted once every 29.55 sec and is flagged in word 3 of subframe 1. This occurs once every 58 frames.

A command system provides for 11 commands associated with the LSPE. Two commands turn the LSPE on and off; two commands control the bit rate; and two commands control down-link formatting. In addition, commands are used to control amplifier gain status, transmission of fire pulses, and calibration of the geophones.

Explosive Package Description and Performance

An LSPE explosive package is shown in figure 10-6. The eight explosive packages are identical

except for the amount of high explosive and the preset runout time of the mechanical timers. An explosive package is activated by removing three pull pins (fig. 10-6). Removal of the first pull pin activates the SAFE/ARM slide timer, which is preset at 89.75, 90.75, 91.75, or 92.75 hr. Removal of the second pull pin releases the SAFE/ARM slide from its constrained SAFE position. Removal of the third pull pin removes a constraint on the firing pin and activates the thermal battery timer.

The LSPE transmitter, which is located within the ALSEP central station, transmits a repetitive pulsed carrier signal. A series of three pulses properly spaced in time is required to elicit a FIRE signal from the signal processor within the explosive package and to detonate the explosives train. The thermal battery, activated by the timer, has a minimum life of 2 min. This 2 min provides a time window long enough to ensure that at least one fire pulse set is received while the explosive package is energized electrically. Because the seismic data subsequently collected must be accurately referenced to the instant of detonation, it is necessary to establish which specific set of pulses is effective. This is done by comparing known times of pulse-set transmission with the time of arrival at the geophones of the initial seismic data. Pulse sets are spaced at 29.55-sec intervals to make such identification possible without ambiguity.

No difficulty was experienced in the deployment of the explosive packages during the periods of extravehicular activity (EVA) (fig. 10-7). The 454-g explosive package (EP-6) was deployed at station 1, and the 227-g explosive package (EP-7) was positioned on the return to the LM from station 1. Explosive packages 4, 1, and 8 were armed and placed on the lunar surface during the second EVA. During the third EVA, explosive packages 3, 5, and 2 were deployed. It was necessary to place the 1361-g

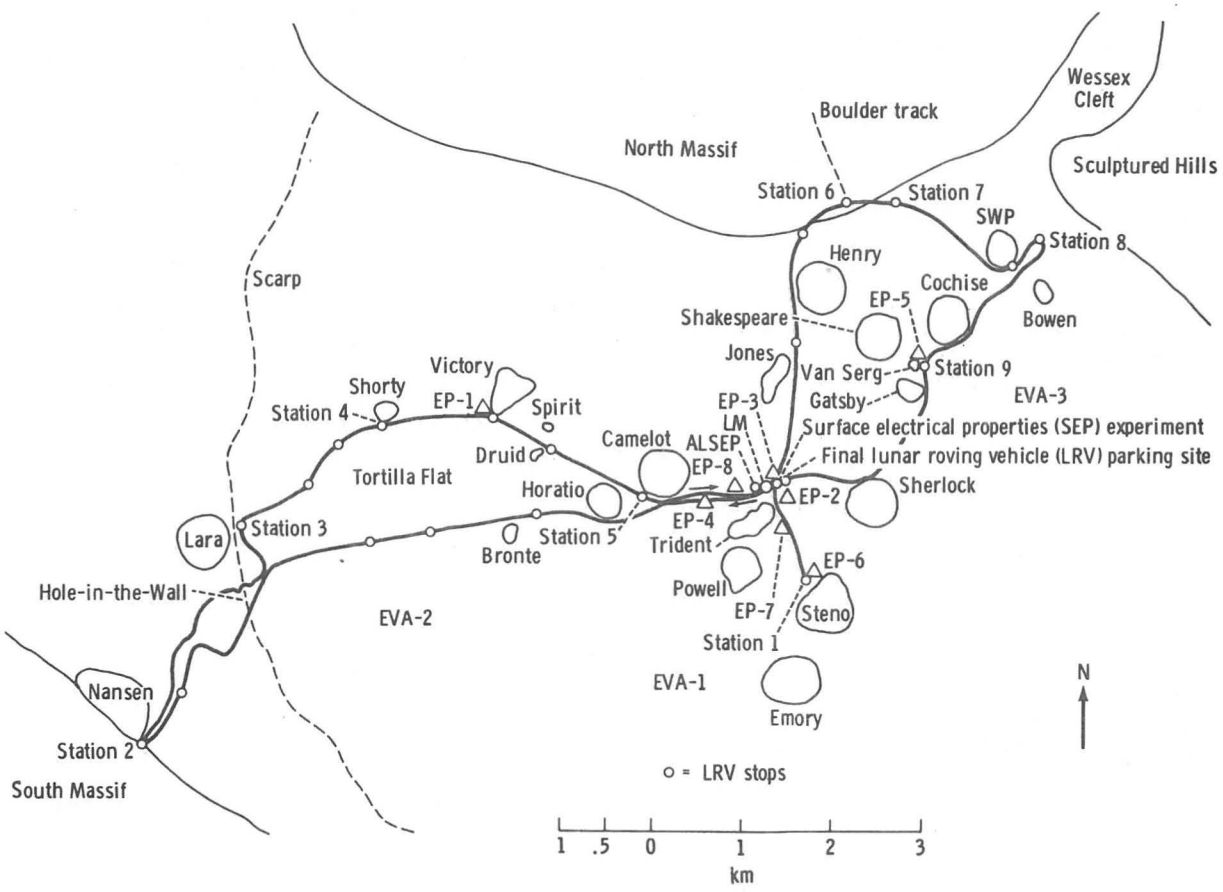

FIGURE 10-7.–Extravehicular activity traverses showing positions of deployed explosive packages at the Apollo 17 landing site.

explosive package (EP-5) at station 9 when it became apparent that insufficient time remained for a visit to the crater Sherlock. All the explosive packages were successfully detonated (table 10-III), and the detonation of EP-7 was visible from the television camera on the lunar roving vehicle (LRV). Figure 10-8 is a photograph showing EP-8 on the lunar surface approximately 296 m west of the LM.

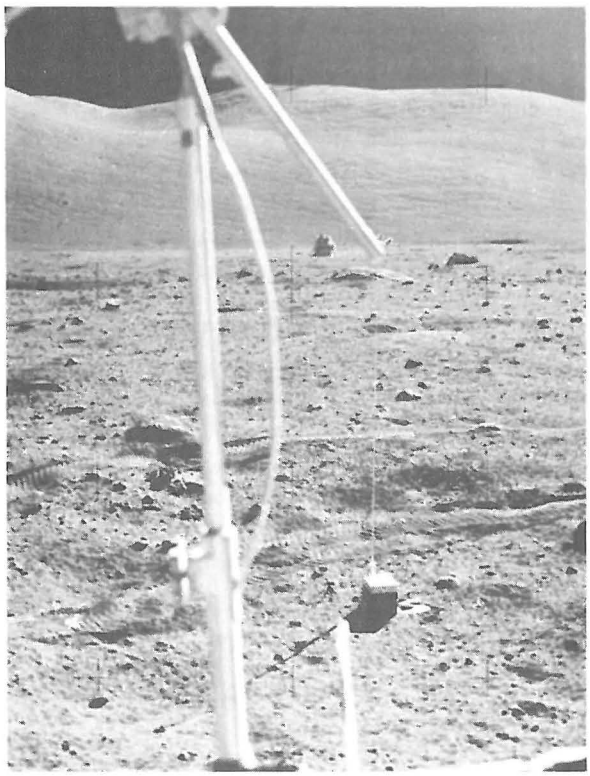

FIGURE 10-8.–Photograph of EP-8 on the lunar surface 296 m west of the LM (AS17-145-22184).

DESCRIPTION OF RECORDED SEISMIC SIGNALS

The Apollo 17 LSPE was planned to contribute to the understanding of the shallow lunar structure in two major ways: (1) by providing traveltimes of the seismic signals from explosive packages, which were to be detonated on the lunar surface at distances ranging from 100 to 2700 m, to the LSPE geophone array and (2) by impacting the Apollo 17 LM at a nominal distance of 10 km to provide traveltime data for deciphering the variation of seismic velocity with depth in the upper 5 km of the Moon. In addition, monitoring of the seismic signals generated by the LM ascent engine at lunar lift-off provided useful data.

Lunar Module Ascent

The LSPE was commanded on at 22:24:00 G.m.t. on December 14, 1972, to record the impulse produced by the thrust of the LM ascent engine. The effective zero time for the seismic impulse from the LM ascent-engine ignition was determined from NASA postflight analyses, which gave engine buildup pressure data at 5-msec intervals for the LM lift-off. The assigned ignition time of 22:54:38.424 G.m.t. corresponds to the time when the LM ascent engine achieved 20 percent of its maximum propulsion pressure. Clear seismic signals were recorded by the LSPE geophone array at distances of 148, 244, 190, and 187 m (fig. 10-9). Interpretation of the traveltime data is presented in the subsection entitled "Shallow Lunar Structure."

TABLE 10-III.–*Detonation Times of Explosive Packages*

Charge no.	*Explosive weight, g (lb)*	*Date, 1972*	*Time, G.m.t.*
EP-6	454 (1)	Dec. 15	23:48:14.56
EP-7	227 (1/2)	Dec. 16	02:17:57.11
EP-4	57 (1/8)	Dec. 16	19:08:34.67
EP-1	2722 (6)	Dec. 17	00:42:36.79
EP-8	113 (1/4)	Dec. 17	03:45:46.08
EP-5	1361 (3)	Dec. 17	23:16:41.06
EP-2	113 (1/4)	Dec. 18	00:44:56.82
EP-3	57 (1/8)	Dec. 18	03:07:22.28

Lunar Module Impact

The LSPE was commanded on at 06:36:00 G.m.t. on December 15 to record the LM ascent-stage impact. The impact occurred at latitude 19.91° N, longitude 30.51° E, 8.7 km southwest of the Apollo 17 landing site. Other pertinent parameters for the LM impact are given in table 10-IV.

A portion of the seismic signal from the Apollo 17 LM impact is shown in figure 10-10 in a compressed time scale. The impact signal is similar in character to previous impact signals; that is, these signals have an emergent beginning and a long duration. The initial portion of the impact signal on an expanded time

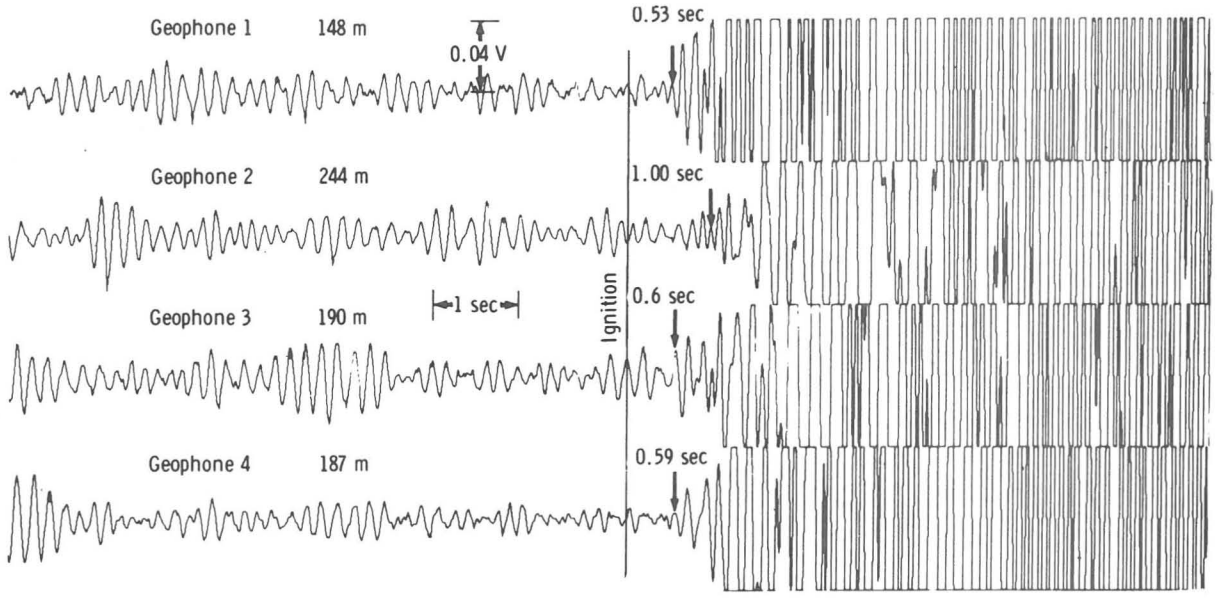

FIGURE 10-9.–Seismic signals recorded by the LSPE geophones from the lift-off of the Apollo 17 LM ascent stage (Dec. 14). Arrows point to onset of the first seismic arrival.

TABLE 10-IV.–*Parameters of Apollo 17 LM Impact*

Parameter	*Value*
Day, G.m.t.	Dec. 15, 1972
Range time,[a] G.m.t., hr:min:sec	06:50:20.84
Real time, G.m.t., hr:min:sec	06:50:19.60
Velocity, km/sec	1.67
Mass, kg	2260
Kinetic energy, J	3.15×10^9
Heading, deg	283

[a]Range time is the time the signal of the event was observed on Earth.

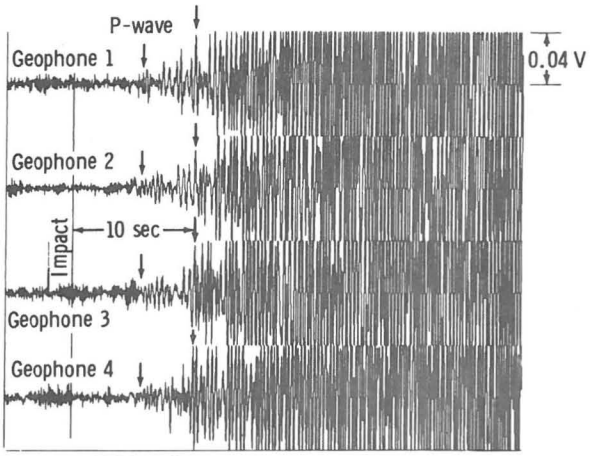

FIGURE 10-10.–Compressed time-scale record of the seismic signal received from the Apollo 17 LM impact (Dec. 15). Arrows point to measured first and second seismic arrivals.

scale is shown in figure 10-11. The arrival time of the first compressional wave (P-wave) is marked at 06:50:25.35 G.m.t., giving a traveltime of 5.75 sec.

The amplitude of the impact signal is of interest when compared with the P-wave amplitudes for previous LM and SIVB impact signals. Comparison of previous LM impact and SIVB impact signal amplitudes demonstrated that the LM impact data had to be adjusted upward by a factor of 17.4 to allow for the lower kinetic energy and a shallower angle of impact. Extrapolating the earlier LM impact data to a distance of 8.7 km leads to a predicted peak-to-peak amplitude of 26 nm. The Apollo 17 LM impact signal is centered at 4 Hz and has a measured peak-to-peak amplitude of 400 nm. This amplitude was caused by the Apollo 17 LM ascent stage striking the side of the mountainous South Massif rather than grazing the lunar surface. In other words, if the predicted amplitude of 26 nm is multiplied by the factor 17.4, the resulting figure is 452 nm, which agrees well with the observed amplitude of 400 nm. The LM impact traveltime data are discussed in the subsection entitled "Shallow Lunar Structure."

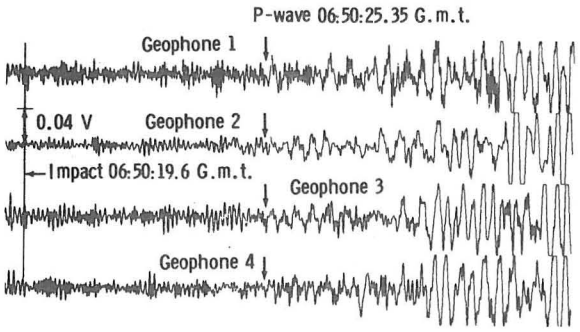

FIGURE 10-11.–Expanded time-scale record of the seismic signal from the Apollo 17 LM impact.

Analyses of previous lunar seismic impact signals (ref. 10-1) have demonstrated that many of their characteristics (signal rise time, duration of signal, and lack of coherence between horizontal and vertical components of motion) can be explained by wave scattering. Seismic energy is considered to spread with a diffusivity ξ proportional to the product of the average seismic velocity and the mean distance between scattering centers; that is, the larger the value of diffusivity, the smaller the amount of scattering. For a surface impact, the theory predicts (ref. 10-1) that the signal rise time (the time from signal onset to its maximum value) is given by R^2/ξ where R is the range.

The Apollo 17 LM impact seismic signal rise time of 56 sec leads to a diffusivity of 1.35 km^2/sec, which is significantly larger than the value of 0.033 km^2/sec inferred at the Apollo 16 site (ref. 10-2) from analysis of the seismic signals generated by the LRV at distances of approximately 4 km. The implication is that the Apollo 17 landing area is more homogeneous, for the dimensions of the seismic waves considered (approximately 25 m), than either the Apollo 15 or 16 landing areas. Such a difference in near-surface properties of these landing sites may be attributable to differing ages of the different areas and to the effects of differing amounts of comminution and gardening by meteoroid impacts.

Explosive Packages

All eight of the explosive packages placed on the lunar surface were successfully detonated. The seismic data recorded for EP-5, which was detonated at station 9, are shown in figure 10-12. The arrows point to the measured onset of the first seismic arrival.

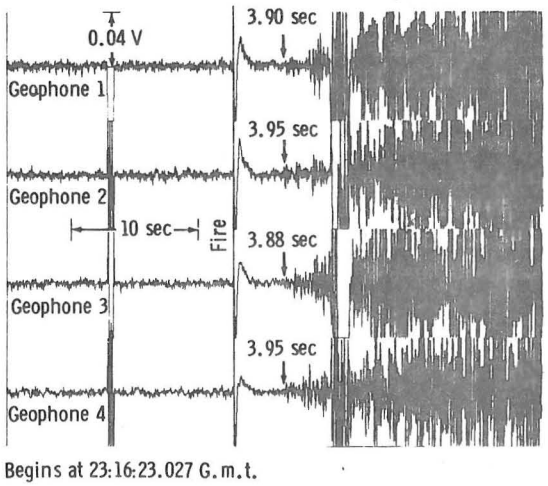

FIGURE 10-12.–Seismic signals produced by detonation of EP-5 on the lunar surface (Dec. 17). Arrows point to onset of seismic arrival.

Transmissions of the fire pulses at 29.55-sec intervals from the LSPE antenna (fig. 10-2) were observable as crosstalk on the individual geophone data channels and produced convenient, accurate references for selecting the detonation time of the individual explosive packages.

The locations of the explosive packages with respect to the LSPE geophone array were taken from preliminary postmission analyses (refs. 10-3 and 10-4). Adjustments in the absolute distances of the explosive packages will undoubtedly be necessary when subsequent analyses of the appropriate Apollo 17 lunar surface photographs are completed. However, it is not anticipated that any revisions in the distances will have a major effect on the traveltime data discussed in the following subsection.

SHALLOW LUNAR STRUCTURE

The traveltime/distance data obtained from the detonation of the eight explosive packages are shown in figure 10-13. Two sets of seismic wave first arrivals were observed traveling at velocities of 250 and 1200 m/sec. The shortest explosive-charge-to-geophone distance was approximately 100 m. If a seismic velocity of 100 m/sec is assumed for the regolith at the Apollo 17 site, a regolith as thick as 25 m would not have been detected. The depth of penetration of seismic waves is nominally one-fourth the explosive-charge-

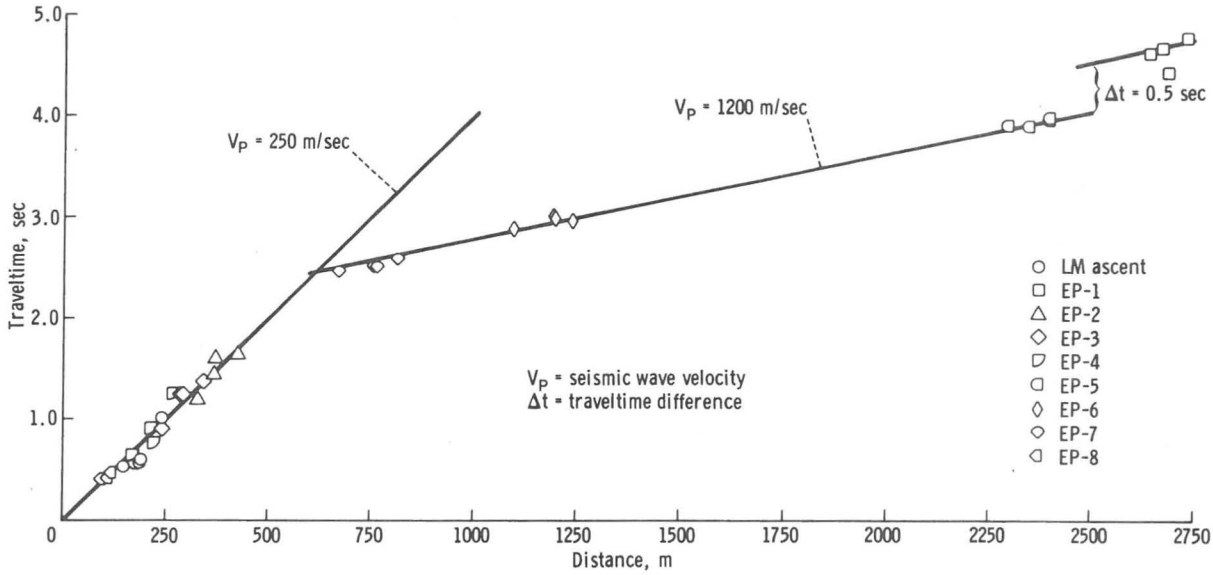

FIGURE 10-13.–Seismic arrivals from the detonation of the explosive charges plotted on a traveltime/distance graph.

to-receiver distance. However, it is probable that the regolith is significantly thinner than 25 m, inasmuch as the 250-m/sec velocity curve extrapolates to a zero intercept time.

The faster seismic arrival with a velocity of 1200 m/sec was observed beginning at a distance of 612 m, indicating that the thickness of the 250-m/sec material was 248 m. Considering uncertainties in the charge distances and in the inferred seismic velocities, the depth estimates are considered accurate to 10 percent. The 1200-m/sec velocity was observed to a distance of approximately 2.5 km. At this distance, the observed traveltimes for EP-1 were offset by approximately 0.5 sec with respect to the 1200-m/sec line.

Examination of the path between EP-1 and the LSPE geophone array revealed that the seismic path was affected by the presence of the 600-m-diameter crater Camelot. The observed time delay on the seismic path can be explained by postulating that low-velocity material extends to a greater depth beneath the crater Camelot than along the remainder of the traveltime path. A simple model approximation for Camelot Crater that explains the observed traveltime delay is shown in figure 10-14.

The traveltime data from the LSPE explosive charges can be combined with the observed traveltime for the LM impact to provide information about the

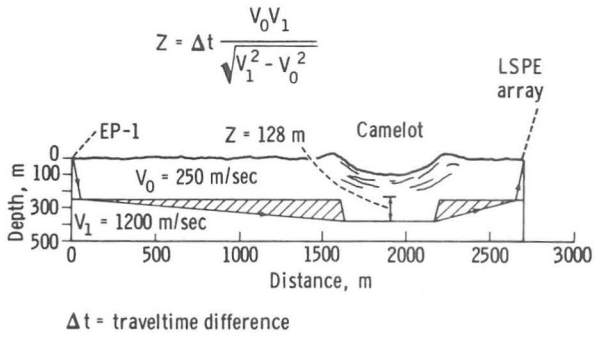

FIGURE 10-14.–Model approximation for seismic ray path from EP-1 to LSPE array that crosses Camelot Crater. Observed time delay is produced by presence of low-velocity material (of thickness Z) beneath crater.

seismic velocity to a depth of several kilometers. Traveltime data from the seismic signals produced by the LM impact and the explosive charges are shown in figure 10-15. A line with an apparent velocity of 4 km/sec can be fitted through the LM impact data point to intersect close to the corrected traveltime data point for EP-1. Because of obvious uncertainties in allowing for the time delay through the crater Camelot, there is no a priori reason to force a specific apparent-velocity line through the EP-1 data point. The first-order conclusion is that high-velocity material (≈4 km/sec) must lie beneath the 1200-m/sec material.

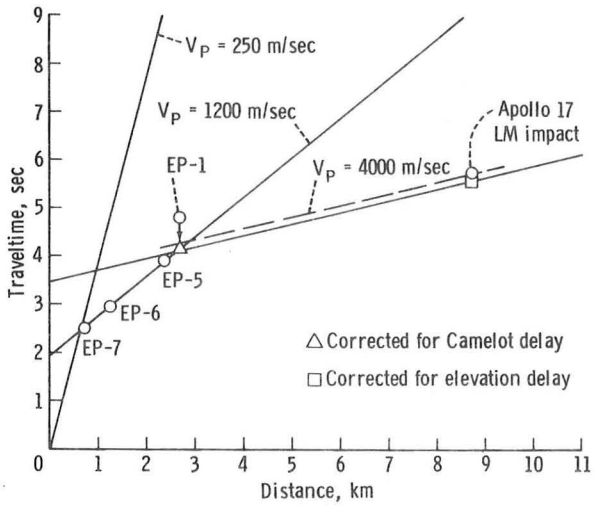

FIGURE 10-15.–Seismic traveltimes from LM impact and LSPE explosive charges. Traveltime for EP-1 has been corrected for Camelot Crater delay, and LM impact traveltime has been corrected for 1.2-km elevation difference between the impact point and the LSPE array. These corrections shift the position of the 4-km/sec apparent velocity slightly downward as shown.

Inasmuch as the LM impacted at an elevation of 1.2 km (fig. 10-1) above the valley floor at the Apollo 17 landing site, the LM impact traveltime can be adjusted to the same reference elevation as the LSPE geophone array. The 1.2-km difference in elevation contributes an additional delay time equal to the ratio of the elevation difference to the seismic velocity of the material traversed multiplied by the cosine of the angle of incidence at which the particular seismic arrival under consideration departed the source (impact point). Inserting the appropriate values in this case leads to a time correction of 0.18 sec. This correction will shift the position of the 4-km/sec apparent-velocity line downward as shown in figure 10-15 such that its zero distance time intercept is decreased. The end result is a decrease in the derived thickness of the 1200-m/sec material from 1020 to 927 m.

It is possible that a dipping interface exists beneath the 1200-m/sec material that might result in a high apparent velocity, or that the particular seismic ray passed through a high-velocity heterogeneity somewhere along its path. Some of the uncertainty may be resolved by subsequent digital velocity filtering (beam steering) of the LM impact signal on the LSPE array.

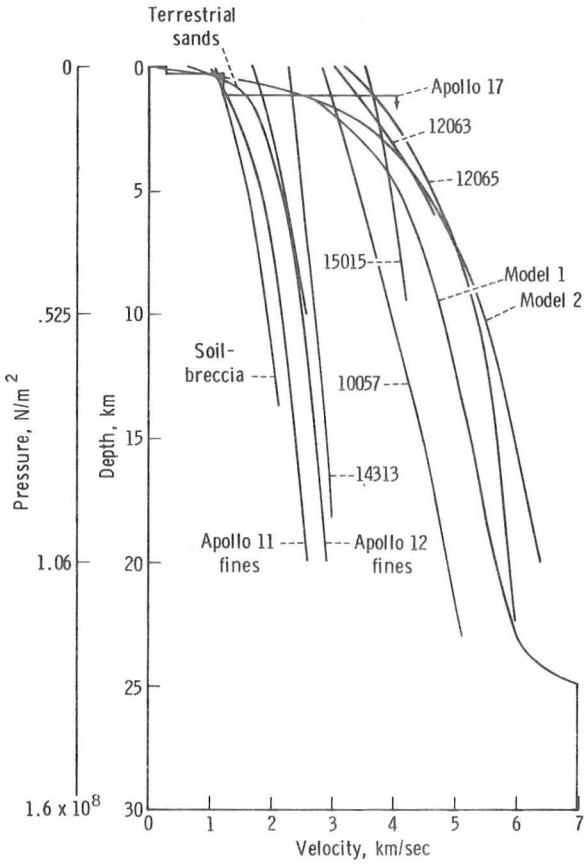

FIGURE 10-16.–Inferred compressional-wave velocity profiles for the Moon and velocities of lunar and terrestrial rocks measured in the laboratory as a function of pressure. Lunar rocks are identified by sample number. Lunar models 1 and 2 are based on results available through Apollo 16. Apollo 17 results reveal a marked stepwise increase in seismic velocity in the upper 2 km of the Moon.

Before the Apollo 17 mission, the best estimates of the seismic velocity variation in the upper 20 km of the Moon were as depicted by lunar model 1 or 2 in figure 10-16. The seismic velocity was known to increase very rapidly from values of 100 to 300 m/sec in approximately the upper 100 m to a value of ≈4 km/sec at a depth of 5 km. Even though the seismic velocity variation was depicted as a smooth increase with depth, it was surmised (ref. 10-5) that such a rapid increase of velocity (≈2 km/sec/km) could not be explained solely by the pressure effect on dry rocks with macrocracks and microcracks nor by the self-compression of any rock powder.

Laboratory velocity measurements on returned lunar soils (refs. 10-6 to 10-10) and recent measure-

ments under hydrostatic pressure conditions on terrestrial sands and basaltic ash have indicated velocity-depth gradients of 0.4 to 0.8 km/sec/km, but such gradients occur only to pressures of $\approx 50 \times 10^5$ N/m^2 (a lunar depth of ≈1 km). The measurements on unconsolidated sands and rock powders also have demonstrated that no unique relation exists between seismic velocity and porosity in granular material. An examination of these experimental data led to the inference that compositional or textural changes must be important in the upper 5 km of the Moon (ref. 10-5).

The LSPE results have shown that, at least beneath the Taurus-Littrow site, the seismic velocity increases in a stepwise manner in the upper several kilometers. It is of interest to examine the in situ velocity information with reference to the surface geological investigations at the Apollo 17 site, the laboratory velocity measurements from returned lunar samples, and the seismic velocity measurements on terrestrial lunar analogs.

Premission analyses indicated that much of the Apollo 17 landing site area is covered by a dark mantling material, possibly volcanic ash (ref. 10-11). Crew observations of the lunar surface revealed that there was no readily discernible boundary between the overlying thin regolith and the dark mantling material. The thickness of the dark mantling material was estimated to be between 5 and 10 m (ref. 10-3). As pointed out earlier, whether the dark mantling material/subfloor interface represents a sharp seismic discontinuity or is gradational cannot be determined because the shortest explosive-charge-to-receiver distance was approximately 100 m.

The dominant rock type observed underlying the dark mantling material is a medium-grained vesicular basalt believed to be primarily mare-type basalt. Crew observations of the crater walls revealed textural variations that suggest the involvement of individual flow units. Seismic observations have indicated 248 m of 250-m/sec material overlying 927 m of 1200-m/sec material.

The abrupt change in seismic velocity from 250 to 1200 m/sec and, by inference, in other physical properties suggests a major change in the nature of the evolution or deposition of the Apollo 17 subfloor basalts. However, a similar range of seismic velocities has been observed with refraction surveys on terrestrial lava flows. Some insight can be gained by considering specific lava flows that have been examined in some detail as possible lunar analogs: the Southern Coulee, the SP flow, and the Kana-a flow (refs. 10-12 and 10-13).

The Southern Coulee is a recent lava flow near the Mono Craters in eastern California. Seismic velocities range from 160 m/sec at the surface to 2000 m/sec at depth. The higher velocities are found in more competent, denser lava that underlies higher porosity, lower density surface material. The SP flow is a blocky basalt flow located in the northern part of the San Francisco volcanic field near Flagstaff, Arizona. Vesicularity ranges from 5 to 50 percent, and in situ seismic velocities range from 700 to 1100 m/sec. The Kana-a flow, also located near Flagstaff, is an olivine basalt flow intermingled with ash; seismic velocities range from 700 to 1200 m/sec.

Observed velocities on terrestrial lava flows bracket the velocities measured at the Apollo 17 site and therefore support the presence of lava flows in the Taurus-Littrow valley. Whether the 250-m/sec velocity is representative of a separate flow or is merely the manifestation of shattered near-surface basalts mixed with pyroclastic materials cannot be resolved from the seismic data. Nevertheless, a surface layer of fractured, loose, blocky material merging into more welded flows is a common occurrence on Earth. Photographs of the walls of Hadley Rille (ref. 10-14) also attest to the blocky nature of the near-surface mare basalts. Because of the similarity in structure and the analogous seismic velocities on the Earth and the Moon, the sum of the 248 m of 250-m/sec material and 927 m of 1200-m/sec material, 1175 m, is designated as representing the full thickness of the subfloor basalts at the Apollo 17 site.

The material underlying the basalts with a seismic velocity of ≈4 km/sec is difficult to classify by rock type. Based on the geological evidence, it seems likely that the highland massif material that rings the narrow, grabenlike valley at the Apollo 17 site underlies the basalt flow or flows. Several rock types were recognized in the North and South Massifs, but the dominant rock type is apparently a coherent breccia believed to be similar to the breccias sampled at the Apennine Front (Apollo 15) and at Descartes (Apollo 16).

Laboratory velocity measurements have been reported for two Apollo 15 breccias, 15418 and 15015 (ref. 10-15). Sample 15418 is described as a dark-gray breccia of chemical composition similar to that of anorthite-rich gabbro. Sample 15015 is a more friable

breccia of unknown composition. The in situ value of ≈4 km/sec is close to the seismic velocities measured in the laboratory for sample 15015 and shown in figure 10-16.

CONCLUSIONS

Before the Apollo 17 mission, the question of how the P-wave velocity increased from 100 to 300 m/sec near the surface (refs. 10-16 to 10-19) to ≈6 km/sec at a depth of 15 to 20 km (ref. 10-2) was unexplained. The main reason for the uncertainty was the gap in traveltime data between the range of a few hundred meters (previous active seismic experiments) and 67 km (Apollo 14 LM impact as recorded by the Apollo 14 passive seismic experiment). The Apollo 17 lunar seismic profiling results have demonstrated that the seismic velocity increases in a sharp stepwise manner in the upper 2.5 km. A surface layer with a seismic velocity of 250 m/sec overlies a layer with a velocity of 1200 m/sec. Beneath the 1200-m/sec layer, the seismic velocity increases sharply to 4000 m/sec. The velocities of 250 and 1200 m/sec agree with those observed for basaltic lava flows, indicating a total thickness of approximately 1200 m for the infilling mare basalts at Taurus-Littrow. When the Apollo 17 results are combined with earlier traveltime data for direct and surface-reflected seismic arrivals from LM and SIVB impacts (ref. 10-2), it will be possible to construct a velocity model for the upper lunar crust believed to be representative for a mare basin. Such work is now underway.

REFERENCES

10-1. Latham, Gary V.; Ewing, Maurice; Press, Frank; Sutton, George; et al.: Passive Seismic Experiment. Sec. 6 of Apollo 14 Preliminary Science Report. NASA SP-272, 1971.

10-2. Latham, Gary V.; Ewing, Maurice; Press, Frank; Sutton, George; et al.: Passive Seismic Experiment. Sec. 9 of Apollo 16 Preliminary Science Report. NASA SP-315, 1972.

10-3. Apollo Lunar Geology Investigation Team: Preliminary Report on the Geology and Field Petrology of the Apollo 17 Landing Site. U.S. Geol. Survey, Interagency Rept.: Astrogeology 69, Dec. 17, 1972.

10-4. Apollo Lunar Geology Investigation Team: Documentation and Environment of the Apollo 17 Samples: A Preliminary Report. U.S. Geol. Survey, Interagency Rept.: Astrogeology 71, Jan. 21, 1973.

10-5. Kovach, R. L.; and Watkins, J. S.: The Velocity Structure of the Lunar Crust. The Moon, vol. 7, Apr. 1973, pp. 63-75.

10-6. Kanamori, Hiroo; Nur, Amos; Chung, D.; Wones, D.; and Simmons, G.: Elastic Wave Velocities of Lunar Samples at High Pressures and Their Geophysical Implications. Science, vol. 167, no. 3918, Jan. 30, 1970, pp. 726-728.

10-7. Kanamori, H.; Mizutani, H.; and Hamano, Y.: Elastic Wave Velocities of Apollo 12 Rocks at High Pressures. Proceedings of the Second Lunar Science Conference, vol. 3, MIT Press (Cambridge, Mass.), 1971, pp. 2323-2326.

10-8. Anderson, Orson L.; Scholz, Christopher; Soga, Naohiro; Warren, Nicholas; et al.: Elastic Properties of a Micro-Breccia, Igneous Rock and Lunar Fines from Apollo 11 Mission. Proceedings of the Apollo 11 Lunar Science Conference, vol. 3, Pergamon Press (New York), 1970, pp. 1959-1973.

10-9. Mizutani, H.; Fujii, N.; Hamano, Y.; Osako, M.; et al.: Elastic Wave Velocities and Thermal Diffusivities of Apollo 14 Rocks. Lunar Science–III (Rev. abs. of the Third Lunar Science Conference (Houston, Tex.), Jan. 10-13, 1972), Feb. 18, 1972, pp. 547-549.

10-10. Warren, N.; Schreiber, E.; Scholz, C.; Morrison, J. A.; et al.: Elastic and Thermal Properties of Apollo 11 and Apollo 12 Rocks. Proceedings of the Second Lunar Science Conference, vol. 3, MIT Press (Cambridge, Mass.), 1971, pp. 2345-2360.

10-11. McGetchin, T. R.; and Head, J. W.: Lunar Cinder Cones. Science, vol. 180, no. 4081, Apr. 6, 1973, pp. 68-71.

10-12. Watkins, J. S.: Annual Report, Investigation of In Situ Physical Properties of Surface and Subsurface Site Materials by Engineering Geophysical Techniques. NASA Contract T-25091(G), July 1966.

10-13. Watkins, Joel S.; Walters, Lawrence A.; and Godson, Richard H.: Dependence of In Situ Compressional-Wave Velocity on Porosity in Unsaturated Rocks. Geophysics, vol. 37, no. 1, Feb. 1972, pp. 29-35.

10-14. Howard, Keith A.; Head, James W.; and Swann, Gordon A.: Geology of Hadley Rille. Proceedings of the Third Lunar Science Conference, vol. 1, MIT Press (Cambridge, Mass.), 1972, pp. 1-14.

10-15. Todd, Terrence; Wang, Herbert; Baldridge, W. Scott; and Simmons, Gene: Elastic Properties of Apollo 14 and 15 Rocks. Proceedings of the Third Lunar Science Conference, vol. 3, MIT Press (Cambridge, Mass.), 1972, pp. 2577-2586.

10-16. Kovach, Robert L.; Watkins, Joel S.; and Landers, Tom: Active Seismic Experiment. Sec. 7 of Apollo 14 Preliminary Science Report. NASA SP-272, 1971.

10-17. Kovach, R. L.; and Watkins, J. S.: The Near-Surface Velocity Structure of the Moon. Lunar Science–III (Rev. abs. of the Third Lunar Science Conference (Houston, Tex.), Jan. 10-13, 1972), Feb. 18, 1972, pp. 461-462.

10-18. Watkins, Joel S.; and Kovach, Robert L.: Apollo 14 Active Seismic Experiment. Science, vol. 175, no. 4027, Mar. 17, 1972, pp. 1244-1245.

10-19. Kovach, Robert L.; Watkins, Joel S.; and Talwani, Pradeep: Active Seismic Experiment. Sec. 10 of Apollo 16 Preliminary Science Report. NASA SP-315, 1972.

Reprinted from
8 June 1973, Volume 180, pp. 1063-1064

SCIENCE

Apollo 17 Seismic Profiling: Probing the Lunar Crust

Robert L. Kovach and Joel S. Watkins

Apollo 17 Seismic Profiling: Probing the Lunar Crust

Abstract. *Apollo 17 seismic data are interpreted to determine the structure of the lunar crust to a depth of several kilometers. Seismic velocity increases in a marked stepwise manner beneath the Taurus-Littrow region at the Apollo 17 site. A thickness of about 1200 meters is indicated for the infilling mare basalts at Taurus-Littrow. The apparent velocity is high (about 4 kilometers per second) in the material immediately underlying the basalts.*

The successful installation of a geophysical station at the Taurus-Littrow landing site of the Apollo 17 mission marked the culmination of an exciting period of manned lunar exploration and vastly improved our knowledge of the lunar interior. Before the Apollo 17 mission there was a surprising gap in our knowledge concerning the nature of the upper 10 km of the lunar crust because of the absence of pertinent seismic travel time data at distances closer than 30 km. Travel times of seismic waves are inverted to determine the seismic velocity structure and provide the direct means of probing the lunar interior.

The seismic velocity in the moon was known to increase rapidly from values of 100 to 300 m/sec in the upper 100 m to a value of about 6 km/sec at a depth of 15 to 20 km. Even though the seismic velocity variation was believed to be a smooth increase with depth it was surmised (*1*) that such a rapid increase of velocity (approximately 2 km/sec per kilometer) could not be explained solely by the effect of increasing pressure on dry rocks with macroscopic and microscopic cracks or by the self-compression of any granular rock powder.

Laboratory velocity measurements on returned lunar soils and on terrestrial sands and basaltic ash (*2*) have indicated velocity-depth gradients of 0.4 to 0.8 km/sec per kilometer, but such gradients occur only to pressures of about 50 bars (corresponding to a lunar depth of about 1 km). An examination of these experimental data led to the inference that compositional or textural changes must be important in the upper 5 km of the moon (*1*).

The purpose of the Apollo 17 lunar seismic profiling experiment was to record on a triangular array of four seismometers the vibrations of the lunar surface as induced by explosive charges, the thrust of the lunar module (LM) ascent engine, and the crash of the LM ascent stage.

Strong seismic signals were recorded from the detonation of eight explosive charges, which were armed and placed on the lunar surface by the Apollo 17 crew at various points along the traverses. The weights of the explosive charges ranged from 0.06 to 2.7 kg. Recording of these signals generated seismic travel time data in the distance range from 0.1 to 2.7 km.

One of the more significant events of the Apollo 17 mission was the recording of the seismic signal from the LM ascent stage, which struck the lunar surface 8.7 km southwest of the landing site in the highlands of the South Massif. The seismic signals from this impact were observed at a greater depth of penetration than could be achieved solely with the use of small explosive charges. The impact signal was similar in character to previous impact signals, having an emergent beginning and a long duration (*3*, *4*).

The observed travel times for the detonation of the explosive charges can be combined with the observed travel time for the LM impact to provide information about the seismic velocity to a depth of several kilometers beneath the Apollo 17 landing site. Since the LM impacted at an elevation of 1.2 km above the recording seismometer array the LM travel time has been adjusted to the same reference elevation as the geophone array. The correction is small and decreases the observed time of 5.75 seconds by 0.18 second. Travel time data from the LM impact and the explosive charges are plotted against distance in Fig. 1. Three *P*-wave (compressional wave) velocities are represented in the travel time data: 250, 1200, and 4000 m/sec. There is some uncertainty in the apparent velocity of 4000 m/sec determined primarily by the LM impact data point at a distance of 8.7 km, but the important fact is that high-velocity material ($\geqslant$ 4000 m/sec) must lie beneath the 1200-m/sec material. The 1200-m/sec material is 925 m thick and it is overlain by a layer with a thickness of 248 m and a velocity of 250 m/sec.

Our results have shown that, at least beneath the Taurus-Littrow site, the seismic velocity increases in a stepwise manner in the upper several kilometers. It is of interest to examine our in situ velocity information in the light of the surface geological investigations at the Apollo 17 site, laboratory velocity measurements from returned lunar samples, and seismic velocity measurements on terrestrial lunar analogs.

Premission analyses have shown that

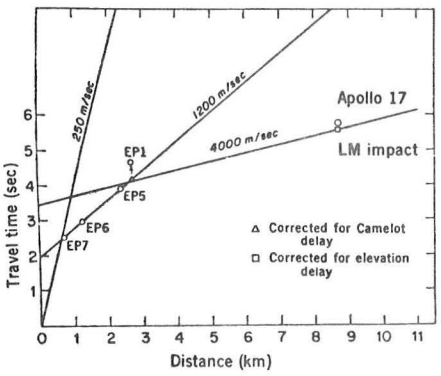

Fig. 1. Travel times of seismic *P*-wave pulses as a function of distance for Apollo 17 explosive charges and the LM impact. The data points defining the 250-m/sec line are omitted for brevity. The travel time for explosive package 1 (EP1) was corrected for propagation delay through a large crater, Camelot, and the LM impact travel time was corrected for an elevation effect.

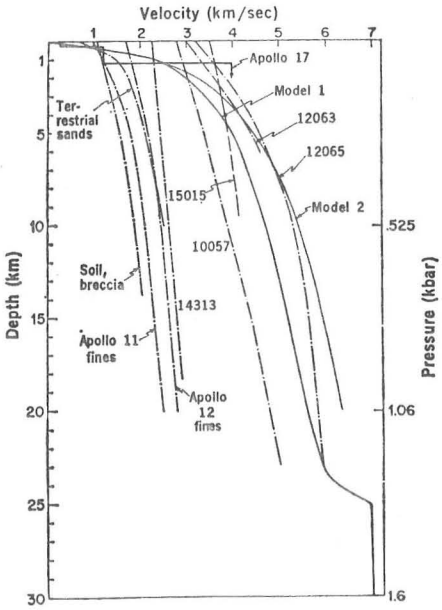

Fig. 2. Velocity model from the Apollo 17 results compared to earlier lunar models [models 1 and 2 (*4*)] and to velocities for lunar rocks and terrestrial sands measured in the laboratory as a function of pressure. Lunar rocks are identified by sample numbers.

much of the Apollo 17 landing site area is covered by a dark mantling material. Observations by the Apollo 17 crew on the lunar surface revealed that any boundary between an overlying thin regolith and the dark mantling material was not readily discernible. Because our closest distance between an explosive charge and the receiver was about 100 m we could not resolve the properties of the upper 20 m or so, and cannot determine whether the interface between the dark mantling material and the subfloor represents a sharp seismic discontinuity or is gradational. However, our data indicate that any horizon, if present, would be less than 20 m from the lunar surface.

Underlying the dark mantling material the dominant rock type observed by the Apollo 17 crew is a medium-grained vesicular basalt believed to be primarily mare-type basalt. Observations in crater walls revealed textural variations, suggesting that individual flow units are involved. Our seismic observations have indicated 248 m of 250-m/sec material overlying 925 m of 1200-m/sec material.

The abrupt change in seismic velocity (and, by inference, in other physical properties) from 250 to 1200 m/sec is suggestive of a major change in the nature of the evolution or deposition of the Apollo 17 subfloor basalts. However, a similar range of seismic velocities is observed with refraction surveys in lava flows on the earth (*5*).

The velocities observed in terrestrial lava flows bracket the velocities measured at the Apollo 17 site and therefore support the presence of lava flows in the Taurus-Littrow valley. Whether the velocity of 250 m/sec is representative of a separate flow or several flows separated by lower-velocity layers of ash or ejecta cannot be resolved from the seismic data. Individual flows may be fractured or brecciated, which could further decrease their seismic velocities. Surface layers of fractured loose blocky material merging into more welded flows are common occurrences on the earth. We believe that the total thickness of the materials with seismic velocities of 250 and 1200 m/sec (1173 m) represents the full thickness of the subfloor basalts at the Apollo 17 site (*6*).

The nature of the 4000-m/sec material underlying the basalts is difficult to unambiguously assign to any particular rock type. It seems likely, based on the geological evidence, that the highland massif material which rings the narrow graben-like valley at the Apollo 17 site underlies the basalt flow or flows. Several rock types were recognized in North Massif and South Massif but the dominant rock type is apparently a coherent breccia believed to be similar to breccias sampled at the Apennine front (Apollo 15) and Descartes (Apollo 16).

Laboratory velocity measurements have been reported for two Apollo 15 breccias, 15418 and 15015 (*7*). Sample 15418 is described as a dark grey breccia of chemical composition similar to anorthite-rich gabbro. Sample 15015 is a more friable breccia of unknown composition. The in situ value of approximately 4000 m/sec is close to the values measured in the laboratory for sample 15015.

Before the Apollo 17 mission the question of how the *P*-wave velocity increased from 100 to 300 m/sec near the surface to about 6 km/sec at a depth of 15 to 20 km was most uncertain. The Apollo 17 lunar seismic profiling results (Fig. 2) have demonstrated that the seismic velocity increases in a sharp stepwise manner in the upper 2.5 km. When our Apollo 17 results are combined with earlier travel time data for direct and surface-reflected arrivals from earlier LM and Saturn (S-IV B) impacts it will be possible to construct a velocity model for the upper lunar crust representative for a lunar mare basin.

ROBERT L. KOVACH
Department of Geophysics, Stanford University, Stanford, California 94305
JOEL S. WATKINS
Marine Biomedical Institute, University of Texas, Galveston 77550

References and Notes

1. R. L. Kovach and J. S. Watkins, *Moon*, in press.
2. H. Kanamori, A. Nur, D. H. Chung, D. Wones, G. Simmons, *Science* **167**, 726 (1970); H. Kanamori, H. Mizutani, Y. Yamano, *Geochim. Cosmochim. Acta* **2** (Suppl. 2), 2323 (1971); N. Warren, E. Schreiber, C. Scholz, J. A. Morrison, P. R. Norton, M. Kumazawa, O. L. Anderson, *ibid.*, p. 2345; O. L. Anderson, C. Scholz, N. Soga, N. Warren, E. Schrieber, *ibid.* **2** (Suppl. 1), 1959 (1970); H. Mizutani, N. Fujii, Y. Hamano, M. Osako, H. Kanamori, in *Revised Abstracts of the Third Lunar Science Conference* (Lunar Science Institute, Houston, 1972), p. 547; P. Talwani, A. Nur, R. L. Kovach, *J. Geophys. Res.*, in press.
3. G. Latham *et al.*, *NASA Spec. Publ. NASA SP-272* (1971), p. 133.
4. G. Latham *et al.*, *NASA Spec. Publ. NASA SP-315* (1973), p. 9-1.
5. J. S. Watkins, L. A. Walters, R. A. Godson, *Geophysics* **37**, 29 (1972).
6. The traverse gravimeter experiment carried out on the Apollo 17 mission suggests basalt flows with a positive density contrast of 0.8 g//cm^3 and a thickness of 1 km (M. Talwani, personal communication).
7. T. Todd, H. Wang, W. S. Baldridge, G. Simmons, *Geochim. Cosmochim. Acta* **3** (Suppl. 3), 2577 (1972).
8. We thank A. Nur for reviewing the manuscript. Supported by NASA contract NAS-9-5632.

6 March 1973

Proceedings of the Fourth Lunar Science Conference
(Supplement 4, *Geochimica et Cosmochimica Acta*)
Vol. 3, pp. 2561–2574

Seismic investigation of the lunar regolith*

JOEL S. WATKINS

Earth and Planetary Sciences Division, University of Texas, Galveston, Texas 77550

ROBERT L. KOVACH

Department of Geophysics, Stanford University, Stanford, California 94305

Abstract—Seismic investigation of the lunar regolith shows that the regolith consists of a layer with an average velocity of 105 m/sec. Seismically determined regolith thicknesses in the highlands average 10 m, about twice the thickness deduced from astronaut observations and photographs from the maria. The difference in thickness is thought to be due to a depositional rate about one order of magnitude greater during the interval between formation of the circular maria and the extrusion of mare basalts than during the post-extrusion interval.

Seismic velocities observed in the regolith indicate that the regolith consists primarily of impact derived ejecta. The regolith at the Apollo 17 site is anomalously thick, probably because the site is in the midst of a crater field and because of irregularities in the surface of the underlying subfloor basalt. The Apollo 17 seismic data do not support the compacted powder model of the lunar near surface but show that the lunar crust to a depth of over 1 km consists of horizontal or subhorizontal strata comprised of breccia, lava flows, and rock.

INTRODUCTION

SEISMIC DATA pertaining to the lunar regolith were obtained at all but the Apollo 11 site. On missions 12, 14, and 15, the Passive Seismic Experiment (PSE) provided seismic data from the regolith; on missions 14 and 16 the Active Seismic Experiment (ASE) provided the seismic data, and on mission 17, the Lunar Seismic Profiling Experiment (LSPE) provided the data.

The ASE included a low energy source of seismic energy designed primarily to obtain seismic data from the regolith. The other experiments gleaned data incidentally in the course of their primary missions of collecting seismic data from rocks beneath the regolith.

Data analyzed to date consist entirely of *P*-wave travel times. From these data it has been possible to deduce velocities of *P*-waves traversing the regolith and/or regolith thicknesses at each site except the Apollo 17 site. At this site it was possible only to obtain a maximum thickness.

The seismic data have been interpreted in terms of rock properties and rock structure. The interpretation is based on properties of similar terrestrial rocks (e.g., basaltic lavas, fragmental rocks and breccias at Meteor Crater, Arizona), theoretical models, and geological evidence. In this paper, we review seismic data obtained during the Apollo missions, discuss the model of the regolith which we feel best explains the data, and discuss some of the implications of the data.

---

*Earth and Planetary Sciences Division, Marine Biomedical Institute. Contribution No. 18.

EXPERIMENTAL RESULTS

Astronauts deployed the PSE on Apollo missions 12, 14, 15, and 16. On missions 12, 14, and 15, the PSE short period vertical (SPZ) seismometer recorded the LM ascent. In each instance, a regolith arrival was observed (Latham *et al.*, 1970, 1971, 1972). Regolith *P*-wave velocities were 108 m/sec, 104 m/sec, and 92 m/sec. Since each ascent was recorded by only one instrument, it was not possible to deduce the thickness of the regolith.

On Apollo 14 and 16, astronauts deployed the ASE, an experiment which depends on explosives for seismic energy. The ASE consists of a thumper, a mortar package assembly (MPA), a linear array of 3 geophones, and associated electronics (Kovach, 1967; McAllister *et al.*, 1969; Watkins *et al.*, 1969). The thumper, which was designed to investigate the regolith, is an astronaut-activated staff containing 21 small explosives in its base. Firing of an explosive produces seismic energy by driving the base plate into the regolith or "thumping" the regolith surface. A pressure transducer in the base detects the instant of detonation. The geophones detect seismic waves radiating away from the thump via the regolith and subjacent strata. ASE electronics compress the geophone data and transmit it to the earth in real time.

Mortar launches provide additional data on the seismic properties of the regolith. Although the MPA was designed to provide seismic data from rocks below the regolith, mortar launches generate a detectible signal which travels through the regolith and immediately subjacent rocks. These signals were used in analysis

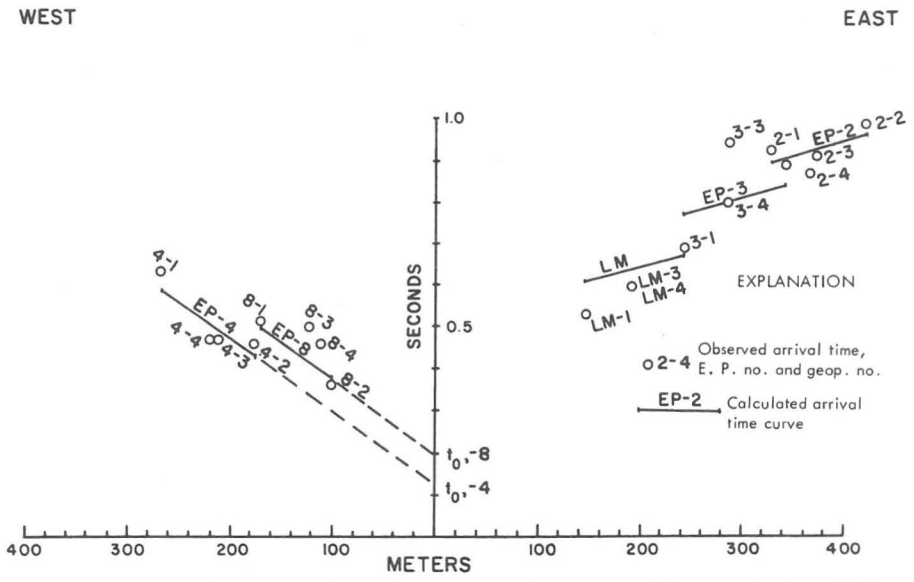

Fig. 1. Arrival time observed from headwaves refracted from EP-2, -3, -4, -8, and LM ascent events; and arrival time ranges calculated for headwaves refracted by a layer 17.4 m beneath geophone 3 and dipping 3° East.

of Apollo 16 data (Kovach *et al.*, 1973a). LM ascent data were recorded by the ASE at the Apollo 16 site (Kovach *et al.*, 1973a) and used in the interpretation. ASE data from Apollo 14 and 16 sites yielded regolith velocities of 104 and 114 m/sec, respectively, and regolith thicknesses of 8.5 and 12.2 m, respectively.

The LSPE consisted of 4 geophones deployed in a triangular array, eight explosive packages (EP), and associated electronics. All EPs were deployed too far from the array to obtain first arrivals of the regolith *P*-wave. It is possible that examination of second arrivals will yield the velocity of the regolith in the vicinity of the LSPE array but examination of second arrivals to date has been cursory and inconclusive.

The first arrivals from explosives detonated near the Apollo 17 LSPE array at Taurus-Littrow are shown in Fig. 1. The pattern of arrivals differs in two important respects from the pattern of arrivals recorded by the ASE at the Apollo 14 and 16 sites.

The first important difference is that velocities calculated from waves traversing the array are significantly higher than the velocities calculated from arrivals at more distant EPs (850 m/sec vs. 280 m/sec). This phenomenon we attribute to the "thin-layer" effect. When a layer has a velocity higher than that of layers above and below, arrivals from the layer will mask arrivals from lower layers. The extent of masking depends on velocities and thicknesses of the layers. If the high velocity is thin (less than a wave length thick) energy will leak from the bottom of the layer at a relatively high rate. As a result, the amplitude of the refracted wave will attenuate more rapidly with distance than it normally would. The refracted wave will quickly die out and disappear into the background noise (Press and Dobrin, 1956). At this point, the refracted arrival from a previously masked lower layer becomes the first arrival. Terrestrial examples of this phenomenon have been reported by Press and Dobrin (1956), Domzalski (1956), and Watkins and Spieker (1972) among others.

The thin-layer phenomenon is not unexpected in mare basalts. Stratigraphy in some terrestrial basalts indicates that thin-layer attenuation should occur. For example, cores from the Kana-a basalt flow near Flagstaff, Arizona (Watkins *et al.*, 1964), revealed a stratigraphy consisting about 2 m of cinders (velocity 300 m/sec) overlying 8 m of basalt and more cinders. The upper 5 m of basalt had a velocity of 900 m/sec while the lower 3 m had a velocity of 2700 m/sec. The difference in velocity is probably due to increased fracturing and vesicularity in the upper 5 m. The cinders had a velocity of 300 m/sec. Another core hole in the same flow successively penetrated 1 m of cinders (350 m/sec), 5 m of basalt (1–350 m/sec; 3–900 m/sec; 1–730 m/sec) and 6 m of cinders (730 m/sec). Only high frequency energy could propagate in these flows because of their small thicknesses.

Stratigraphy observed in Hadley Rille during Apollo 15 would lead to thin layer attenuation. Photographs of Hadley Rille showed 3 sequences of outcropping rocks in the upper 50 m of the rille wall (Swann *et al.*, 1972). These outcrops consisted of a sequence of massive units sandwiched between discontinuous exposures of less massive units. The massive sequence is about 25 m thick. The

velocity of mare basalt at the Apollo 17 site is in excess of 800 m/sec and the dominant frequency less than 20 Hz. These values would require 40 m or more in thickness in order to efficiently transmit the seismic energy, or almost twice the thickness of the Hadley Rille sequence. Actually, the effective thickness of the massive interval in Hadley Rille may be significantly less than the total thickness if fracturing and vesicularity decrease the seismic velocity in the upper few meters. We suggest that a similar stratigraphy at Taurus-Littrow causes the anomalously high velocities observed in data from EP-2, -3, -4, and -8.

In a companion paper devoted to a discussion of deeper structure (Kovach and Watkins, 1973c) it was necessary to estimate an average velocity for the zone containing the thin, high-velocity layers because seismic refraction theory does not permit unique inversion of data where high-velocity layers are intercalated with low-velocity layers. Average shot point-array travel times for EPs -2, -3, -4, -8, the LM ascent, and the travel time to the geophone nearest EP-7 indicate that the average velocity in this zone is about 280 m/sec.

The second important difference derives from the fact that the EPs were detonated over a dipping subsurface layer. The dipping refractor causes arrivals from EPs detonated on the updip (western) side to be earlier than arrivals from EPs detonated at comparable distances on the downdip side. The earlier arrivals result from a smaller thickness of low-velocity regolith traversed by waves generated on the updip side. A dipping refractor coupled with the array-EP configuration causes the "shingle" effect (an echelon pattern) of arrival times shown in Fig. 1. The shingle effect does not occur unless the refracting layer dips. The analysis of these data differs slightly from analysis of conventional data. Analysis procedures are discussed below.

Analysis of the data in Fig. 1 is complicated by noise originating in the ALSEP electronics (probably in the LSPE firing-pulse transmitter) and picked up by LSPE detectors and/or cables. The noise makes it difficult to precisely pick the first arrivals from all EPs. Picks were especially difficult in EP-2 and -3 data. Therefore, EP-2 and -3 data are treated with less confidence than data from EP-4 and -8 where first arrivals are more distinct. Analysis of the noise suggests that some of it can be removed. Therefore, it may be possible to improve on the following interpretation at a later date.

In spite of the scatter in the first arrivals it is clear that for given distances arrivals from EPs detonated east of the array are later than arrivals from EPs detonated west of the array. As previously mentioned, this difference in arrival times suggests that the refractor is tilted to the east causing refracted waves from EP-2, -3 and the LM ascent to traverse a thicker low velocity layer (probably the regolith) than waves from EP-4 and -8. The dipping refractor suggestion is further supported by the obvious shingling of arrivals from EP-4 and -8. The shingling of EP-2, -3 and LM arrivals is less obvious but still apparent.

The shingling effect is explained in terms of the travel time equations for a two layer case with dipping refractor:

$$t = t_0 + mx \qquad [111]$$

t = travel time; t_0 = shot-intercept time as shown in Fig. 1; m = slope; and x = distance from shot point to detector, where,

$$t_o = \frac{2z \cos\theta \cos\phi}{v_1} \quad \text{and} \quad m = \frac{\sin(\theta \pm \phi)}{v_2}$$

z = depth of refractor beneath the EP; v_1, v_2 = velocity in surface layer and underlying refractor, respectively; $\theta = \sin^{-1}(v_1/v_2)$; and ϕ = dip of the refractor; the sign in the expression $(\theta \pm \phi)$ is negative when shooting updip and positive when shooting downdip. All updip data have the same slope and all downdip data have the same slope. The downdip slope is always greater than the updip slope. The shingling effect derives from the fact that changes in z alone affect the t_0 terms since ϕ, v_1, and θ are all constant for a given model.

If arrivals from EP-2, -3 and the LM were better, the travel time data could be uniquely inverted to give the depth of the refractor and its dip. However, values from EPs east of the array were not considered sufficiently well established for inversion, so depths and dip were calculated by the approximate method discussed below.

If $v_2 \geq 600$ m/sec, $v_1 = 105$ m/sec, and the $\phi < 5°$, then $\cos\theta \cos\phi = 0.99 \pm 0.01$. It has previously been shown that the regolith velocity v_1 is relatively constant 105 m/sec. Analysis indicates that $v_0 \geq 600$ m/sec and $\phi < 5°$. Thus, z can be accurately estimated for EPs-4 and -8 from the t_0 term alone. Estimates of z were not made for EP -2, -3 and LM ascent arrivals.

A least squares fit of the EP-4 data (which had the least scatter of all data) yielded an apparent velocity v_2' of 560 m/sec and an intercept time (t_0) of 0.115 sec or a depth (z) of 6.2 m. Projecting a line with a slope of 1/560 through the mean position of EP-8 data points results in $t_0 = 0.220$ sec and $z = 11.8$ m. The distance from EPs -4 and -8 to the center of the array (geophone 3) were 215 and 122 m, respectively. Hence the dip is about 3.4°. Use of 3.4° in the "m" term yields a true velocity for the refractor of 910 m/sec which is well within the range of velocities observed in terrestrial basalts and close to the velocity observed in the next deeper refractor (1130 m/sec) at Taurus-Littrow (Kovach and Watkins, 1973c). The agreement of velocities support our interpretation of the layer as a basalt flow. Use of the above values to calculate arrival time from EP-2, -3, and LM ascent yielded approximately correct values. Better agreement (that shown in Fig. 1) was obtained by reducing the average dip to 3° which changed the average velocity of the refractor to 850 m/sec. The recalculated depth of the refractor beneath the center of the array (geophone 3) is 17.4 m.

Electrical properties of lunar near-surface rocks at the Apollo 17 site are consistent with at least two different model interpretations (Simmons *et al.*, 1973). One model bears no resemblance to the seismic model of the regolith and subjacent layering, but the other model consists of an eastward dipping layer about 20 m below the ALSEP, a second interface about 300 m below the surface and no other interfaces up to depths of 1.5 km or more. This model closely resembles the Apollo 17 seismic model.

No craters penetrate the regolith within the area encompassing the geophone

array and EPs -2, -3, -4, and -8, therefore we have no direct geological evidence of regolith thickness from the area of where seismic data were obtained. Outside the area, however, astronaut observations suggest that the regolith varies in depth from 5–20 m (ALGIT, 1973). For example, rims of craters less than 30 m in diameter or near LRV-1 (west of the array) were block free except for one crater 10–15 m in diameter whose rim included blocks with diameters up to 1 m (ALGIT, 1973). Data reported by Baldwin (1949) and Short (1970) indicate that small craters excavate to depths equal to 0.25–0.35 of their diameters. Therefore, regolith is probably 3–10 m thick in the LRV-1 area, a range of depths consistent with LSPE data. East of the array, 15–20 m of surficial fragmental material were exposed in the walls of Van Serg Crater. These data agree qualitatively with our interpretation of the seismic data to the extent that the regolith is shallower west of the array than it is east of the array. The dip of the refractor indicated by the seismic data is somewhat greater than the dip of the subfloor basalt indicated from crater data, however.

We believe that the answer to these apparently conflicting dip data derive from the constricted, sloping nature of the Taurus-Littrow valley floor coupled with an anomalously high density of medium-sized craters surrounding the array. The valley of Taurus-Littrow slopes from an elevation of about 4800 m in the northwest to an elevation of about 4220 m in the southeastern corner. Lee scarp, a prominent feature in the western part of the valley, slopes eastward at angles up to 17°, which is much steeper than the 3° indicated by the LSPE data. The undulating, dipping surface suggests that a local increase in slope may be responsible for the change in depth of the refractor beneath the LSPE.

The anomalous average depth of the refractor is probably due to an anomalous regolith thickness. The LSPE array and the four closest explosives are within an area with an unusually high density of both young craters and old, subdued craters. The array is underlain by ejecta from Camelot, Horatio, Trident, Sherlock, and others. The ejecta from these craters and others near the array is probably responsible for the anomalously large (17.4 m) regolith thickness observed by the astronauts and deduced from LSPE data.

We conclude that the substrate is probably subfloor basalt and that it has an undulating surface. The LSPE array is located over a portion of the subfloor basalt where the dip is slightly oversteepened to the east. Ejecta from an anomalously large number of medium-sized craters in the vicinity of the array smoothed the topography and created an unusually thick regolith.

DISCUSSION

The regolith is a moonwide phenomenon. Photography from orbiting satellites reveals everywhere a smoothed, pockmarked lunar surface now associated with the mantling effect of the regolith. Bodies of rock larger than a few meters are exposed only in small areas or inside craters. Apollo seismic data suggest that the regolith observed in different lunar geological habitats is also remarkably uniform in its properties moonwide.

Low, uniform P-wave velocity

The *P*-wave velocity of the regolith is very low and uniform. The average velocity determined from Apollo data is 105 m/sec and the standard deviation is 8 m/sec (Table 1). Velocities in terrestrial soils have much greater variability. For example, Watkins and Spieker (1972) found that unconsolidated surface materials in the Miami River Valley of southwestern Ohio had velocities ranging from 460 m/sec to over 1000 m/sec. Standard deviations in specific areas of more or less homogeneous surface material ranged from 9 to 34% of the mean velocity. *In situ* velocity measurements of terrestrial rock outcrops show similar variations. Watkins *et al.* (1972) reported standard deviations equal to 14% of the mean velocity in outcrops of the welded, rhyolitic Bishop Tuff in eastern California, 27% of the mean velocity in Navajo Sandstone outcrops in northern Arizona, and 22% of the mean velocity in Amboy basalt outcrops in the Mojave Desert, California. Figure 2 shows scatter in lunar regolith and selected terrestrial rocks.

Brecciation and high porosity are probably the major causes of the extremely low velocities observed in the lunar regolith. Watkins and Kovach (1972) compared velocity data from brecciated rock (Apollo 14 regolith, Apollo 11 returned samples and ejecta from Meteor Crater, Arizona) with velocity data from terrestrial rocks of comparable porosity (Fig. 3). They found that the lunar regolith and Meteor Crater ejecta had significantly lower velocities than common terrestrial rocks with comparable porosities, a relationship which they attributed to brecciation of the Apollo 14 regolith and Meteor Crater ejecta.

Watkins *et al.* (1972) reported that only very fine, extremely porous (60%) terrestrial materials had velocities as low as 100 m/sec. The velocity in basaltic cinders was 300 m/sec, a value significantly greater than that of the lunar regolith. The low regolith velocities thus indicate that the regolith probably contains no significant amounts of volcanic ash at Apollo 12, 14, 15, and 16 sites. The regolith velocity was not established at the Apollo 17 site but absence of ash in returned samples from the Apollo 17 site (ALGIT, 1973) seems to preclude its existence there, too.

Table 1. *P*-wave velocity and thickness of the regolith at the Apollo sites. Although mare basalt underlies the Apollo 17 site, the site is in a small valley surrounded by highlands and is located within a local crater field which probably accounts for the unusual range of regolith thickness values.

Mission	Velocity (m/sec)		Thickness (meters)		Geologic Setting
	PSE	ASE	Craters	Seismic	
11	—	—	3–6	—	Mare
12	108	—	2–4	—	Mare
14	104	104	—	8.5	Highlands
15	92	—	5	—	Mare
16	—	114	—	12.2	Highlands
17	—	—	3–20	6.2–36.9	Restricted Mare

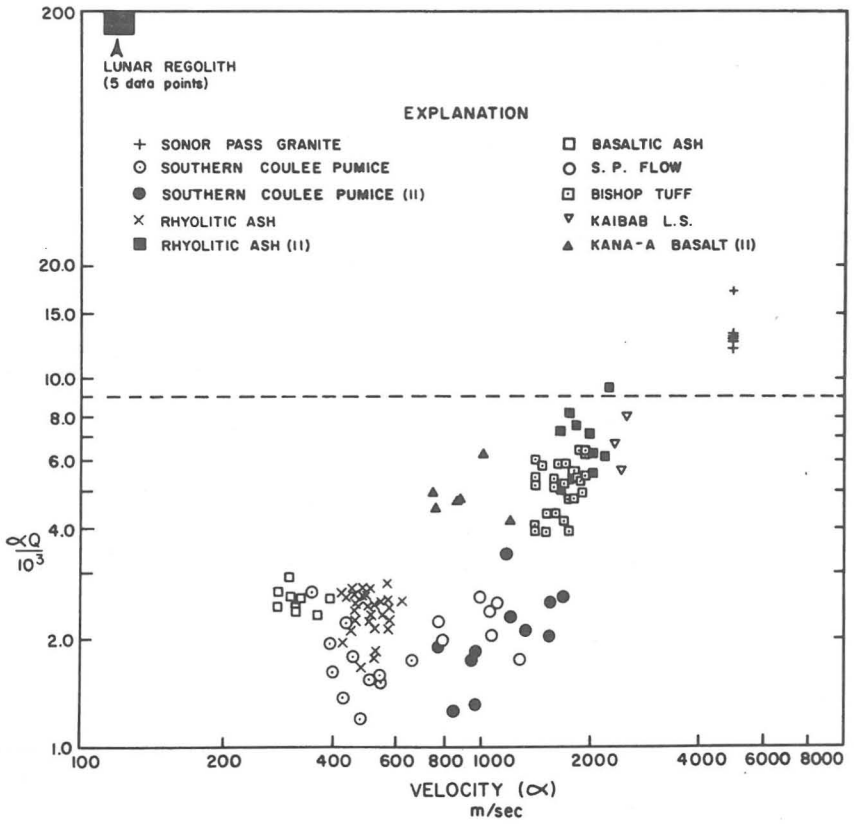

Fig. 2. Velocity-Q product as a function of velocity (α) for the lunar regolith and selected unsaturated *in situ* terrestrial rocks. Note the small scatter in the lunar regolith velocities relative to the scatter observed in the terrestrial rocks. A high Q is characteristic of lunar crustal rocks. (Q of the lunar regolith was provided by Y. Nakamura, personal communication, 1973.)

Regolith thickness

Variation in the thickness of the regolith is small. At the Apollo 11 site the regolith is estimated to be 3–6 m thick (LSPET, 1970); at the Apollo 12 site it is estimated to be 2–4 m thick (LSPET, 1970); at the Apollo 15 site measurements from photographs indicate that it is 5 m thick; ASE data indicate it is 8.5 m thick at the Apollo 14 site and 12.2 m thick at the Apollo 16 site; and anomalous Apollo 17 seismic data indicate an average depth of 10–15 m (*see* Table 1). The range of thickness is thus less than one order of magnitude. When maria and highland thicknesses are considered separately, the ranges in thickness are even less; the maria determinations differing by no more than a factor of 3 and the two highland determinations differing by a few tens of percent.

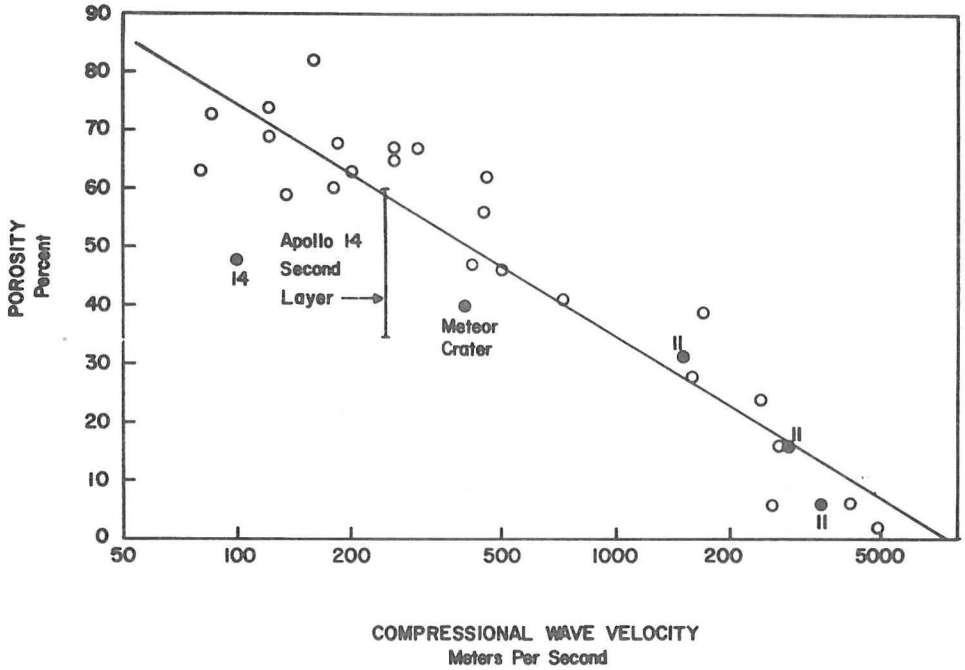

Fig. 3. Terrestrial velocity-porosity data (open circles) and lunar velocity-porosity data (solid circles). Numbers refer to Apollo missions that provided data. Note the progressively lower seismic velocities observed in shocked rocks (Apollo and Meteor Crater data) relative to the least-squares fit calculated for all terrestrial data. (Apollo 11 data are from Kanamori *et al.*, 1970).

Impact ejecta models and the origin of the regolith

The thickness of the regolith is an important parameter in attempts to deduce models of regolith formation, cratering mechanics, and meteorite flux. The many investigators who have studied the problem of crater formation and ejecta thicknesses have reached diverse conclusions. Part of the diversity derives from the use of different assumed crater and/or meteorite populations. Other differences derive from differing assumptions regarding the impact mechanism and the regolith formation process.

Among the investigators whose estimates agree reasonably well with observations of the regolith thickness are Gault (1970), Short and Forman (1972), and Hu (1971). Gault, using the Naumann–Hawkins meteorite flux rate to estimate the equilibrium ejecta accumulation due from craters up to 2.5 km in diameter, obtained an average ejecta thickness of 6 m at Sinus Medii. Short and Forman (1972), using volumes excavated from all lunar craters, estimated that the ejecta thickness would be 1–20 m on the maria and about 2 km in the highlands. Their estimate of ejecta thickness on the maria agree with observed regolith thicknesses, and their highland thickness estimate is in approximate agreement with the

depth to "hard rock" (4 km/sec) determined from LSPE data. Hu (1971) developed an empirical model of the variation of ejecta thickness as a function of crater size and distance from the center of the crater. His estimates of total ejecta thicknesses from post-Imbrian impacts near Apollo 11, 12, and 14 sites agreed closely with observed thicknesses and support a post-Imbrian age for the regolith at these locations. Hu's calculated thicknesses and stratigraphic sequences agreed well with observed thicknesses and stratigraphic sequence in the Apollo 12 drive sample. This close agreement indicates that mixing of ejecta is not as effective as some investigators have suggested.

Age of the regolith

Since the oldest portion of the regolith overlies mare basalts ranging in ages from 3.1 to 3.7 billion years (Tera *et al.*, 1973), mare regolith ranges in age from 0–3.7 billion years. The regolith in the highlands appears to include slightly older ejecta.

Radiometric ages of soil from the Apollo 16 site fall mainly in a narrow range of ages between 3.9 and 4.2 billion years (Tera *et al.*, 1973; Hussain and Schaeffer, 1973). The soil from which these ages were determined probably consists mainly of ejecta from the 250 m/sec layer immediately subjacent to the regolith. Although we cannot calculate the exact thickness of the 250 m/sec layer, the fact that it transmits seismic energy peaking at 8 Hz indicates that it is at least 30 m thick. Since most nearby craters bottom at lesser depths, we can conclude that the 250 m/sec layer is the source of most of the surface fragments.

At the Apollo 14 site, the Fra Mauro Formation is thought to be 3.9 billion years (Alexander *et al.*, 1973). Thus the maximum age of overlying regolith ejecta is very nearly the same as that at the Apollo 16 site.

The greater thickness of the lunar regolith on the highlands relative to the younger regolith in the maria regions suggests that the rate of deposition of regolith was almost in order of magnitude greater during the period between the great cataclysm about 4 billion years ago (Tera *et al.*, 1973) and the middle of the period of maria formation (about 3.4 billion years ago) than during the subsequent time interval.

Compacted powder model

Unusual seismic properties of the lunar regolith and underlying crustal breccias led Gold and Soter (1970) and Gangi (1972) to suggest that the lunar near-surface consists of a deep layer of powder. Their powder model is gravitationally self-compressed in such a way as to provide a linear velocity increase with depth (Gold and Soter, 1970) or a velocity which increases as the sixth root of the depth (Gangi, 1972).

ASE and LSPE data do not support this model. Figure 4 shows velocity-depth models deduced from Apollo 14, 16, and 17 data. Depth is plotted on a logarithmic scale so that a power law velocity-depth function appears as straight line. From

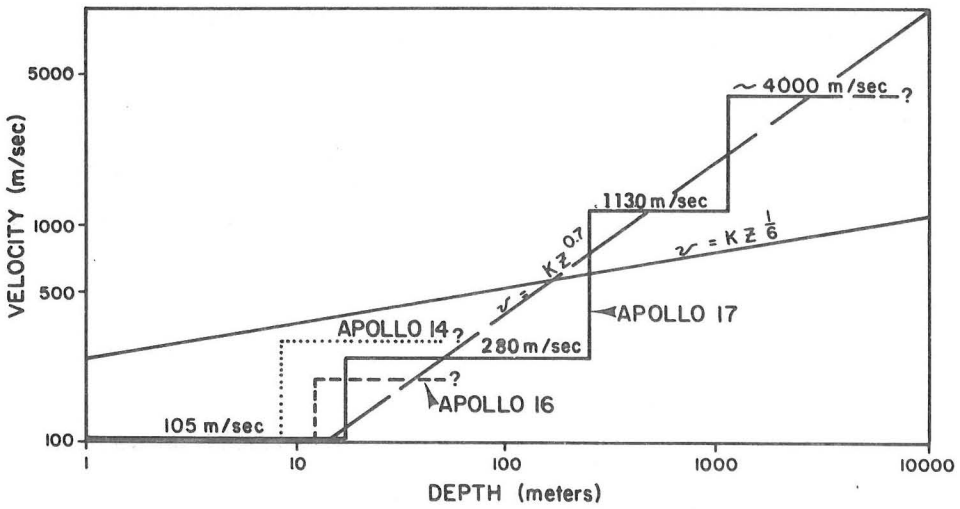

Fig. 4. Velocity-depth models deduced from Apollo 14, 16, and 17 data. Depth is plotted on a logarithmic scale in order to show power law velocity-depth functions as straight lines.

this figure it is clear that if one attempts to fit a sixth root velocity-depth function to the regolith and immediately subjacent rocks and breccia, the curve is badly in error at greater depths. Conversely, a sixth root function fitted in the 1130 and 4000 m/sec region is badly in error in the 100–300 m/sec region. It is possible to fit a power law velocity-depth function ($v = kz^{0.7}$) over much of the range of the lunar crust but this is probably coincidental. A linear increase of velocity with depth fits the data worse than the sixth root curve.

A major reason for the recurrence of the compacted dust hypothesis is the extremely low seismic velocity of near-surface rocks. Although seismic velocities in lunar near-surface rocks are low by terrestrial standards, comparable velocities have been observed in terrestrial rocks with extremely high porosities (Fig. 3).

Brecciation tends to enhance the decrease in velocity accompanying an increase in porosity. Todd *et al.* (1973) have observed anomalously low seismic velocities in shocked rock samples from the Ries impact crater and from lunar samples, and Watkins *et al.* (1972) observed similar results during *in situ* measurements of velocities in shocked rocks near Meteor Crater.

In Fig. 3, velocities reported by Kanamori *et al.* (1970) proportionately average only slightly less than velocities observed in unshocked terrestrial rocks of comparable porosity; Meteor Crater rock velocities average about 50% of comparable unshocked rock; and the lunar regolith velocities average about 20% of comparable unshocked rock. These data indicate that the relative decrease in velocity due to brecciation increases in magnitude with increasing porosity.

Interpolation of Meteor Crater and Apollo regolith data suggests that unshocked rock comparable to the 299 m/sec and 250 m/sec layers observed at Apollo 14 and 16 sites would have velocities between 500 and 800 m/sec. These

velocities are comparable to velocities observed in unsaturated terrestrial soils. A layer of very porous soil overlying a layer of normal soil would thus constitute a good velocity analog of unshocked lunar regolith and unshocked subjacent breccia at the Apollo 14 and 16 sites. Without the reduction in velocity due to brecciation, the velocities of the lunar regolith and substrate at the Apollo 14 and 16 sites are within the normal range of velocities observed in terrestrial soils.

We conclude that the anomalously low *in situ* velocities observed in the lunar regolith and in lunar breccias result primarily from shock induced microcracks and high porosity. Without microcracks, velocities in these rocks would be comparable to velocities in terrestrial soils.

SUMMARY AND CONCLUSIONS

Synthesis of seismic, geological, and crater ejecta calculations suggest the following conclusions.

1. The regolith consists primarily of impact ejecta having an average compressional wave velocity of 105 m/sec. Pyroclastics do not appear to comprise a significant portion of the ejecta in the areas investigated.

2. In the maria areas the regolith averages between four and five meters in thickness and represents the sum of the post-maria ejecta blankets. The regolith was deposited during the interval of 0 to 3.7 billion years ago.

3. In the highlands the regolith thickness averages about 10 m. The highland regolith represents the sum of post-cataclysm ejecta blankets and was formed during the interval between 0 and 4 billion years ago. Differences in thicknesses of highland and maria suggest that the regolith deposition rate was approximately an order of magnitude greater in the period between 3.5 and 4 billion years ago than during the period 3.5 billion years ago to present.

4. The regolith in the valley of Taurus-Littrow (Apollo 17) is anomalously thick, ranging from 6.2 to 36.9 m in the area of investigation. The anomalous thickness is attributed to the combined effects of an unusually high concentration of medium-sized craters and irregularities in the surface of underlying mare basalts.

5. Apollo seismic data do not support the compacted power model of the lunar crust but indicate that lunar near-surface regolith, breccia, and crust consist of discrete layers. Anomalously low seismic velocities observed in the regolith and subjacent breccia are due to impact fracturing.

REFERENCES

Alexander E. C., Jr., Davis P. K., Reynolds J. H., and Srinauason B. (1973) Age exposure history, and trace element composition of some Apollo 14 and 15 rocks as determined from rare gas analysis (abstract). In *Lunar Science—IV*, pp. 27–28. The Lunar Science Institute, Houston.

Apollo Lunar Geology Investigation Team (1973) Documentation and environment of the Apollo 17 samples: A preliminary report. U.S. Geol. Survey Interagency Rpt., *Astrogeology* **71**, 322 pp.

Domzalski W. (1956) Some problems of shallow refraction investigation. *Geophys. Prosp.* **4**, 140–166.

Gangi A. F. (1972) The lunar seismogram. *The Moon* **4**, 40–48.

Gold T. and Soter S. (1970) Apollo 12 seismic signal: Indication of a deep layer of powder. *Science* **169**, 1071–1075.

Hu T. (1971) The crater ejecta component in the lunar regolith. Univ. North Carolina Master's Thesis, 41 pp.

Hu T. and Watkins J. S. (1971) The crater ejecta component in the lunar regolith. *Trans. Am. Geophys. Union* **52**, 273.

Hussain L. and Schaeffer O. A. (1973) ^{40}Ar–^{39}Ar crystallization ages and ^{38}Ar–^{37}Ar cosmic ray exposure ages of samples from the vicinity of the Apollo 16 landing site (abstract). In *Lunar Science—IV*, pp. 406–407. The Lunar Science Institute, Houston.

Kanamori H., Nur A., Chung D., Wones D., and Simmons G. (1970) Elastic wave velocities of lunar samples at high pressures and their geophysical implications. *Science* **167**, 726–728.

Kovach R. L. (1967) Lunar seismic exploration. *Physics of the Moon* (editor S. F. Singer). *Am. Astronautical Soc.* **13**, 189–198.

Kovach R. L., Watkins J. S., and Landers T. (1971) Active seismic experiment. In *Apollo 14 Preliminary Science Report*, NASA SP-272, pp. 163–174.

Kovach R. L., Watkins J. S., and Talwani P. (1973a) Active seismic experiment. In *Apollo 16 Preliminary Sciences Report*, NASA SP-315, Chap. 10, 14 pp.

Kovach R. L., Watkins J. S., Nur A., and Talwani P. (1973b) The properties of the shallow lunar crust: An overview from Apollo 14, 16 and 17 (abstract). In *Lunar Science—IV*, pp. 444–445. The Lunar Science Institute, Houston.

Kovach R. L. and Watkins J. S. (1973c) The structure of the lunar crust at the Apollo 17 site. *Proc. Fourth Lunar Sci. Conf., Geochim. Cosmochim. Acta.* This volume.

Latham G. V., Ewing M., Press F., Sutton G., Dorman J., Nakamura Y., Toksöz N., Wiggins R., and Kovach R. (1970) Passive seismic experiment. In *Apollo 12 Preliminary Science Report*, NASA SP-235, pp. 39–54.

Latham G. V., Ewing M., Press F., Sutton G., Dorman J., Nakamura Y., Toksöz N., Duennebier F., and Lammlein D. (1971) Passive seismic experiment. In *Apollo 14 Preliminary Science Report*, NASA SP-272, pp. 133–162.

Latham G. V., Ewing M., Press F., Sutton G., Dorman J., Nakamura Y., Toksöz N., Lammlein D., and Duennebier F. (1972) Passive seismic experiment. In *Apollo 15 Preliminary Science Report*, NASA SP-289, Chap. 8, 25 pp.

Lunar Sample Preliminary Examination Team (1970) Preliminary examination of lunar samples from Apollo 12. *Science* **167**, 1325–1339.

McAllister D. B., Kerr J., Zimmer J., Kovach R. L., and Watkins J. S. (1969) A seismic refraction system for lunar use. *Trans. IEEE*, **GE-7**, pp. 164–171.

Press F. and Dobrin J. (1956) Seismic wave studies over a high-speed surface layer. *Geophysics* **21**, 285–298.

Short N. M. (1970) Anatomy of a meteorite impact crater: West Hawk Lake, Manitoba, Canada. *Bull. Geol. Soc. Am.* **81**, 609–648.

Short N. M. and Forman M. L. (1972) Thickness of impact crater ejecta on the lunar surface. *Mod. Geol.* **3**, 69–91.

Simmons G., Baker R. H., Bannister L. A., Brown R., Kong J. A., LaTorraca G. A., Tsang L., Strangway D. W., Cubley H. D., Annan A. P., Redman J. D., Rossiter J. R., Watts R. D., and England A. W. (1973) Electrical structure of Taurus-Littrow (abstract). In *Lunar Science—IV*, p. 675. The Lunar Science Institute, Houston.

Swann G. A., Bailey N. G., Batson R. M., Freeman V. L., Haiit M. H., Head J. W., Holt H. E., Howard K. A., Irwin J. B., Larson K. B., Muehlberger W. M., Reed V. S., Rennilson J. J., Schaber G. G., Scott D. R., Silver L. T., Sutton R. L., Ulrich G. E., Wilshire H. G., and Wolfe E. W. (1972) Preliminary Geologic Investigation of the Apollo 15 landing site. In *Apollo 15 Preliminary Science Report*, NASA SP-289, Chap. 5, 112 pp.

Tera F., Papanastassiou D. A., and Wasserburg G. J. (1973) A lunar cataclysm at 3.95 Ae and the structure of the lunar crust (abstract). In *Lunar Science—IV*, pp. 723–725. The Lunar Science Institute, Houston.

Todd T., Wang H., Richter D., and Simmons G. (1973) Unique characterizations of lunar samples by physical properties (abstract). In *Lunar Science—IV*, pp. 731–733. The Lunar Science Institute, Houston.

Watkins J. S. and Kovach R. L. (1972) Apollo 14 active seismic experiment. *Science* **175**, 1244–1245.

Watkins J. S. and Spieker A. M. (1972) Seismic refraction survey of pleistocene drainage channels in the lower Great Miami River Valley, Ohio. *U.S. Geol. Survey Prof. Paper* **605-B**, 17 pp.

Watkins J. S., Loney R. A., and Godson R. H. (1964) Investigation of *in situ* physical properties. *Proj. Ann. Rept.*, 1964. *U.S. Geol. Survey* open-file rpt., 78 pp.

Watkins J. S., Walters L. A., and Godson R. H. (1972) Dependence of *in situ* compressional-wave velocities on porosity in unsaturated rocks. *Geophysics* **37**, 29–35.

Watkins J. S., Whitcomb J. H., Weeks E. L., Graves T. J., Kovach R. L., and Godson R. H. (1969) A lunar engineering seismic system. *Bull. Assoc. Eng. Geol.* **6**, 119–130.

Proceedings of the Fourth Lunar Science Conference
(Supplement 4, *Geochimica et Cosmochimica Acta*)
Vol. 3, pp. 2549–2560

The structure of the lunar crust at the Apollo 17 site

ROBERT L. KOVACH

Department of Geophysics
Stanford University
Stanford, California 94305

JOEL S. WATKINS

Earth and Planetary Sciences Division
The Marine Biomedical Institute
The University of Texas Medical Branch
Galveston, Texas 77550

Abstract—A seismic profiling experiment was successfully executed on the lunar surface during the Apollo 17 mission allowing a determination of the structure of the lunar crust to a depth of several kilometers. The most outstanding feature of the seismic velocity variation, in the Taurus–Littrow region, is the stepwise increase with depth. A total thickness of about 1200 meters for the infilling mare basalts at the 17 landing site is also indicated from the seismic results. The apparent velocity is high (about 4 km/sec for *P* waves) in the material below the basalts.

INTRODUCTION

WITH THE successful installation of a geophysical station at the Taurus–Littrow landing site of the Apollo 17 mission an exciting period of manned lunar exploration was brought to an end. Prior to the Apollo 17 mission there was a surprising gap in our knowledge concerning the nature of the properties of the upper 10 km of the lunar crust, because of the absence of pertinent seismic travel time data at distances (Δ) closer than 30 km. Travel times of seismic waves are inverted in a classical fashion to determine seismic velocity structure and as a result provide the direct means of probing the lunar interior.

On the Apollo 17 mission a Lunar Seismic Profiling Experiment (LSPE) was successfully executed. Eight explosive charges were armed and placed on the lunar surface by the Apollo 17 astronauts at various points along the geological traverses. In addition, the impact of the Lunar Module (LM) ascent stage, at a distance of 8.7 km from the 17 landing site, was recorded on an array of miniature seismometers. In this paper we describe the seismic data, the velocity structure in the lunar crust beneath the Taurus–Littrow area and the implications for lunar history. The interpretation is more expansive than in previous reports (Kovach *et al.*, 1973; Kovach and Watkins, 1973a). Post-mission analyses of the Apollo 17 lunar surface photography has necessitated some adjustments in the absolute positions of the deployed explosive charges.

SEISMIC DATA

The LSPE recorded the LM ascent stage impact on December 15, 1972. The location of the impact was at 19.91 degrees north latitude and 30.51 degrees east longitude, at a distance 8.7 km southwest of the Apollo 17 landing site. Pertinent parameters for the LM impact are shown in Table 1.

A portion of the seismic signal from the Apollo 17 LM impact is shown in Fig. 1. The impact signal is similar in character to previous impact signals, possessing

Table 1. Parameters of Apollo 17 LM impact.

Impact parameters	LM
Day, G.m.t.	December 15, 1972
Range time,* G.m.t. hr:min:sec	06:50:20.84
Real time, G.m.t. hr:min:sec	06:50:19.60
Velocity, km/sec	1.67
Mass, kg	2260
Kinetic energy, ergs	3.15×10^{16}
Heading, deg	283

*Range time is the time that the signal of the event was observed on Earth.

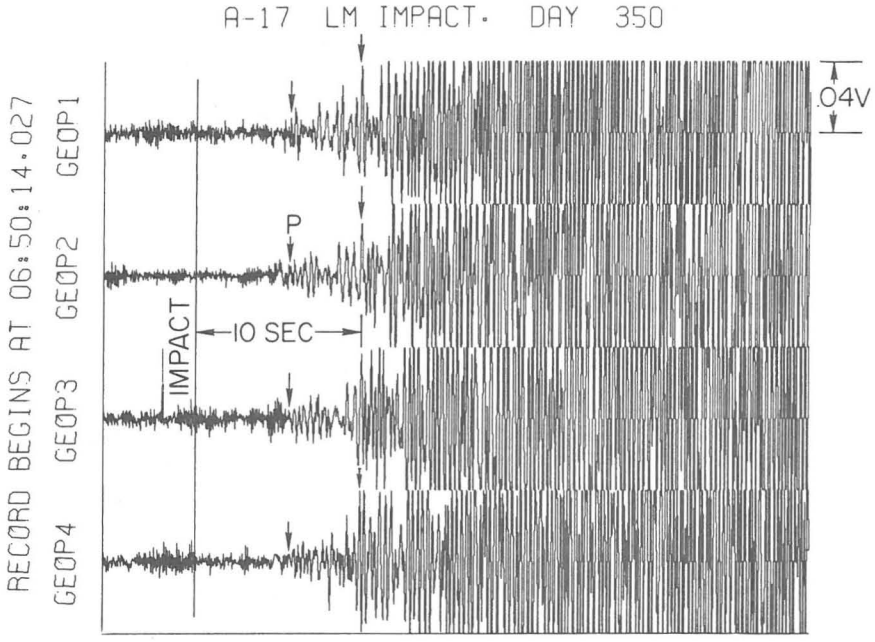

Fig. 1. Compressed time scale record of the seismic signal received from the LM impact of the Apollo 17 mission. Arrows point to the onset of first and second arrivals. The first arrow indicates a travel time of 5.75 seconds.

an emergent beginning and a long duration. The travel-time of the first P wave is 5.75 sec. A prominent second arrival with a travel time of 10 sec can also be identified on the seismograms. Whether this arrival represents a shear wave arrival or a later P wave arrival cannot be resolved from only a vertical component seismogram.

The observed amplitude of the impact signal is of interest when compared with the P wave amplitudes for previous impact signals. Comparison of previous LM impact signal amplitudes of SIVB impacts (Latham *et al.*, 1972) demonstrated that the LM impact amplitude data had to be adjusted upwards by a factor of 17.4 to be directly compared to the amplitudes observed for SIVB impacts. Extrapolating the observed amplitudes of the earlier LM impacts to a distance of 8.7 km leads to a predicted peak to peak amplitude of 26 nm. The Apollo 17 LM impact signal is centered at 4 Hz and has a measured peak to peak amplitude of 400 nm. It is interesting that, if we multiply the predicted amplitude of 26 nm by the scale factor 17.4 we obtain 452 nm which is in good agreement with the observed amplitude of 400 nm.

Analyses of previous lunar seismic impact signals (Latham *et al.*, 1973) have demonstrated that many of their characteristics (signal rise time, duration of signal, and lack of coherence between horizontal and vertical components of motion) can be explained by scattering. Seismic energy is considered to spread with a diffusivity ξ. The larger the value of diffusivity the smaller the amount of scattering. For a surface impact one can show that the signal rise time (the time from signal onset to its maximum value) is given by R^2/ξ where R is the range.

The Apollo 17 LM impact seismic signal has a rise time of 56 seconds leading to a diffusivity of 1.35 km^2/sec, a larger value than that inferred at the Apollo 15 and 16 sites from analysis of the seismic signals generated by the lunar roving vehicle out to distances of about 4 km (Latham *et al.*, 1973). The implication is that the Apollo 17 site is more homogeneous (for dimensions on the order of the wavelengths of seismic waves considered, i.e., approximately 25 m) than either the Apollo 15 or 16 landing areas. A difference in the near-surface properties of these landing sites may be due to differing ages for the areas and the effects of varying amounts of comminution and gardening by meteoroid impacts.

Figure 2 shows the seismogram recorded on the LSPE geophone array from the detonation of one of the explosive charges placed on the lunar surface at the 17 landing site. The arrows point to the onset of the first seismic arrival.

The locations of the explosive packages with respect to the geophone array are shown on the map in Fig. 3. Explosive charge weights ranged from 1/8 to 6 lbs. The one-pound explosive package (EP-6) was deployed on the outgoing traverse to the south and the one-half pound charge (EP-7) was positioned on the return leg to the lunar module. EP-4 (1/8 lb) and EP-8 (1/4 lb) were placed west of the geophone array. EP-2 (1/4 lb) and EP-3 (1/8 lb) were positioned east of the geophone array. EP-1 (6 lbs) was placed at a distance of 3 km NW from the LM and EP-5 (3 lbs) at a distance of 2.1 km NE of the LM.

The observed travel times from EP's 4 and 8 to the west of the geophone array and EP's 2 and 3 to the east are shown in Fig. 1 of Watkins and Kovach (1973).

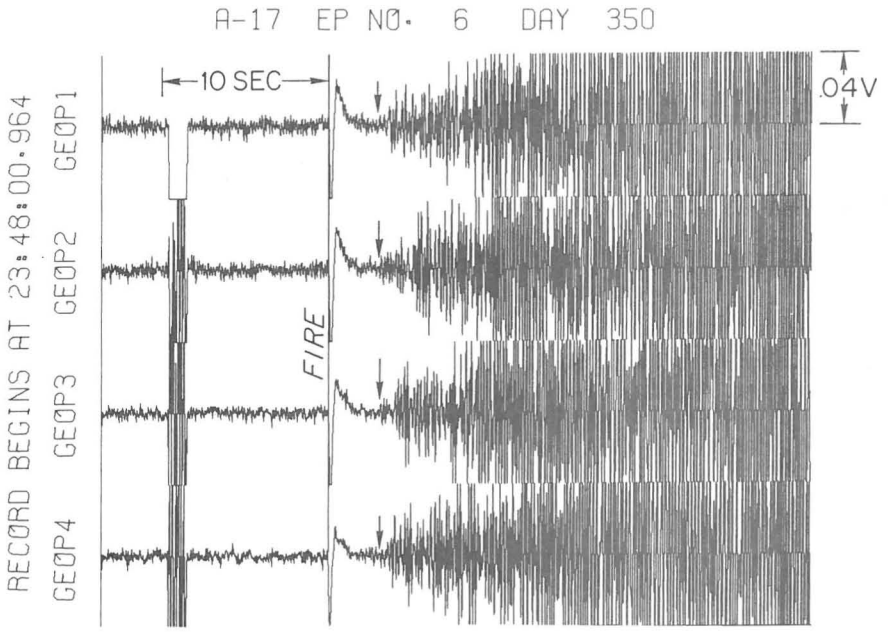

Fig. 2. Seismic signals produced by the detonation of explosive package 6 on the lunar surface as recorded on Apollo 17 geophone array. Arrows point to the onset of the seismic arrival.

These data yield a partially reversed profile and are discussed in detail in Watkins and Kovach (1973).

It is useful at this point to restate the assumptions (Ewing *et al.*, 1939) underlying the method of interpreting a seismic refraction profile: (1) the top and bottom of any layer is planar and propagates seismic waves with constant velocity; (2) at a layer interface the path of a seismic wave is governed by Snell's law; (3) a seismic wave propagating in a layer with a velocity V, which is incident on the surface of the layer at an angle α with the normal, travels with an apparent velocity V/sin α along the surface; (4) travel time is the same if the shot point and recording position are interchanged. Departures from these stated assumptions are revealed by the departure of the observed travel time data from straight lines drawn on the travel time graph.

Figure 4 shows the travel time data obtained from the detonation of the eight explosive packages. The digital sampling interval for the seismic data is 0.0085 sec. Using expanded scale time plots the onset of the seismic first arrivals could be picked to an accuracy of ± 0.05 sec. Subsequent array processing techniques on the digital data may contribute some additional information on apparent velocities, but it is not believed that subsequent processing will have any major effect on the travel time data discussed here. Inasmuch as complete reversal information was not obtained we shall interpret the travel time data on the assumption of zero dip of all interfaces. When treated *in toto* the close in shot

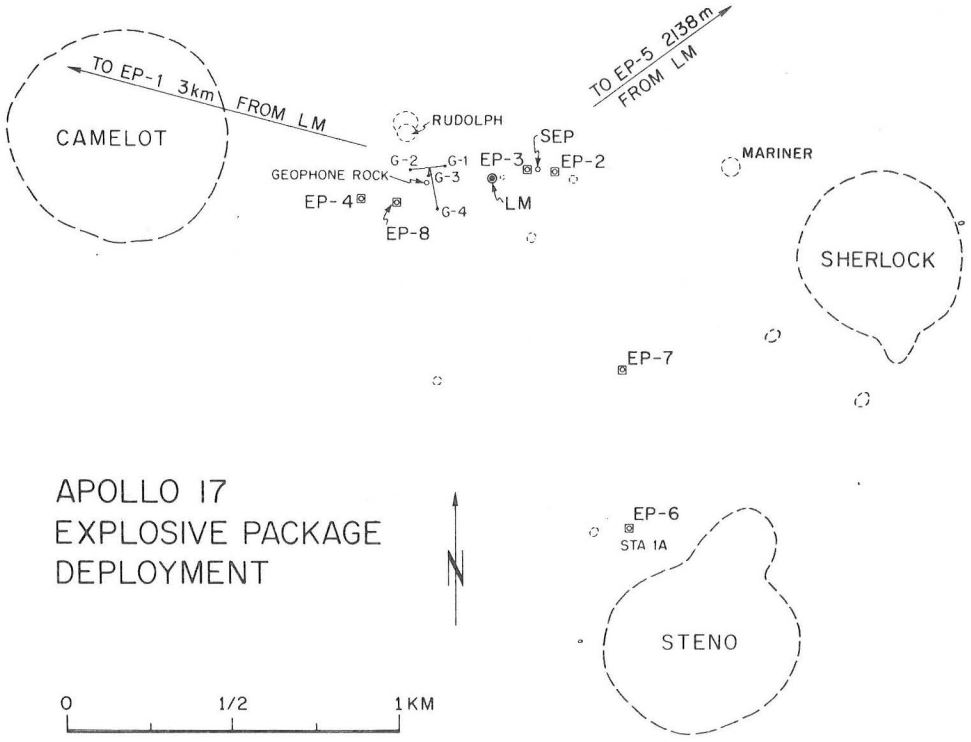

Fig. 3. Planimetric map of the Apollo 17 landing site showing location of geophone array and positions of explosive packages.

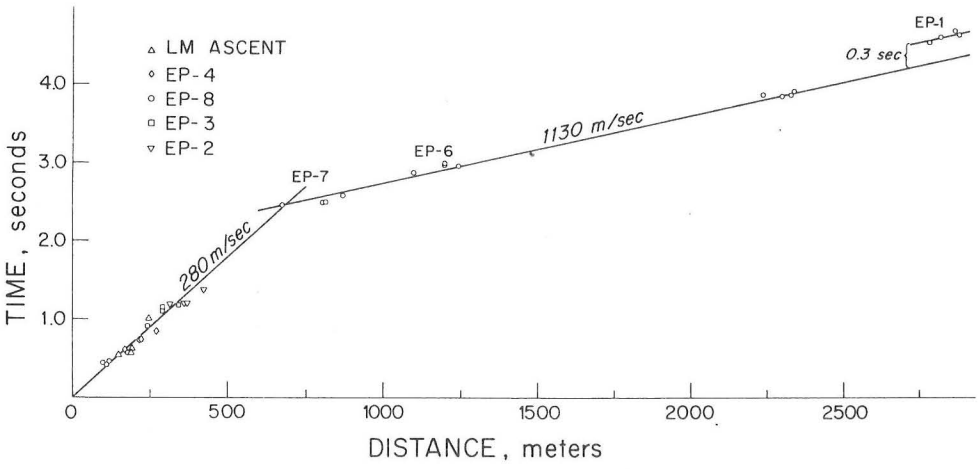

Fig. 4. Travel time distance graph for *P* wave pulses recorded from detonation of explosive packages and thrust of LM ascent engine.

points (EP's 2, 3, 4, and 8) define an *average* velocity arrival of 280 m/sec. Travel times from EP's 7, 6, and 5 define an apparent velocity of 1130 m/sec. The calculated thickness of the 280 m/sec layer is 264 m.

One can note that the travel time data for EP 1 are offset by about 0.3 sec with respect to the 1130 m/sec line. Examination of the path between EP 1 and the LSPE geophone array reveals that the seismic path is affected by the presence of the 600 m diameter crater Camelot. We can explain the observed time delay by postulating that the low-velocity 280 m/sec material extends to a greater depth beneath the crater Camelot than along the remainder of the travel time path. Figure 5 shows diagrammatically a simple model approximation for Camelot crater which can be constructed to explain the observed travel time delay. Subsequent digital velocity filtering (beam steering) of the seismic signals from EP 1 should allow more detailed models to be considered.

The travel time data from the explosive charges can be combined with the observed travel time for the LM impact to provide information about the seismic velocity to a depth of several km. Travel time data from the seismic signals produced by the LM impact and the explosive charges are shown in Fig. 6. A line with an apparent velocity of 4 km/sec can be fit through the LM impact data point to intersect very close to the corrected travel time data points for EP 1.

Inasmuch as the LM impacted at an elevation of 1.2 km above the valley floor at the 17 landing site the LM impact travel time should be adjusted to the same reference elevation as the LSPE geophone array. The effect of a difference in elevations is to contribute an additional delay time equal to the ratio of the elevation difference to the seismic velocity of the material traversed times the cosine of the angle of incidence that the particular seismic arrival under consideration departed the source (impact point). We shall assume that the underlying 4000 m/sec material in the Taurus–Littrow valley extends to the surface beneath the LM impact point in the South Massif. If we further assume that at a distance of 8.7 km (LM impact point) on the travel time graph the seismic velocity increases to 4500 m/sec (say) the angle of incidence for a refraction at this depth and the related angle of incidence at the source can be straightforwardly calculated.

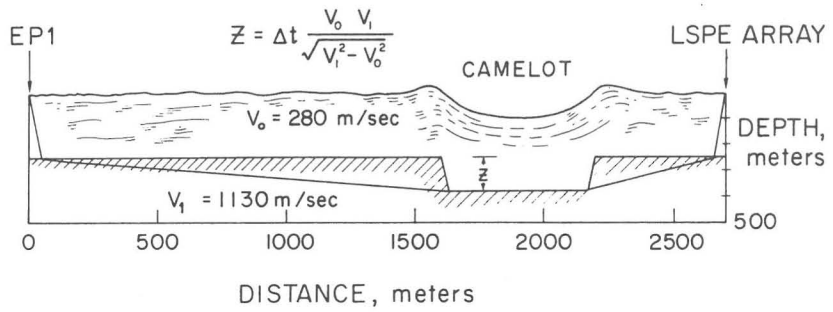

Fig. 5. Model approximation for seismic ray path from explosive package 1 to geophone array. Ray path crosses Camelot crater and observed time delay is produced by presence of low-velocity material beneath crater.

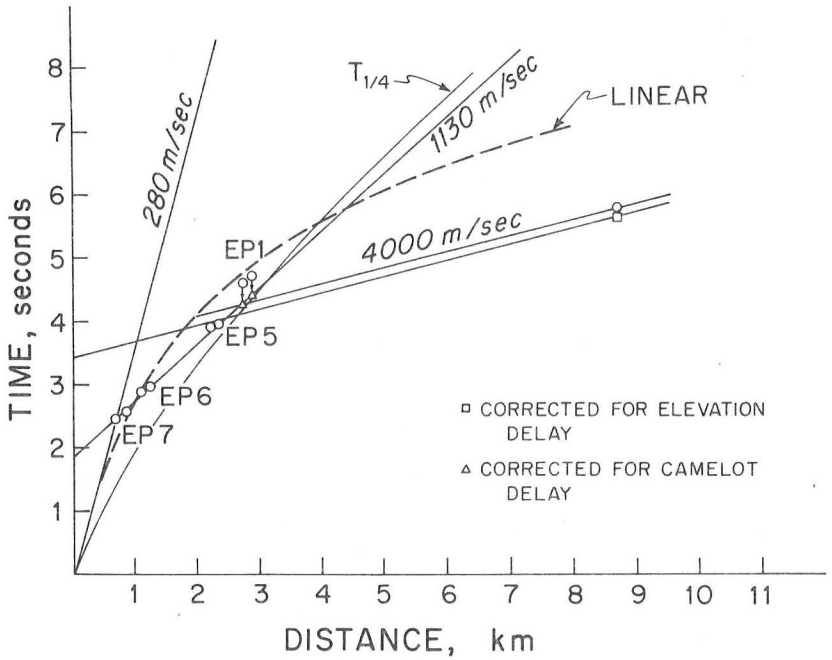

Fig. 6. Seismic travel times from LM impact and explosive charges. Travel time for EP 1 has been corrected for Camelot crater delay and LM impact travel time for 1.2 km elevation difference between impact point and LSPE geophone array. These corrections shift position of 4 km/sec apparent velocity line slightly downward as shown.

Inserting appropriate values for our case leads to a delay time correction of 0.14 sec. This correction will shift the position of the 4 km/sec apparent velocity line downward as shown in Fig. 6 such that its zero distance time intercept is decreased. There are obvious uncertainties in correcting for the elevation delay but the *important first order* consideration is that high velocity material (~4 km/sec) must lie beneath the 1130 m/sec material. The end effect of the elevation correction is to decrease the derived thickness of the 1130 m/sec material from 1006 m to 923 m.

Various power laws for the variation of seismic velocity with depth in the moon have been proposed (Gold and Soter, 1970; Gangi, 1972). Among these are that the seismic velocity increases as either the fourth or sixth power of the depth. It is of interest to compare the Apollo 17 *observed* travel times with some of these proposed velocity-depth variations.

The fourth power model with velocity variation of the form $v = v_0(z/z_0)^{1/4}$ gives a travel time relationship

$$t = \frac{2\pi z_0}{v_0}[2x/3\pi z_0]^{3/4},$$

where v_0 is the assigned velocity at a depth of z_0. Normal practice is to choose v_0

such that the observed travel time agrees with that observed at a distance x. We shall select $z_0 = 1$ km and the observed travel time of 4.2 sec at a distance x of 2.75 km. In this case $v_0 = 0.998$ km/sec. Using these parameters a travel time curve has been calculated and is shown as the curved marked $T_{1/4}$ in Fig. 6. It is seen that the fourth root velocity variation predicts travel times that are too slow at distances greater than 3 km, implying that the velocities are too low at depth.

We can also examine a uniform increase of velocity with depth. In this case $v = v_0 + Kz$, where v_0 = velocity at surface, K = rate of increase with depth and

$$t = \frac{2}{K} \sinh^{-1} \left(\frac{Kx}{2v_0} \right).$$

Let us assume a surface velocity of 280 m/sec and a value for K of 0.92/sec. This linear gradient model gives a travel time graph marked linear in Fig. 6. The agreement is quite good out to a distance of about 1 km but at greater distances the predicted velocity is again too slow. Nevertheless, it is to be emphasized that both the fourth-power and linear gradient models cannot satisfy the well defined linear segments of the observed travel times.

DISCUSSION

Prior to the Apollo 17 mission our best estimates of the seismic velocity variation in the upper 20 km of the moon were as depicted by lunar models 1 or 2 (Latham *et al.*, 1973; Toksoz *et al.*, 1972) in Fig. 7. The seismic velocity was known to increase very rapidly from values of 100–300 m/sec in the upper 100 m or so to a value of ~ 4 km/sec at a depth of 5 km. Even though the seismic velocity variation was taken to be a smooth increase with depth it was surmised (Kovach and Watkins, 1973b) that such a rapid increase of velocity (~ 2 km/sec/km) could not be solely explained by the pressure effect on dry rocks with macrocracks and microcracks nor by the self-compression of any rock powder.

Laboratory velocity measurements on returned lunar soils (Kanamori *et al.*, 1970, 1971; Anderson *et al.*, 1970; Mizutani *et al.*, 1972; Warren *et al.*, 1971) and recent measurements under hydrostatic pressure conditions on terrestrial sands and basaltic ash (Talwani *et al.*, 1973) have indicated velocity-depth gradients of 0.4 to 0.8 km/sec/km but such gradients occur only to pressures of 50 bars (lunar depth of ~ 1 km). An examination of these experimental data led to the inference that compositional or textural changes must be important in the upper 5 km of the moon (Kovach and Watkins, 1973b).

The lunar seismic profiling results have shown that, at least beneath the Taurus–Littrow site, the seismic velocity increases with depth in a stepwise manner in the upper several km. It is of interest to examine our *in situ* velocity information in the light of the surface geological investigations at the 17 site, laboratory velocity measurements from returned lunar samples and seismic velocity measurements on terrestrial lunar analogs.

Underlying the regolith at the 17 site the dominant rock type observed is a

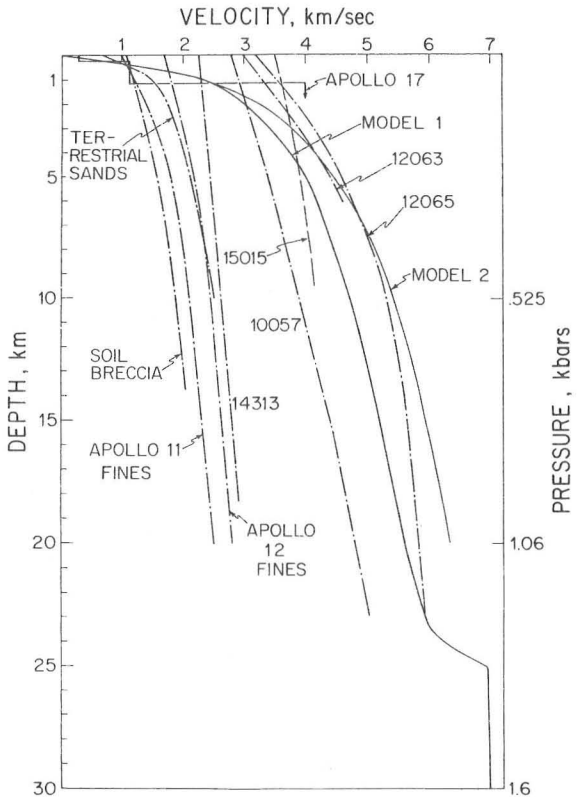

Fig. 7. Inferred compressional wave velocity profiles for moon and velocities of lunar and terrestrial rocks measured in the laboratory as a function of pressure. Lunar rocks are identified by a sample number. Lunar models 1 and 2 are based on results available through Apollo 16 (Toksoz *et al.*, 1972). Apollo 17 results reveal marked stepwise increase in seismic velocity in upper 2 km.

medium grained vesicular basalt believed to be primarily a mare type basalt. Observations by the crew in crater walls revealed textural variations suggesting that individual flow units are involved. Our seismic observations have indicated 264 m of material with an average velocity of 280 m/sec overlying 923 m of 1130 m/sec material. We suspect the 280 m/sec layer contains several higher velocity lava flow units (Watkins and Kovach, 1973).

The abrupt change in seismic velocity and, by inference in other physical properties, from 280 m/sec to 1130 m/sec is suggestive of a major change in the nature of the evolution or deposition of the Apollo 17 subfloor basalts. However, a similar range of seismic velocities is observed with refraction surveys on lava flows on earth. Some insight can be gained when we consider specific lava flows which have been examined in some detail as possible lunar analogs: the Southern Coulee, the SP flow and the Kana-a flow (Watkins, 1966; Watkins *et al.*, 1972).

The Southern Coulee is a recent lava flow near Mono Craters in eastern California. Seismic velocities range at the surface, from 160 m/sec to 2000 m/sec at depth. The higher velocities are found in more competent denser lava which underlies higher porosity, lower density surface material. The SP flow is a blocky basalt flow located in the northern part of the San Francisco volcanic field near Flagstaff, Arizona. Vesicularity ranges from 5 to 50% and *in situ* seismic velocities range from 700 to 1100 m/sec. The Kana-a flow, also located near Flagstaff, is an olivine basalt flow intermingled with ash; velocities range from 700 to 1200 m/sec.

We see that observed velocities on terrestrial lava flows bracket the velocities measured at the 17 site and therefore are consistent with the presence of lava flows in the Taurus–Littrow valley. The 280 m/sec velocity is probably representative of several flows separated by lower velocity layers of ash or ejecta. Individual flows may be fractured or brecciated which would further decrease their seismic velocities. Surface layers of fractured loose blocky material merging into more welded flows are common occurrences on earth. We therefore believe that the sum of the 280 m/sec and the 1130 m/sec materials (1187 m) represent the full thickness of the subfloor basalts at the Apollo 17 site.

The nature of the material underlying the basalts with a seismic velocity of ~4 km/sec is difficult to assign unambiguously to any particular rock type. It seems likely, based on the geological evidence, that the highland massif material which rings the narrow graben-like valley at the 17 site underlies the basalt flow(s). Several rock types were recognized in the North and South Massifs but the dominant rock type is apparently a coherent breccia believed to be similar to breccias sampled at the Apennine Front (Apollo 15) and Descartes (Apollo 16).

Laboratory velocity measurements have been reported for two Apollo 15 breccias, 15418 and 15015 (Todd *et al.*, 1972). Sample 15418 is described as a dark gray crystalline breccia of chemical composition similar to anorthite rich gabbro. Sample 15015 is a more friable breccia of unknown composition. The *in situ* value of ~4 km/sec is close to the values measured in the laboratory for sample 15015.

CONCLUSIONS

Prior to the Apollo 17 mission the question of how the *P*-wave velocity increased from 100 to 300 m/sec near the surface to 6 km/sec at a depth of 15 to 20 km was most uncertain. The main reason for this uncertainty was the gap in travel time data between the ranges of a few hundred meters (previous Active Seismic Experiments) and 67 km (Apollo 14 LM impact as recorded by the Apollo 14 PSE). The Apollo 17 Lunar Seismic Profiling results have demonstrated that the seismic velocity increases in a sharp stepwise manner in the upper 2.5 km. A surface layer with a seismic velocity of 280 m/sec overlies a layer with a velocity of 1130 m/sec. Beneath the 1130 m/sec layer the seismic velocity increases sharply to a velocity of 4000 m/sec. The velocities of 280 m/sec and 1130 m/sec are in

agreement with those observed for basaltic lava flows on earth and therefore suggest a total thickness of about 1200 m for the infilling mare basalts at Taurus–Littrow. When the Apollo 17 results are combined with earlier travel time data for direct and surface reflected arrivals from LM and SIVB impacts it will be possible to construct a velocity model for the upper lunar crust believed to be representative for a mare basin.

Acknowledgments—This work was supported by the National Aeronautics and Space Administration under contract NAS9-5632 and grant NGL05-020-232.

REFERENCES

Anderson O. L., Scholz C., Soga N., Warren N., and Schreiber E. (1970) Elastic properties of a micro-breccia, igneous rock and lunar fines from Apollo 11 mission. *Proc. Apollo 11 Lunar Sci. Conf., Geochim. Cosmochim. Acta*, Suppl. 1, Vol. 3, pp. 1959–1973. Pergamon.

Ewing M., Woollard G., and Vine A. (1939) Geophysical investigations in the emerged and submerged Atlantic coastal plain: Part III: Barnegat Bay, New Jersey, section. *Bull. Geol. Soc. Amer.* **50**, 257–296.

Kanamori H., Nur A., Chung D. H., Wones D., and Simmons G. (1970) Elastic wave velocities of lunar samples at high pressures and their geophysical implications. *Science* **167**, 726–728.

Kanamori H., Mizutani H., and Hamano Y. (1971) Elastic wave velocity of Apollo 12 rocks at high pressures. *Proc. Second Lunar Sci. Conf., Geochim Cosmochim. Acta*, Suppl. 2, Vol. 3, pp. 2323–2326. MIT Press.

Kovach R. L. and Watkins J. S. (1973a) Apollo 17 seismic profiling—probing the lunar crust. *Science* **180**, 1063–1064.

Kovach R. L. and Watkins J. S. (1973b) The velocity structure of the lunar crust. *The Moon* **7**, 63–75.

Kovach R. L., Watkins J. S., and Talwani P. (1973) Seismic profiling experiment. *Apollo 17 Preliminary Science Report.* In press.

Latham G., Ewing M., Press F., Sutton G., Dorman J., Nakamura Y., Toksoz N., Lammlein D., and Duennebier F. (1972) Passive seismic experiment. *Apollo 15 Preliminary Science Report*, NASA SP-289, section 8.

Latham G., Ewing M., Press F., Sutton G., Dorman J., Nakamura Y., Toksoz N., Lammlein D., and Duennebier F. (1973) Passive seismic experiment. *Apollo 16 Preliminary Science Report*, NASA SP-315, section 9.

Mizutani H., Fujii N., Hamano Y., Osako M., and Kanamori H. (1972) Elastic wave velocities and thermal diffusivities of Apollo 14 rocks (abstract). In *Lunar Science—III*, p. 547. The Lunar Science Institute, Houston.

Gangi A. F. (1972) The lunar seismogram. *The Moon* **4**, 40–48.

Gold T. and Soter S. (1970) Apollo 12 seismic signal: Indications of a deep layer of powder. *Science* **169**, 1071–1075.

Talwani P., Nur A., and Kovach R. L. (1973) Compressional and shear wave velocities in granular materials to 2.5 kilobars. *J. Geophys. Research.* In press.

Todd T., Wang H., Baldridge W., and Simmons G. (1972) Elastic properties of Apollo 14 and 15 rocks. *Proc. Third Lunar Sci. Conf., Geochim. Cosmochim. Acta*, Suppl. 3, Vol. 3, pp. 2577–2586. MIT Press.

Toksoz M. N., Press F., Dainty A., Anderson K., Latham G., Ewing M., Dorman J., Lammlein D., Sutton G., and Duennebier F. (1972) Structure, composition and properties of lunar crust. *Proc. Third Lunar Sci. Conf., Geochim. Cosmochim. Acta*, Suppl. 3, Vol. 3, pp. 2527–2544. MIT Press.

Warren H., Schreiber E., Scholz C., Morrison J. A., Norton P. R., Kumazala M., and Anderson O. L. (1971) Elastic and thermal properties of Apollo 12 and Apollo 11 rocks. *Proc. Second Lunar Sci. Conf., Geochim. Cosmochim. Acta*, Suppl. 2, Vol. 3, pp. 2345–2360. MIT Press.

Watkins J. S. (1966) Annual Report. Investigation of *in situ* physical properties of surface and subsurface site materials by engineering geophysical techniques. NASA Contract T-25091 (G).
Watkins J. S. and Kovach R. L. (1973) Seismic investigation of the lunar regolith. *Proc. Fourth Lunar Sci. Conf., Geochim. Cosmochim. Acta.* In press.
Watkins J. S., Walters L. A., and Godson R. H. (1972) Dependence of *in situ* compressional-wave velocity on porosity in unsaturated rocks. *Geophysics* **37**, 29–35.

Lunar Near-Surface Structure

MICHAEL R. COOPER AND ROBERT L. KOVACH

Department of Geophysics, Stanford University, Stanford, California 94305

JOEL S. WATKINS

Earth and Planetary Sciences Division, Marine Biomedical Institute
University of Texas Medical Branch, Galveston, Texas 77550

Seismic refraction data obtained at the Apollo 14, 16, and 17 landing sites permit a compressional wave velocity profile of the lunar near surface to be derived. Although the regolith is locally variable in thickness, it possesses surprisingly similar seismic characteristics. Beneath the regolith at the Apollo 14 Fra Mauro site and the Apollo 16 Descartes site is material with a seismic velocity of ~300 m/s, believed to be brecciated material or impact-derived debris. Considerable detail is known about the velocity structure at the Apollo 17 Taurus-Littrow site. Seismic velocities of 100, 327, 495, 960, and 4700 m/s are observed. The depth to the top of the 4700-m/s material is 1385 m, compatible with gravity estimates for the thickness of mare basaltic flows, which fill the Taurus-Littrow valley. The observed magnitude of the velocity change with depth and the implied steep velocity-depth gradient of >2 km/s/km are much larger than have been observed on compaction experiments on granular materials and preclude simple cold compaction of a fine-grained rock powder to thicknesses of the order of kilometers. The large velocity change from 960 to 4700 m/s is more indicative of a compositional change than a change of physical properties alone. This high velocity is believed to be representative of the material that forms the lunar highlands.

Seismic refraction experiments were executed on the lunar surface by Apollo astronauts during missions 14, 16, and 17 as part of an integrated set of geophysical experiments called Alsep (Apollo lunar surface experiments package). For the study of the earth's crust, seismic refraction techniques are often used. The basic technique involves the recording of seismic waves produced by the detonations of explosive charges placed at different distances from an array of seismometers (geophones). The travel times of the resulting seismic waves are analyzed in a straightforward fashion to determine the variation of seismic velocity with depth and as a result provide a direct method of probing the lunar interior.

The results of these experiments when they are combined with the seismic signals from other man-made impacts from spent rocket stages have allowed a model of the near-surface lunar structure to be constructed. In this paper we describe and analyze the seismic data pertinent to the near surface of the moon.

SEISMIC INSTRUMENTATION

At the Apollo 14 and 16 sites the astronauts deployed a 91-m linear array of three geophones, and several seismic energy sources were used: an astronaut-activated thumper device with small explosive initiators, a mortar package containing earth-controlled rocket-launched grenades, and the impulse produced by the thrust of the lunar module (LM) ascent stage as it departed from the lunar surface. Technical details of these experiments can be found in *McAllister et al.* [1969], *Kovach et al.* [1971], and *Kovach et al.* [1972].

The seismic refraction experiment on Apollo 17 differed in scale from the earlier experiments and offered an unusual opportunity to study the properties of the lunar crust to a depth of several kilometers. Four geophones were positioned in a T-shaped array, and eight explosive packages were placed at distances ranging from 60 m to 3 km from the array during traverses on the lunar surface by the astronauts (Figure 1). The explosive charges were fired by command from earth after the astronauts had departed. In addition to the explosive packages the thrust of the LM ascent and the crash of the LM ascent stage back into the moon served as seismic sources for the array. Figure 2 is a view from behind explosive package 8 (EP 8 in Figure 1) looking eastward with the LM in the background.

ANALYSIS OF LUNAR SEISMIC SIGNALS

Apollo 14. The Apollo 14 astronauts landed on the moon in an area referred to as the Fra Mauro region (3°40'S latitude, 17°27'W longitude). The region is underlain by the Fra Mauro formation, presumed to be the ejecta deposit produced by the large impact that formed the Imbrium basin [*Sutton et al.*, 1972]. Surface topography is characterized by a series of hummocks, ridges, and valleys trending radially from the Imbrium basin. At the landing site the astronauts placed three geophones in a southerly direction across the lunar surface and used the handheld thumper device to generate seismic signals at different positions along the geophone line.

Figure 3 shows typical seismic signals recorded at the Apollo 14 site. Thumper firings within 9 m of a geophone produced seismic signals with very impulsive beginnings. As the distance between the thumper firings and the geophones increases, the seismic signals possess much more emergent beginnings. The peak amplitude of the signals typically decreases by a factor of 60 over a distance of 60 m.

It is of some help at this point to recognize the common assumptions underlying the interpretation of a seismic refraction profile [*Ewing et al.*, 1939]: (1) layers are considered planar and propagate seismic waves with a constant velocity, (2) at a layer boundary the path of a seismic wave is governed by Snell's law, (3) a seismic wave traveling in a layer at an angle α with the normal travels with an apparent velocity $V/\sin\alpha$ along the surface, and (4) the travel time of a seismic wave is the same if the point of detonation of the explosive

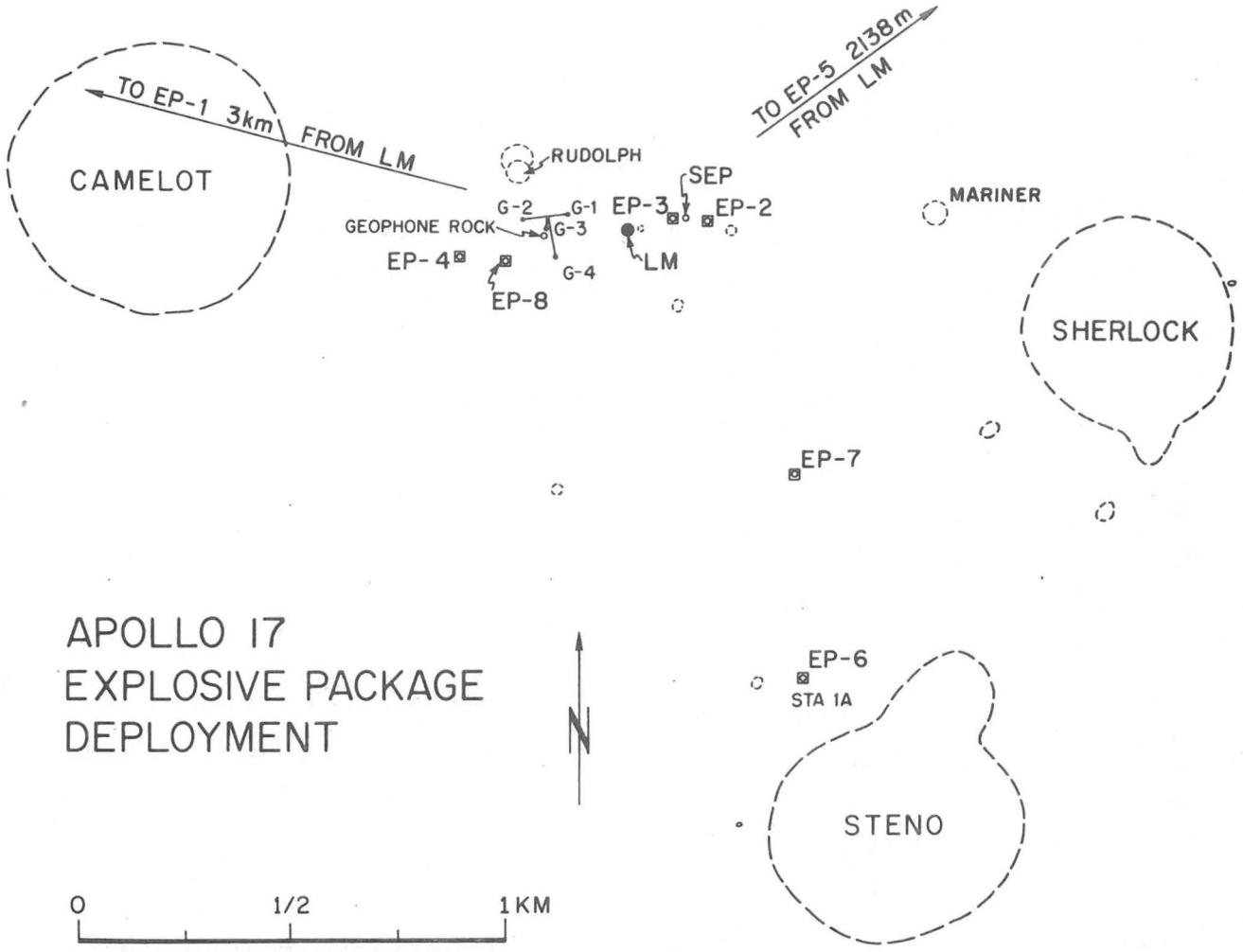

Fig. 1. Map of Apollo 17 landing site showing position of geophone array (G-1 to G-4) and locations of explosive charges (EP 4 etc.) deployed during traverses. Location of lunar module is shown as LM.

charge (shot point) and recording point are interchanged. Departures from these assumptions are indicated by deviations of the observed seismic travel time data from linear segments drawn on a travel time versus distance graph.

Two compressional wave (*P* wave) velocities were identified in the lunar near surface at the Apollo 14 site. The first seismic arrival was observed to travel with a velocity of 104 m/s out to a distance of 22.7 m, where the first arrival then traveled with a velocity of 299 m/s. At the Apollo 14 location the near surface can be described as a surface layer with 104-m/s velocity material overlying material possessing a seismic velocity of 299 m/s.

The rocket thrust produced by the ascent of the LM from the moon produced seismic signals that were recorded by the Apollo 14 passive seismometer at a distance of 178 m. The travel time data of these signals are compared in Figure 4 with the extrapolated travel time distance curves measured from the astronaut thumper firings. As can be seen, the LM ascent travel times are in close agreement with the extrapolated travel times; however, the first arrival arrives somewhat earlier than that predicted from the 299-m/s horizon, this situation revealing that material with a faster velocity lies beneath the 299-m/s material. If the critical distance for the arrival traveling through the underlying material is taken as the length of the geophone array (100 m), a minimum velocity of 386 m/s is inferred for the underlying material (Figure 4).

The thickness of the 104-m/s layer is 8.5 m. This low seismic velocity is suggestive of a porous or highly fractured and brecciated rock material and is believed to be representative of the lunar regolith, the veneer of unconsolidated and 'gardened' material that covers much of the lunar surface. Examination of the depth at which blocky floors can be seen in fresh craters has determined that the regolith at the Apollo 14 site ranges in thickness from 5 to 12 m [*Offield,* 1970].

The underlying velocity of 299 m/s is in agreement with velocities measured in the upper part of the terrestrial Meteor crater ejecta blanket and therefore is compatible with the idea that this velocity is indicative of ejecta material from the Imbrium basin (the Fra Mauro formation). The Fra Mauro returned samples are almost entirely composed of complex breccias [*Sutton et al.,* 1972].

Apollo 16. The lunar central highlands were the site of the Apollo 16 landing (8°59′29″S latitude, 15°30′52″E longitude). The location of the LM and the traverses was on the Cayley formation, near the western edge of the Descartes Mountains. Premission photogeologic analysis had concluded that both of these features were the products of igneous activity; the Cayley formation was believed to be of volcanic origin, and lava domes (intrusive or extrusive masses of very viscous lava) made up the rounded topography of the Descartes Mountains. Apollo 16 astronauts, however, found only breccia samples at the landing site; no evidence of any local igneous activity was

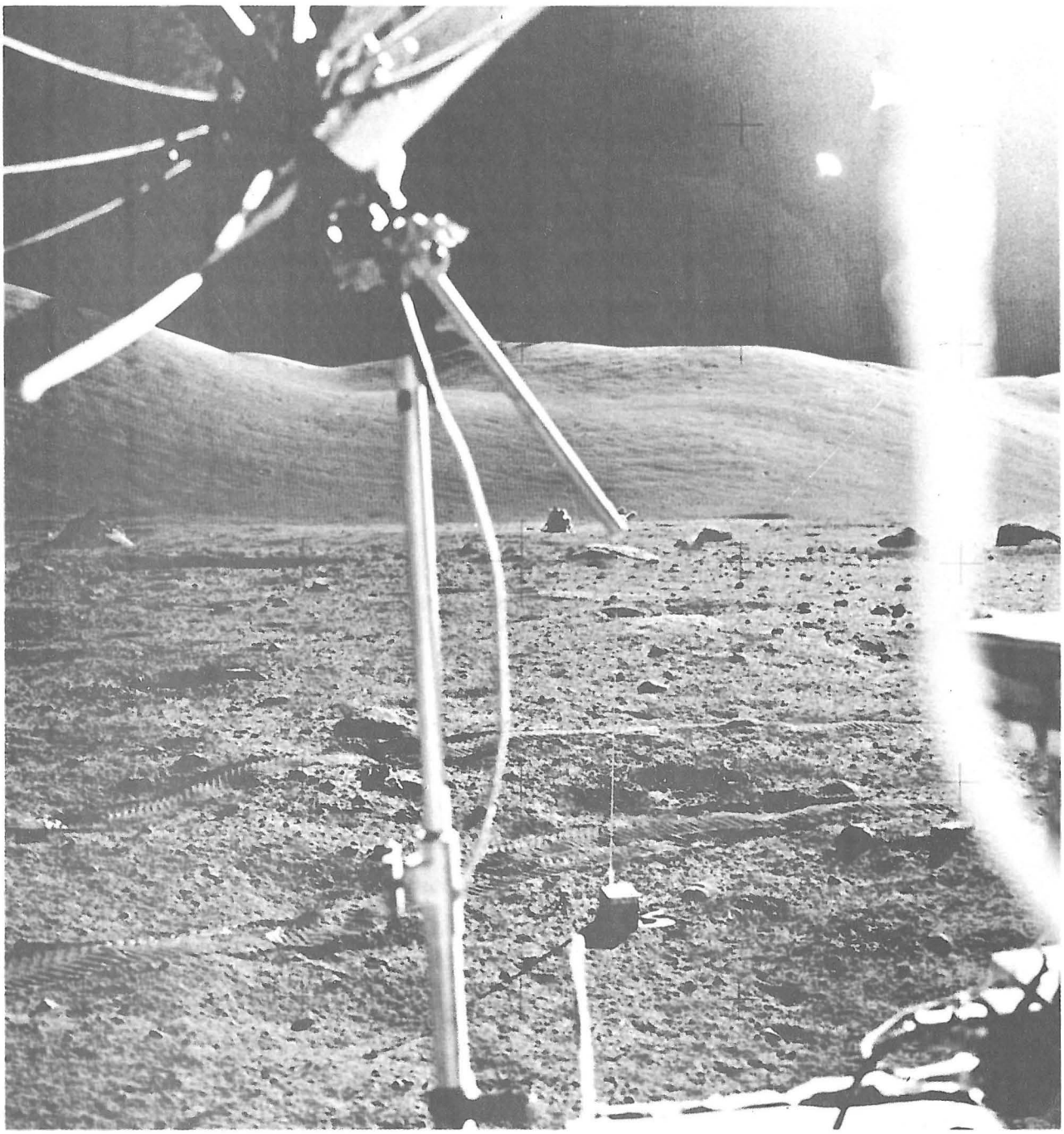

Fig. 2. Photograph of Apollo 17 landing site looking eastward toward LM with EP 8 in foregound (NASA photograph AS17-145-22184).

detected [*Hodges et al.*, 1973]. More current interpretations of the Cayley formation view it as an ejecta blanket from the Imbrium impact.

The three geophones were arranged in a line trending WNW from the central station. As was mentioned above, energy sources consisted of the astronaut-activated thumper, rocket-propelled grenades, and the thrust of the LM ascent stage.

The thumper experiment provided travel time data over distances ranging between 4 and 91 m. Figure 5 shows a typical series of thumper shots as recorded at geophone 2. All of the thumper signals arrived with a first arrival velocity of 114 m/s, as is indicated by the travel time plot shown in Figure 6.

Data for shot distances between 55 and 450 m were supplied by the grenades. The signals recorded from a close grenade are shown in Figure 7. The LM ascent was located 100–150 m from the various geophones and also supplied useful data. Travel time data for the grenades and LM ascent are shown in Figure 8. In addition to the 114-m/s velocity observed from thumper shots a velocity of 250 m/s was detected at distances up to 160 m. It is likely that this arrival persists but is too weak to be detected at greater distances (Figure 8).

The 114-m/s layer is found to be 12.2 m thick. If we assume that whatever underlies the 250-m/s layer has a velocity of at least 1.0 km/s and if we also assume that the refractions from the faster horizon begin just after the last detection of the 250-m/s arrival, a minimum thickness of 70 m for the 250-m/s

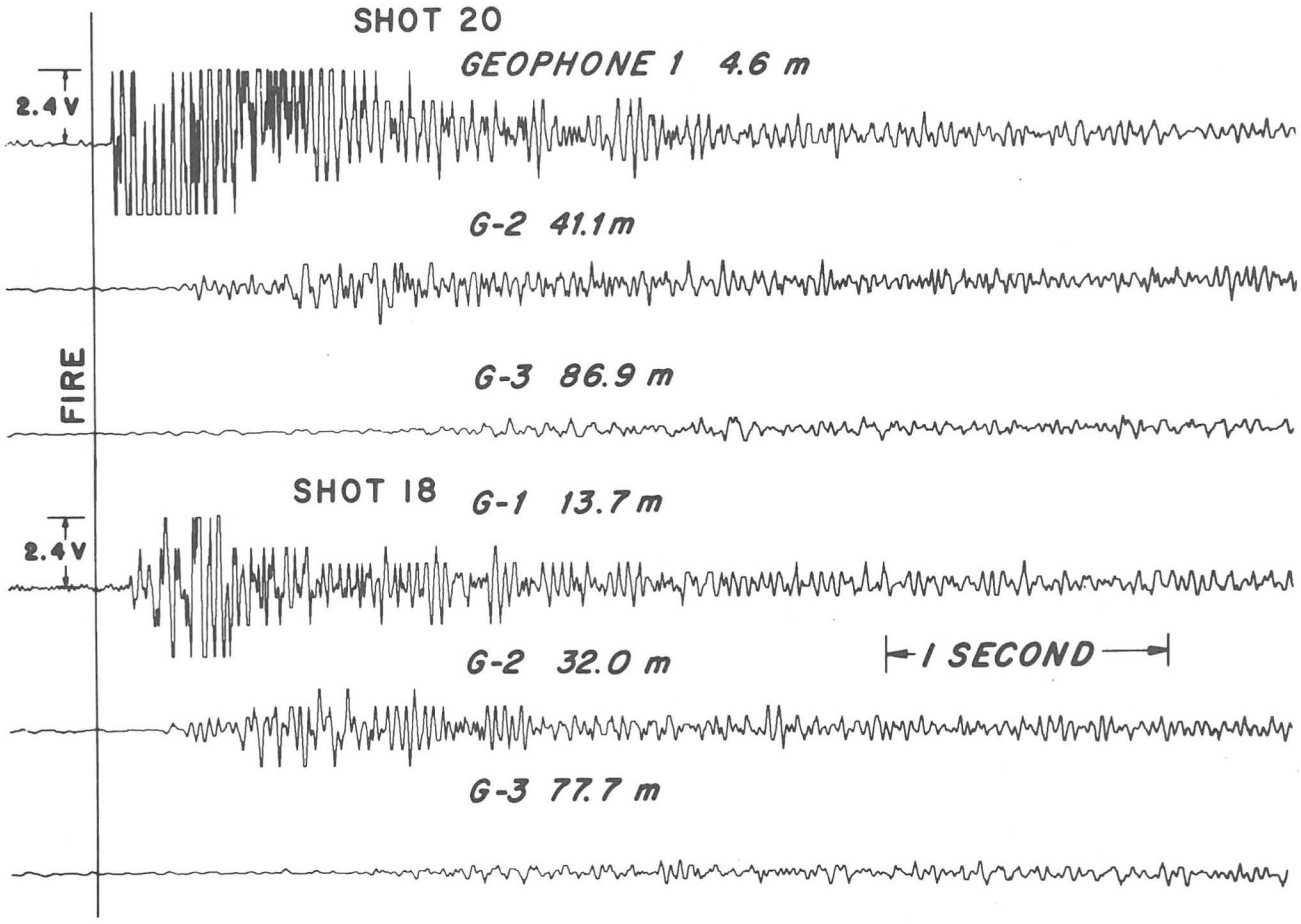

Fig. 3. Seismic signals recorded at the Apollo 14 site at different distances. Note the strong signal attenuation with distance and except for the thumper shot to receiver distance of 4.6 m the emergent onsets of the first seismic arrivals.

layer may be estimated. Alternately, if we assume that the first (undetected) arrival at 445 m is still from the 250-m/s material, it must be at least 220 m thick [*Kovach and Watkins,* 1973*a*].

The uppermost layer (114 m/s) may be identified with the lunar regolith. The 12.2-m thickness is within limits estimated [*Oberbeck,* 1971] by crater counting. The base of the regolith was not unambiguously observed in any of the craters investigated by the astronauts. The underlying material with a 250-m/s velocity is thought to be representative of the Cayley formation. Returned lunar samples indicate that the formation

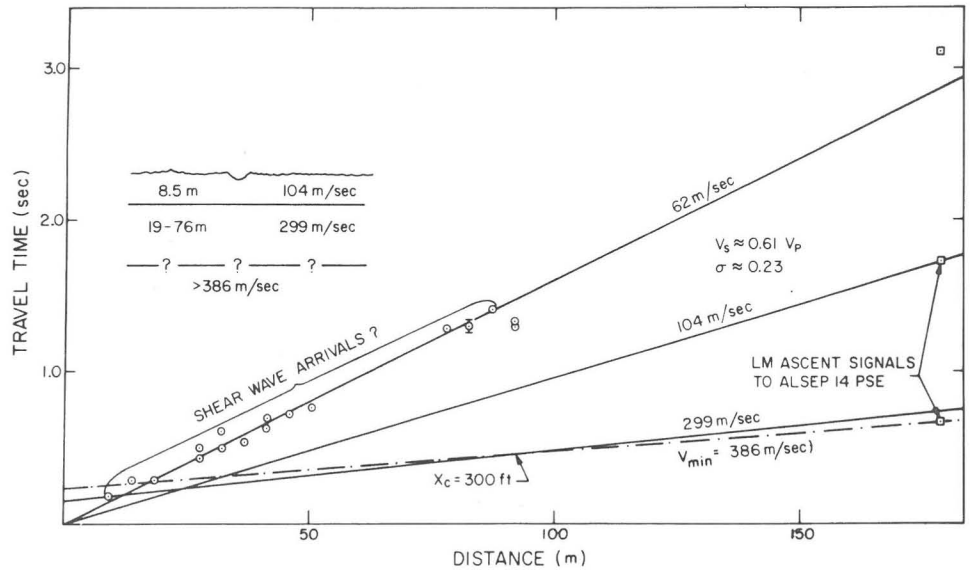

Fig. 4. Apollo 14 travel time curve combining data from the thumper shots and the thrust of the LM ascent stage. Velocities of 104 m/s and 299 m/s are recognized in the thumper data. A faster horizon with a minimum velocity of 386 m/s is inferred from the LM ascent signal.

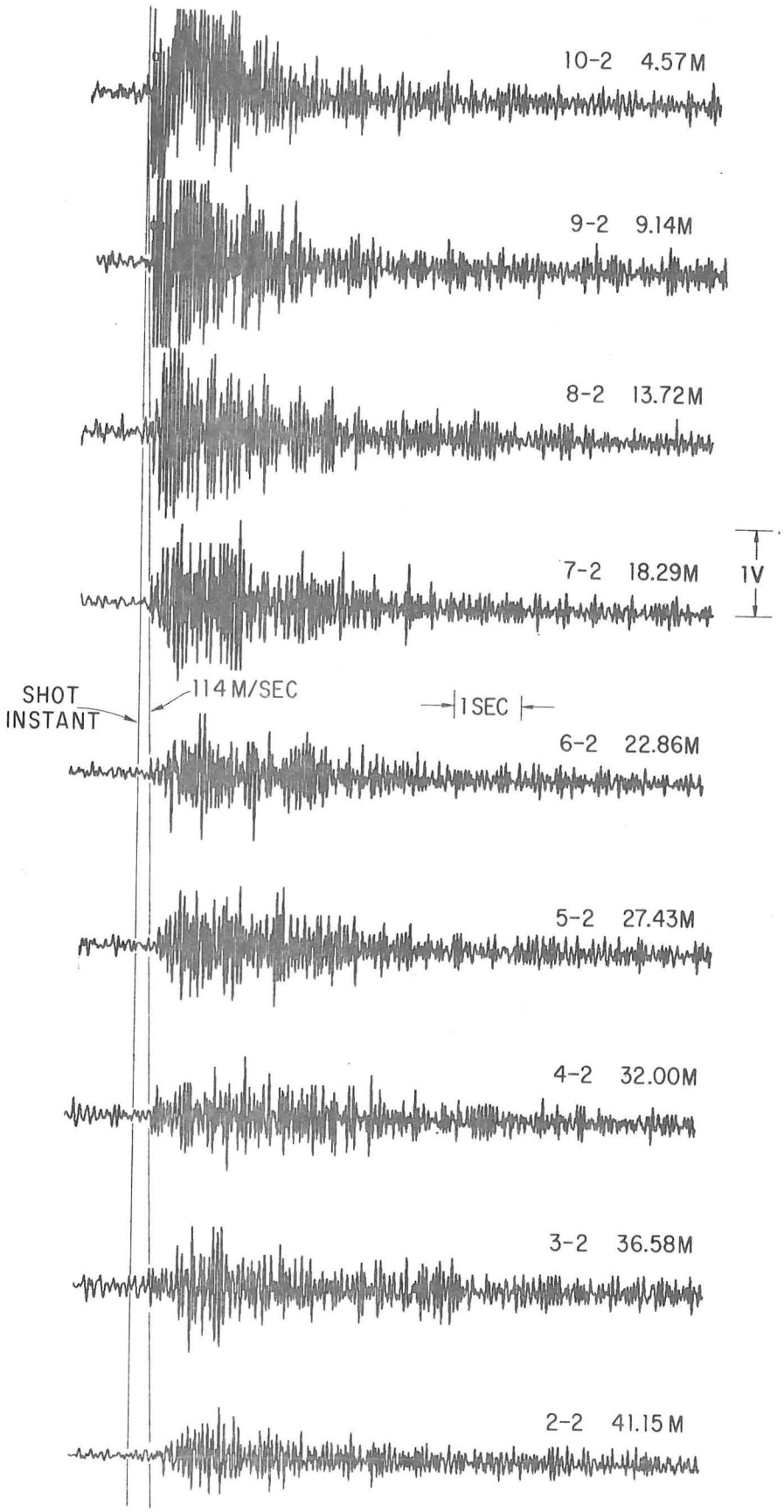

Fig. 5. Seismic signals produced by thumper firings at the Apollo 16 site. The traces are aligned to the same relative instant of the thumper firings, indicated by the vertical line labeled shot instant. The line marked 114 m/s indicates the velocity inferred from the measured onsets of the seismic signals. (The first number in the data identifier reflects the thumper firing, and the second refers to the geophone on which the data were recorded.)

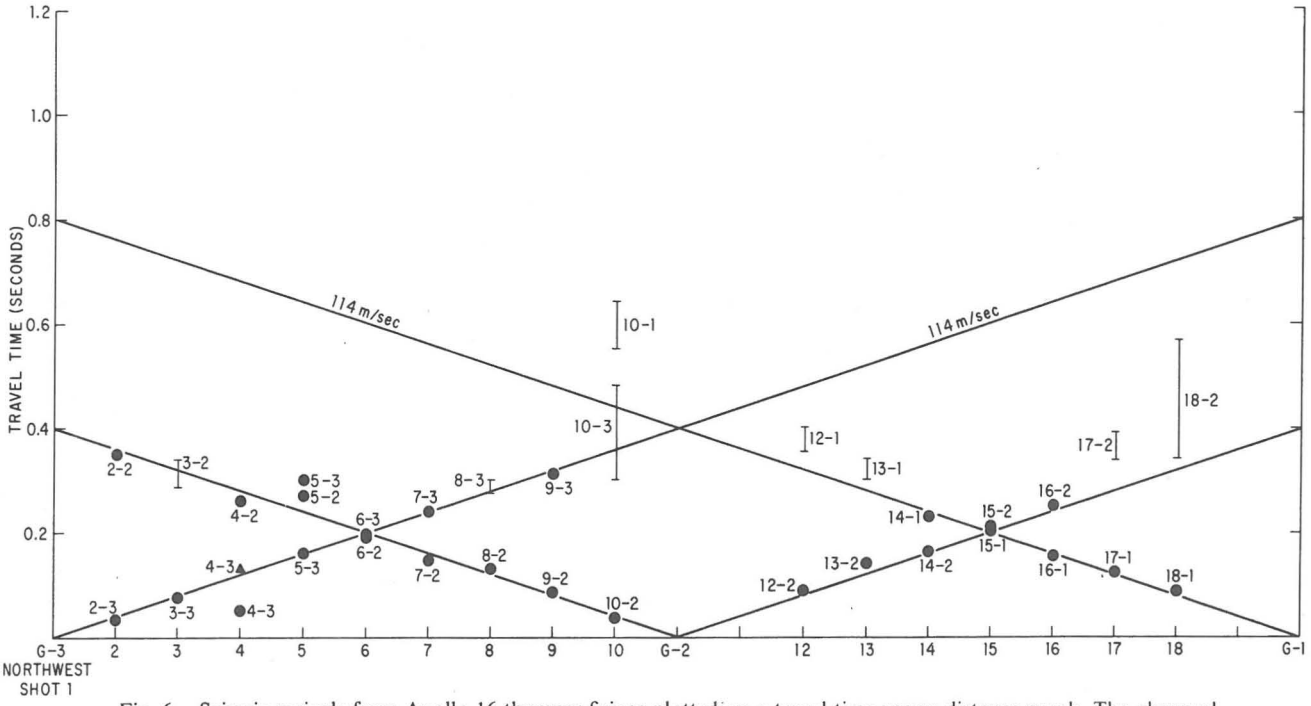

Fig. 6. Seismic arrivals from Apollo 16 thumper firings plotted on a travel time versus distance graph. The observed travel times for the first arrivals are shown as black circles. The distance between tick marks on the horizontal axis is 4.75 m. Shot 4-3 has an anomalously early arrival. (The first number in the data point identifier is the thumper firing, and the second number is the geophone on which the data were recorded.)

is a breccia. The 70- to 220-m thickness estimates of the Cayley formation are representative of the depths to the associated Descarte material that is part of the lunar highlands [*Hodges et al.*, 1973].

Apollo 17. The Apollo 17 mission landed in the Taurus Mountains at the southeastern edge of Mare Serenitatis (20°10′N latitude, 30°46′E longitude). This site provided access to both the highland material, which makes up the massifs of the Taurus Mountains, and the mare basalts, which fill the Taurus-Littrow valley, where the LM landed. Located near the center of the valley, the four-geophone array recorded seismic signals from eight explosive sources, the thrust of the LM ascent engines on the valley floor, and also the crash of the LM impact on the adjacent highlands (Figure 1).

Typical signals are shown in Figures 9–11 for EP 3, 5, and 6. In each case the center four traces show the seismic data as they were received from the moon. For all but the closest explosive sources the first arrival has an emergent onset contaminated by periodic noise generated by the transmitter used to send fire commands to the explosive charges. Prediction filtering was applied in two slightly different ways to separate the noise and the signal. In the first approach a filter was designed that could predict the pattern of the noise, given a sufficient length of noise with no seismic signal. Starting before the onset of the signal, the noise was predicted well into the future, and this predicted time series of noise was subtracted from the observed data. The result of this process is shown in the top four traces of Figures 9–11 and labeled 'prediction filtering.'

The second approach utilized the same predictive filter as the first but applied it in a different manner. Instead of starting the filter before the arrival of the signal the filter was convolved with the entire record of data. In other words, instead of predicting well into the future, only the next point beyond the filter is predicted. The error between this prediction and the next actual data point is the output of a prediction error filter shown in the bottom four traces of Figures 9–11.

A failing of the first method is that its predictive accuracy diminishes markedly as it looks farther and farther ahead. The second method maintains a uniform accuracy of prediction but may alter the character of the seismic signal as it is convolved with it. Specifically, the prediction error filter may 'accidentally' begin to predict part of the signal as well as the noise, this behavior thus removing some of the information that we seek along with the noise. Comparisons of the two analyses were made, and arrival times of the signals were chosen to be consistent with both techniques. Both of these more sophisticated approaches detected the onset of the seismic arrivals significantly earlier than they could be observed in the raw data (Figures 9–11).

The arrangement of EP 2, 3, 4, and 8 (EP 2 etc.) and the LM approximates a straight E-W line through the geophone array. Such geometry may be used to gain information about the inclination of the layers beneath the surface [*Ewing et al.*, 1939]. The times of arrival of the first signal received at each geophone and of later impulses recorded there are shown in Figure 12, plotted against the distance of the source from the various geophones.

The *P* wave velocities of 100 m/s, 327 m/s, and 750 m/s can be seen on both the east and the west side of the array. It can be seen that the 750-m/s arrival takes longer to travel to the array on the east side than it does on the west. Such a delay would be expected over an eastward-dipping bed with an approximate velocity of 750 m/s at a depth of about 65 m beneath geophone 3. These data indicate an eastward apparent dip of about 3° in agreement with photographic observations made on the regional tilting of the lunar surface.

The signals from EP 2 arrive at the array slightly earlier than the signals from the closer EP 3. If the EP 3 data are indeed first arrivals, this delay most likely represents relief of the

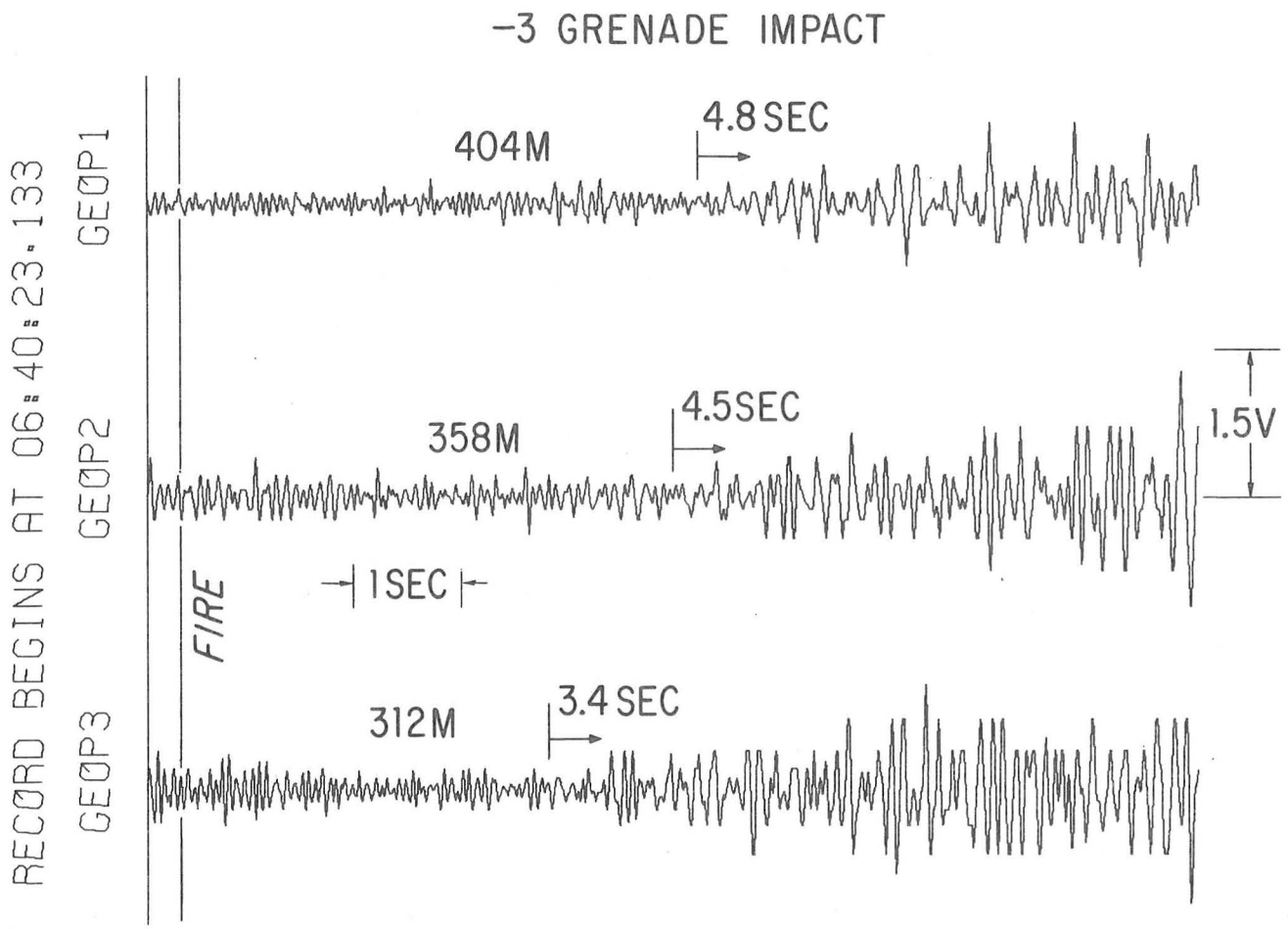

Fig. 7. Seismic signals produced by the detonation of an Apollo 16 grenade on the lunar surface. The detonation time is marked by the vertical line marked fire. The small horizontal arrows indicate the onset of the seismic signal.

order of 6 m on the surface of the 750-m/s layer. Relief of this magnitude could be produced by the fracturing and crushing due to impacting meteorites after emplacement and solidification of the lunar material.

If it is assumed that all the layers are horizontal, all of the data may be incorporated into the analysis of lunar crustal structure. A model derived under this assumption, however, will only be a regional average. In Figures 13 and 14 the arrival times of first and later signals are plotted against distance from the geophone array for all the seismic sources. Five different

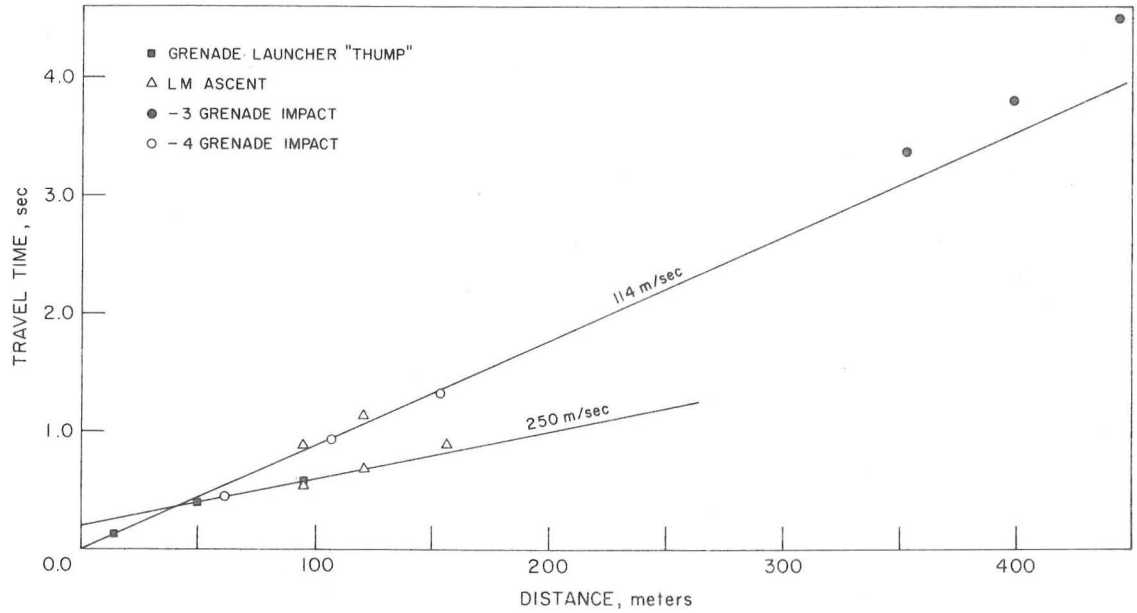

Fig. 8. Travel times measured at the Apollo 16 site.

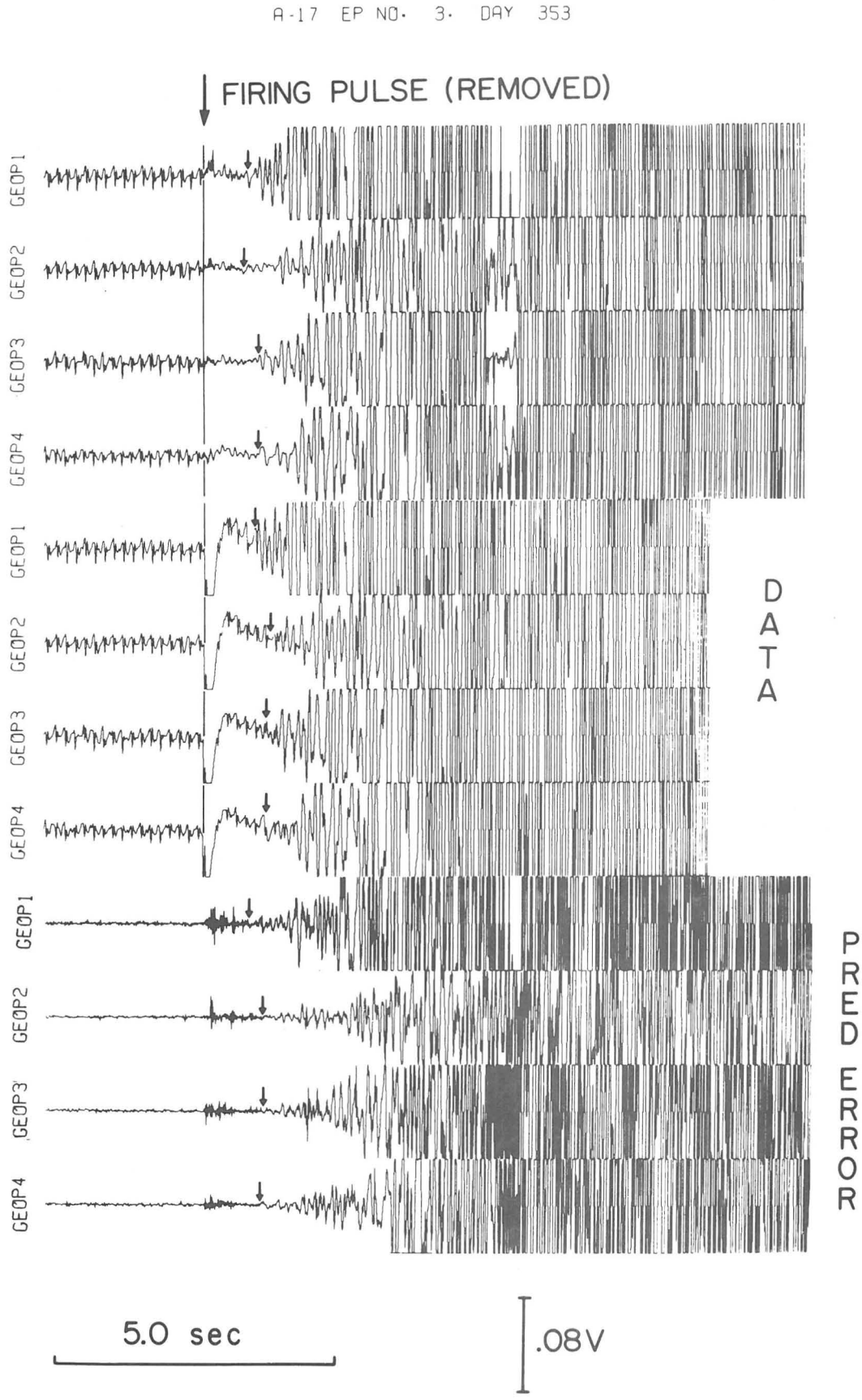

Fig. 9. Seismic signals recorded at the Apollo 17 site at a distance of approximately 300 m from the detonation of 113.5 g of high explosive. The four center traces show the raw data as received from the moon. The top four traces have been filtered to predict the pattern of the noise, and the lower four traces represent the output of a 'prediction error' filter, as discussed in the text. The arrows point to the measured onset of the first seismic arrival. Observe the improvement over the raw data.

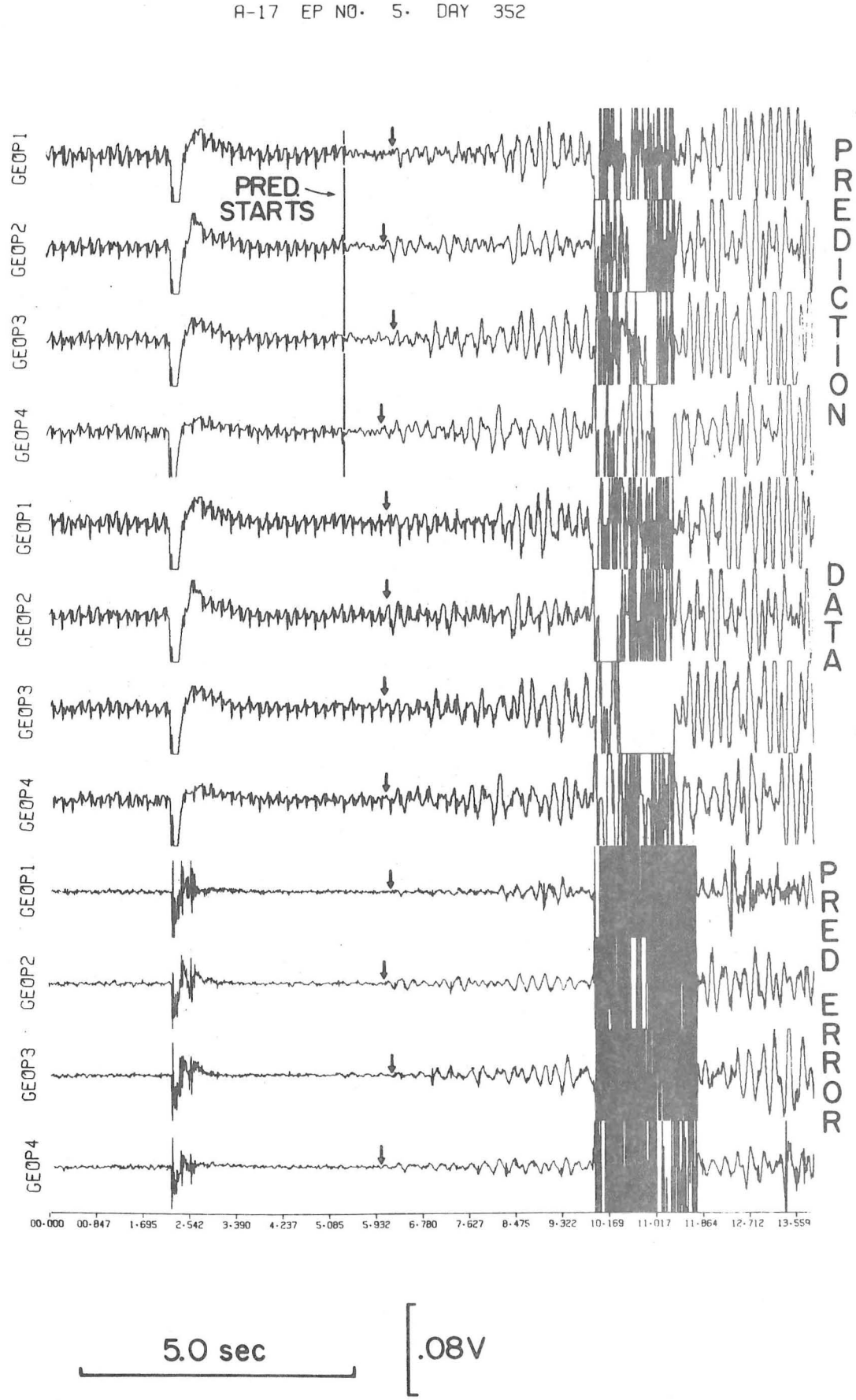

Fig. 10. Seismic signals recorded at the Apollo 17 site at a distance of approximately 2.2 km from the detonation of 1362 g of explosive. The signals have been processed digitally, as is described in the caption for Figure 9. The dark closely spaced lines midway into the seismic signals were produced by a momentary telemetry loss from the moon.

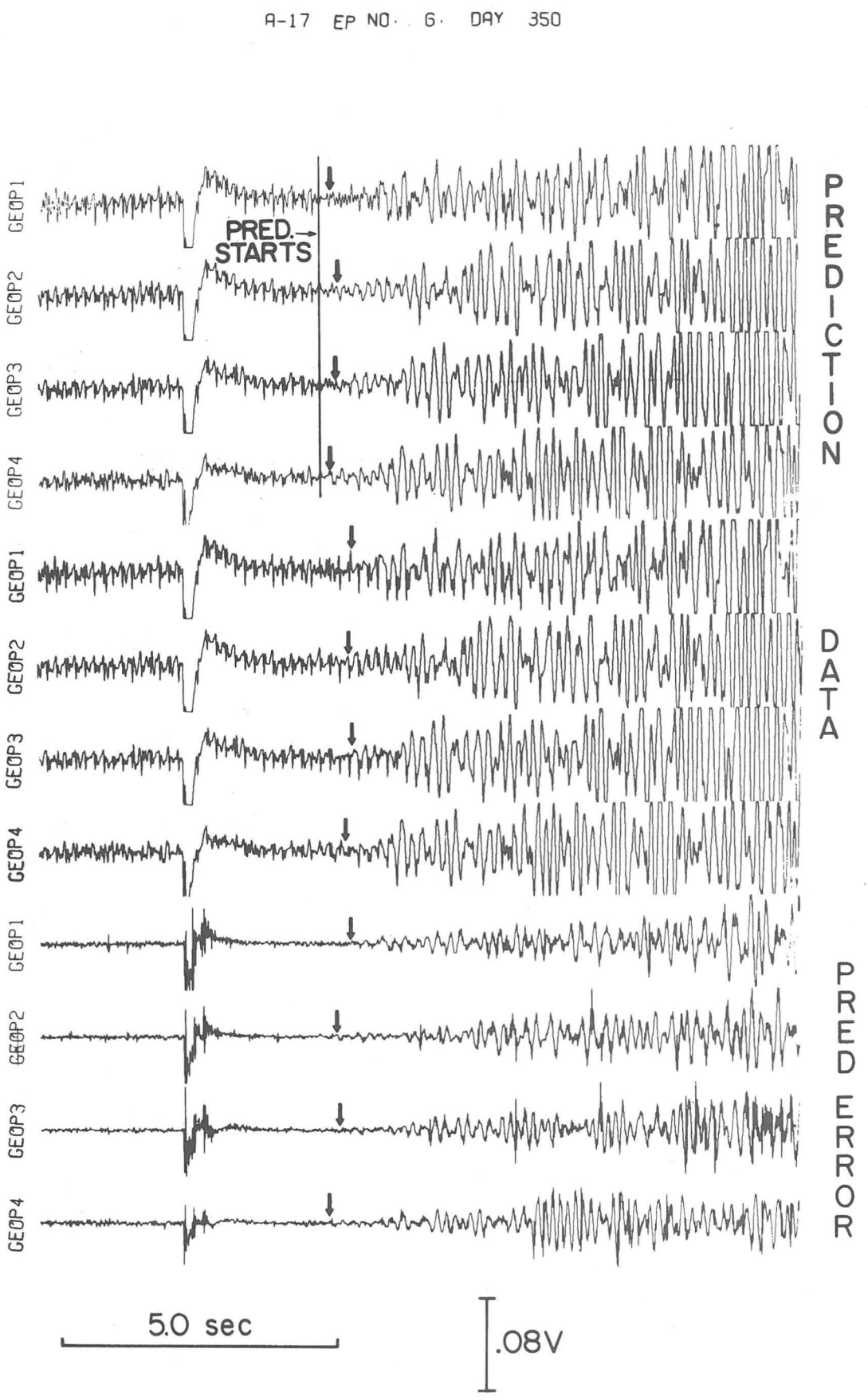

Fig. 11. Seismic signals recorded at the Apollo 17 site at a distance of approximately 1.2 km from the detonation of 454 g of explosive. The four center traces are the raw data as received from the moon; the upper four traces have undergone the operation of prediction filtering. The lower four traces are the output of a 'prediction error' filter. Note that the onset of the seismic signal is detected significantly earlier than can be observed in the raw data.

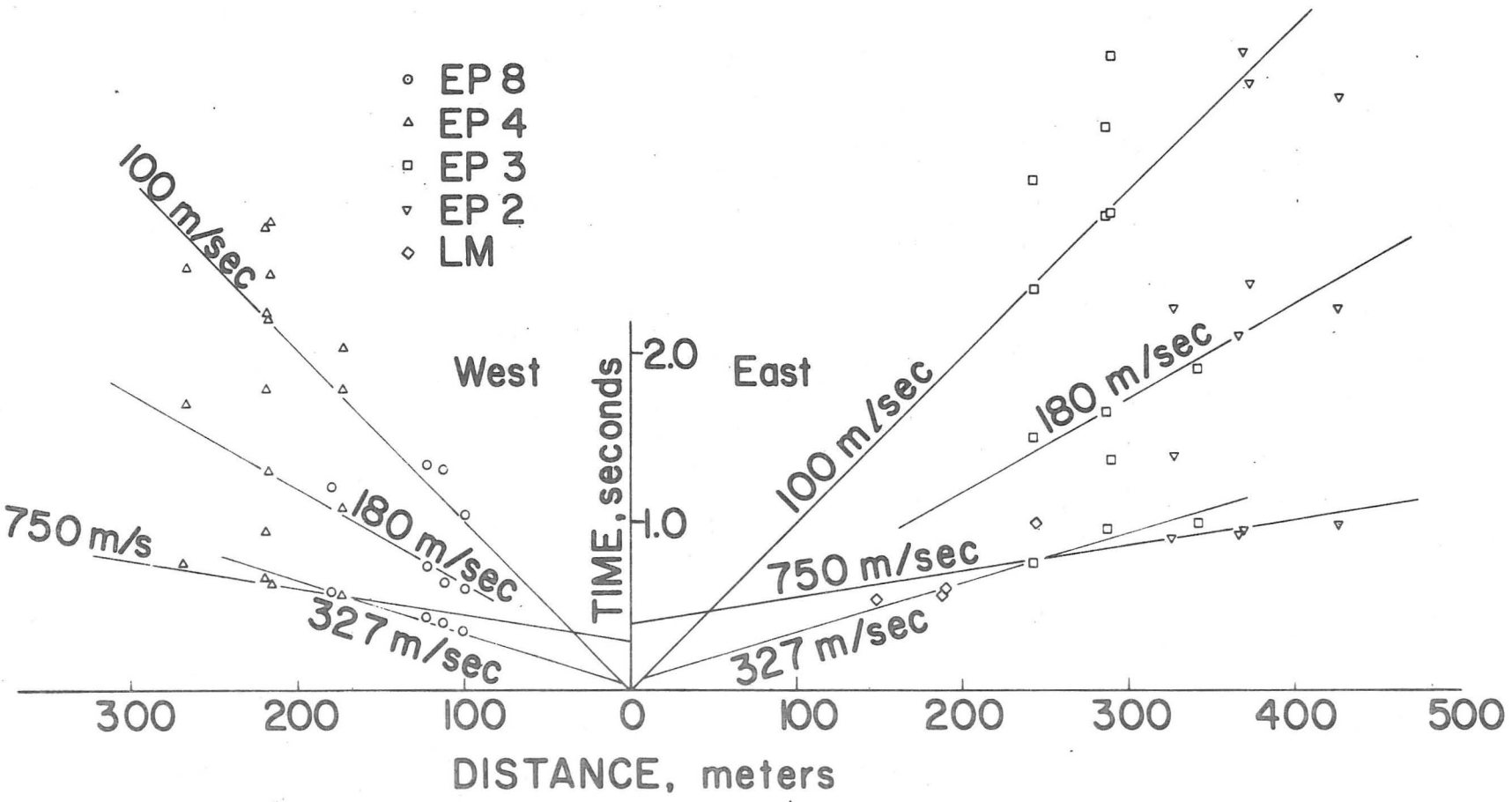

Fig. 12. Reversed travel time curve for EP 2, 3, 4, and 8 and LM ascent for the Apollo 17 site. Both first and later arrivals are shown. Note 180-m/s arrival that can never be observed as a first arrival.

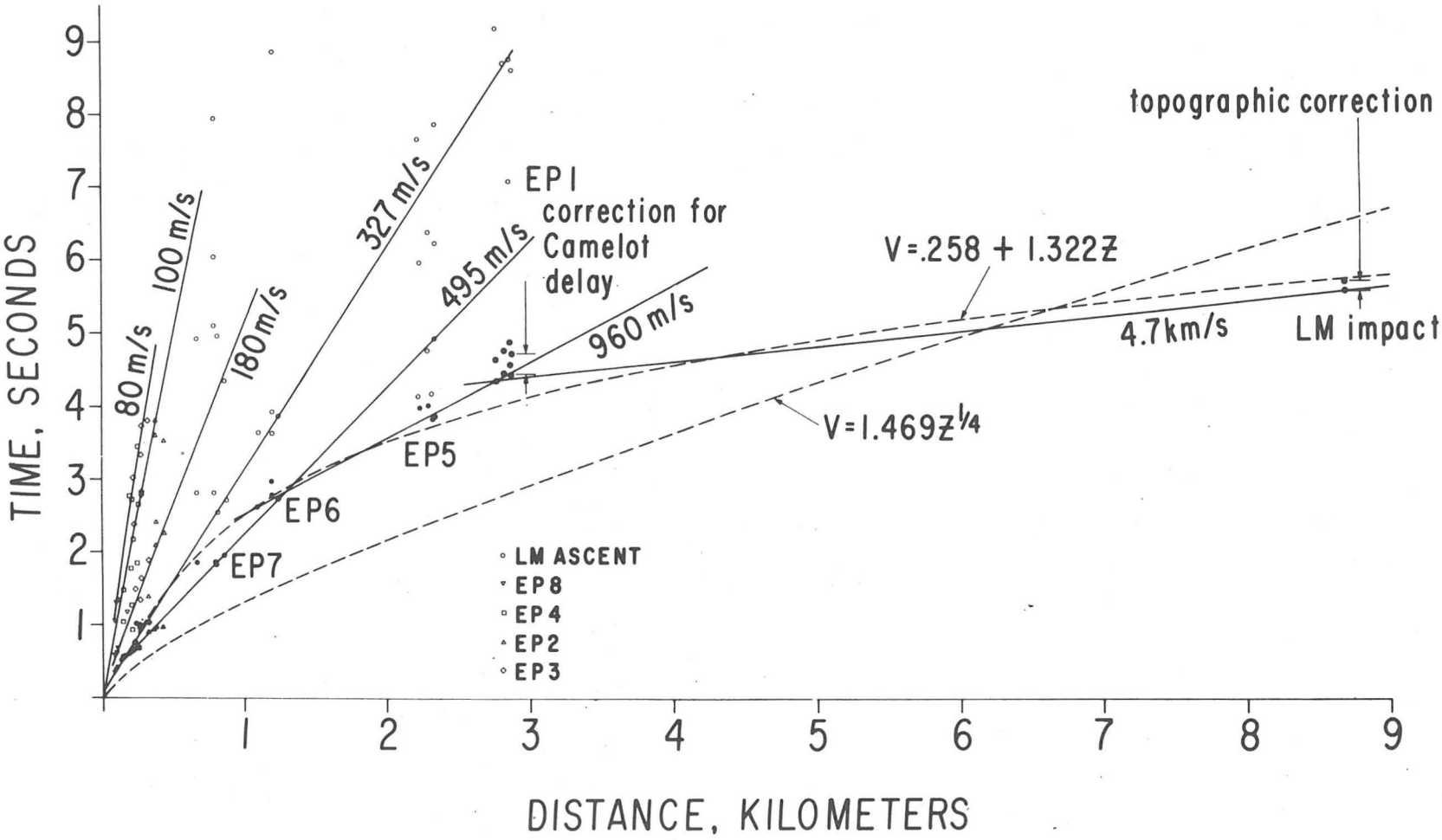

Fig. 13. Apollo 17 regional travel time curve for all explosion packages and the LM impact. The travel time for EP 1 and the LM impact have been corrected for delay through the crater Camelot and a difference in elevation, respectively [*Kovach and Watkins*, 1973*b*]. First arrival velocities are 100, 327, 495, 960, and 4700 m/s. Dashed lines refer to travel time curves for best-fitting linear and power law velocity-depth relationships.

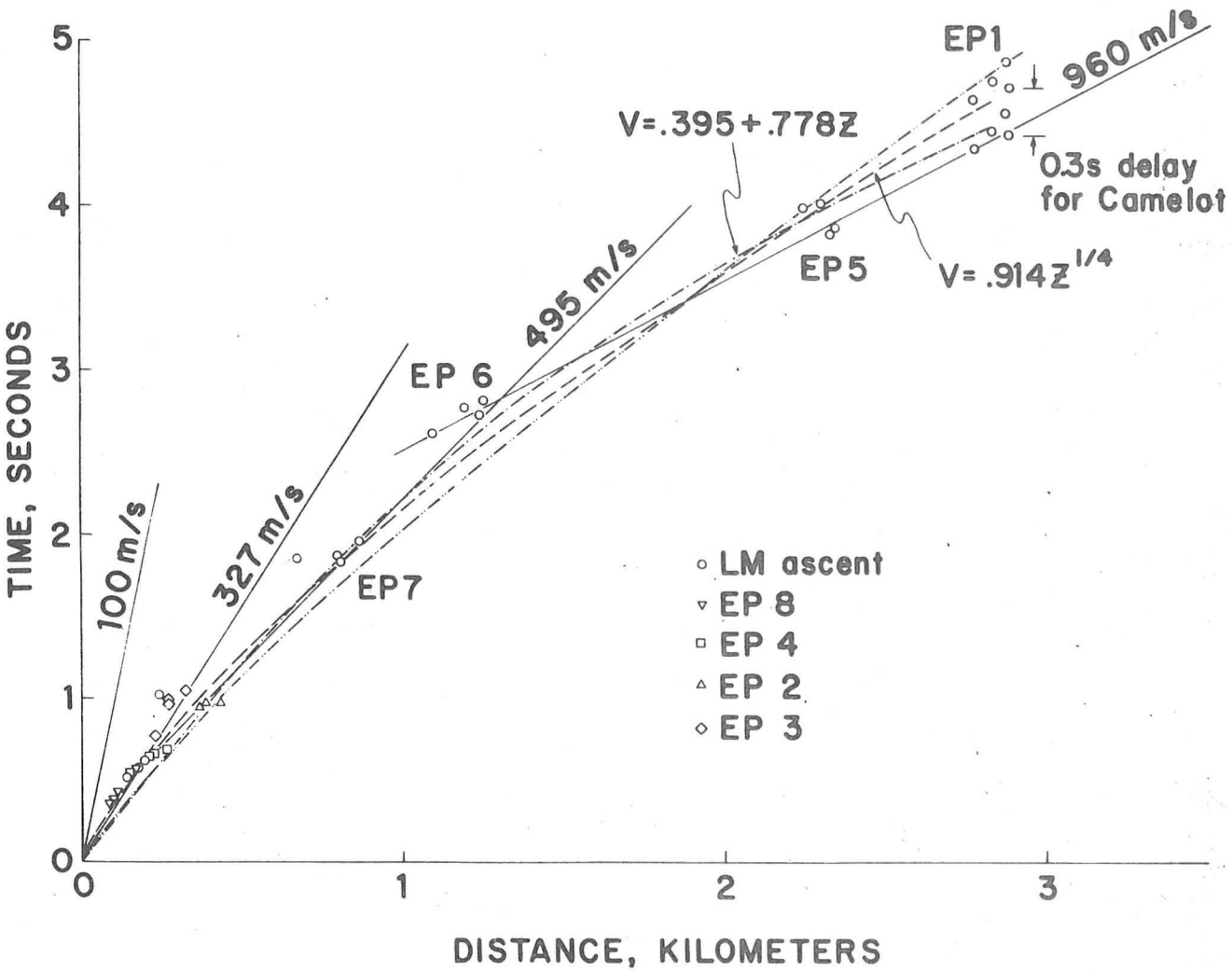

Fig. 14. Apollo 17 regional travel time curve for only the explosion packages. Dot-dash and dashed curves are best-fitting travel time curves derived for linear and power law velocity-depth relationships, respectively. The double dot-dash curve refers to a power law relationship $V = 0.793Z^{1/6}$.

apparent signal velocities are observed as possible first arrivals: 100 m/s, 327 m/s, 495 m/s, 960 m/s, and 4700 m/s. If the layers are horizontal, these velocities equal the P wave velocity in the subsurface layers. The depths to the tops of these five velocity layers may easily be computed and are found to be 0 m, 4 m, 32 m, 390 m, and 1385 m. A schematic cross section of the Taurus-Littrow valley, showing seismic velocity structure, is given in Figure 15. All velocities and depths have approximately a 10% error.

To reach this interpretation, it has been necessary to make

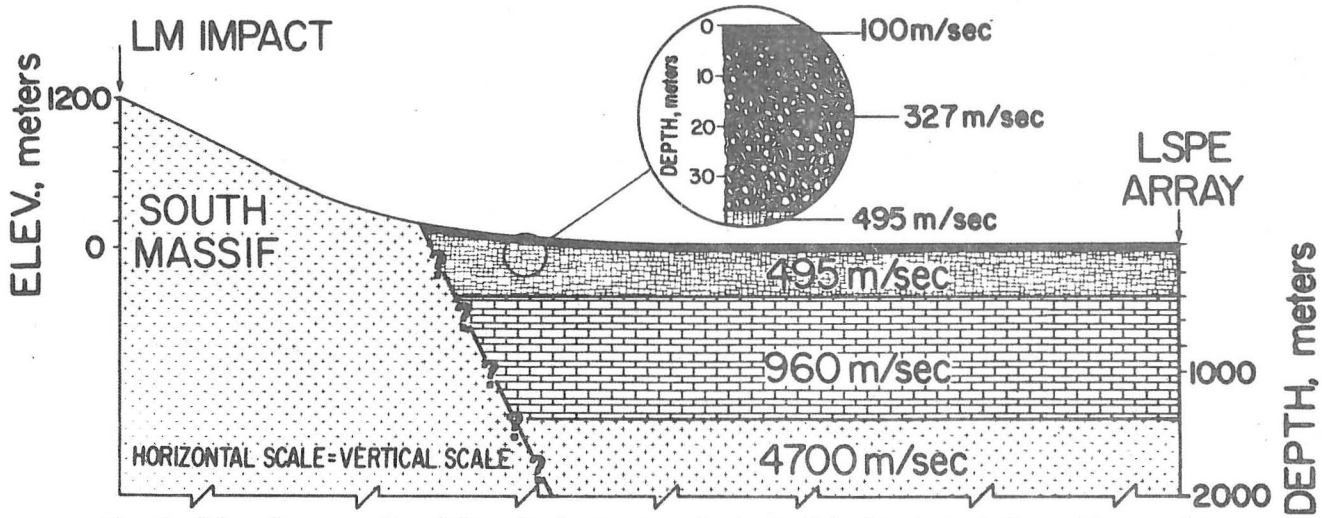

Fig. 15. Schematic cross section of the regional structure at the Apollo 17 landing site in the Taurus-Littrow valley.

some corrections to the data. The LM impacted on the lunar highlands 8.7 km from the array at an elevation 1.2 km higher. It is estimated that it takes 0.14 s to traverse this additional distance [*Kovach and Watkins,* 1973*b*]. In addition, the seismic signal from EP 1 is almost certainly delayed when it passes through or beneath the rubble underlying the crater Camelot. This delay has been estimated at 0.3 s.

The topmost 4 m, with the very low velocity of 100 m/s, is taken to be the lunar regolith. Beneath this to a depth of 32 m is another slow (327-m/s) layer. This low-velocity material is probably indicative of rubble and broken rock, perhaps partially consolidated by later impacts. At a depth of 32 m the velocity rises to 495 m/s. This is interpreted to be the fractured or vesicular top of the basalt layers that are assumed to fill the Taurus-Littrow valley. This interpretation is in agreement with the geologic observations that basalt boulders are excavated from craters reaching to a depth of 20 m or more below the valley floor [*Muehlberger et al.,* 1973]. At a depth of 390 m below the surface the velocity increases to 960 m/s. An increase in velocity is to be expected beneath the surface of lunar basalts, since the surface velocity will be very low owing to the intense fracturing induced by numerous meteorite impacts. The deepest and fastest (4.7-km/s) layer revealed by the seismic data is at a depth of 1.4 km. Such a large jump in velocity is more indicative of a compositional change than a change of physical properties alone. This high-velocity material is believed to be the anorthositic breccia of the highlands, probably very similar to the samples collected from the massifs surrounding the site.

Regolith thickness determined by seismic methods may differ from measurements based on crater morphology, boulder distribution, etc., since these techniques measure different properties of the lunar surface material. The 4 m of 100-m/s material is very unconsolidated and may correspond to only younger regolith (above the central cluster ejecta) [*Muehlberger et al.,* 1973]. The 327-m/s layer could then be older regolith, extremely fractured bedrock, or a mixture of both. The 4-m thickness may apply only to the LM region, which is on top of the relatively young central cluster ejecta. An alternate, less detailed regional-model omits the 327-m/s layer and has 7–12 m of 80- to 120-m/s material above the 494-m/s layer.

A velocity of 4.7 km/s is in very good agreement with the *P* wave velocities of small breccia samples measured in laboratories. This agreement can be seen in Figure 16, where the density of various terrestrial and lunar breccia samples is plotted against *P* wave velocity. The in situ lunar measurements of the velocity of the inferred basaltic layer, however, are significantly lower than the laboratory measurements of lunar basalt samples. Figure 17 shows velocity-density data for basalts. This discrepancy may be explained by noting that terrestrial field measurements of basalt velocities also are markedly lower than laboratory-measured velocities. The large-scale fracturing and jointing and thick vesicular layers, major factors in lowering in situ seismic velocities, would not be present in small laboratory samples, very likely chosen for their coherence. This same mechanism does not affect the lunar breccia because the higher pressures to which it is subjected (at a depth of 1.4 km) probably inhibit larger-scale fracturing and jointing [*Johnson,* 1970].

In addition to the first arrivals discussed above there appear to be arrivals that never appear first at any distance from the array (Figure 13), specifically the arrivals with apparent

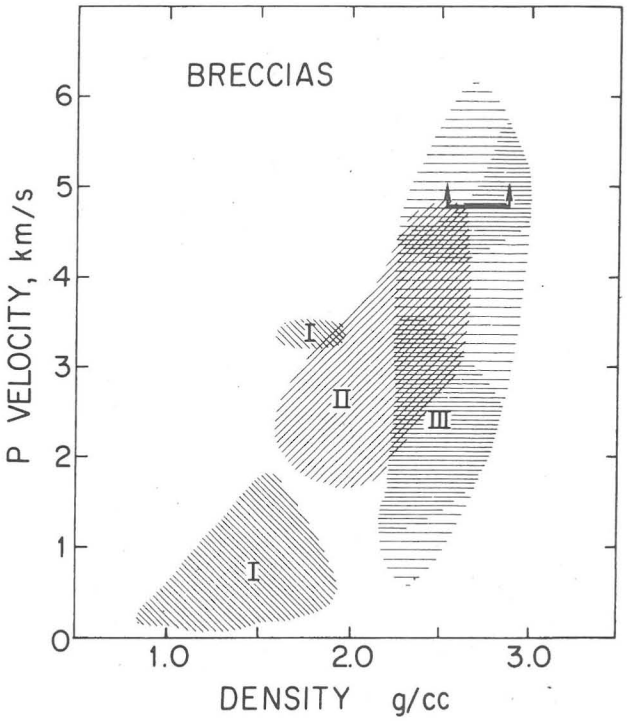

Fig. 16. Plot of density versus *P*-wave velocity for terrestrial and lunar breccias. Data include both laboratory and in situ measurements. The horizontal line with arrows indicates the velocity and density postulated for the highland breccia presumed to underlie the Taurus-Littrow valley. The shaded area I represents field measurements on tuffs, impact breccias, and volcanic ashes. Shaded area II represents laboratory measurements on terrestrial impact breccias. Shaded area III represents laboratory measurements on lunar breccias, shown lighter where they are uncertain. Data are compiled from *Anderson et al.* [1970], *Chung* [1973], *Clark* [1966], *Kanamori et al.* [1970, 1971], *Mizutani et al.* [1972], *Mizutani and Newbigging* [1973], *Tittman et al.* [1972], *Todd* [1973], *Todd et al.* [1972], *Wang et al.* [1971], *Warren et al.* [1971, 1972], *Watkins et al.* [1965], and *Watkins* [1966*a*, *b*].

velocities of 80 m/s and 180 m/s. The 180-m/s signal can be explained as a shear (*S*) wave traveling on the highly fractured basalt below 32 m. The 80-m/s arrival does not correspond to an *S* wave in the surface layer or to multiple reflections of either *P* or *S* waves in any of the shallow layers; it may represent surface waves in the upper layers.

Internal consistency of all data with the proposed model should be one of the first tests. But in the two interpretations offered on the Apollo 17 data a paradox appears. The regional profile, incorporating data from all the seismic sources, implies a fairly low velocity (327 m/s) to a depth of 34 m, where the velocity increases to roughly 500 m/s. This layer appears to extend to 390-m depth. But in the end-to-end profile with the utilization of only EP 2, 3, 4, and 8 and the LM ascent as seismic sources, the 327-m/s layer continues to 65 m, where the velocity increases to something distinctly greater than 500 m/s. (The data do not accurately define this velocity. It is taken as 750 m/s in Figure 12.) No data are available for greater depths. The data do not preclude the existence of a thin 495-m/s layer, but why has the higher-speed layer disappeared in the regional velocity model?

On the assumption that the limited data of Figure 12 do indicate an arrival with a velocity of about 750 m/s, the absence of this arrival in the regional model may be explained by two possibilities. First, terrestrial basalt flows are quite commonly

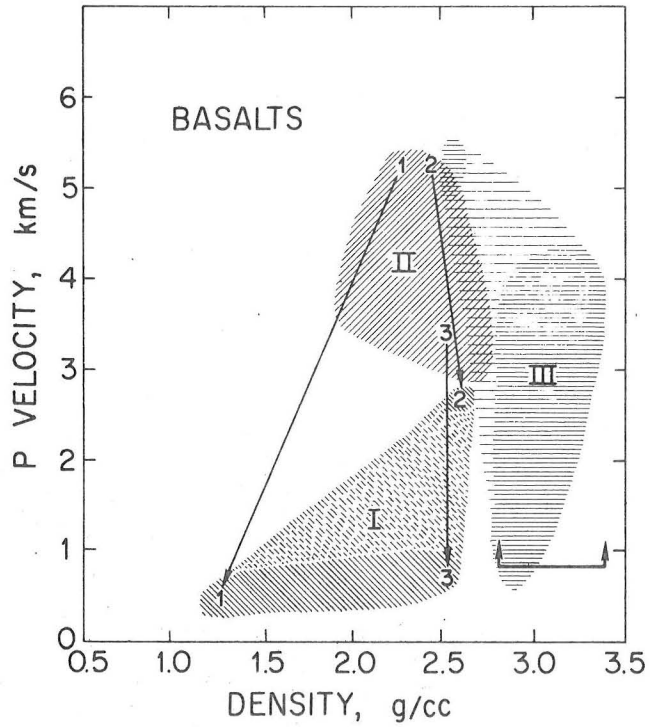

Fig. 17. Plot of density versus *P* wave velocity for terrestrial and lunar basalts. Shaded area I represents field measurements on terrestrial basalts, shown lighter where they are uncertain. Shaded area II represents laboratory measurements on terrestrial basalts. Shaded area III represents laboratory measurements on lunar basalts, shown lighter where they are uncertain. The numbers refer to laboratory and field measurements on the same basalt unit: number 1 is S-P basalt, number 2 is Amboy basalt, and number 3 is Kana-a basalt. The arrows labeled 1–3 represent laboratory and in situ measurements on the same basalt unit emphasizing the importance of in situ fractures and cracks in larger-scale experiments. The horizontal line with arrows indicates the velocity and density postulated for the basalts filling the Taurus-Littrow valley. Data are compiled from same sources given in caption to Figure 16.

thinly layered, and thinly layered units have been observed at the Apollo 15 landing site [*Swann et al.*, 1972]. The resulting 'thin layer' effect [*Watkins and Kovach*, 1973] causes the energy traveling as a head wave in any thin strata to gradually 'leak' out the bottom of the unit. Thus an easily detectable first arrival from a thin bed will at greater distances give way to later arrivals from deeper layers, even though the thin bed may still be present. This situation could account for the disappearance of the 750-m/s arrival (observed to 420 m) at distances of 800 m (EP 7), 1200 m (EP 6), and 2300 m (EP 5). Alternately, of course, the higher-speed layer may not extend to the shot points of EP 5, 6, or 7. Such discontinuities could be caused by either original flow characteristics or subsequent impact brecciation. As the energy passes downward out of this thin layer of basalt, it will encounter various flow boundaries, vesicular layers, massive jointing, and perhaps breccia lenses. All of these will tend to decrease the average velocity. As was mentioned earlier, the observed average velocity, 495 m/s, is not unreasonable for in situ velocity measurements on basalts (Figure 17).

Second, the higher velocity tends to disappear in the regional model because arrivals from different depths are being averaged. If the first arrivals from EP 2, 3, 4, and 8 and the LM ascent (Figure 12) were plotted together, a single 750-m/s line would not fit as well as a line representing a lower velocity with a smaller intercept time. Thus the 750-m/s arrival is absent at great distances owing to the 'thin layer' effect (or discontinuity of the layer) and is hidden in the regional travel time curve because of the averaging effects of the eastward dip.

DISCUSSION

Stratigraphy. Velocity models of near crustal structure are now available at three widely spaced locations on the lunar surface. Can any generalizations be made about lunar structure from this limited set of data?

At each site the shallowest layer had a velocity between 100 and 114 m/s. At the Apollo 14 site this layer was 8.5 m thick; at the Apollo 16 site it had a thickness of 12.2 m. Only 4 m of this material was found at the Apollo 17 site. From the low velocity it was expected that this material would correspond to the lunar regolith. Earlier estimates of regolith thickness based on crater density had postulated a relatively thin regolith at the Apollo 17 site [*Muehlberger et al.*, 1972]. Drill cores at the Apollo 17 site encountered more resistant material at a depth of 2–3 m [*Muehlberger et al.*, 1973]. It would thus appear that the loose and powdery lunar regolith has a characteristic *P* velocity very close to 100–110 m/s but has varying thickness over the lunar surface. The process of fragmentation by meteoroid impacts has produced a moonwide surface layer of very similar acoustic properties.

Underlying the regolith at the Apollo 14 site was material with a 299-m/s velocity, presumed to be the Fra Mauro formation. Its thickness is not well determined but must lie between 17 and 88 m. At the Apollo 16 site at least 70 m of 250-m/s material underlies the regolith, and it may be as thick as 220 m. This is the material that is thought to represent the Cayley formation. Both the Cayley formation and the Fra Mauro formation are impact-derived breccias thought to be generated by the Imbrium impact. At least 30 m, and perhaps as much as 62 m, of 327-m/s material underlies the regolith at the Apollo 17 site. High-velocity material, presumed to be basalt, is first detected 65 m below the geophone array. Between 32 and 65 m the velocity structure is uncertain. It is likely that 327-m/s material that grades into faster material with depth is present. Samples of breccia have been found near the Van Serg crater in the Taurus-Littrow valley, which is thought to overlie the basalt in this region. In addition to the breccia, sources of large boulders of basalt must be present below 20–30 m, since basalt ejecta are commonly found around craters excavating to this depth.

All lunar landing sites show the presence of material with a velocity of 300 m/s (±50 m/s), poorly controlled estimates of thicknesses ranging between 17 and 220 m. The somewhat better controlled estimate at Taurus-Littrow, 30–60 m, fits well into the range of the other data. As was mentioned earlier, 300 m/s is similar to velocities observed in ejecta at Meteor crater, Arizona. At both Apollo 14 and Apollo 16 sites this material was identified with the breccia generated by large basin-forming impacts. It cannot be resolved if the similar material at the Apollo 17 site is derived from a similar larger impact, from brecciation due to more local smaller impacts, or from partial pulverization of bedrock basalt.

The breccia layer was the deepest unit seen at both the Apollo 14 and the Apollo 16 landing site. As was discussed above, the deeper layers filling the valley at the Apollo 17 site include a 495-m/s layer and a 960-m/s layer believed to represent fractured and relatively intact mare-type basalt, respectively.

Gravity. A traverse gravimeter obtained data about the relative changes in the moon's gravity at the Apollo 17 landing site. Such data provide additional constraints on the local structure.

Preliminary analysis of the data (G. Thompson, personal communication, 1974) indicates a dense valley fill with a Bouguer anomaly of 32 ± 5 mGal between the edge of the south massif and the center of the valley. The seismic refraction data indicate a sharp increase in velocity (to 4.7 km/s) at 1400-m depth. When the valley is modeled as slab 1400 m thick with sloping sides, a density contrast of 0.5–0.7 g/cm³ between the infill and the surrounding highlands and basement is required to explain the gravity anomaly. Are the materials, basalt and anorthositic breccia, that are postulated for the valley fill and its surroundings consistent with this constraint?

Figure 16 shows the *P* velocities and densities of various breccias, both lunar and terrestrial, measured both in the field and in the laboratory. The horizontal line indicates the velocity measured at the Apollo 17 site. A density of 2.5–2.9 g/cm³ would be expected with a 4.7-km/s breccia. Thus to meet the above constraint, the basalt would have to show a density between 3.0 and 3.5 g/cm³ at a velocity of 960 m/s. Basalt *P* velocities and densities, shown in Figure 17, indicate that a reasonable density for basalt showing such a low velocity would be 3.2 g/cm³. Near-surface field measurements of seismic velocity yield much lower velocities than laboratory measurements on comparable samples. The heavy black lines connecting the numerals 1, 2, and 3 show typical differences between laboratory and field measurements. With the corroboration by the gravity data, basalt and anorthositic breccia remain the most likely candidates to compose the structure in the Taurus-Littrow valley.

Compacted powders. The standard methods of seismic interpretation, as described above, assume the propagation medium to be composed of distinct layers, each with a unique velocity. The velocity models derived in this way are shown in heavy lines in Figures 18 and 19. These were derived from the travel time data given in Figures 13 and 14, respectively. Within each layer, velocity may increase slightly with depth without violating the assumptions behind the interpretation, but the first arrivals observed on the surface must have traveled as head waves, waves critically refracted along the top of each layer. Thus each layer generates one straight line segment in the travel time curve (Figures 13 and 14).

If the *P* wave velocity in the medium does not increase in a stepwise fashion with depth, i.e., if $V(z) = az^b$, where z is depth, the travel time data will plot as a smooth continuous curve. Such a velocity function might be expected in any material whose composition or physical properties gradually change with depth.

Motivated by the long duration of the seismic signals observed after impacts, various authors [*Gold and Soter,* 1970; *Gangi,* 1972] have suggested that the topmost layers of the moon consist of compacted powders. Can the lunar seismic data be represented satisfactorily by smooth functions, and are the implied velocity-depth relationships consistent with our knowledge of compacted powders? To investigate these questions, Apollo 17 data will be used, since a deeper velocity structure is available here than at the other sites.

The data points in Figures 13 and 14 certainly by themselves do not preclude the possibility of a smooth functional relationship describing the travel time observations. Power laws of the form $V(z) = az^b$ have been used to describe the velocity-depth relationship in powders [*Gangi,* 1972]. The values taken for b are 1/4 and 1/6. *Gold and Soter* [1970] used a linear velocity-depth model.

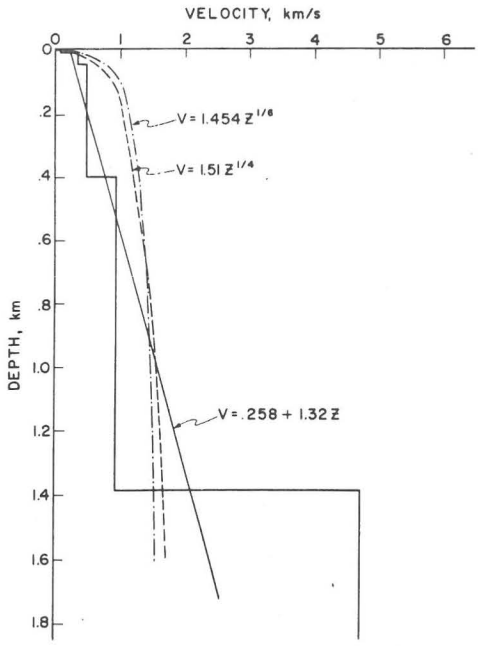

Fig. 18. Plot of velocity as a function of depth at the Apollo 17 site. Heavy solid line shows the layered velocity model. The thin solid line and dashed lines show best-fitting linear and power law velocity models. Note that linear and power law models cannot account for the 4.7-km/s velocity.

In Figures 13 and 14 the travel time curves that would result from these velocity-depth functions are plotted. They are 'best fits' in the sense that they are least squares fits to evenly spaced samples along the standard segmented travel time curve. This precaution was taken to avoid biasing our results by the concentration of data obtained within 400 m of the array.

The velocity functions determined by the travel time data are shown in Figures 18 and 19 for comparison with the standard refraction velocity model.

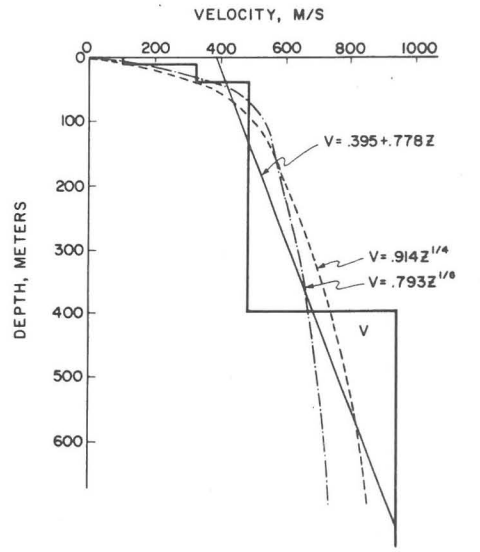

Fig. 19. Plot of velocity as a function of depth at the Apollo 17 site excluding the LM impact data point. Heavy solid line shows the layered velocity model. The thin solid line and dashed lines show best-fitting linear and power law models.

Figure 13, showing all the seismic data out to a distance of 8.7 km and hence reflecting velocities to a depth of 1.4 km, indicates that a power law model ($b = 1/4$; very little difference was observed for $b = 1/6$) gives a very poor fit to the data. Better agreement can be obtained by a linear velocity model $V(z) = 0.258 + 1.32z$. This is very close to the model $V(z) = 0.150 + 1.35z$ taken by Gold and Soter. However, this linear velocity gradient model is unable to account for the sharp velocity increase that causes the small difference in travel time between the LM impact and EP 1. This model predicts that the signal for EP 1 should arrive 0.4 s before it actually does.

Travel time data from only the explosive charges (excluding the LM impact) are shown in Figure 14. Various power law velocity models can be made to fit the observed data, and a particularly good agreement can be obtained with a linear velocity gradient model. (This situation is not too surprising, since the linear model has two adjustable parameters.) However, the linear velocity model has a velocity-depth gradient of 1.32 km/s/km. Data on compacted lunar and terrestrial rock powders [*Warren et al.* 1971; *Talwani et al.*, 1973] have indicated that such high gradients are possible but only at very shallow pressures. Simple cold compaction of a fine-grained rock powder might be important in the upper tens of meters of the lunar near surface, but the seismic data preclude thicknesses of the order of kilometers.

CONCLUSIONS

Seismic velocities of 104, 108, 92, 114, and 100 m/s were measured for the lunar regolith at the Apollo 12, 14, 15, 16, and 17 landing sites, respectively [*Kovach and Watkins*, 1973*a*, *b*; *Watkins and Kovach*, 1973]. These seismic data indicate that the process of fragmentation and comminution by meteoroid impacts has produced a layer of remarkably uniform seismic properties moonwide. Brecciation and high porosity are believed to be the major causes of the extremely low velocities observed in the lunar regolith [*Watkins and Kovach*, 1973].

The Apollo 17 seismic data have revealed that the seismic velocity increases very rapidly with depth in the near-lunar surface, at least at this particular site. Velocities of 100 m/s are observed at the surface increasing to 4.7 km/s at a depth of 1.4 km. These data are not compatible with the premise that a rock powder layer extends to a depth of 1 km or so in the moon. The observed magnitude of the velocity change and the implied steep velocity-depth gradient of >2 km/s/km are much larger than have been observed on compaction experiments on granular materials [*Talwani et al.*, 1973]. Such a large velocity change is indicative of compositional and textural changes and in view of the geologic observations at the Apollo 17 site is compatible with the proposed model of basaltic flows (fractured near the surface) overlying the presumably anorthositic breccias that form the lunar highlands.

Acknowledgments. We thank Brian Dent for compiling much of the velocity-density data and Don C. Riley and John Burg for providing the prediction error filter used in enhancing the Apollo 17 seismic data. This research was supported by the National Aeronautics and Space Administration under contract NAS9-5632 and grant NGL 05-020-232.

REFERENCES

Anderson, O. L., C. Scholz, N. Soga, N. Warren, and E. Schreiber, Elastic properties of a micro-breccia, igneous rock, and lunar fines from Apollo 11 mission, *Proc. Lunar Sci. Conf. 1st*, 1959, 1970.

Chung, D. H., Elastic wave velocities in anorthosite and anorthositic gabbros from Apollo 15 and 16 landing sites, *Proc. Lunar Sci. Conf. 4th*, 2591, 1973.

Clark, S. P. (Ed.), *Handbook of Physical Constants, Geol. Soc. Amer. Mem. 97*, 195–218, 1966.

Ewing, M., G. Woollard, and A. Vine, Geophysical investigations in the emerged and submerged Atlantic coastal plain, 3, Barnegat Bay, New Jersey, section, *Geol. Soc. Amer. Bull., 50*, 257–296, 1939.

Gangi, A. F., The lunar seismogram, *Moon, 4*, 40–48, 1972.

Gold, T., and S. Soter, Apollo 12 seismic signal: Indication of a deep layer of powder, *Science, 169*, 1071–1075, 1970.

Hodges, C. A., W. R. Muehlberger, and G. E. Ulrich, Geologic setting of Apollo 16, *Proc. Lunar Sci. Conf. 4th*, 1, 1973.

Johnson, A. M., *Physical Processes in Geology*, pp. 356–399, Freeman, Cooper, San Francisco, Calif. 1970.

Kanamori, H., A. Nur, D. H. Chung, and G. Simmons, Elastic wave velocity of lunar samples at high pressures and their geophysical implications, *Proc. Lunar Sci. Conf. 1st*, 2289, 1970.

Kanamori, H., H. Mizutani, and Y. Hamano, Elastic wave velocities of Apollo 12 rocks at high pressures, *Proc. Lunar Sci. Conf. 2nd*, 2323, 1971.

Kovach, R. L., J. S. Watkins, and T. Landers, Active seismic experiment, Apollo 14 Preliminary Science Report, *NASA SP-272*, sect. 7, 1971.

Kovach, R. L., J. S. Watkins, and P. Talwani, Active seismic experiment, Apollo 16 Preliminary Science Report, *NASA SP-315*, sect. 10, 1972.

Kovach, R. L., and J. S. Watkins, The velocity structure of the lunar crust, *Moon, 7*, 63–75, 1973*a*.

Kovach, R. L., and J. S. Watkins, The structure of the lunar crust at the Apollo 17 site, *Proc. Lunar Sci. Conf. 4th*, 2549, 1973*b*.

McAllister, B. D., J. Kerr, J. Zimmer, R. L. Kovach, and J. S. Watkins, A seismic refraction system for lunar use, *IEEE Trans. Geosci. Electron., GE-7*, 164–171, 1969.

Mizutani, H., N. Fujii, V. Hamano, and M. Osako, Elastic wave velocities and thermal diffusivities of Apollo 14 rocks, *Proc. Lunar Sci. Conf. 3rd*, 2557, 1972.

Mizutani, H., and D. F. Newbigging, Elastic-wave velocities of Apollo 14, 15, and 16 rocks, *Proc. Lunar Sci. Conf. 4th*, 2601, 1973.

Muehlberger, W. R., et al., Preliminary report on the geology and field petrology at the Apollo 17 landing site, Interagency Report: Astrogeology 69, U.S. Geol. Surv., Reston, Va., 1972.

Muehlberger, W. R., et al., Preliminary geologic analysis of the Apollo 17 site, Interagency Report: Astrogeology 72, U.S. Geol. Surv., Reston, Va., 1973.

Oberbeck, V. R., Implications of regolith thickness in Apollo 16 landing site, *NASA TM X-62089*, 1971.

Offield, T. W., Geological map of the Fra Mauro site—Apollo 13, scale 1:5000, U.S. Geol. Surv., Reston, Va., 1970.

Sutton, R. L., M. H. Hait, and G. A. Swann, Geology of the Apollo-14 landing site, *Proc. Lunar Sci. Conf. 3rd*, 27, 1972.

Swann, G. A., et al., Preliminary geologic investigation of the Apollo 15 landing site, Apollo 15 Preliminary Science Report, *NASA SP-289*, chap. 5, p. 112, 1972.

Talwani, P., A. Nur, and R. L. Kovach, Compressional and shear wave velocities in granular materials to 2.5 kilobars, *J. Geophys. Res., 78*, 6899–6909, 1973.

Tittman, B. R., R. M. Housley, E. H. Cirlin, and M. Abdel-Gawad, Rayleigh wave studies of two Apollo 15 rocks, in *Apollo 15 Lunar Samples*, p. 244, Lunar Science Institute, Houston, Tex., 1972.

Todd, T., H. Wang, W. S. Baldrige, and G. Simmons, Elastic properties of Apollo 14 and 15 rocks, *Proc. Lunar Sci. Conf. 3rd*, 2577, 1972.

Todd, T., Unique characterization of lunar samples by physical properties, *Proc. Lunar Sci. Conf. 4th*, 2639, 1973.

Wang, H., T. Todd, D. Weidner, and G. Simmons, Elastic properties of Apollo 12 rocks, *Proc. Lunar Sci. Conf. 2nd*, 2327, 1971.

Warren, N., E. Schreiber, C. Scholz, J. A. Morrison, P. R. Norton, M. Kumazawa, and O. L. Anderson, Elastic and thermal properties of Apollo 11 and Apollo 12 rocks, *Proc. Lunar Sci. Conf. 2nd*, 2345, 1971.

Warren, N., O. L. Anderson, and N. Soga, Applications to lunar geophysical models of the velocity-density properties of lunar rocks, glasses, and artificial lunar glasses, *Proc. Lunar Sci. Conf. 3rd*, 2587, 1972.

Watkins, J. S., J. C. DeBremaecker, R. A. Loney, J. H. Whitcomb, and R. H. Godson, Investigation of in situ physical properties of surface and subsurface site materials by engineering geophysical

techniques, *Annu. Rep. FY 1965,* NASA contract T-25091(G), 1965.
Watkins, J. S., Investigation of in situ physical properties of surface and subsurface site materials by engineering geophysical techniques, *Quart. Rep. Oct.–Dec., 1965,* NASA contract T-25091(G), 1966*a*.
Watkins, J. S., Investigation of in situ physical properties of surface and subsurface site materials by engineering geophysical techniques, *Annu. Rep. FY 1966,* NASA contract T-25091(G), 1966*b*.
Watkins, J. S., and R. L. Kovach, Seismic investigation of the lunar regolith, *Proc. Lunar Sci. Conf. 4th,* 2561, 1973.

(Received March 22, 1974;
accepted April 19, 1974.)

Proc. Lunar Sci. Conf. 6th (1975), p. 2863–2879.
Printed in the United States of America

Energy, frequency, and distance of moonquakes at the Apollo 17 site

MICHAEL R. COOPER and ROBERT L. KOVACH

Department of Geophysics, Stanford University, Stanford, California 94305

Abstract—"Thermal" moonquakes have been detected at the Apollo 17 site. A typical event releases about 10^6–10^7 ergs of energy. The annual seismic energy release for the events observed in the Taurus-Littrow Valley is estimated at 10^{11} ergs. Such small events would not cause impossibly rapid erosion on either the North Massif or within the craters of the Central Cluster. Seismic events become increasingly frequent after sunrise and reach a maximum at sunset. The largest events, however, occur most commonly near lunar noon. Rise times of the seismic signals, after being calibrated by the well-located Lunar Seismic Profiling Experiment (LSPE) seismic sources, were used to estimate distances to the seismic events. Most seismic events (~90%) appear to occur within 2.5 km of the seismometer array.

INTRODUCTION

SHORT-PERIOD SEISMIC INSTRUMENTS were successfully deployed on Apollos 14, 15, 16, and 17. The short-period seismic signals detected on the first three missions have been analyzed by Duennebier and Sutton (1974a). Seismic activity at these three stations showed generally similar characteristics; activity was concentrated in daylight hours, natural events were observed to recur identically at about the same time each lunar day, and the events were all very small (by terrestrial standards). These characteristics led to the suggestion that the most likely source mechanism for these moonquakes was downslope movement of material.

The similarity of the observations on Apollos 14, 15, and 16 suggested that seismicity at the Apollo 17 landing site would not be markedly different. At the Apollo 17 landing site four geophones are arranged in a T-shaped array. Characteristics of the seismic instrumentation are given in Kovach *et al.* (1973). These devices were part of the Lunar Seismic Profiling Experiment (LSPE), which involved the detonation of eight explosives to investigate the structure of the Taurus-Littrow Valley (Cooper *et al.*, 1974). In the ensuing months, the experiment was activated periodically in a listening mode to detect seismic signals. In this paper we discuss the seismicity at the Apollo 17 site and its differences with seismicity at other sites. The explosive packages of the LSPE serve as controlled sources at known locations and origin times. The amplitudes of these records enable us to estimate the energies of moonquakes. The envelope of the explosion seismograms was found to vary systematically with source distance, in agreement with scattering theory. One aspect of the envelope, the rise time, increases with source distance and, following calibration by the explosion packages, may be used to estimate the distance to natural seismic sources.

ENERGY OF MOONQUAKES

To estimate the source energy of seismic events, the relationship between source energy and ground displacement (or some other observed quantity) must be determined. The most direct method is to compare the observed maximum ground displacements with the known source energies of the LSPE artificial sources (Dunnebier and Sutton, 1974a; Criswell and Lindsay, 1974). Figure 1 shows the overall system sensitivity to ground motion for the Apollo 17 seismic system.

We use the empirical relation:

$$A = \frac{k \cdot E^{1/2}}{r} \tag{1}$$

where A is the maximum peak-to-peak amplitude (nm), r is the source distance (km), and E is the source energy (ergs). k is the coupling factor to be determined, and is proportional to the square root of seismic efficiency. The coupling coefficient has been determined for total amplitudes and for amplitudes at specific frequencies. Power density at particular frequencies and times was determined by maximum entropy spectral analysis (J. P. Burg, personal communication, 1974; Ulrych, 1972; Ulrych *et al.*, 1973). Amplitude of ground motion was then

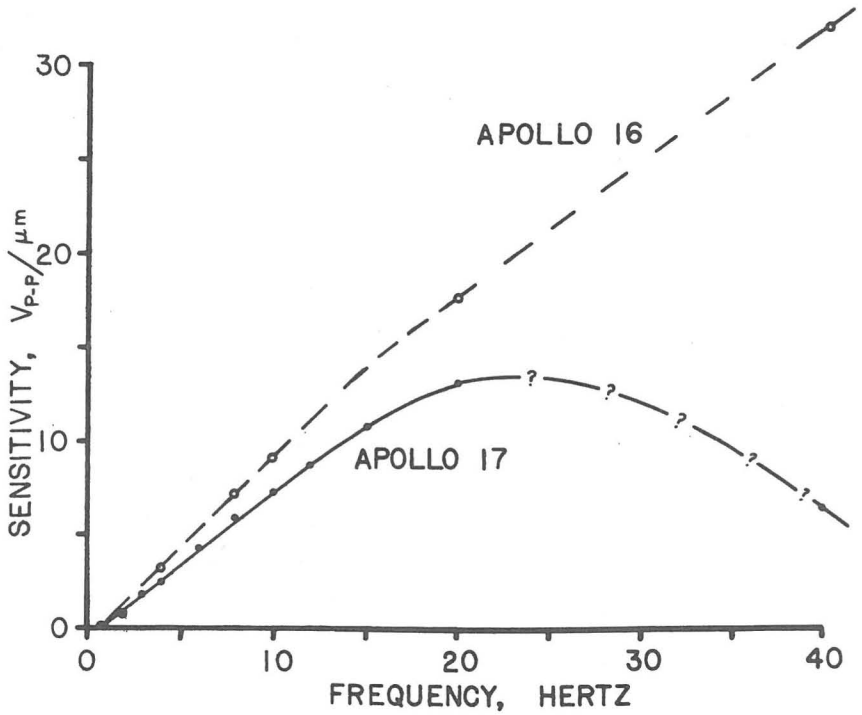

Fig. 1. Sensitivity of Apollo 16 and 17 seismic instrumentation to ground displacement (zero-to-peak). The values were computed from shake table tests on the seismic system.

computed at intervals of 0.47 Hz between 3 and 20 Hz, after correcting for instrument response. Total ground displacement was estimated by

$$U_{\mathrm{TOT}} = \left(\sum_{f=3}^{20} [U(f)]^2\right)^{1/2} = \sqrt{2}\, U_{\mathrm{RMS}} \tag{2}$$

The maximum amplitudes (zero-peak) determined in this way are listed in Table 1. Also included are the energies of the LSPE artificial sources and the distances from these sources to each of the four geophones.

The coupling factor has been computed from Eq. (1) and values averaged for each source are plotted in Fig. 2. The k computed from the maximum U_{TOT} (labeled "RMS," in Fig. 2) maintains a reasonably constant value as distance increases. But at any individual frequency, corresponding to measurements on band-pass-filtered seismograms, the coupling factor changes markedly between the near and the distant sources. This is due to changes in the spectral characteristics of the seismograms of more distant sources. For nearby sources, the dominant frequency component is 7 Hz with a strong second peak at 10–11 Hz. As source distances increased, the peak frequencies decreased, the second peak became weaker and eventually disappeared at distances beyond

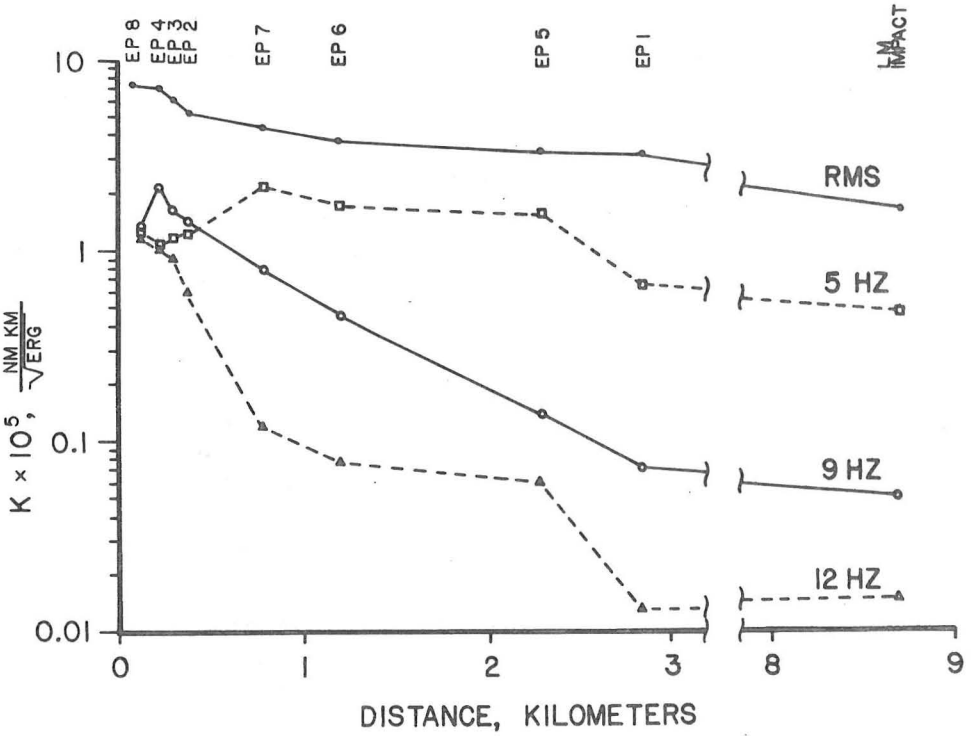

Fig. 2. Comparison of coupling coefficients of the LSPE seismic sources at distances from 128 m to 8.7 km. Coupling coefficients were determined for $\sqrt{2} \cdot$ RMS ground displacement (labeled "RMS"), and for displacement components at 5, 9, and 12 Hz.

Table 1.

EP #	Geophone no.	Dist. (m)	Mass expl., g (energy, ergs)	$o-p$ Max. displacement, nanometers			
				U_{TOT}	5 Hz	9 Hz	12 Hz
8	1	179	113	508	105	86	74
	2	101	(4.25×10^{12})	854	95	132	142
	3	122		543	110	143	78
	4	112		559	82	121	101
4	1	269	57	179	28	47	17
	2	172	(2.1×10^{12})	290	43	95	33
	3	215		noise	noise	56	44
	4	220		187	42	34	40
3	1	242	57	206	30	45	29
	2	341	(2.1×10^{12})	102	16	31	16
	3	288		173	23	54	28
	4	287		165	26	44	21
2	1	327	113	171	31	42	16
	2	425	(4.25×10^{12})	120	50	27	14
	3	371		168	30	44	19
	4	366		139	26	42	19
7	1	800	227	108	44	15	3
	2	865	(8.5×10^{12})	76	34	12	2
	3	810		88	36	14	2
	4	672		74	34	14	3
6	1	1195	454	74	31	8	1
	2	1240	(19×10^{12})	67	23	9	1
	3	1195		84	42	10	2
	4	1095		68	40	8	2
5	1	2230	1361	51	35	2	1
	2	2330	(57×10^{12})	72	13	2	<1
	3	2290		62	34	3	1
	4	2320		52	29	2	1
1	1	2855	2722	71	10	1.5	0.2
	2	2758	(110×10^{12})	60	10	1.0	0.1
	3	2818		75	16	1.5	0.4
	4	2870		57	16	1.5	0.2
LM impact	1	8700		212	50	5	1.3
	2	8700	(3.15×10^{16})	161	64	6	1.6
	3	8700		199	60	6	1.5
	4	8700		159	38	6	1.5
Background noise					<0.4	<0.2	<0.1

1.2 km. A spectrogram computed on the seismogram of the lunar module (LM) impact has a single, relatively narrow peak at 4 Hz. This change in character is influenced by at least two factors: more rapid attenuation of the higher frequencies and different source characteristics as explosion sizes were increased to

compensate for greater source distances. It can be seen from Fig. 2 that any estimate of moonquake source energy must use either total power or some low frequency that is excited uniformly for all sources. The use of any higher frequency would require information about both source distance (to choose the appropriate value of the coupling factor) and the moonquake source mechanism. Since the source spectrum of moonquakes is unknown, the coupling coefficient for total power will be used for all moonquake energy estimates.

It is generally assumed that moonquakes are more efficient than surface explosions, since it is unlikely that moonquakes excavate craters or toss up much regolith. Following Duennebier and Sutton (1974a) we allow k_{mq} to be 32–100 times larger to compensate for this difference. This corresponds to moonquakes being 10^3–10^4 times more efficient. Choosing 3×10^{-5} nm km erg$^{-1/2}$ as a representative k_{ep}, we can determine k_{mq} to be in the range 9.6×10^{-4} to 30×10^{-4}. Typical moonquake amplitudes are about 1 nm (peak-to-peak). Assuming a typical source distance to be 2 km, an average moonquake releases 0.4–4.3×10^6 ergs. If the events are as distant as 5 km, the source energy is 0.3–2.7×10^7 ergs. Purely for purposes of comparison, assume the empirical relationship between source energy and magnitude (Richter, 1958):

$$\log E = 11.4 + 1.5 M_L$$

the "magnitude" of a large moonquake would be -2.0 to -2.6. Similar assumptions about the relationships between magnitude, seismic moment and fault length (Wyss and Brune, 1968), imply a fault area of about 10 m^2 and 6-cm slip for a large event. We do not necessarily expect these empirical, terrestrial relationships to be valid for lunar seismic events; we merely want to illustrate that these short-period moonquakes are very small compared to earthquakes. The annual release of seismic energy detected at the Apollo 17 site may be crudely estimated at about 10^{11} ergs, based on the number of "average moonquakes." Duennebier and Sutton (1974a) suggested that these moonquakes were possibly the result of gravitational slumping on lunar slopes. Erosion rates may be calculated from these seismic energies, if it is assumed that all the energy released originated as gravitational potential energy. Using a simple geometrical model of a planar slope, a 1° change in slope in a small (150 m deep) crater could occur over as short a time as 4 m.y. (Duennebier and Sutton, 1974a). Our estimates of energy release imply that such slope degradation would occur over 750 m.y.

Both estimates are based on 100 "typical" events within the crater; the energy of a "typical" moonquake (1-nm peak-to-peak, 2 km away), based on our k_{mq} was taken to be 4×10^5 ergs. Duennebier and Sutton (1974a) using a much smaller k_{mq} of about 7×10^{-7} nm km erg$^{-1/2}$, employed a typical moonquake of 7×10^7 ergs. Their k_{ep} was derived from near-source Apollo 16 grenade and thumper data filtered around 5 Hz; a comparison of their data (Duennebier and Sutton, 1974b) with the values in Table 1 (e.g. EP 2, geophone 2; EP 4, geophone 2) suggest that they may have been given incorrect maximum displacement values. If their displacement values are correct, the 5-Hz seismic efficiency of the thumper and grenade shots at the Apollo 16 site would have to be at least 200 times smaller than

the efficiency at the Apollo 17 site, even though the material properties at the two sites seemed to be generally similar (Cooper *et al.*, 1974). Criswell and Lindsay (1974) looked at lunar surface exposure ages and concluded that the earlier computed erosion rates were impossibly high. Their suggested mechanism, booming sand dunes, had such small source energies due to their high efficiencies (1–5%) that they would induce only very slight erosion. Our results show that gravitational slumping can account for the moonquakes without requiring massive erosion of all lunar slopes. Landslides, with our energy estimates, would cause a given amount of erosion in 20–80% of the time suggested for booming sand dunes.

SEISMICITY

Following the detonation of the LSPE explosions, the seismic array was activated for numerous short (usually 30 min) listening periods. Since the short-period seismicity on earlier Apollo missions showed very similar properties over numerous lunations, it was decided to accumulate data that would cover the moon's orbit by eight short (4 earth-day) listening modes during various lunations. The times of the seven completed listening modes are given in Table 2, and the

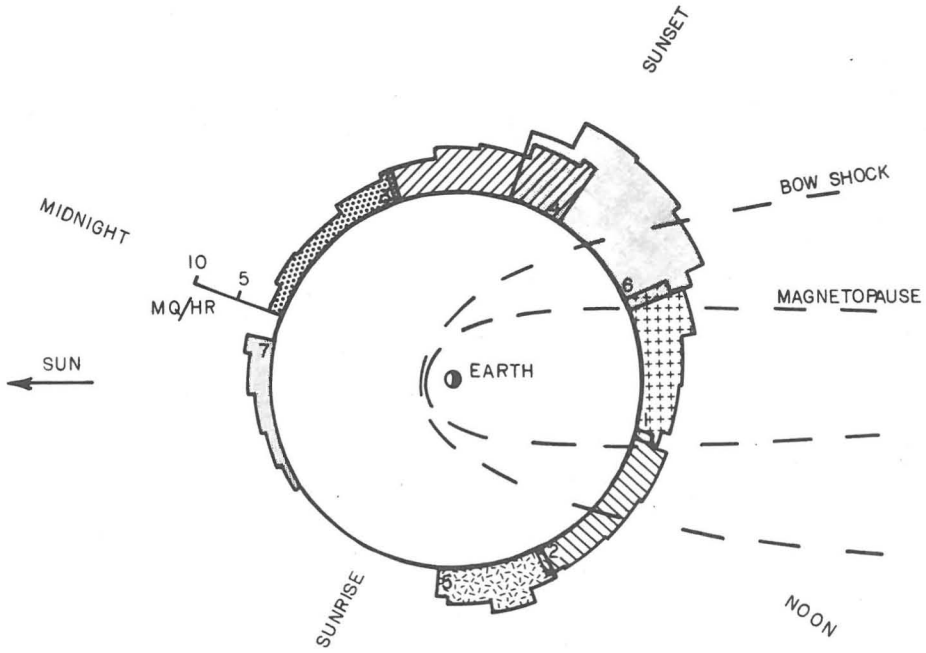

Fig. 3. Earth–moon diagram showing position of moon during each of the seven Apollo 17 listening modes. Small numbers in hatchured blocks represent the chronological order of listening periods (Table 2). The moon's position at sunrise, noon, etc. at Taurus-Littrow is indicated. Histograms outside of moon's orbit show average number of seismic events (≥4 mm on compressed seismogram, ~ ≥0.2-nm zero-to-peak ground displacement) per hour.

Table 2. Apollo 17 LSPE listening modes.

No.	Date	No. events	Cutoff amp. (mm)
1	July 13–17, 1973 (194–198)	121	8 mm
2	March 3–6, 1974 (62–65)	114	8 mm
3	August 12–16, 1974 (224–228)	261	3 mm
4	September 6–10, 1974 (249–253)	234	7 mm
5	October 22–25, 1974 (295–298)	106	7 mm
6	November 1–5, 1974 (305–309)	365	7 mm
7	December 12–16, 1974 (346–350)	54	7 mm

position of the moon relative to the earth–sun line during these modes is shown in Fig. 3.

Compressed seismograms (Fig. 4) of all the listening periods were obtained. These were used for all subsequent measurements on the moonquakes.

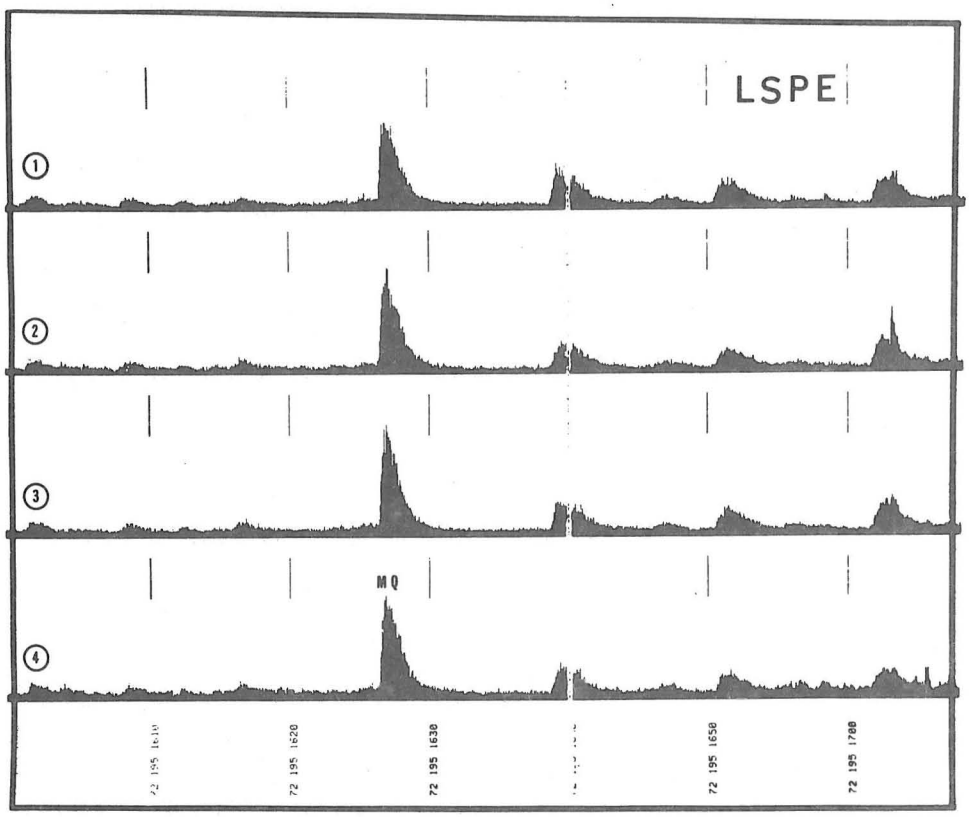

Fig. 4. Compressed seismogram from July 1973 listening period (Day 195: 1600–1708 hr). Time between the short vertical lines is 10 min. Geophones are numbered at the left. The largest event (labeled MQ) had an amplitude of 25 mm. (Original photo courtesy of F. Duennebier.)

Plotted around the moon's orbit in Fig. 3 are histograms depicting the average number of moonquakes per hour for each earth-day of all the listening periods. This activity includes all events with amplitudes greater than 4 mm on the compressed seismograms (zero-peak ground motion greater than about 0.2 nm). These events comprise natural moonquakes, impacts, and noises generated in the abandoned Apollo equipment. The consistency of seismic activity between adjacent listening modes in Fig. 3 which were separated in time indicates that the seismic activity probably changes little from one lunation to the next. Activity increases slowly after sunrise, reaches a maximum of about 10 events/hour at sunset, then slowly decreases to a nighttime value of about 0.5 events/hour. Over 60 short (30 min) listening periods between April 1973 and July 1974 were analyzed, and showed levels of activity almost identical to those in Fig. 3.

Seismic activity at the Apollo 14 site showed a "boxcar-like" distribution (Duennebier and Sutton, 1974a) over a lunation beginning shortly after sunrise and ending just after sunset. The Apollo 17 activity is distinctly different, showing much more gradual changes in activity. The reason for this difference is not clear. It may be related to the steep-walled graben in which the Apollo 17 landing site lies. The various slope angles in the valley may "smooth out" the otherwise sudden terminator crossing and concomitant thermal effects. The sharp changes in seismicity detected on the earlier missions could also be partially explained if the thermal noises from the insulating shroud that covered the seismometer (Latham *et al.*, 1971, 1972) were not completely removed.

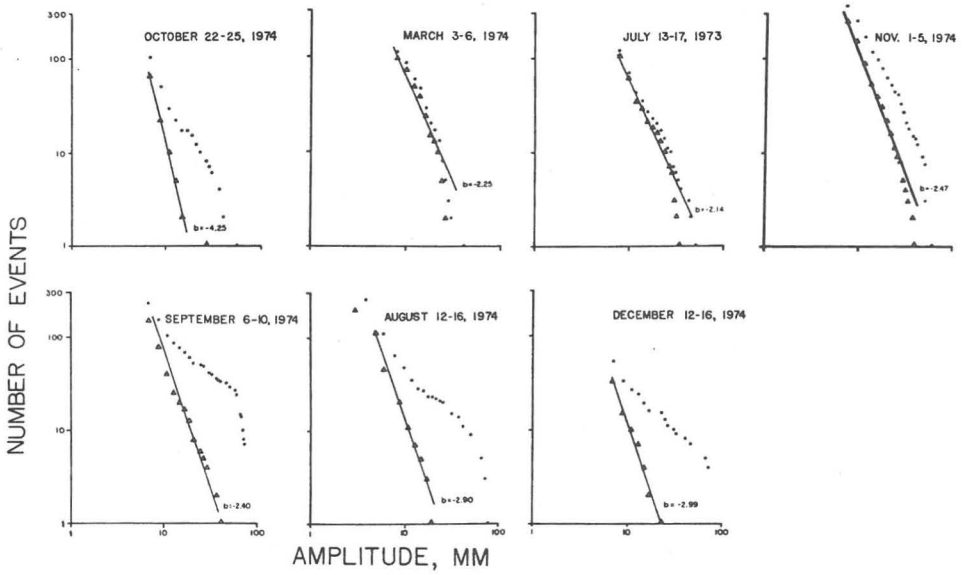

Fig. 5. Frequency–amplitude plots of the seven listening periods, in the order of their occurrence in the lunar day (cf. Table 2; Fig. 3). Black dots represent all events, open triangles represent events with rise times greater than 20 sec. Straight lines shown have been fit by eye.

Frequency–amplitude plots have been made for each period and compared to the relation $\log N = a + b \log A$ in Fig. 5. In this relation A is amplitude (nm) on the compressed seismograms and N is the number of events with amplitude equal to or greater than A (Isacks and Oliver, 1964). The steeper the slope (b) in such a diagram, the more extensively small events dominate the seismic activity. Each plot shows two data sets: (1) all events on the compressed seismograms with amplitudes greater than a cutoff amplitude (generally 7 mm; see Table 2), and (2) the subset of the above with rise times greater than 20 sec. Rise time, the time the seismic wave envelope takes to reach a maximum, depends on properties of the lunar crust and source distance (Latham, *et al.*, 1972). Events that originate within the abandoned Apollo equipment or the remaining ALSEP experiments show very short rise times—10 sec or less. A 20-sec minimum rise time was chosen for the second set to insure that no artificial events are included in the second data set. Although it has been suggested that it is possible to differentiate moonquakes from impacts in short-period, full-scale seismograms, they cannot be separated in the compressed seismograms used for this study. High-frequency events (significant energy at frequencies above 5 Hz) were taken to be meteor impacts by Duennebier and Sutton (1974b). Using their frequency–amplitude relation for impacts detected by the Apollo 14 short-period instrument (after converting to the scale used on the compressed seismograms), 51 impact events larger than 4 mm and 7 impacts larger than 30 mm could be expected *per year*. In the four-day-long listening periods, 0.55 events larger than 4 mm, and 0.05 events larger than 30 mm would be likely to be high-frequency events; i.e. caused by impacts. Thus the inclusion of these few impact events will not affect the results we present here.

Straight lines have been drawn by eye through the distant subset of the data (Fig. 5) and the slopes are recorded in Table 3. The nighttime listening mode is characterized by a steep slope of -3 or -4. As seismic activity increases during sunlit periods, the b values drop sharply to -2.0 and slowly rise during the day and following night.

The b values are so large that, contrary to terrestrial experience, more of the total source energy is released by the more common small events. For example, in

Table 3.

Time	b	Maximum likelihood b	$\bar{A}$ (mm)
October 1974	−4.25	−6.80	9.26
March 1974	−2.25	−2.89	11.30
July 1973	−2.14	−3.86	10.37
November 1974	−2.47	−4.34	10.07
September 1974	−2.40	−4.80	9.86
August 1974	−2.90	−4.79	9.86
December 1974	−2.99	−3.30 (−5.30)*	10.83

*Obtained using all events with $A \geq 7$ mm, $t_R \geq 21$ sec.

the September 1974 listening period ($b = -2.40$; distant events only), the seventy-three 7–9-mm events imply almost three times the energy of the three 15–16-mm events. This may be seen by considering the frequency–amplitude relationship for the number of events with amplitude between A and $A + dA$ (Isacks and Oliver, 1964), where A is maximum trace amplitude (mm) on the compressed seismograms:

$$n(A) = kA^{-(b+1)}.$$

(Note the difference between this and the frequency–magnitude relationship $n(M) = k\ 10^{-bM}$.) Fix r in Eq. (1). The energy of each of the $n(A)$ events may then be calculated (after correcting for the response of the compressed seismogram). The frequency–amplitude formula will yield the ratio of the numbers of events, $n(A_1)$ and $n(A_2)$, with amplitudes A_1 and A_2 (assume $A_1 < A_2$), and Eq. (1) will give the ratio of the energies: $E_1/E_2 = (A_1/A_2)^2$. Thus the ratio of source energy of each of the sets will be

$$\frac{n(A_1)}{n(A_2)} \cdot \frac{E_1}{E_2} = \left(\frac{A_2}{A_1}\right)^{b-1}.$$

Since $A_2 > A_1$, more energy will be released by the small events whenever $b > 1$. Although we have assumed a fixed source distance, the inclusion of this parameter would increase the amount of energy in small events, since random large events would probably have been detected from distant regions where a small event would generate a seismogram too small to notice. This unusual energy relationship casts doubt on the accuracy of the energy estimate obtained earlier. Clearly, significant energy is being released by events below the amplitude cutoff of our investigation. The frequency–amplitude plots (Fig. 5) may be leveling off at 6–7 mm (as they eventually must); whether this reflects an actual reduced frequency of small events—or is only an observational limitation—cannot be determined. It should be remembered that the energy release figures are minimal estimates based on the sequences of events with amplitudes between (roughly) 7 and 70 mm.

Utsu (1966), has devised a maximum likelihood estimate of b values, computed by

$$b = \frac{\log_{10} e}{\bar{M} - M_s}$$

where M_s is the smallest magnitude in the set of s earthquakes, e is the base of natural logarithms, and $\bar{M} = 1/s\ \Sigma\ M_i$. We have applied this to the distant data, using 8 mm as the lowest amplitude, and defining $M = \log_{10} A$. These b values are also listed in Table 3, as is the mean amplitude. Ten millimeters on the compressed seismograms are generated by a ground motion of approximately 1-nm peak-to-peak. A change in amplitude of 1 mm would correspond to about 0.08-nm peak-to-peak in actual ground displacement. The same systematic change is seen in the maximum likelihood b values, and therefore is reflected in the trends of the mean amplitudes. The actual values of the mean amplitudes, of course, reflect the

arbitrary cutoff amplitudes: the means refer to the means of particular sets of events. Largest events seem to be most predominant after sunrise, decreasing in importance throughout the remainder of the thermal cycle. The December 1974 listening period detected very few events; its b values and $\bar{M}$ were extremely sensitive to choice of M_s. Until more events can be obtained with the moon in this position, the values should be taken as approximations of questionable significance.

Thus the b values indicate that the increase in activity during the day does not seem to be reflected in large and small sources equally. One explanation of this is that there may be two populations of sources, for example, slumps in unconsolidated material, and thermal creaking in rocks, which react differently to the lunar heating cycle.

Rise-Time analysis

Lunar seismograms of natural or artificial events appear quite different from terrestrial seismograms. Lunar records are emergent, lack or show only poorly developed phases, and continue ringing much longer than expected. These properties have been explained (Latham *et al.*, 1972) by scattering in the near-surface layers. Arrival energy is then determined using the two dimensional diffusion equation (assuming an instantaneous point source):

$$E(t) = \frac{E_0}{\pi \xi t} \exp\left[-\frac{r^2}{\xi t} - \frac{\omega t}{Q}\right]$$

where $E(t)$ = seismic energy density observed at a time t after origin
E_0 = source energy
r = source distance
ξ = diffusivity
ω = angular frequency
$1/Q$ = dissipation constant.

This equation determines the "shape" of the moonquakes in Fig. 4. Rise time, the time between origin and maximum of the signal, may be determined by differentiation:

$$t_r = \frac{Q}{2\omega}\left[\sqrt{1 + \frac{4\omega R^2}{\xi Q}} - 1\right].$$

This should increase monotonically with increasing r, assuming the material properties ξ and Q remain constant. Thus, knowledge of the rise time of an event will yield an estimate of its distance. The rise times of the eight LSPE explosions and the LM impact were measured for total power and at 5, 9, and 12 Hz. The averaged rise times are plotted in Fig. 6. Poorly defined maxima on the more distant shots limited resolution of these rise times to a 10-sec window. The P-travel time from the most distant sources was less than 6 sec, so errors caused

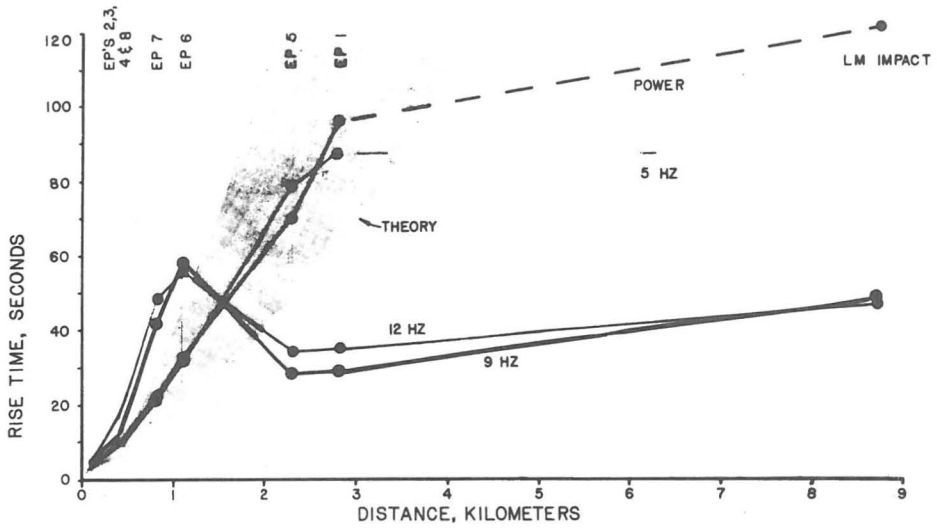

Fig. 6. Rise times of seismograms generated by LSPE sources. Rise times were measured at total power, and at 5, 9, and 12 Hz ($1\frac{1}{2}$-Hz bandwidth). Sources are indicated at the top. The theoretical zone was computed using $\xi = 0.017$–0.033 km^2/sec, $Q = 1700$–3000.

by differences between total rise time, and rise time after signal onset will be slight.

The observed rise times in Fig. 6 deviate from theoretical predictions beyond 1 km, the deviation being most apparent at higher frequencies. One possible explanation of this discrepancy is variable material properties along the deeper ray paths. Rise times at higher frequencies are clearly of little value in estimating source distance. A 35-sec rise time at 9 Hz could come from 0.7, 2, or 3–7 km. Similar ambiguities probably affect total power and 5-Hz rise times at distances greater than 3 km ($t_r = 95$ sec). Rise times of total power of 1255 events in the seven listening periods were measured from the compressed seismograms, and are plotted as frequency histograms in Fig. 7. The t_r versus distance relationship observed in Fig. 6 for total power is plotted at the top. Both the explosion and moonquake seismograms carry most of their energies at low frequencies. The "spectral peaks" of moonquakes range between 3 and 9 Hz, and average about 4–6 Hz. As mentioned earlier, high-frequency events would be relatively rare, if they occurred as often as at the Apollo 14 site. Thus, moonquakes should exhibit a dependence of total power rise time on distance that is similar to that of the explosion packages. Two peaks—at 10 sec and at 40 sec—are apparent. The first peak represents very local events, many of which are probably "LM burps" and other artificial signals. These appear to be most numerous near sunrise and sunset (in October, November, and September). The second peak corresponds to events at a distance of about 1.5 km. The source distance to any of the rare 10–20-Hz events would, however, be significantly underestimated by this technique. Moonquakes exhibit very emergent beginnings, so the rise times may be systematically low if a low-amplitude early arrival were missed. The measurements were

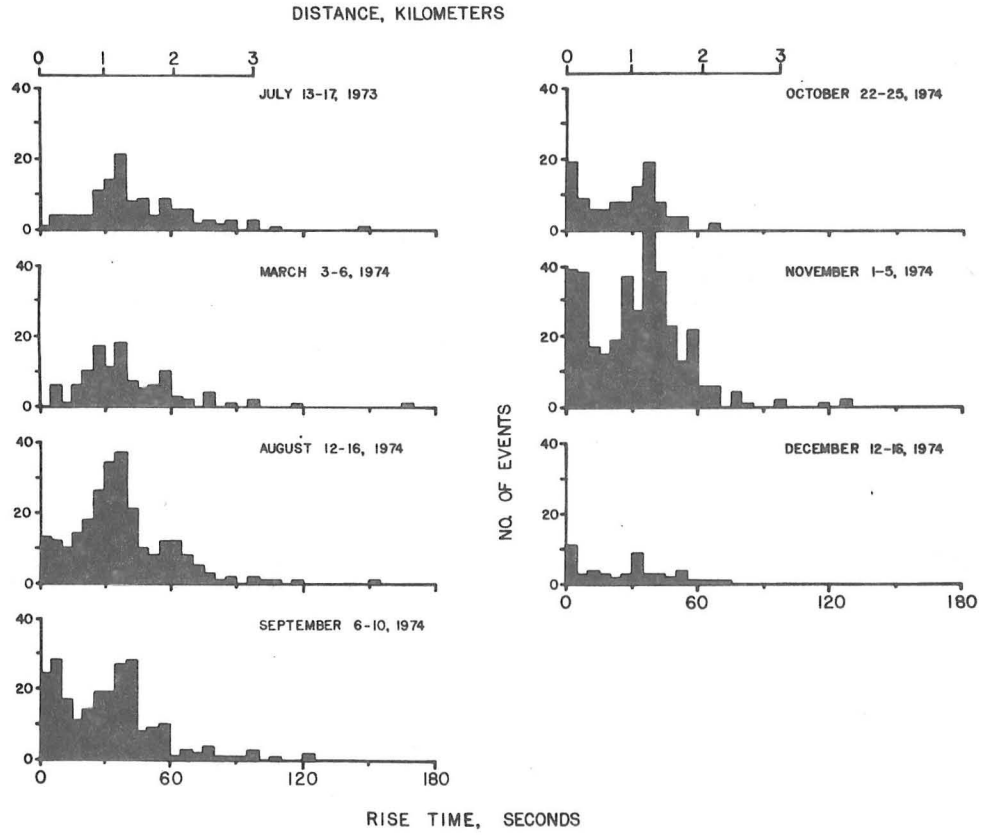

Fig. 7. Histograms, showing the frequency of occurrence of different rise times (5-sec blocks) in each of the seven listening periods. The distance scale at the top is adopted from the rise time–distance relationship for total power in Fig. 6.

consistent with similar measurements made on over 50 detailed seismograms, and repeatable within 5 sec, and it is unlikely that our measurements of rise times consistently missed any detectable onset by more than 10 sec. But, if the first arrivals were undetectable; i.e. below the detection level of the instrument, the resulting bias would lead to measured rise times that were consistently short. To estimate the size of this error, rise times were measured from the explosion package spectrograms, but much higher noise levels were added. Measurements were made by assuming the background noise level was 4, 10, 20, and 30 db below the signal's maximum. At any fixed source distance, the relative error in detectable rise time stayed approximately constant. With a signal only 4 db above noise level, only 62% of the true rise time was seen; for 10 db, 70%, for 20 db, 82%, and for a signal 30 db above noise level, 92% of the rise time would be observed. Thus a 40-sec rise time measured on a signal 10 db above background noise may actually be closer to a 57-sec rise time. Most events seem to be 15–20 db above noise level, so that a typical bias would be on the order of 25%. Due to the

elementary nature of this error estimate, we have presented the data in Fig. 7 without any correction. The reader is warned that any distance estimates from these histograms are minimal, but are probably not incorrect by more than a factor of two.

Even assuming that the total power rise times are always low by a 6-sec error, 90% of the events occur within 2.5 km of the array. However, distance estimates based on the rate of signal decay appear to be somewhat greater (F. Duennebier, personal communication, 1975).

DISCUSSION

The central question concerning short-period moonquakes still remains—What causes them? The various studies of short-period moonquakes have pointed out phenomena which will bear on the source mechanisms. The waveforms of short-period moonquakes have been observed to repeat themselves exactly (Latham *et al.*, 1972). Two events which generate identical seismograms must have the same source function and must occur in the same place (to within one wavelength). The correlation with the 300°K diurnal temperature variation implies that moonquakes must at least be initiated in regions that have a significant temperature variation. Langseth *et al.* (1973) reported that the diurnal temperature variation was attenuated to 0.3°K only 57 cm beneath the surface. If the values of k_{mq}, derived from data generated by surface explosions, are applicable, the 1–3-nm displacements are indicative of very small source energies. Whatever the source energy of the events may be, however, the sources cannot have significant erosive power; the persistence of lunar slopes over billions of years and the great exposure ages measured on returned lunar samples preclude significant erosive ability. Any source mechanism must then satisfy the following constraints: (1) a nearly repeatable source time function; (2) correlation with the 29-day lunar thermal cycle—hence source depths very close to the surface; (3) small source energy; and (4) implied low erosive power.

Since the first observation of these events, a number of explanations have been suggested—tectonic events, slumping or landsliding (Latham *et al.*, 1970), thermal noises from basalt or breccia blocks (Latham *et al.*, 1971) and booming sand dunes (Criswell and Lindsay, 1974). The marked correlation of activity with the thermal cycle would appear to eliminate tectonic fault movements as the source for most moonquakes. It is also unlikely that the same motion would recur over the same slip region, a phenomenon that is required by the occurrence of duplicate events. It is not clear that thermal stresses in boulders can build up as high as 10^6 ergs. Booming sand dunes (Criswell and Lindsay, 1974) or gravitational slumping (Duennebier and Sutton, 1974a) appear as the most likely source mechanisms. Both of these sources depend on gravitational potential energy—in the former case to accelerate sand grains to the point of seismic emission, and in the latter to provide the force for downward motion. The simplest "device" for this energy change is a sloping surface.

Our estimates of source energy do not rule out either of these mechanisms.

Landslides releasing sufficient energy are relatively small and do not cause undue erosion. Little is known about the mechanism or efficiency of booming sand, but 10^4-erg booming events have been suggested (Criswell and Lindsay, 1974) as being sufficient to account for the moonquakes.

If the changes in b value reflect changes in applied stress (Scholz, 1968), stresses in the source must be low just after sunrise and rise "rapidly" reaching a maximum near lunar noon. The stresses remain roughly constant or decrease gradually through the lunar afternoon and night. No change in b value, and, by implication, in applied stress is observed at sunset. It is expected that b slopes in the period preceding sunrise would show the steady increase seen since noon (excepting the small sample obtained in the December 1974 period). This stress history is consistent with thermoelastic stresses induced by heating, but an aseismic stress release mechanism is then required to release stresses generated during cooling. Such a "one-way" mechanism is in agreement with the observation that the repeating seismic events never repeat with reversed polarity (Duennebier and Sutton, 1974a). Warren and Latham (1970) reported thermal cracks generated by the heating and cooling of laboratory samples. These events also showed high b values, in the range -1 to -3. They suggested that high b values are indicative of all thermally induced events. They mention that "activity ... starts rather abruptly, increases rapidly to a maximum, and decays slowly." Such a mechanism might explain the lunar activity—activity starts suddenly at dawn, but only in a thin surface layer. Total activity increases as the thermal wave penetrates deeper into the regolith, with new, deeper activity adding to the "slowly decaying" shallower events. The larger events in the experiment occurred predominantly in the first half of each activity episode. These results would predict a repetition of daytime activity after sunset as the "cooling wave" penetrated the regolith. Such effects are not observed. Finally, no activity was observed in the laboratory specimens after repeated (15–20 times) thermal cycling. Although these events could explain some of the characteristics of lunar seismicity, the absence of a post-sunset increase and the mere presence of events after millions of diurnal thermal cycles on the moon suggest that thermal cracking is not the source of moonquakes, or, at best, is modified and constrained by other phenomena.

If rise times can be accurately measured and the explosion-derived relationship between rise time and distance is valid, most events must occur within 2 km of the array. The fresh-appearing Lee–Lincoln scarp is never closer than 5.4 km from the seismic array. The edge of North Massif is almost 3 km away. Since distance estimates based on rise time are minimal estimates, we cannot conclude that the North Massif is too far away to account for the seismic sources. While the scarp to the west could provide a possibly active fault, it seems too distant to account for the events. Such a source would imply a total power rise time of 100 sec or greater, and thus observational errors on the order of 60 sec. The array lies on the north edge of the Central Cluster of craters which range up to a diameter of about 650 m. A 2-km circle around the array would include many of the larger craters. The crater Camelot may be crudely modeled by a 20° planar

slope, 100 m high (to allow for a gentler slope near bottom), and 2 km long (Camelot's circumference). A 1° degradation of this slope releases 7.9×10^{17} ergs. If all this energy is transformed into typical seismic events (5×10^6 ergs), it would account for 1.6×10^{11} events. Assuming that the Central Cluster is equivalent to 10 Camelots, the 1.6×10^{12} events would take approximately 100 m.y. The energy detected at the Apollo 17 array could come from moonquakes occurring within the Central Cluster craters, but yet not causing excessively rapid erosion of the crater walls.

If slumping of local crater walls, rather than slumping on the North Massif, were the cause of moonquakes, the seismic signals would originate closer and arrive generally from the south. Present distance estimates do not unequivocally differentiate between these hypotheses. The determination of the azimuths toward the sources has been complicated by the emergent nature of the moonquake signals and the lack of distinct phases. Brief time windows have been found in the explosion package seismograms and possibly in some moonquake records that show the Rayleigh-wave dispersion expected for the structure in the Taurus-Littrow Valley. A dispersive character would imply direct, not scattered, Rayleigh waves, which could in turn be investigated in a beam steering study to determine their direction of approach. Such a study, now in progress, may shed light on the location of the moonquake sources.

Although many of the local (short rise time) events have unusual spectral characteristics indicative of thermally generated equipment noises, some of these local events appear to be natural moonquakes (F. Duennebier, personal communication, 1975) within 400 m of the array. No large craters are this close to the array, and slopes near the landing site are typically no more than 5°–10° (W. R. Muehlberger, personal communication, 1975). It is difficult to see how a process involving the release of gravitational energy could operate in such a flat region.

CONCLUSIONS

The source mechanism of "thermal" moonquakes still remains an enigma, but further constraints may now be placed on it. A typical 1-nm (peak-to-peak) moonquake releases 10^6–10^7 ergs; the annual seismic energy release detected at the Taurus-Littrow Valley is about 10^{11} ergs. Landslides on the massifs and crater walls, previously believed to cause impossibly rapid erosion, can be the source of moonquakes without degrading all lunar slopes. Seismic activity reaches a distinct peak near sunset, in contrast to the seismicity observed on earlier Apollo missions. The variation in b values during the lunar day may be interpreted to indicate stress buildup in the source near lunar noon. This is consistent with a mechanism that releases stresses seismically during heating, but aseismically during cooling. Finally, rise times indicate that the sources are very close, within 2.5 km of the array. The crater walls in the Central Cluster may be the source location of landslide-induced moonquakes. Surface wave studies, now in progress, may determine the azimuth to moonquake sources, and differentiate between a North Massif source and a Central Cluster source.

Acknowledgments—We would like to thank Fred Duennebier for supplying us with compressed seismograms of the listening periods, and for the original photograph from which Fig. 4 was made. We also appreciate several anonymous reviewers' comments. This research was supported by the National Aeronautics and Space Administration under contract NAS 9-5632.

References

Cooper M. R., Kovach R. L., and Watkins J. S. (1974) Lunar near-surface structure. *Revs. Geophys. Space Phys.* **12**, 291–308.

Criswell D. R. and Lindsay J. F. (1974) Thermal moonquakes and booming dunes (abstract). In *Lunar Science V*, p. 151–153. The Lunar Science Institute, Houston.

Duennebier F. and Sutton G. H. (1974a) Thermal moonquakes. *J. Geophys. Res.* **79**, 4351–4363.

Duennebier F. and Sutton G. H. (1974b) Meteoroid impacts recorded by the short-period component of Apollo 14 lunar passive seismic station. *J. Geophys. Res.* **79**, 4365–4374.

Isacks B. and Oliver J. (1964) Seismic waves with frequencies from 1 to 100 cycles per second recorded in a deep mine in northern New Jersey. *Bull. Seis. Soc. Amer.* **54**, 1941–1979.

Kovach R. L., Watkins J. S., and Talwani P. (1973) Lunar seismic profiling experiment. In *Apollo 17 Preliminary Sci. Report*, NASA publication SP-330, p. 10-1 to 10-12.

Langseth M. G., Jr., Keihm S. J., and Chute J. L., Jr. (1973) Heat flow experiment. In *Apollo 17 Preliminary Sci. Report*, NASA publication SP-330, p. 9-1 to 9-24.

Latham G. V., Ewing M., Press F., Sutton G., Dorman J., Nakamura Y., Toksoz N., Wiggins R., Derr J., and Duennebier F. (1970) Apollo 11 passive seismic experiment. *Proc. Apollo 11 Lunar Sci. Conf.*, p. 2309–2320.

Latham G. V., Ewing M., Press F., Sutton G., Dorman J., Nakamura Y., Toksoz N., Duennebier F., and Lammlein D. (1971) Passive seismic experiment. In *Apollo 14 Preliminary Sci. Report*, NASA publication SP-330, p. 6-133 to 6-161.

Latham G. V., Ewing M., Press F., Sutton G., Dorman J., Nakamura Y., Toksoz N., Lammlein D., and Duennebier F. (1972) Passive seismic experiment. In *Apollo 16 Preliminary Sci. Report*, NASA publication SP-315, p. 9-1 to 9-29.

Richter C. F. (1958) *Elementary Seismology.*

Scholz C. H. (1968) The frequency–magnitude relationship of microfracturing in rock and its relation to earthquakes. *Bull. Seis. Soc. Amer.* **58**, 399–415.

Ulrych T. J. (1972) Maximum entropy power spectrum of truncated sinusoids. *J. Geophys. Res.* **77**, 1396–1400.

Ulrych T. J., Smylie D. E., Jensen O. G., and Clark G. K. C. (1973) Predictive filtering and smoothing of short records by using maximum entropy. *J. Geophys. Res.* **78**, 4959–4964.

Utsu T. (1966) A statistical significance test of the difference in b-value between two earthquake groups. *J. Phys. Earth* **14**, 37–40.

Warren N. W. and Latham G. V. (1970) An experimental study of thermally induced microfracturing and its relation to volcanic seismicity. *J. Geophys. Res.* **75**, 4455–4464.

Wyss M. and Brune J. N. (1968) Seismic moment, stress, and source dimension for earthquakes in the California–Nevada region. *J. Geophys. Res.* **73**, 4681–4694.